THE DEVELOPMENT OF SHAFT FRICTION AND END BEARING RESISTANCE FOR DYNAMICALLY DRIVEN MODEL PILES

by

G. C. LAKE B.Sc., F.G.S.

Thesis presented in partial fulfilment of the requirement for the Degree of Doctor of Philosophy, Council for National Academic Awards, London.

Sponsoring Establishment

Department of Civil Engineering and Building, The Polytechnic of Wales, United Kingdom

Collaborating Establishment

Building Research Establishment, Watford, United Kingdom

April 1986

I FY NHAD,

AM EI HOLL GYMORTH A CEFNOGAETH.

Certificate of Research

This is to certify that, except when specific reference to other investigations is made, the work described in this thesis is the result of the investigation of the candidate.

Gwyn C Lake
G. C. Lake
(Candidate)

15/4/86
(Date)

G.O. Rowlands
Mr. G. O. Rowlands
(Director of Studies)

15/4/86
(Date)

R. Delpak
Dr. R. Delpak
(Supervisor)

15/4/86
(Date)

Declaration

This is to certify that neither this thesis, nor any part of it has been presented, or is being currently submitted, in candidature for any degree at any other Academic Institution.

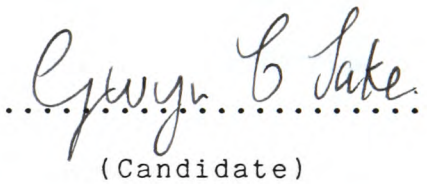

(Candidate)

ACKNOWLEDGEMENTS

The candidate wishes to express his gratitude to Mr. G. O. Rowlands, his Director of Studies, and Dr. R. Delpak, his Supervisor, for their constant help and encouragement. He wishes to thank Mr. R. W. Cooke formerly of the Building Research Establishment for his helpful discussions and criticisms.

Special thanks must go to the following:-

(1) Mr. W. M. Hague of the Department of Mechanical and Production Engineering for his help in developing instrumentation for measuring transient signals and also making available the specialist equipment needed to monitor and record these signals.

(2) Mr. C. Bennett of the Department of Civil Engineering and Building Technical Staff for manufacturing the candidates apparatus.

(3) Mr. M. Coundly for all his help in reducing many of the candidates original drawings.

(4) Extra special thanks to J & J Secretarial Services for typing an almost illegible manuscript with good humour and alacrity.

(5) Mr. L. Whiteman and Mr. B. Lloyd for their help in performing the experimental work.

(6) M. A. Hoskins for invaluable help in all matters electrical.

(7) Mr. R. B. Robinson (Research Assistant) for help in performing the experimental work and liaison with the Department subsequent to the candidate leaving the Polytechnic.

Thanks should also go to Blaenau Gwent Borough Council for affording the candidate a leave of absence to pursue his studies.

He would finally like to thank all the people at the Polytechnic who gave help and encouragement and are not mentioned by name.

CONTENTS

SUMMARY

THE DEVELOPMENT OF SHAFT FRICTION AND END BEARING RESISTANCE FOR DYNAMICALLY DRIVEN MODEL PILES

by

G. C. LAKE

This thesis describes a laboratory investigation of the behaviour of a 60 mm diameter tubular steel model pile dynamically driven into sand and into sand overlying clay. The soil was placed and instrumented under controlled conditions in a 3 m diameter concrete tank 3 m deep.

A pilot study was initially undertaken using a 38 mm pile to check the proposed static and dynamic instrumentation. A sophisticated control programme was then developed for the main tests using an Orion Data Logger interfaced with a Commodore PET micro computer. The static load data was stored on discs whilst the transient data was recorded on magnetic tape for later analysis.

A pneumatically controlled rig was designed for driving the piles. The piles were driven from the surface adding sections at selected intervals. Inclinometers were installed in the soil to monitor vertical movements. The density of the soil was also measured at selected points at the end of the tests.

The pile was driven to an embedded depth of 2 metres and then test loaded using the conventional CRP, MTL and Pull Out tests. The load distribution along the pile, together with the vertical movement of the soil was monitored at all stages. Changes in the shear and vertical stresses at the sand clay interface were also monitored and the final deformation of the clay beneath the pile tip.

The data showed:-

(1) The pile top impact force was dependant on ram impact velocity only.

(2) The transient forces at the pile tip could be less than equal to or greater than the impact force depending on the nature of the bearing surface.

(3) The stress transfer curves exhibited a large value at shallow depth diminishing in value towards the toe.

(4) Vertical sand displacement decreased with increasing depth and radius.

(5) Insitu density increased towards the pile shaft by an appreciable amount.

(6) Soil movements were recorded across the sand clay interface during driving and test loading.

(7) Dragdown of sand into the clay along with a wedge of sand which preceded the pile tip was also observed.

A theoretical approach for predicting static bearing capacity using the dynamic equations of motion and dynamic measurements is also outlined and compared with the authors experimental results. The agreement between experimental and theoretical thus achieved are encouraging.

LIST OF FIGURES

CHAPTER 1

CHAPTER 2

CHAPTER 3

CHAPTER 7

LIST OF PLATES

CHAPTER 3

CHAPTER 4

CHAPTER 5

CHAPTER 6

CHAPTER 1

OBJECTIVES OF THE PRESENT INVESTIGATION AND LITERATURE REVIEW

1.1 Introduction and Relation to Previous Work

The work described in this thesis forms part of an ongoing research project currently being conducted at the Polytechnic which concerns the development of shaft friction and end bearing in piles passing through a granular medium into clay. Kay (1980) used a 110 mm tubular steel pile in a frictionless cylinder to eliminate end bearing. In this way he was able to study the development of shaft friction on a pile passing through sand into a clay stratum. Kay (1980) placed the sand around the pile in layers and observed linear increase in shaft friction at shallow depths becoming constant at greater depths as previously observed by Vesic (1963).

Wersching (1986) extended this work by jacking a 110 mm tubular steel pile from the surface into both a sand and sand/clay profile. He used more sophisticated axial load cells than Kay (1980) and also incorporated contact stress transducers along the surface of the pile to measure shear and normal stresses directly. Wersching (1983) also developed a means of determining insitu density in dry sand along with a method of measuring insitu vertical soil displacements using electrolytic levels.

The present research programme changes the method of installation from static to dynamic by using a drop hammer and examines the transmission of transient forces along the pile as well as static load distribution and insitu soil

movement. It was orginally envisaged that the results obtained from the present investigation would be compared with those of Wersching's in order to study the variations encountered by changing from static to dynamic installation. However, the two research investigations overlapped and at the time of publication Wersching's results were not available.

A search of the available literature shows that very little work has been conducted on the development of shaft friction in piles passing through sand into a clay stratum.

The most relevant work conducted outside the Polytechnic was that of Meyerhof and Sastry (1978) who presented test results on instrumented model piles and field data for both jacked and driven piles. They showed that as the pile approaches the sand/clay interface it may fail by 'punching' into the underlying stratum. They also noticed that the shaft load curves and the tip load/settlement curves were similar in shape to each other.

Tomlinson (1971) described results of examination of the surfaces of bearing piles and sheet piles which had been driven through granular materials into stiff to very stiff clays. It was observed that the overburden material was carried into the clay to a limited distance (3D). Radial cracking of the clay and heave of the surface was also observed.

A comprehensive 'State of the Art' review of piling is given by Kay (1980) and therefore only work of direct relevance will be included in the literature review.

1.2 Literature Review

1.2.1 Effects of Installation of Driven Piles

1.2.2 Sand

It is well established that when a pile is driven into sands or cohesionless soils there is considerable compaction due to displacement and vibration by the pile. This process leads to permanent changes in the sand structure and even crushing of the sand particles. Therefore installing a pile in loose sands by driving has advantages over other non-displacement type processes due to the increase in relative denisty caused by the driving process. There has been a number of notable contributions in determining the extent of this zone of increased density and compaction, namely Meyerhof (1959), Robinsky and Morrison (1964) and Kishida (1963).

Using driven piles Meyerhof (1959) found a radial zone of volume change around the pile shaft of 8D and a further failure zone below the pile tip of 4D.

Kishida (1963) observed widths of 4D for the failure zone and 8D for the compaction zone. In careful laboratory tests on a model pile, Robinsky and Morrison (1964) studied the displacement and compaction zone around the pile using radiography techniques. Robinsky and Morrison found that in loose sand the soil movement extended from 3 to 4D to the side and 2.5 to 3.5D below the pile tip. In dense sand they found these zones to be 4.5 to 5.5D and 3 to 4.5D respectively. Robinsky and Morrison also found that the process of compaction and displacement below the pile tip leads to sand movement and loosening of the soil immediately in the vicinity of the pile shaft. This process tends to nullify some of the benefits of the primary compaction.

Meyerhof and Sastry (1978) found the zone of compaction around a 76 mm diameter pile to be 8D.

1.2.3 Clay

De Mello (1969) classified the effects of pile driving in clays into four categories:-

(a) Remoulding or partial structural alteration of the soil surrounding the pile.

(b) Alteration of the stress state in the soil in the vicinity of the pile.

(c) Dissipation of the excess pore pressures developed around the pile.

(d) Long term phenomena of strength regain in the soil.

1.2.4 Changes in Soil Properties due to Driving

A correlation between load tests to failure on piles in clay at different times after installation indicate a considerable increase in bearing capacity. This phenomenon has been observed by many authors, among others, Cummings, Kerkhoff and Peck (1950), Orrje and Broms (1967), Cooke, Price and Tarr (1979) and O'Neill, Hawkins and Audibert (1982).

From the observations it can be inferred that initially considerable loss in the undrained shear strength of the clay takes place with subsequent regain as time passes. This increase in strength may be attributed to a combination of two factors (Poulos and Davis (1980)):-

(1) Thixotropic regain of undrained shear strength.

(2) Local Consolidation produced by dissipation of excess pore water pressure with time.

Cooke, Price and Tarr (1979) have shown that for piles jacked into London Clay the global shear modulus (G) increased by as much as 50% over a period of 32 months. The extent of the disturbance caused by pile driving has again been reported upon by numerous authors with varying results.

The extent of this disturbed zone is fully discussed in Chapter 4, Section 4.6.1 where conclusions are drawn on the suitability of the sand tanks used for the pile tests. De Mello (1969) based on available evidence suggested that immediately after driving, the amount of remoulding decreased from about 100% at the pile soil interface to virtually zero at about 1.5 to 2.0D from the pile surface.

Apart from thixotropic regain of strength, the rate of increase of soil strength with time is related to the dissipation of excess pore water pressure. Soderberg (1962) presented data that showed that the increase in strength of the soil was related to the rate of dissipation of the excess pore water pressure.

Much work has been carried out on the amount of excess pore water pressure developed during driving, for example: Bjerrum, Hansen and Sevallson (1958), Bjerrum and Johannessen (1960), Milligan et.al (1962), Lambe and Horn (1965), Lo and Stermac (1965), Orrje and Broms (1967), Hanna (1967), Koizumi and Ito (1967) and D'Appolonia and Lambe (1971).

It is generally agreed that excess pore water pressures generated in the vicinity of the pile may be greater than

or equal to the effective overburden stress. Data presented by Airhart (1969) has shown that even larger pore pressures than those developed around the pile may be developed at the pile tip.

1.3 Load Distribution in Piles and Stress Transfer

1.3.1 Sand Only

The axial load distribution in piles in sand for increasing load increments is shown in Fig. 1.1 and has been shown to be the case by among others Vesic (1963), Meyerhof and Valsanker (1977), Chan and Hanna (1979) and Gregerson et.al (1973). Vesic (1967) and Kerisel (1961) have shown that skin resistance and base resistance do not necessarily increase linearly with depth but reach a constant value after a certain critical depth. These findings have been confirmed by Tavenas (1971) and Hanna and Tan (1973).

Mansur and Kaufman (1956) demonstrated that the slope of the load distribution curve at any depth, is a measure of the rate at which the load is transferred from the pile to the soil at that depth. The slope is also a measure of the frictional resistance mobilised at that point.

1.3.2 Clay

A typical load distribution for piles in clay is shown in Fig. 1.2 (Cooke, Price and Tarr (1979)) and differs slightly from the curve for sand only (Fig. 1.1) in that increase in base resistance with increasing applied load is less than for the sand case. This leads to an increasing stress transfer towards the toe (Cooke, Price and Tarr (1979)) as opposed to a decreasing stress transfer shown by Tan (1983).

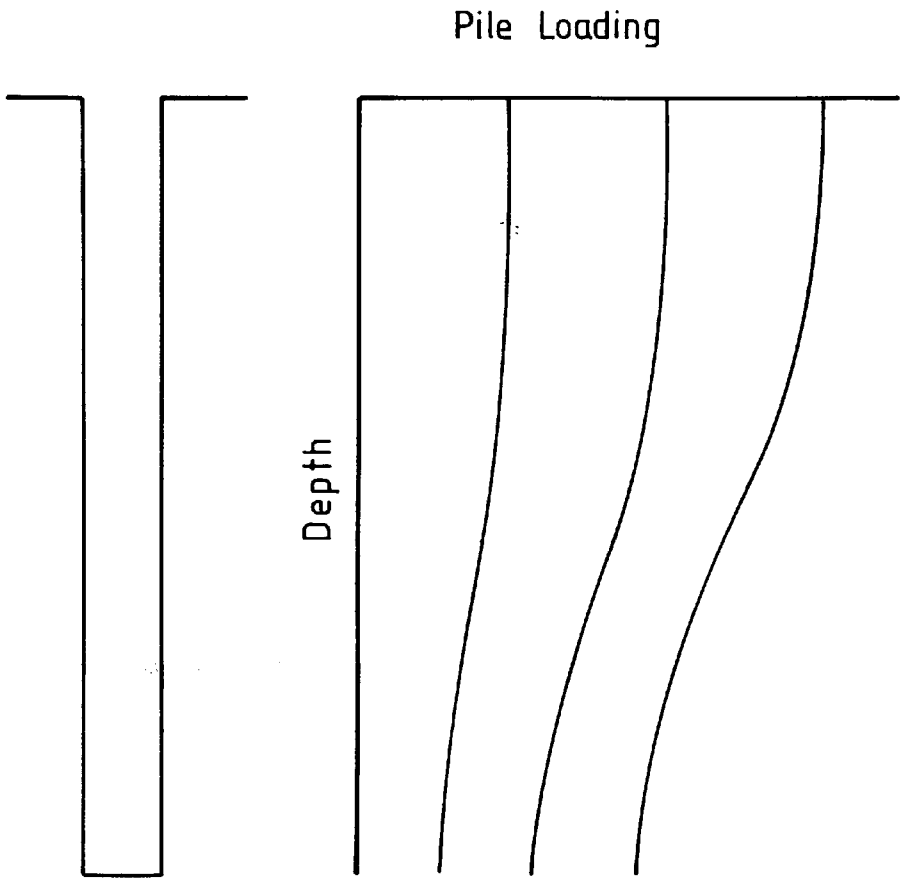

FIG. Nº 1.1 TYPICAL LOAD DISTRIBUTION CURVES FOR DIFFERENT APPLIED LOADS (Sand)

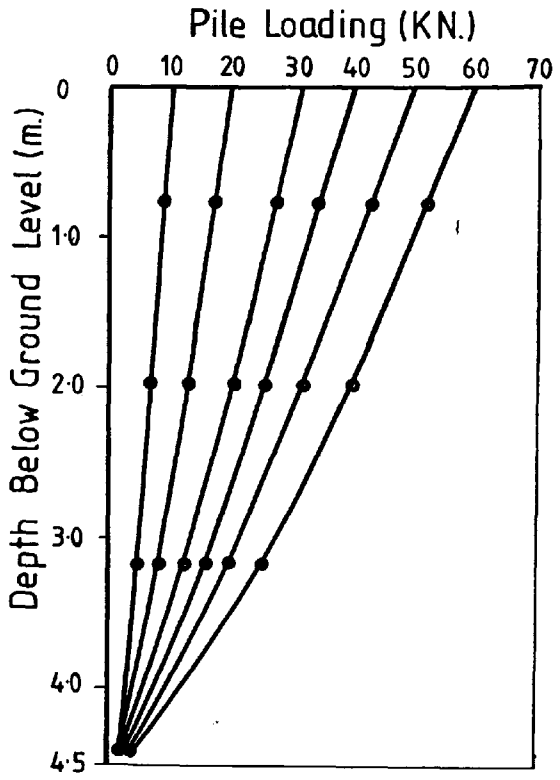

FIG. Nº 1.2 TYPICAL LOAD DISTRIBUTION CURVES FOR DIFFERENT APPLIED LOADS (Clay, After Cooke, Price & Tarr)

Coyle and Reese (1966) found the load transferred to the clay to be a function of depth and pile movement.

Tomlinson (1977) suggested that the stress distribution along a pile depends on the soil density and method of installation of the pile.

1.4 Dynamic Pile Driving Formulas

All pile driving formulae attempt to relate pile set to the ultimate load carrying capacity of the pile and assume that driving resistance is equal to the static capacity of the pile.

The derivation of the more reliable formulae are given by Whitaker (1970) while details of some of the required parameters are given by Chellis (1961).

A fairly recent development in predicting static bearing capacity from dynamic measurements is the case of the wave equation, which examines the transmission of compressive waves down the pile as opposed to the driving formulae which assume instantly generated force throughout the pile. Use of the wave equation is discussed in some detail in Section 1.5.

The majority of the driving formulae are based on Newton's Second Law of Impact with some being modified to account for energy losses. Taylor (1948) gave the derivation of a general pile formula while the reliability of such formulae have been reported upon by among others Sorensen and Hansen (1957), Agerschou (1962), Flaate (1964), Housel (1966) and Olsen and Flaate (1967). Tavenas and Audibert (1977) have

also conducted a comparison of the reliability of the one dimensional wave equation with other driving formulae and will be discussed in Section 1.5.9.

A table summarising the more well known formulae is given by Poulos and Davis (1980) and is reproduced in Figure No. 1.3 for the readers interest.

Sorensen and Hansen (1957) showed that there is little difference in the Danish, Hiley, Janbu and wave equation while the Eytelwein formula was found to be very inaccurate.

The work of Agerschou was based mainly on the reliability of the Engineering News formula but nevertheless broadly confirmed the findings of Sorensen and Hansen (1957) with regard to the reliability of the Janbu, Hiley and Dutch formulas. Agerschou concluded that the Engineering News formula was very unreliable with failure loads as determined from the formula having actual safety factors as high as 30.0. The reliability of the Janbu, Hiley and Engineering News formula was given by Flaate (1964) for a number of different material piles in sand and confirmed Agerschou's findings with regard to the unreliability of the Engineering News formula. Flaate again found the Janbu and Hiley formulas to be the most reliable. In contrast to the findings of Sorensen and Hansen, Agerschou and Flaate, Housel (1966) showed a greater reliability obtained from the Engineering News formula than from the Hiley. This reversal may well stem from the fact that two sites of differing soil profiles were used in the investigation. One site was predominantly sand while the other was clay. Poulos and Davis (1980)

FORMULA	EQUATION FOR Ru	REMARKS
Sanders	$\frac{WH}{S}$	
Engineering News	$\frac{WH}{S+C}$	C = 1·0 in. for drop hammer 0·1 in for steam hammer 0·1 Wp/W in. for steam hammer on very heavy piles
Eytelwein (Dutch)	$\frac{WH}{S} \cdot \frac{W}{W+Wp}$	
Weisbach	$\frac{SAEp}{L} + \sqrt{\left(\frac{2WHAEp}{L}\right) + \left(\frac{SAEp}{L}\right)^2}$	
Hiley	$\frac{e_f WH}{S+1/2(C_1+C_2+C_3)} \cdot \frac{W+n^2Wp}{W+Wp}$	For values of e_f, C_1, C_2, C_3 and n see Poulos & Davis (1980)
Janbu	$\left(\frac{1}{Ku}\right)\left(\frac{WH}{S}\right)$	$ku = Cd(1+\sqrt{1+\gamma e/Cd})$ $Cd = 0·75 + 0·15\, Wp/W$ $\gamma e = WHL/AES^2$
Danish	$\frac{e_f WH}{S+(2e_f WHL/AEp)^{1/2}}$	For values of e_f see Poulos & Davis (1980)
Gates	$5·6\sqrt{e_f WH \log_{10}(10/S)}$	Units are inches and tons (short)
	$4·0\sqrt{e_f WH \log_{10}(25/S)}$	Units are metric tons (1000 kg.) and centimeters

FIG. Nº 1.3 SUMMARY OF PILE DRIVING FORMULAS (After Poulos & Davis (1980))

suggested that the reason for this reversal in reliability may be due to the significant friction encountered in piles in clay (which is not allowed for in the formulae leading to the reported differences.

The work of Flaate (1964) was extended by Olsen and Flaate (1967) to examine the reliability of the pile driving formulae on different material piles. They concluded that for steel and timber piles the Janbu formula was most reliable while for precast concrete piles no formula was clearly the best. Again the Engineering News formula was found to be unsatisfactory with the Danish, Janbu and Gates formula found to be the most reliable.

It is obvious from these findings that a more consistent approach for all pile type and soil conditions which takes into account such factors as pile vibration due to impact and side and point soil resistance should be adopted. The one dimensional wave equation appears to be one such approach and will be discussed in the ensuing sections.

1.5 One Dimensional Wave Equation

Today predictions of static bearing capacity from dynamic measurements are mostly based on the solution of the one dimensional wave equation first presented by St. Venant (1866) and first considered for use in piling by Isaacs (1931). Glanville et.al (1938) published a comprehensive report on the mathematical and experimental aspects of the problem.

The basic differential equation being:-

$$\frac{\delta^2 D}{\delta t^2} = \frac{E}{\rho} \frac{\delta^2 D}{\delta x^2} \pm R$$

R = soil resistance term

D = longitudinal displacement of a point on a bar from its original position

t = time

x = direction of longitudinal axis

Explicit solutions can only be calculated for idealised cases : therefore it was not until the advent of the digital computer on which numerical solutions could be performed that the approach received wide acclaim.

The first numerical solution for one dimensional longitudinal wave impact of an elastic bar was given by Smith (1955), followed by a further paper (Smith (1960)) which gave an extensive treatment of the application of the wave equation to pile driving analysis.

As the majority of subsequent wave equation type analysis are based on the work of Smith a brief outline of the approach will now follow.

1.5.1 Pile Driving Analysis by the Wave Equation

The numerical solution proposal by Smith is based on a finite difference representation of the wave equation.

Figure 1.4(a) illustrates the idealisation of the pile/soil system suggested by Smith.

As can be seen from Figure 1.4(b) the pile is split up into a number of discrete elements connected by weightless springs.

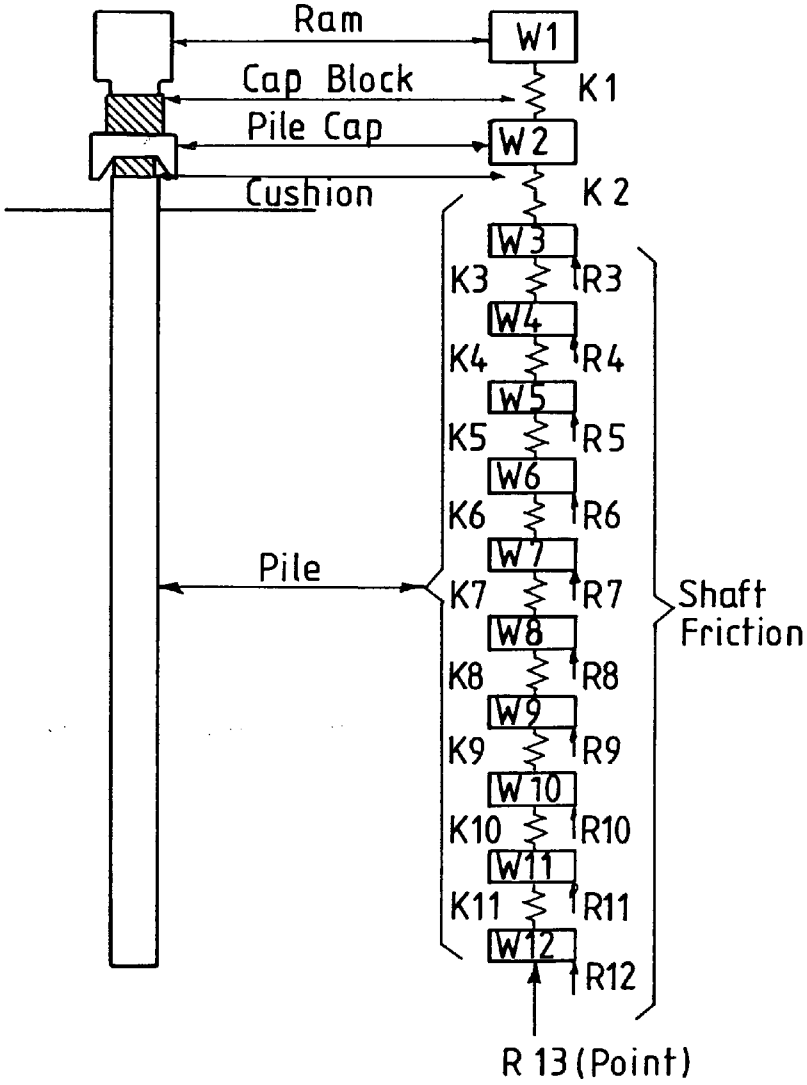

(a) Actual Pile (b) Idealised Pile

FIG. Nº 1.4 IDEALISATION OF PILE USED FOR THE WAVE EQUATION ANALYSIS

The frictional resistance on the side of the pile is accounted for by a spring with friction link and viscous damper. (Fig. 1.5(a)).

The role of the friction link will be discussed in a later section.

The basic equations as developed by Smith are as follows:-

$$D(m,t) = D(m,t-1) + 12\Delta t\ V(m,t-1) \qquad 1.1$$

$$C(m,t) = D(m,t) - D(m+1,t) \qquad 1.2$$

$$F(m,t) = C(m,t)\ K(m) \qquad 1.3$$

$$R(m,t) = [D(m,t) - D'(m,t)]\ K'(m)[1+J(m)V(m,t-1)] \qquad 1.4$$

$$V(m,t) = V(m,\ t-1) + [F(m-1,t) + W(m) - F(m,t) - R(m,t)] \times \frac{g\Delta t}{W(m)} \qquad 1.5$$

where $()$ = functional designation

m = element number

t = number of time interval

Δt = size of time interval (sec)

$C(m,t)$ = compression of internal spring m in time interval t (in)

$D(m,t)$ = displacement of element m in time interval t(in)

$F(m,t)$ = force in internal spring m in time interval t(lb)

g = acceleration due to gravity (ft per sec)

$K(m)$ = spring constant associated with internal spring m, lb/in

$R(m,t)$ = force exerted by external spring m on element m

$V(m,t)$ = velocity of element m in time interval t(ft per sec)

$W(m)$ = weight of element m (lb)

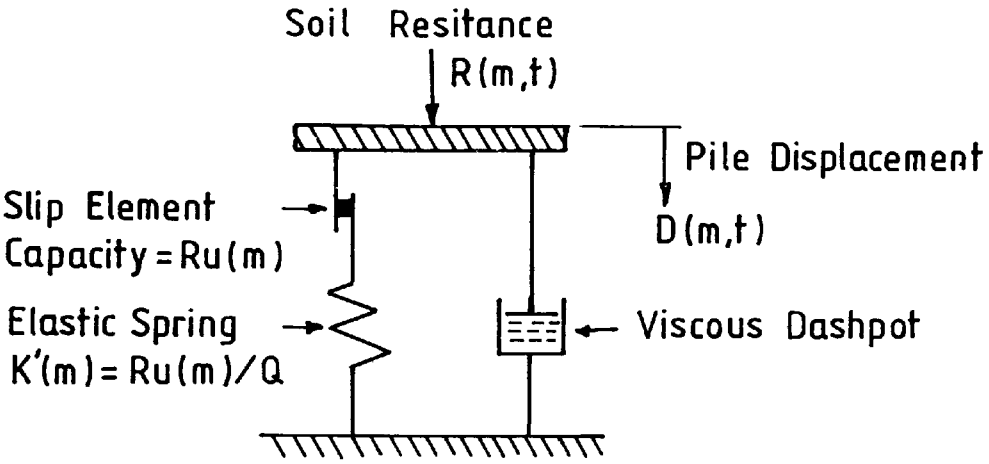

(a) RHEOLOGICAL MODEL

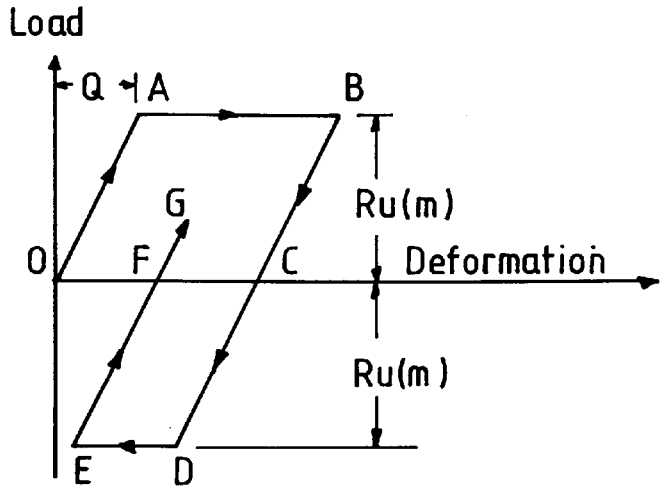

(b) STATIC

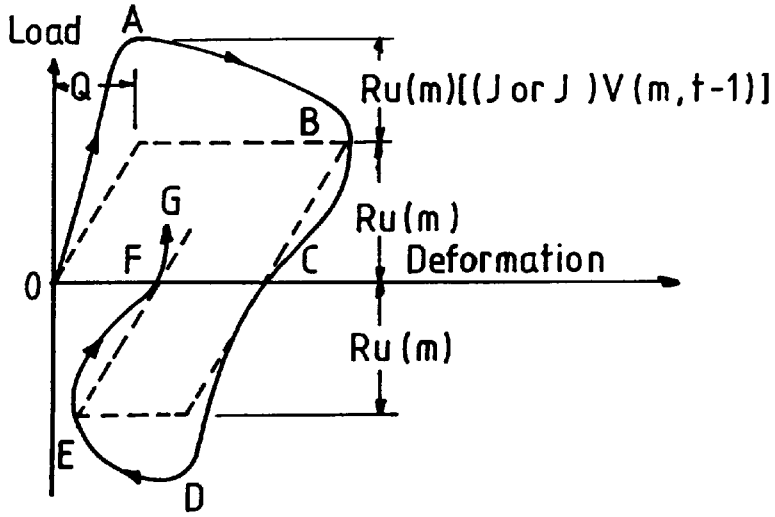

(c) DYNAMIC

FIG. Nº 1.5 LOAD DEFORMATION RELATIONSHIPS FOR SOIL (After Smith)

The spring constant K(m) for the pile, capblock and cushion is calcualted from the relationship:

$$K(m) = \frac{E(m)\ A(m)}{L(m)}$$

where $A(m)$ = cross sectional area of element m (in^2)

$E(m)$ = modulus of elasticity of element m (lb/in^2)

$L(m)$ = length of element m (in)

In order to account for internal damping in the capblock and cushion equation 1.3 was modified to:-

$$F(m,t) = \frac{K(m)}{[e(m)]^2}\ C(m,t) - \frac{1}{[e(m)]^2} - 1\ K(m)C(m,t)_{max} \qquad 1.6$$

where $e(m)$ = coefficient of restitution of internal spring m and

$C(m,t)_{max}$ = temporary maximum value of $C(m,t)$

1.5.2 Soil Springs

Figure 1.5(b) shows the load deformation relationship assumed by Smith excluding any damping effects. The path OABCDEFG represents loading and unloading for side friction. Only compressive loading is possible for the pile point and so the loading and unloading path is OABCF.

This model has been shown by Lowery et.al (1969) to be equivalent to a Kelvin rheological model.

The important characteristics of the model are defined by the terms Q and Ru. The term Q is designated as the quake and is taken as the maximum deformation which may occur elastically. Ru is the ultimate static soil resistance, or the load at which a spring K' behaves in a purely plastic manner.

Thus for each individual soil spring the soil stiffness relationship is:-

$$K'(m) = \frac{Ru(m)}{Q(m)}$$

where K'(m) is the spring constant for elastic deformation for external spring m.

By introducing a damping constant J(m) and multiplying by the velocity term the soil resistance R(m,t) in equation 1.4 takes into account effects due to velocity changes and the dynamic load deformation relationship thus becomes that shown in Figure 1.5(c).

Smith used two values of J, one for side resistance and one for point resistance. Based on back analysis, the values were 0.05 and 0.15 in. respectively.

1.5.3 Smiths Computer Solution

The computation proceeds as follows:-

1. The initial velocity of the ram is determined from the properties of the pile driver. Other time dependant quantities are initialised at zero or to produce equilibrium of forces under gravity.

2. Displacements D(m,1) are calculated by equation 1.1. It should be noted that V(1,0) is the initial velocity of the ram.

3. Compressions C(m,1) are calculated by equation 1.2.

4. Internal spring forces F(m,1) are calculated by equation 1.3 or equation 1.6 as appropriate.

5. External spring forces R(m,1) are calculated by equation 1.4.

6. Velocities V(m,1) are calculated by equation 1.5.

7. The cycle is repeated for successive time intervals.

1.5.4 Important Contributions to Wave Equation Analysis

The work of Smith opened peoples eyes to the practical uses of a wave equation type analysis and spurred many researchers into in depth analysis of the approach. Some important contributions to the approach are now outlined.

Samson et.al (1963) have shown that by using a wave equation analysis the influence on pile behaviour of factors such as ram weights, ram velocity, diesel hammer pressure, capblock and cushion block stiffness, pile material properties and soil properties may be evaluated. They compared Smith's approximate solution for the influence of gravity on the solution with their own influence coefficient method and concluded that in both cases the effect was negligable giving a maximum difference in results of 10%. Later work conducted by Litkouhi (1979) on offshore piles has shown that in the case of very large piles the effect of gravity on the overall solution cannot be ignored.

Forehand and Reese (1966) concluded that Smith's mathematical model was indeed valid and that attempts to correlate 24 pile driving records with their respective load tests showed encouraging results. They also showed that Smith's method of representing ground resistance is reasonably consistent when compared with experimental findings of others for high

loading rates. Also Forehand and Reese demonstrated that Smith's value for quake of 0.1 inches was not unreasonable and compared favourably with the values given by Hiley (1930) of 0.05 - 0.5 inches.

They further contended that in the case of a clay soil the two values of J and J' used by Smith were unreasonable.

Since that time much work has been carried out on obtaining experimental values for J and Q. Hirsche et.al (1969) showed graphs of the difference in soil resistance (Ru) against blows per foot by varying Q.

Hirsche et.al (1970) have shown that for a pipe pile in a relatively dense medium to fine sand with thin seams of clay (Arkansas test site) that for a given blow count Ru decreases as J(p) increases.

Coyle and Gibson (1970) have attempted to measure J(p) from static and dynamic tests on triaxial specimens.

However it has been found that J(p) is dependant on the velocity of deformation for both sands and clays.

Litkouhi (1979) developed a system for measuring J directly using an hydraulically controlled apparatus. The system was capable of delivering penetration velocities of between 0.03 cm/sec. up to 475 cm/sec.

Over the past fifteen years considerable extensions and refinements to Smith's original approach have been achieved and are discussed in the following section under the headings 'Limitations of the Linear Spring Soil Model' and 'Updating of the Pile/Hammer Model'.

1.5.5 Limitations of the Linear Spring Soil Model

The commonly used bi-linear model has a number of limitations, one of those being that it can not represent loading conditions at high stress levels. The soil behaves non-linearly when the ultimate capacity of the soil is approached. However, in the case of sandy sub-soils Van Koten et.al (1980) has shown that a bi-linear spring does model toe resistance satisfactorily. Holloway et.al (1978) included a hyperbolic load deformation curve in their wave equation analysis. Holloway further stated that in predicting the load-settlement behaviour a non-linear soil model performs better than the bi-linear one. Matlock and Foo (1980) pointed out that the unloading path, reloading path and subsequent hysteresis are not yet fully explained. They also pointed out the fact that in a conventional wave equation analysis the total soil resistance during driving is assumed to be constant and this assumption may be a principal cause of many drivability prediction failures. Published data by Heerima (1978) demonstrated the progressive reduction in the soil resistance as the pile was being driven. Matlock and Foo (1980) contended that due to volume changes, temporary pore pressure build-ups, near field liquafaction and subsequent re-consolidation the total resistance must be variable with time and with the history of pile displacement. They therefore included in their analysis a degrading soil model in which soil resistance is progressively lost as reversals of displacement occur during impact and rebound of the pile.

An alternative approach is to use the theory of elasticity thereby changing the discrete point model to that of an

elastic half space. The dynamic response of an Homogeneous, Isotropic elastic half space has been studied by, among others Reissner (1936), Sung (1953), Bycroft (1956), Lysmer (1965) and by Lysmer and Richart (1966). The response of an elastic half space can be approximately modelled by a linear spring with spring constant:

$$K \simeq Ed$$

E = Young Modulus of the material in the elastic half space

d = diameter of pile point

Again, however, the model is in some cases a very crude approximation of the real behaviour of soil. Important factors which are not taken into account are, for example, pore-water and pore-air pressures (Biot 1956(a), 1956(b)).

1.5.6 Updating of the Pile Model

1.5.7 Inclusion of Residual Stress

Holloway and Dover (1978) have shown that residual stresses remaining in the pile and soil at the end of a hammer blow can be included in a wave equation analysis and can be important. Holloway, Clough and Vesic (1978) further stated that "by neglecting residual driving stress in analysing pile load test results one usually (1) overestimate pile shaft capacity, (2) underestimate point capacity and (3) determine incorrectly the actual resistance distribution at failure".

They incorporated a residual stress analysis in a one dimensional wave equation analysis with proprietary name DUKFOR (Holloway et.al (1978)).

1.5.8 Improvements to the Hammer and Pile Model

Goble and Rausche (1976) have included a hammer model that takes into account the complex thermodynamic effects of diesel hammers in a computer program WEAP sponsored by the U.S. Department of Transportation.

Rempe and Davisson (1977) conducted studies on the influence of soil resistance and fuel energy on ram stroke and examined overall hammer performance by means of a wave equation analysis. They included a simulation of diesel hammer performance in a wave equation program DIESEL1. Litkouhi (1979) incorporated pile joint slackness into his analysis both for gravity and Rockwell connectors and showed a better correlation with experimental results using the modified analysis than with a normal wave equation program. Litkouhi concluded that joint slackness reduced drivability due to the loss of energy caused by closing the joints.

1.5.9 Reliability of the Wave Equation

There has been conflicting reports as to the reliability of the wave equation. Rempe (1975) showed very good bearing capacity predictions with errors less than 10% when compared with experimental. Litkouhi (1979) has also shown the same sort of aggrement as Rempe.

Ramey and Hudgins (1977) performed a statistical analysis on 21 steel and 6 concrete piles and compared the accuracy of the wave equation for predicting bearing capacity with the commonly used dynamic formulas. They found that the wave equation was consistently the most accurate both for

steel and concrete piles. Tavenas and Audibert (1976) found no correlation at all between wave equation results and field pile performance. Goble et.al (1980) suggested that "the difference in the observations is probably a result of different construction control, on the one hand, well controlled tests; on the other hand, normally supervised pile driving".

1.6 Other Analytical Methods of Note

As an extension of the wave equation approach Foo and Matlock (1977) presented a discrete algorithm that may be used either for static or dynamic prediction. To achieve this they used an implicit finite difference Crank - Nicholson type solution used to solve partial differential equations of the heat conduction types. The numerical method employed was developed as the axial counterpart of the dynamic bending model of Matlock et.al (1969), Chan et.al (1972) and Chan et.al (1973).

The latest improvement to the method was outlined in Section 1.5.5 (Matlock and Foo (1980)) in which they included a hysteretic and degrading soil model in their analysis. A variation of the original wave equation program was developed at the Case Western Reserve University and uses either the measured pile top force or integrated velocity as boundary values in either a closed form or normal wave equation analysis. The computation seeks to match measured force or velocity with theoretical by varying soil parameters. Once a best match is obtained static computations can then be used to predict the static load test curve for the pile.

The original application of the technique was attributed to Rausche (1970) and later produced the Case Pile Wave Analysis Program (CAPWAP), (Rausche et.al (1972)).

Concurrently with the CAPWAP method the CASE method was developed and again used the measured force and acceleration records from the pile top to predict static bearing capacity.

Different from both the CASE and CAPWAP methods of predicting static bearing capacity is the TNO method (Van Koten and Middendorp (1980)). Here a special hammer is used and the displacement of the pile head is measured by an electronic theodolite. The prediction of static bearing capacity is based upon the assumption of an ideal plastic behaviour of the pile. The difference between the force and the velocity before the reflected wave from the pile point reaches the pile head is attributed to skin-friction resistance.

1.7 Computer Programs

There are many programs today available to determine ultimate static bearing capacity. The more well known of which are included below. Some of the programs included have already been mentioned but are included for completeness.

	Program	Purpose
1.	CAPWAP	Used recorded force and acceleration at pile top to match theoretical and experimental.
2.	PEBWAB	Similar to CAPWAP but for point bearing piles.

	Program	Purpose
3.	WEAP	Special program for diesel hammers.
4.	DIESEL1	As WEAP.
5.	DUKFOR	Incorporates residual stress analysis.
6.	TTI	Similar to Smiths original program developed by the Texas Transportation Institute.
7.	The Raymond International Program	Similar to the TTI program.
8.	DRIVE-1	Contains a hysteretic and degrading scil model in its analysis.
9.	MASTER-WAVE	Similar to Smiths original program but incorporates routines for the inclusion of joint slackness and gravity.
10.	SWEAP	A combination of 3 and 5.

1.8 Measurement Techniques

As was stated in Section 1.5 the first attempt to make dynamic stress measurements in piling was by Glanville et.al (1938). They used piezoelectric force transducers attached to the concrete pile reinforcement and recorded the data on oscilliscope.

In the early 1960's a large research project was conducted by the Michigan Department of Highways and concerned energy transfer from hammer to pile (Housel (1966)). They used specially designed force transducers to measure force at the pile top and also added a strain gauge accelerometer in the transducer.

Rausche and Goble (1972) rationalised and explained their results which were at the time considered controversial.

Their problem with the measuring system did not however stop them from performing the primary aim of the project, i.e. the study of hammer energy delivered to the pile. The most extensive program of stress wave measurement was begun in 1964 at the Case Western Reserve University and continued until 1976.

Strain measurements were obtained by mounting electrical resistance strain gauges directly onto the pile wall which were then amplified on an A.C. amplifier and recorded on a high speed oscillograph. At this early stage in the development high impedence quartz crystal accelerometers were used to measure the motion of the pile.

Although this measuring system produced satisfactory results a much more easy to use system which could be used with any pile type was later designed and tested.

The system is shown schematically in Goble and Rausche and Likens (1980). The system consists of a pair of bolt-on strain transducers and a pair of low output impedance quartz accelerometers connected through a terminal box to a pile driving analyser that processes the signals for output onto an oscilloscope and anolog magnetic tape recorder for later analysis. This system has been used to test thousands of piles since its inception and is used throughout the world by various piling concerns under licence to Goble and Associates, Cleveland, Ohio, U.S.A.

The system has proved to be both flexible and easy to use and is considered by many to be the best field system for testing piles using dynamic measurements.

Since 1978 an intensive programme of work has been conducted at Queen Mary College, London into monitoring pile driving. To measure strain the team at Queen Mary College used strain gauged quarter bridge waterproof, fully encapsulated weldable gauges manufactured by 'Aitech' (Cuthbert et.al 1980).

Two types of accelerometers have been used, one piezoelectric (PCB) and the other piezo-resistive (strain gauge) with equal success (Cuthbert et.al (1983)). One proviso for using such accelerometers is that the natural frequency of the accelerometer should be well above those likely to be exited in the pile.

The TNO system (Van Koten and Middendorp (1980)) has been briefly described in Section 1.6 and includes besides analog signal conditioning and recording equipment a microcomputer which performs all necessary calculations. Finally, Broms and Bredenberg (1982) provided a table of companies who manufacture equipment for field applications and is reproduced below.

1. Goble and Associates.
2. Fugro.
3. TNO.
4. Piling Development KB.
5. Elf Aquataine.

1.9 Critical Appraisal of the Literature Review

It can be seen from the review of literature that research has mainly been conducted in a one soil medium, i.e. either

sand or clay. Furthermore, of the research conducted, emphasis has either been placed on load distribution through the pile or the effects of pile installation on the surrounding soil. Very few authors have studied both and even fewer have achieved this under controlled laboratory conditions. A notable exception is the work of Cooke, Price and Tarr (1979) who studied both load distribution through the pile and soil disturbance for jacked piles in London clay.

Also measurement of transient load has mainly been concerned with pile top forces and accelerations and their use in dynamic analysis such as the wave equation. Few authors have actually studied the transfer of transient load along the pile and the magnitude of the transient load at the pile tip. Bredenberg and Broms (1982) have shown that for piles resting on rock that the tip force is larger than the top force due to stress wave superposition a phenomenon that appears worthy of further research.

Over the past 20 years there has been considerable advancement in the prediction of static bearing capacity from dynamic measurements based on the wave equation with conflicting reports on its accuracy. A great deal of research is still being conducted on the topic by establishments with private funding and large resources of equipment and expertise. Because of this it was thought more practical to develop a simple analysis that although not as sophisticated as the wave equation would be used for short piles to predict static bearing capacity form dynamic measurements.

Finally, it is evident that there is a need for research projects that combine transient pile force measurements with static pile load measurements along with insitu soil measurements under controlled laboratory conditions. This also needs to be conducted in a way that simulates as far as possible what happens under field conditions, i.e. pile installation (drop hammer), and subsequent test loading in soils of more than one profile.

CHAPTER 2

RESPONSE ANALYSIS OF A PILE/SOIL SYSTEM SUBJECTED TO HAMMER IMPACT

2.1 Introduction

The assessment of the response of a pile/soil system is desirable in order to:-

1. Determine the stresses in the pile due to impact.
2. To correlate the static pile/soil parameters with dynamic parameters.
3. To determine a suitable combination of a pile/hammer system to avoid pile damage due to driving.

In this Chapter two methods of pile response developed by the author are described. The first is an approximate method where the soil elastoplastic behaviour is simulated using a linear type analysis. This may be regarded as the first step in the development of the second method which considers a more rigorous non-linear approach.

A similar type of discretisation as used by Smith (1960) in the wave equation analysis has been used but in the solutions direct matrix integration procedures are employed.

The two methods are compared with each other by using a numerical example based upon experimental work conducted at the Polytechnic on a 110 mm diameter tubular steel model pile. The shortcomings of the approximate approach are highlighted and conclusions drawn as to the validity and stability of the two methods.

2.2 Mathematical Representation of Pile

The pile/soil system is modelled in a conventional manner as a series of springs, masses and dashpots. The soil is represented rheologically as a spring with friction link (bilinear model) with a linear viscous damper included to represent the rate dependant part of the motion and also to simulate energy radiated from the pile.

A typical representation is shown in Fig. 2.1.

2.2.1 Dynamic Equation of Motion

As can be seen from Fig. 2.1 the pile is split into N elements with N+1 nodes. Each node is represented by a generalised differential relationship of the form:-

$$Ki(x(i-1)-xi)-K(i+1)(xi-x(i+1))+Ci(\dot{x}(i-1)-\dot{x}i)$$
$$-C(i+1)(\dot{x}i-\dot{x}(i+1)) = Mi\ddot{x}i \quad \text{-2.1 (appendix 2.1)}$$

Only axial changes are considered so that stiffness and lumped mass element matrices are of the form:-

$$\left[Kp\right]_i = \begin{bmatrix} \frac{EA}{L} & -\frac{EA}{L} \\ -\frac{EA}{L} & \frac{EA}{L} \end{bmatrix}_i$$

$$\left[Mp\right]_i = \begin{bmatrix} \frac{\rho AL}{2} & 0 \\ 0 & \frac{\rho AL}{2} \end{bmatrix}_i$$

Where Kp_i = elemental pile stiffness matrix

and Mp_i = elemental pile mass matrix.

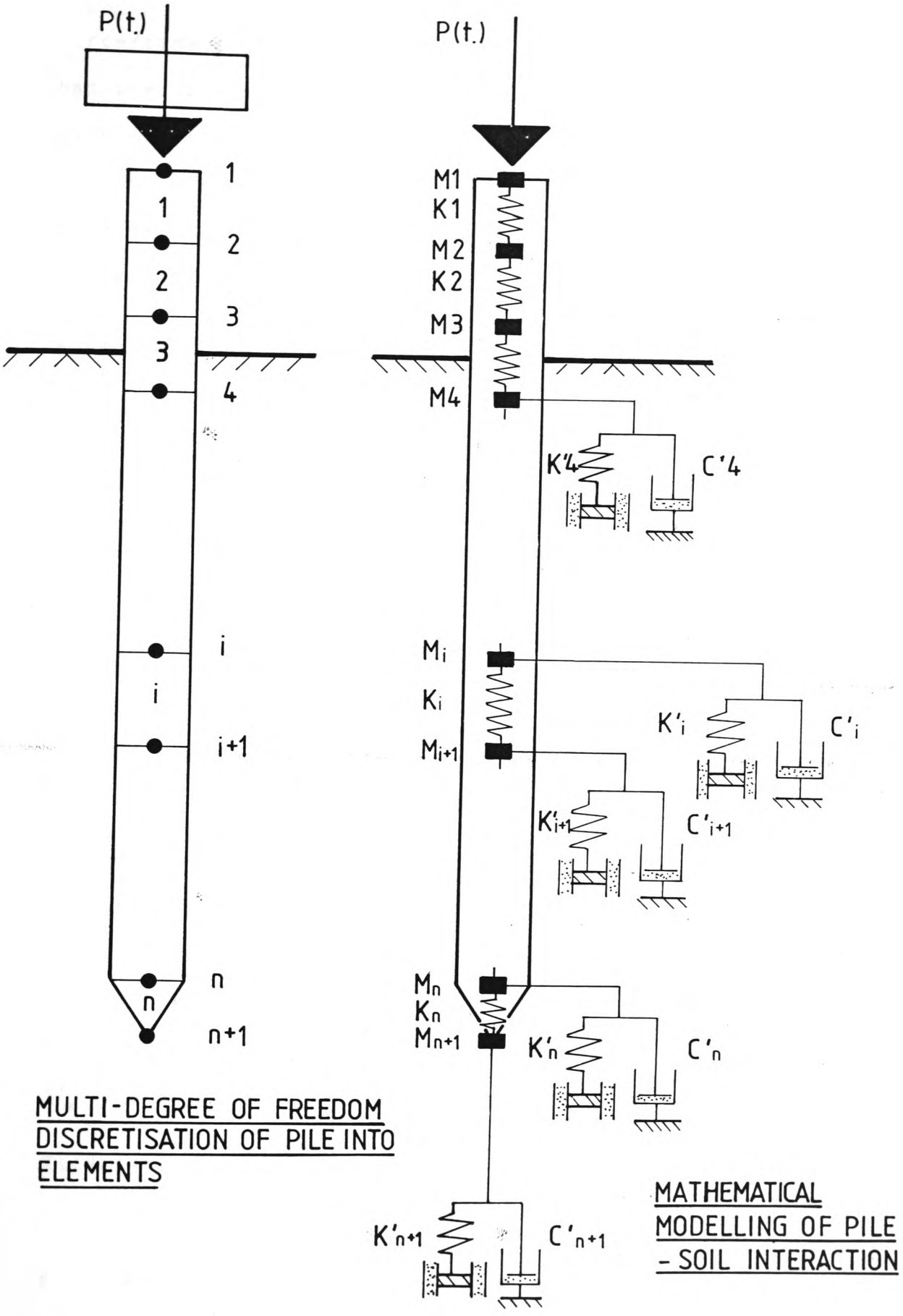

FIG. N° 2.1. PHASE 1 IDEALISATION OF PILE-SOIL SYSTEM

The force vector P(t) is obtained from the measured force/time history due to the hammer impact. This method has the advantage of eliminating any problems associated with modelling of the driving system. The main disadvantage is that energy transfer consideration between the hammer and pile may not be considered. However as this is not a primary target of the analysis this is not a major drawback.

A typical force vector is represented as:-

$$\begin{Bmatrix} P_{(t)} \\ 0 \\ 0 \\ 0 \\ 0 \end{Bmatrix} \begin{matrix} i=1 \\ \\ \\ \\ i=n+1 \end{matrix}$$

Where P(t) represents the dynamic force on the pile top at time t(sec.).

2.2.2 Soil Stiffness

Estimation of soil stiffness is the method used in the wave equation technique (Smith 1960) where an estimated static bearing capacity is assumed for the pile and is then distributed to each embedded node according to any specified relationship. Thus for any node other than the pile point the differential equation of motion for the ith node becomes:-

$$Ki(\ddot{x}(i-1)-xi)-K(i+1)(x_i-x(i-1))+Ci(\dot{x}(i-1)-\dot{x}i)-C(i+1)(\dot{x}i-\dot{x}(i+1))$$
$$+K'ixi = Mi\ddot{x}i \text{ (appendix 2.1)} - (2.2)$$

Where $K'i$ = Soil stiffness for node i = ri/x.i

and ri = Portion of static bearing capacity assigned to node i

and $X_o i$ = Maximum elastic displacement of soil associated with node i (Fig. 2.2).

The maximum elastic displacement is the soil displacement considered to be fully recoverable on cessation of driving.

2.2.3 Soil Mass

As the pile and soil are considered to interact with each other it seemed logical to include soil mass in the differential equations of motion.

However Whitman and Richart (1967) in their work on vibration of machine foundations stated that the use of an effective soil mass is justified only to the extent that an increased mass is needed to fit theoretical and experimental results more closely. They contended that an effective soil mass is purely fictitious, and hence no soil mass is included in the analysis.

2.2.4 Damping Coefficient

The amount of damping in the pile/soil system is calculated from experimental results using logarithmic decrement. This is a standard method of determining system damping experimentally assuming viscous damping.

The basic concept and equations are as follows:-

Taking the experimental acceleration/time curve and denoting by t_1 and t_2 the times corresponding to two consecutive displacements x_1 and x_2 measured one cycle apart it can be

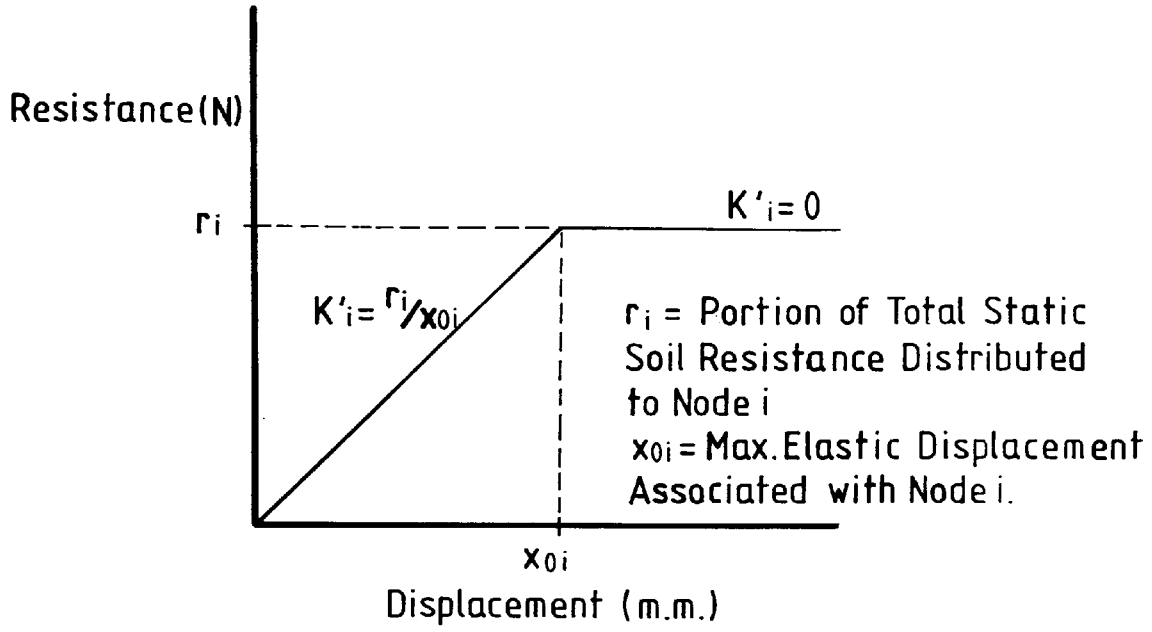

REPRESENTATION OF SOIL STIFFNESS FOR THE ith NODE

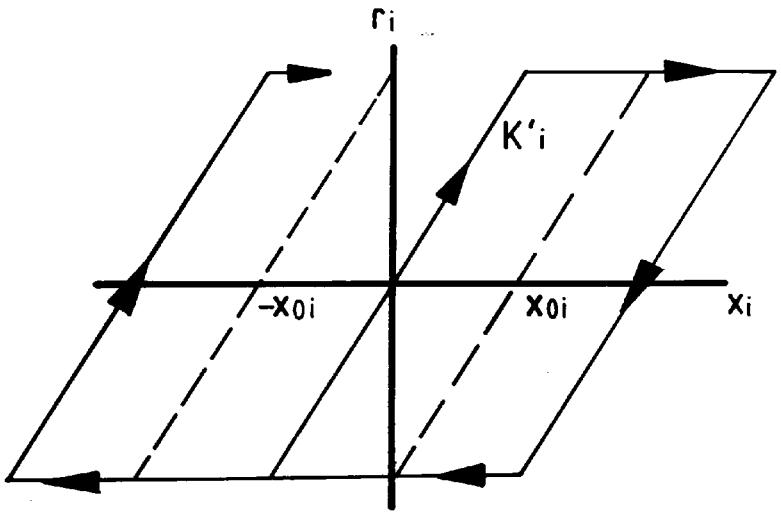

BILINEAR ELASTO-PLASTIC SOIL BEHAVIOUR FOR THE ith NODE (Indicating Full Loading and Reverse Loading Cycle).

FIG. N° 2.2 IDEALISATION OF SOIL BEHAVIOUR

shown that $\frac{x_1}{x_2} = \frac{e^{-\xi\omega n t 1}}{e^{-\xi\omega n(t1+\tau)}} = e^{\xi\omega n\tau}$

Where $T = \frac{2\pi}{\omega D}$ i.e. the period of damped oscillation.

Due to the exponential form of the above equation it is customary to introduce the notation:

$$\delta = \ln \frac{x_1}{x_2} = \xi\omega nT = \frac{2\pi\xi}{\sqrt{1-\xi^2}}$$

Where ωn = natural frequency (rad/s)

ωD = damped frequency (rad/s)

δ = logarithmic decrement

ξ = viscous damping ratio

Therefore to obtain the amount of damping in the pile/soil system any two consecutive displacements x_1 and x_2 are measured (usually the first and second peak values) and δ determined from $\delta = \ln \frac{x_1}{x_2}$. The viscous damping ratio ξ may be obtained from $\xi = \frac{\delta}{\sqrt{(2\pi)^2 - \delta^2}}$

For small values of δ this may be approximated to $\xi = \frac{\delta}{2\pi}$

Because the solution procedure is a step by step direct integration procedure, an actual damping coefficient for each node must be calculated. This is achieved using the relationship:

$$\xi = \frac{C}{C_C}$$

Where C_C is critical damping.

Thus $C = \xi 2m\omega n$

If ξ is high ωn may be calculated from $\omega = \frac{\omega D}{\sqrt{1-\xi^2}}$

otherwise $\omega \approx \omega D$.

The value of C so calculated is the total damping coefficient for the pile/soil system, how much damping is due to the pile and how much is due to the soil is not clear. It would not be practical to determine the different amounts of pile and soil damping for each individual case and so arbitary values to give a best fit will be taken.

Thus the damping coefficient for node i will be split between soil and pile according to the relationship:

$$\alpha Cixi+\beta Ci(\dot{x}(i-1)-\dot{x}i)$$

where $\alpha+\beta = 1$ and are empirical constants.

Obviously damping in the pile/soil system is much more complex and may consist of various different forms of damping such as hysteretic, coulomb, etc., however, for the present analysis damping is taken as linear viscous only.

2.2.5 Complete Differential Equations of Motion

The complete differential equation of motion for the ith embedded node therefore becomes:-

$$Ki(x(i-1)-xi)-K(i+1)(xi-x(i+1))-K'ixi-\alpha Ci\dot{x}i+$$
$$\beta(Ci(\dot{x}(i-1)-\dot{x}i)-C(i+1)(\dot{x}i-\dot{x}(i+1))) = Mi\ddot{x}i \quad - \quad 2.3.$$

The only non-linear term in the equation is that of soil stiffness which varies according to pile displacement.

2.3 Approximate Solution - Two Phase System

Once the dynamic equations of equilibrium have been set up in a matrix form (Appendix 2.1), the coupled equations are intergrated directly. There are many standard solution algorithms available to accomplish this task; the two used by the author are the Newmark and Wilson θ - methods. Appendix 2.2 gives a brief derivation of the two methods.

If the standard algorithms are used the solution is entirely linear, something that a pile/soil system is evidently not.

The approximate solution is a somewhat contrived method of achieving some amount of non-linearity while still using a linear algorithm and may be regarded as an initial step in developing the more rigorous system.

The approximate approach attempts to separate the elastic and rigid body contributions of pile/soil response into individual phases. Scanlan and Tomko (1969) have shown that in the case of short piles the elastic contribution contains almost all the oscilliatory part of the pile motion and is relatively unimportant in predicting pile response. The rigid body contribution however is one of almost a straight line decreasing velocity, suggesting the action of a rigid body under constant deceleration from constant soil resistance and is the major contributing factor to pile response.

The different phases of the analysis are outlined below:-

1. Phase one is represented by a lumped mass, multi degree of freedom system - representing the elastic compression of the pile. (Fig. 2.1).

2. Phase two is represented by a continuously penetrating rigid pile subject to constant soil resistance (Fig. 2.3) with governing equation:

M = total mass of pile

$\ddot{x}$ = rigid body pile acceleration

$M\ddot{x}=P(t)-R$ $\quad P(t)$ = external load at time t

$$R = \sum_{C=n+1}^{C=1} ri \quad \text{[for embedded nodes]}$$

- 2.4

3. When the acceleration first reaches zero the multi degree of freedom system is re-entered with the following initial conditions prevailing:

$$\left\{\ddot{x}\right\}_{i=n+1}^{i=1} = \ddot{x}o, \quad \left\{\dot{x}\right\}_{i=n+1}^{i=1} = \dot{x}, \quad \left\{x\right\}_{i=n+1}^{i=1} = o$$

This has two effects on the overall matrix solution.

a) It helps to prevent numerical instability due to the change of phase.

b) Redefines the displacement zero axis about a new spatial position.

2.3.1 Algorithm - Approximate Solution

The important steps in the algorithm are as follows:-

1. The pile stiffness, mass and damping matrices are set up from pile material properties and assumed damping relationships.

2. The estimated static bearing capacity is distributed to each pile node in a triangular form beginning with zero at the surface. The soil stiffnesses are formed as described in Section 2.2.2.

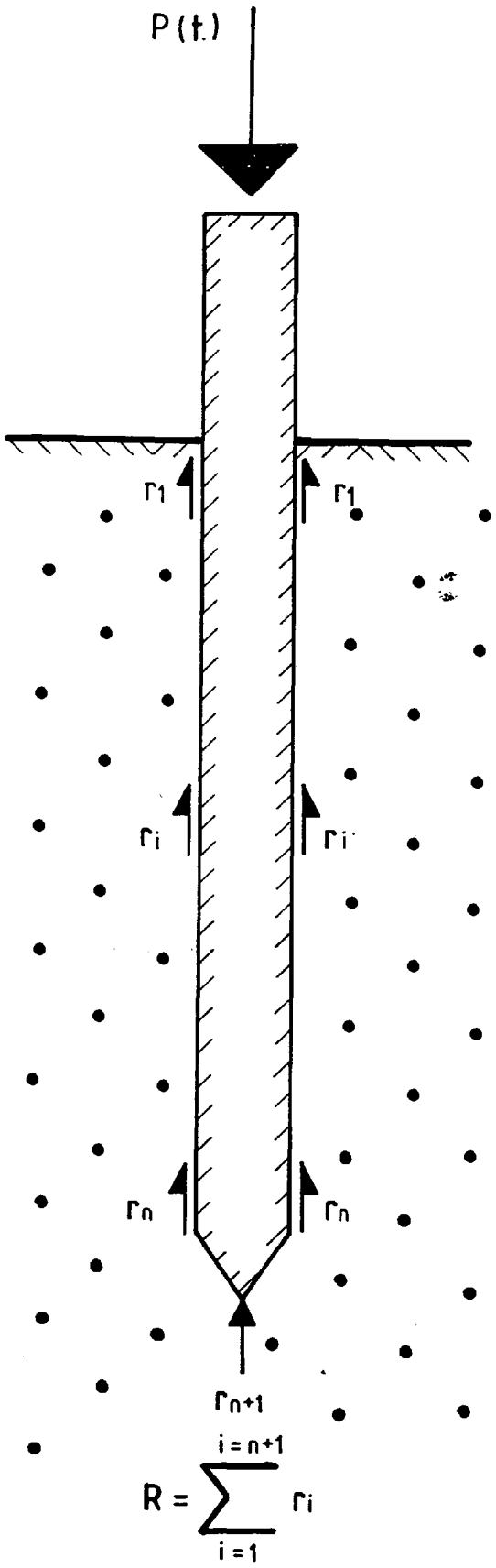

CONTINUOUSLY PENETRATING RIGID PILE

FIG. N° 2.3 PHASE 2 IDEALISATION OF PILE SOIL SYSTEM

3. These are then combined with the pile stiffness matrix as shown in the preceding sections and an equivalent stiffness matrix is set up as shown in Appendix 2.1 and 2.2.

4. A Newmark iterative procedure is then used to solve for nodal displacements, velocities and accelerations due to the measured input force/time history.

5. This process is repeated for consecutive time increments until any nodal displacements exceeds the maximum elastic displacement for that node at which time the soil stiffness is set to zero. This is equivalent to following the first section of the bilinear model (Fig. 2.2). The normal Newmark iterative scheme has no provision for allowing for a non-linear stiffness force/displacement relationship. In an effort to compensate for this the soil resistance is then introduced into the external load vector so that for the ith node the load term becomes - ri. Thus equation 2.3 becomes:

$$Ki(x(i-1)-xi)-K(i+1)(xi-x(i+1))+Ci(\dot{x}(i-1)-\dot{x}i) -C(i+1)(\dot{x}i-\dot{x}(i+1))-ri = Mi\ddot{x}i \quad - \quad 2.5.$$

6. This process continues until all maximum elastic soil displacements are exceeded. At this time the rigid body motion is taken to be the most prominent part of the response and phase two is entered as discussed in section 2.3. The change of phase may in some circumstances cause discontinuity between phases in the acceleration/time graph and will be discussed later.

7. The iterative process continues until the acceleration first becomes zero at which time the multi degree of freedom system is re-entered again as discussed in section 2.3.

8. The iterative process then continues until a user specified limit is reached.

Apart from the variations outlined in this section, the overall approach is the same as given in Appendix 2.2.

2.4 Non-Linear Solution - Single Phase System

The non-linear method is based on sound mathematical principles and uses none of the assumptions used in the approximate solution. The basic pile/soil model is again the lumped mass system. Any form of soil non-linearity may be included; however, for the purpose of comparison the bilinear model is used. An incremental form of the Wilson-θ method is used which calculated increments of $\ddot{x}$, $\dot{x}$, and x for each time step as opposed to the total values calculated using the algorithm given in appendix 2.2.

As demonstrated in appendix 2.1 the equilibrium of forces acting on any mass M gives:

$$FD_{(t)} + FS_{(t)} + FI_{(t)} = P(t) \quad - \quad 2.6$$

rewriting 2.6 to represent a pile/soil system gives:

$$FDS_{(t)} + FD_{(t)} + FSS_{(t)} + FS_{(t)} + FI_{(t)} = P(t) \quad - \quad 2.7$$

Where FSS = soil stiffness force

FDS = soil damping force.

An incremental time later equation 2.7 will change to:-

$$FDS_{(t+\Delta t)} + FD_{(t+\Delta t)} + FSS_{(t+\Delta t)} + FS_{(t+\Delta t)} + FI_{(t+\Delta t)} = P(t+\Delta t) \quad - \quad 2.8$$

Subtracting 2.7 from 2.8 leads to the incremental equation of equilibrium for time t:

$$\Delta FDS_{(t)} + \Delta FD_{(t)} + FSS_{(t)} + \Delta FS_{(t)} + \Delta FI_{(t)} = \Delta P(t) \quad - \quad 2.9$$

The force increments can be expressed as:

$$\left.\begin{aligned}
\Delta FDS_{(t)} &= FDS_{(t+\Delta t)} - FDS_{(t)} = \alpha C \Delta \dot{x}_{(t)} \\
\Delta FD_{(t)} &= FD_{(t+\Delta t)} - FD_{(t)} = \beta C \Delta \dot{x}_{(t)} \\
\Delta FSS_{(t)} &= FSS_{(t+\Delta t)} - FSS_{(t)} = K'_{(t)} \Delta x_{(t)} \\
\Delta FS_{(t)} &= FS_{(t+\Delta t)} - FS_{(t)} = K \Delta x_{(t)} \\
\Delta FI_{t)} &= FI_{(t+\Delta t)} - FI_{(t)} = M \Delta \ddot{x}_{(t)} \\
\Delta P_{(t)} &= P(t+\Delta t) - P(t)
\end{aligned}\right\} \quad - \quad 2.10$$

Where C is the total incremental damping matrix consisting of elements $\alpha C_{ij} + \beta C_{ij}$ and α and β are as defined in section 2.2.4.

The elements of the total incremental stiffness matrix K are influence coefficients $K'_{ij}(t) + K_{ij}(t)$ defined for the time increment.

As can be seen from equation 2.10 the only non-linear term is the soil stiffness $K'_{(t)}$. In order to avoid iterations at each step of the solution a tangent slope is used for the influence coefficient $K'_{ij}(t)$ defined at the beginning of the time increment. Hence the influence coefficient is given by:-

$$K'_{ij}(t) = \frac{dFSSi}{dx_j}_{(t)} \quad - \quad 2.11$$

Substituting equation 2.7 into equation 2.8 gives the incremental equations of motion:-

$$M\Delta\ddot{x}_{(t)} + C\Delta\dot{x}_{(t)} + K\Delta x_{(t)} = \Delta P_{(t)} \quad - \quad 2.12$$

Where $K = K + K'_{(t)}$

The solution procedure for this set of incremental equations follows closely the Wilson-θ algorithm given in appendix 2.2 but again written in incremental form.

Writing the equations for velocity and displacement for the extended time step in an incremental form gives:-

$$\Delta\dot{x}_{(t+\theta\Delta t)} = \theta\Delta t\ddot{x}_{(t)} + \frac{\theta\Delta t}{2}\Delta\ddot{x}_{(t+\theta\Delta t)} \quad - \quad 2.13$$

$$\Delta x_{(t+\theta\Delta t)} = \theta\Delta t\dot{x}_{(t)} + \frac{(\theta\Delta T)^2}{2}\ddot{x}_{(t)} + \frac{(\theta\Delta t)^2}{6}\Delta\ddot{x}_{(t+\theta\Delta t)} \quad - \quad 2.14$$

Solving these equations to express $\Delta\ddot{x}_{(t+\theta\Delta t)}$ and $\Delta\dot{x}_{(t+\theta\Delta t)}$ in terms of $\Delta x_{(t+\theta\Delta t)}$ and substituting into equation 2.12 (written for the extended time step) leads to:

$$K_{(t)}\Delta x_{(t+\theta\Delta t)} = \Delta P_{(t+\theta\Delta t)} \quad - \quad 2.15$$

$$\text{Where } K_{(t)} = K_{(t)} + \frac{6}{(\theta\Delta t)^2}M + \frac{3}{\theta\Delta t}C_{(t)} \quad - \quad 2.16$$

$$\text{and } \Delta P_{(t+\theta\Delta t)} = \Delta P_{(t)} + M\left[\frac{6}{\theta\Delta t}\dot{x}_{(t)} + 3\ddot{x}_{(t)}\right] C_{(t)}\left[3\dot{x}_{(t)} + \frac{\theta\Delta t}{2}\ddot{x}_{(t)}\right] \quad - \quad 2.17$$

Solving 2.15 for $\Delta x_{(t+\theta\Delta t)}$ and substituting into the following equation yields the increment of acceleration for the extended time step, i.e.

$$\Delta\ddot{x}_{(t+\theta\Delta t)} = \frac{6}{(\theta\Delta t)^2}\Delta x_{(t+\theta\Delta t)} - \frac{6}{\theta\Delta t}\dot{x}_{(t)} - 3\ddot{x}_{(t)} \quad - \quad 2.18$$

This equation is again identical to that given in appendix 2.2 but written in incremental form.

Dividing equation 2.18 by Θ yields the acceleration increment for the normal time step.

$$\Delta\ddot{x}_{(t)} = \frac{1}{\Theta}\Delta\ddot{x}_{(t+\Theta\Delta t)} \qquad - \quad 2.19$$

The displacement and velocity vectors at the end of the time step are then given by $x_{(t+\Delta t)} = x_{(t)} + \Delta x_{(t)}$,

$$\dot{x}_{(t+\Delta t)} = \dot{x}_{(t)} + \Delta\dot{x}_{(t)} \qquad - \quad 2.20$$

Because of the use of the initial tangent value for soil stiffness (equation 2.11) the left-hand side of equation 2.12 is only approximate. Therefore errors will tend to arise in the incremental equations of motion from time step to time step due to the assumption that soil stiffness properties remain constant over the whole time increment. To avoid the obvious accumulation of errors due to this factor a simple method proposed by Clough and Penzien is adopted.

A condition of total equilibrium is imposed at each step of the analysis. This is easily accomplished by expressing the acceleration at the beginning of the time step in terms of the total external load minus the total damping and stiffness forces, i.e.

$$\ddot{x}_{(t)} = \frac{1}{M}\left[P_{(t)} - FDS_{(t)} - FS_{(t)} - FSS_{(t)} - FD_{(t)}\right] \qquad - \quad 2.21$$

and is merely a rearrangement of equation 2.12.

2.4.1 Non-Linear Solution - Algorithm

It is convenient to use the format of the algorithm given in Appendix 2.2 as the setting up of soil stiffness, use of the measured input force, time history, etc., has been discussed in previous sections.

2.4.2 Initial Conditions

1.0 Initialise x_o, $\dot{x}_o$, $\ddot{x}_o$

2.0 Assume a static bearing capacity and set up soil stiffness as previously discussed.

3.0 Select time step (Δt) and calculate integration constants.

For each time increment

1. Form effective stiffness matrix

$$K = K + A_0 M + A_1 C$$

Where $K = K + K'$ and $C = C + C'$

2. **Triangularise** $K : K = LDL^T$

3. Calculate effective load increment at time $(t+\Theta\Delta t)$

$$\Delta P_{(t+\Theta\Delta t)} = \Delta P_{(t+\Theta\Delta t)} + M\left[\frac{6}{\Theta\Delta t}\dot{x}_{(t)} + 3\ddot{x}_{(t)}\right] + C_{(t)}\left[3\dot{x}_{(t)} + \frac{\Theta\Delta t\ddot{x}}{2}(t)\right]$$

4. Solve for increments of displacements at time $(t+\Theta\Delta t)$

$$LDL^T\Delta x_{(t+\Theta\Delta t)} = \Delta P_{(t+\Theta\Delta t)}$$

5. Calculate the increment of acceleration and velocity for the normal time step

$$\Delta\ddot{x}_{(t)} = \frac{1}{\Theta}\left[\frac{6}{(\Theta\Delta t)^2}\Delta x_{(t+\Theta\Delta t)} - \frac{6}{\Theta\Delta t}\dot{x}_{(t)} - 3\ddot{x}_{(t)}\right]$$

7. $$\Delta\dot{x}_{(t)} = \frac{3}{\Delta t}\Delta x_{(t)} - 3\dot{x}_{(t)} - \frac{\Delta t\ddot{x}}{2}(t)$$

8. Calculate displacement and velocity vectors at the end of the increment by

$$x_{(t+\Delta t)} = x_{(t)} + \Delta x_{(t)} \quad : \quad \dot{x}_{(t+\Delta t)} = \dot{x}_{(t)} + \Delta\dot{x}_{(t)}$$

9. Calculate the acceleration vector at the end of the increment using

$$\ddot{x}_{(t+\Delta t)} = \frac{1}{M}\left[P_{(t+\Delta t)} - FD_{(t+\Delta t)} - FDS_{(t+\Delta t)} - FS_{(t+\Delta t)} - FSS_{(t+\Delta t)}\right]$$

10. Repeat from step 1.

The algorithm presented is a reiteration of section 2.4 but written in an abridged form for the purpose of clarity.

2.5 Parametric Study of the Two Methods

In the following sections the two methods are compared with each other using a numerical example based on research conducted at the Polytechnic on a 110 mm diameter tubular steel pile. The following input data was used to model the pile:-

1. Number of elements = 11
2. Time increment in seconds = 0.4×10^{-4}
3. Embedded length of pile in metres = 2.125
4. C/S area of pile in sq.m. = $0.7846 \times 6 \times 10^{-3}$
5. No. of pile elements = 10
6. Length of pile element in metres = 0.25
7. Density of pile material (steel) in Kg/cu.m = 7860.0
8. Modulus of elasticity of pile material in N/Sq.m = 0.21×10^{12}
9. Percentage of load on pile tip = 0.733
10. Assumed ultimate load on pile = Various
11. Duration of imput force in seconds = 0.5×10^{-2}
12. Time in seconds to peak value of input force = 0.1×10^{-2}

13. Peak value of input force in N = 0.56×10^5

14. First peak acceleration in m/sec.sec = 0.69449×10^4

15. Second peak acceleration in m/sec.sec = 0.17445×10^4

16. Soil damping coefficient (α) = Various

    Pile damping coefficient (β) = Various

17. Damped frequency in rad/sec = 0.107237×10^5

18. Logarithmic decrement = 1.3815

    Total damping coefficient = 0.2198

While the example is a numerical one, items 14-18 are actual experimental results obtained from small scale tests. The only items that are not experimental values are 11 to 13, however, these are order of magnitude values calculated from the small scale tests described in the next chapter.

2.5.1 Sensitivity of the Two Methods to Various Combinations of Pile and Soil Damping

In this section the effect on the average displacement/time graph of varying the values of α and β is studied.

The displacement/time graph is used as the illustration because of the evenness of the trace, which makes any difference arising from varying the damping parameters readily discernable. Because of the formulation used in the approximate method it is not possible to distinguish between pile and soil stiffness forces and hence only values of $\alpha = 1$, $\beta = 0$ or $\beta = 1$, $\alpha = 0$ are acceptable. In the rigorous method various combinations of α and β are used and are shown in Fig. 2.4 along with the trace for $\alpha = 1$, $\beta = 0$ for for the approximate method.

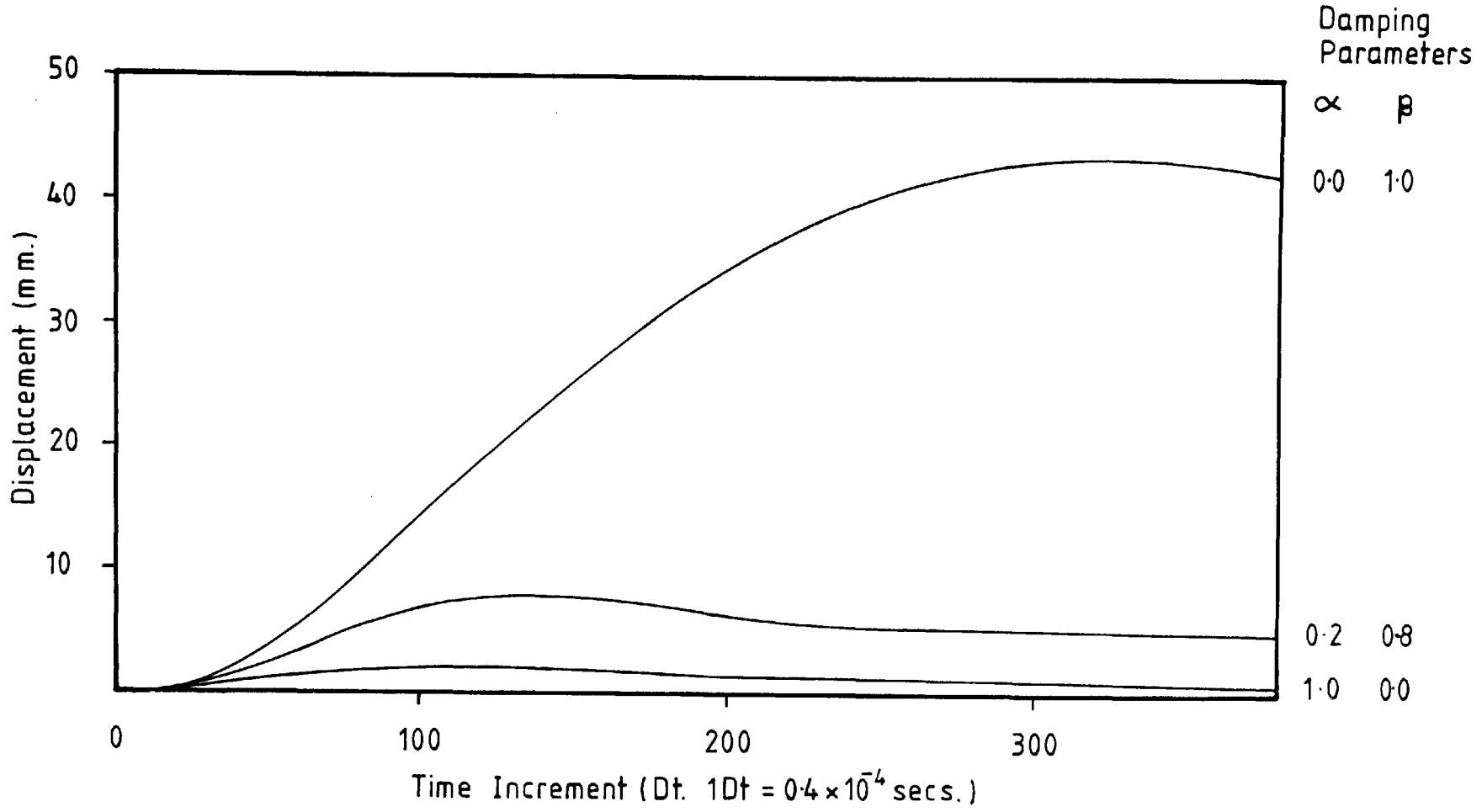

FIG. Nº 2.4 SHOWING THE VARIATION OF DISPLACEMENT / TIME RESPONSE FOR DIFFERENT VALUES OF PILE AND SOIL DAMPING

Figure 2.4 highlights two important facts:-

1. That the two methods where comparable ($\alpha = 1$, $\beta = 0$) bear close resemblance to one another up to the maximum value of displacement. The two methods from then on gradually diverge showing the effects of the various assumptions used in the approximate method on the overall solution.

2. In the case of the rigorous method it becomes evident that the soil damping constant α is the most important parameter when determining pile response, the pile damping constant β being only a trimming parameter. The reason for this can be easily explained by recourse to the way soil and pile stiffness forces are calculated. The pile stiffness force for the ith node is given by $\beta Ci(\dot{x}i-\dot{x}_{i+1})$. The soil stiffness force for the ith node however is given by $\alpha Ci(\dot{x}i)$. Obviously the numerical value of soil damping is very much greater than the numerical value of pile damping and hence has a greater effect on the differential equations of motion.

Because of the inflexibility of the approximate method with regard to damping allied with the effect the various assumptions have on the overall solution the rigorous method will be concentrated on in the following sections.

2.5.2 Sensitivity of the Rigorous Solution to Varying Bearing Capacities

Using the numerical example outlined in section 2.5 with soil and pile damping values of $\alpha = 0.2$, $\beta = 0.8$ the sensitivity of the method to various bearing capacities is examined.

Figure 2.5 shows a nest of displacement/time curves using the same pile model and input data but varying the assumed ultimate static bearing capacity from one to one hundred kN.

Experimental work conducted at the Polytechnic using the same diameter and length of pile used in the numerical example yeilded a bearing capacity of around 10 kN.

This value was taken as the actual static bearing capacity and used to obtain an idea as to the sensitivity of the method to assumed bearing capacity changes.

Obviously as the bearing capacity increases the change in displacement response will decrease as refusal becomes imminent. This makes an actual comparison of percentage changes in peak displacement against percentage changes in ultimate static bearing capacity impractical. However, Figure 2.5 does show considerable and significant changes in displacement/time response for the inputed values of static bearing capacity showing that the approach is fairly sensitive to such changes.

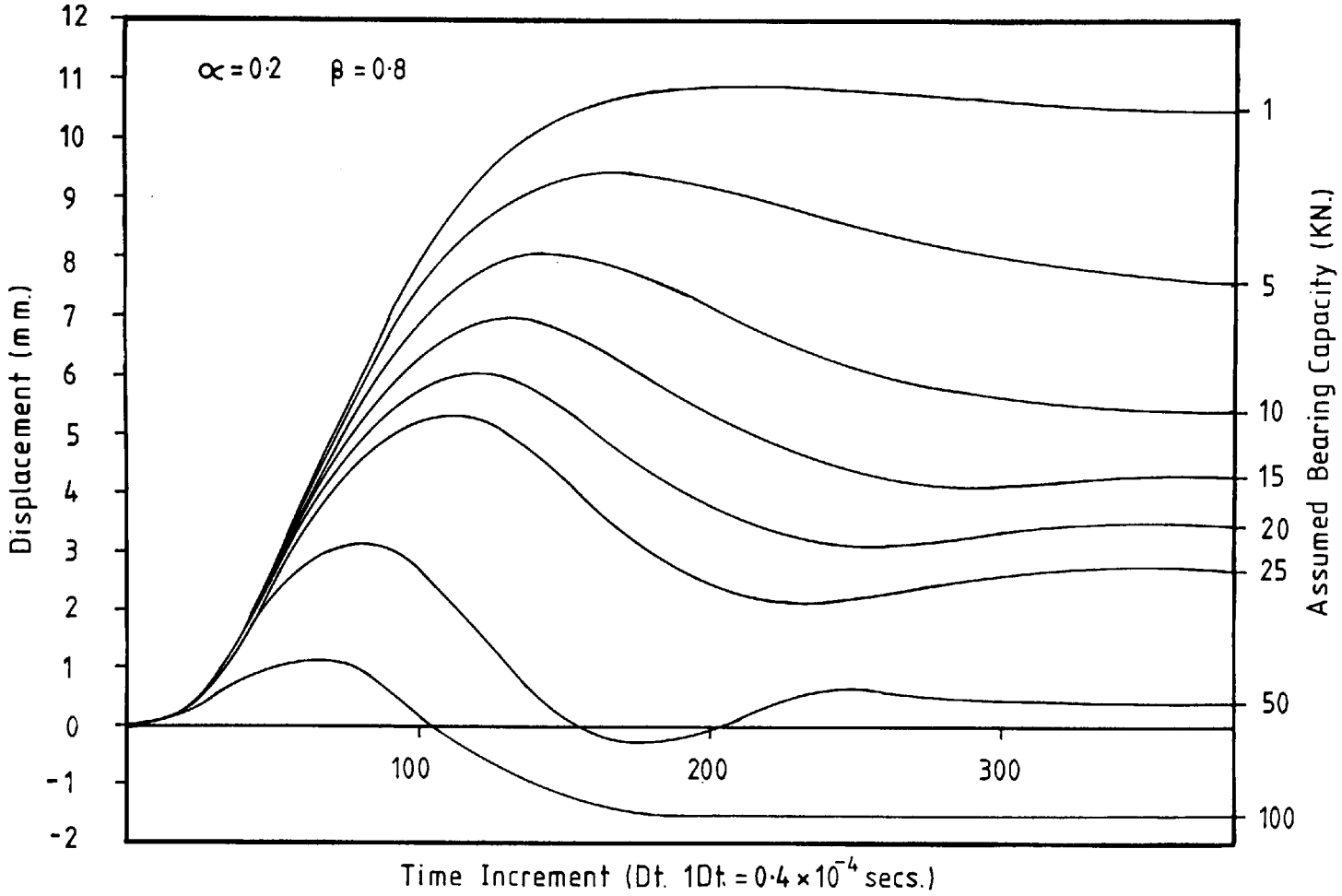

FIG. Nº 2.5 SHOWING THE VARIATION IN DISPLACEMENT/ TIME RESPONSE FOR DIFFERENT ASSUMED BEARING CAPACITYS

2.6 Conclusions as to the Reliability and Stability of the Two Methods

Reliability of the Two Methods

Based on the numerical example used it would appear that:-

(a) The approximate method, due to its obvious limitations with respect to damping and the assumed phase changes involved, is of very limited use only.

(b) The rigorous method although still only using a rough approximation of soil stiffness and force/displacement behaviour is versatile enough and sensitive enough to cope with various values of damping.

Stability

If the displacement/time curve for the approximate solution is compared with the rigorous one it would appear that the method is stable upto the peak displacement with instability gradually appearing from then on. However, instability in the acceleration/time graph may occur at an earlier stage when a change of phase occurs. The governing equation of the second phase reiterated is:-

$$M\ddot{x} = P(t)-R$$

Thus the sign of the acceleration depends only on the magnitude of P(t) and R and is in no way related to the sign of acceleration of the initial phase. This discontinuity may occur between phases which are not evident on the displacement/time curve.

APPENDIX 2.1

DIFFERENTIAL EQUATIONS OF MOTION AND THEIR MATRIX FORMATION

The work described in this appendix is standard mathematics and included in many vibrational analysis textbooks. It is included in the present work as a help to the reader who may not be readily acquainted with the formulations.

2.1.1 Equation of Motion

Consider the single degree of freedom system in Fig. 2.1.1(a), 2.1.1(b).

Figure 2.1.1(a) shows the basic dynamic system with the lumped mass M constrained to move in one plane only. The elastic resistance to motion is provided by the weightless spring K, while the energy loss component is provided by the damper C. An external time varying load P(t) is applied to produce the dynamic response.

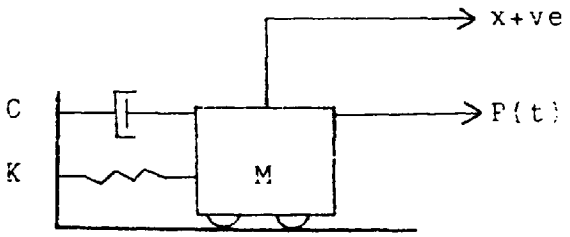

(a)

Fig. 2.1.1

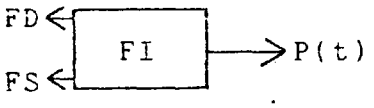

(b)

Considering the equilibrium of forces acting on the mass M gives

$$FD + FS + FI = P(t)$$

Where FD = damping force

FS = stiffness force

FI = inertial force

The elastic force is given by the product of K x x

i.e. $FS = Kx$

D'Alembert's principle states that $FI = M\ddot{x}$

If the damping force is considered to be viscous then

$$FD = C\dot{x}$$

Thus the equation becomes:-

$$M\ddot{x}+C\dot{x}+Kx = P(t)$$

Figure 2.1.2(a) shows a 3 degree of freedom lumped mass system with external resistance and damping denoted by K and C and acted on by an external force P(t).

Figure 2.1.2(b) shows the Freebody diagram for this system. Displacements of mass M1, M2 and M3 are denoted by x1, x2 and x3 with similar nomenclature applying for spring stiffness and damping.

Applying Newtons 2nd law to each mass in turn leads to the following equations of equilibrium.

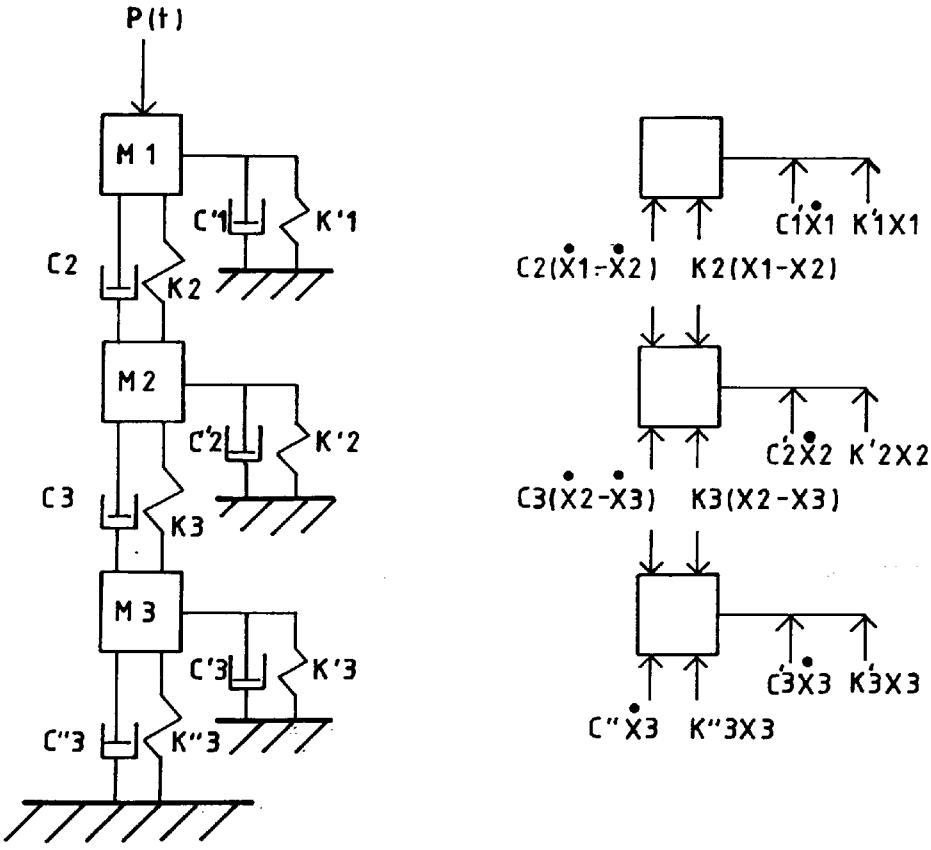

(a) Lumped Mass System (b) Freebody Diagram

FIG. Nº 2.1.2 3 D.O.F. LUMPED MASS SYSTEM

$$P(t)-K2(x1-x2)-C2(\dot{x}1-\dot{x}2)-C'1\dot{x}1-K'1x1 = M1\ddot{x}1 \quad - \quad 1$$

$$K2(x1-x2)-K3(x2-x3)-K'2x2-C2\dot{x}2$$
$$+C2(\dot{x}1-\dot{x}2)-C3(\dot{x}2-\dot{x}3) = M2\ddot{x}2 \quad - \quad 2$$

$$K3(x2-x3)+C3(\dot{x}2-\dot{x}3)-K''3x3-C''3\dot{x}3-C'3\dot{x}3-K'3x3 = M3\ddot{x}3 \quad - \quad 3$$

Rearranging and grouping terms gives

$$M1\ddot{x}1+(K2+K'1)x1+(C2+C'1)\dot{x}1-K2x2-C2\dot{x}2 = P(t)$$

$$M2\ddot{x}2+(K3+K2+K'2)x2+(C3+C2+C'2)\dot{x}2-K2x1-K3x3-C2\dot{x}1-C3\dot{x}3 = 0$$

$$M3\ddot{x}3+(K3+K''3+K'3)x3+(C3+C''3+C'3)\dot{x}3-K3x2-C3x2 = 0$$

Arranging the equation in matrix form gives

$$[M] = \begin{bmatrix} M1 & 0 & \\ 0 & M2 & 0 \\ 0 & & M3 \end{bmatrix} \quad [K] = \begin{bmatrix} (K2+K'1) & -K2 & 0 \\ -K2 & (K3+K2+K'2) & -K3 \\ 0 & -K3 & (K3+K''3+K'3) \end{bmatrix}$$

$$[C] = \begin{bmatrix} (C2+C'2) & -C2 & 0 \\ -C2 & (C3+C2+C'2) & -C3 \\ 0 & -C3 & (C3+C''3+C'3) \end{bmatrix} \quad \text{and} \quad \{P\} = \begin{Bmatrix} P \\ 0 \\ 0 \end{Bmatrix}$$

In general therefore the equation for the ith node of a multi degree of freedom system containing N nodes will be

$$Ki(x(i-1)-xi)-K(i+1)(xi-x(i+1))-K'ixi-Cixi$$
$$+Ci(\dot{x}(i-1)-\dot{x}i)-C(i+1)(\dot{x}i-\dot{x}(i+1)) = Mi\ddot{x}i$$

The solution of these equations and the way non linearity is introduced into the spring stiffness K is described in detail in both Chapter 2 and the subsequent appendicies.

APPENDIX 2.2

Numerical Techniques

The Newmark and Wilson θ direct integration techniques are standard solution routines well documented and therefore not included in the main text. The brief explanation of the procedures together with simple algorithms are included in the appendix for the perusal of the reader and are the same as those given in Bathe and Wilson with only the nomenclature changed to be consistent with the main text.

Wilson - θ Method

The Wilson θ method is an extension of the linear acceleration method in which a linear variation of acceleration is assumed from a time t to t+Δt. The Wilson - θ method assumes that the acceleration varies linearly for an extended time step i.e. (t-t+θΔt) where for unconditional stability $\theta > 1.37$ (usually 1.4).

Thus referring to Fig. 2.2.1

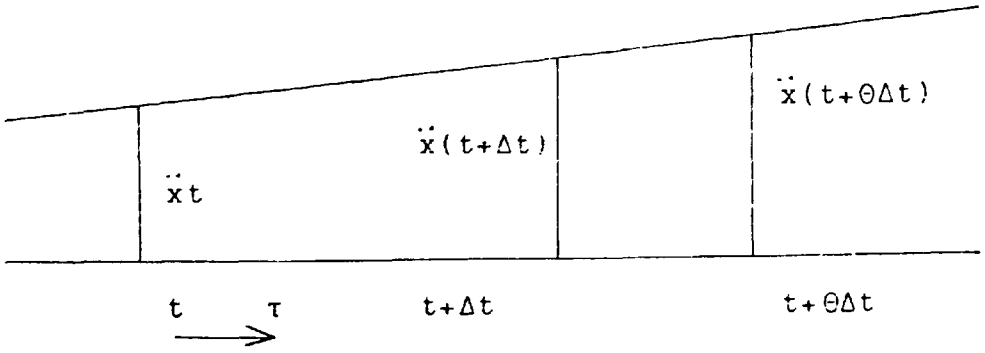

Figure 2.2.1

Let τ equal the time increase where $0 \leq \tau \leq \theta\Delta t$.

Thus for time $t+\theta\Delta t$ assuming a linear increase in acceleration.

$$\ddot{x}(t+\tau) = \ddot{x}t + \frac{\tau}{\theta\Delta t}(\ddot{x}(t+\theta\Delta t) - \ddot{x}t) \quad -2.1$$

Integrating 2.1 we obtain

$$\dot{x}(t+\tau) = \dot{x}t + \ddot{x}t\tau + \frac{\tau^2}{2\theta\Delta t}(\ddot{x}(t+\theta\Delta t) - \ddot{x}t) \quad -2.2$$

and

$$x(t+\tau) = xt + \dot{x}t\tau + \tfrac{1}{2}\ddot{x}t\tau^2 + \frac{1}{6\theta\Delta t}\tau^3(\ddot{x}(t+\theta\Delta t) - \ddot{x}t) \quad -2.3$$

Using 2.1 and 2.2 we have at time $t+\theta\Delta t$

$$\dot{x}(t+\theta\Delta t) = \dot{x}t + \frac{\theta\Delta t}{2}(\ddot{x}(t+\theta\Delta t) + \ddot{x}t) \quad -2.4$$

$$x(t+\theta\Delta t) = xt + \theta\Delta t\dot{x}t + \frac{\theta^2\Delta t^2}{6}(\ddot{x}(t+\theta\Delta t) + 2\ddot{x}t) \quad -2.5$$

From which we can solve for $\ddot{x}(t+\theta\Delta t)$ and $\dot{x}(t+\theta\Delta t)$ in terms of $x(t+\theta\Delta t)$

$$\ddot{x}(t+\theta\Delta t) = \frac{6}{\theta^2\Delta t^2}(x(t+\theta\Delta t) - xt) - \frac{6}{\theta\Delta t}\dot{x}t - 2\ddot{x}t \quad -2.6$$

and

$$\dot{x}(t+\theta\Delta t) = \frac{3}{\theta\Delta t}(x(t+\theta\Delta t) - xt) - 2\dot{x}t - \frac{\theta\Delta t}{2}\ddot{x}t \quad -2.7$$

To obtain the solution for the displacements, velocities, and accelerations at time $t+\Delta t$, the equilibrium equation (2.1, 2.2) are considered at time $t+\theta\Delta t$. The accelerations are assumed to vary linearly therefore a linearly projected load vector is used and the equation employed is

$$M\ddot{x}(t+\theta\Delta t) + Cx(t+\theta\Delta t) + Kx(t+\theta\Delta t) = \hat{P}(t+\theta\Delta t) \quad -2.8$$

Substituting 2.6 and 2.7 into 2.8, an equation is obtained from which $x(t+\theta\Delta t)$ can be solved. Then substituting $x(t+\theta\Delta t)$ into 2.6, we obtain $x(t+\theta\Delta t)$ which is used in 2.1, 2.2 and 2.3, all evaluated at $\tau = \Delta t$ to calculate $x(t+\Delta t)$, $\dot{x}(t+\Delta t)$ and $\ddot{x}(t+\Delta t)$. The complete algorithm used in the integration follows:-

Initial Calculations

A. 1. Form stiffness matrix K, mass matrix M, and damping matrix C.

2. Initialise $\ddot{x}_0$, $\dot{x}_0$ and x_0

3. Select time step Δt and calculate integration constants ($\theta \geq 1.4$)

$$a0 = \frac{6}{(\theta\Delta t)^2}, \quad a1 = \frac{3}{\theta\Delta t}, \quad a2 = 2a1, \quad a3 = \frac{\theta\Delta t}{2}$$

$$a4 = \frac{a0}{\theta}, \quad a5 = -\frac{a2}{\theta}, \quad a6 = 1-\frac{3}{\theta}, \quad a7 = \frac{\Delta t}{2}$$

$$a8 = \frac{\Delta t^2}{6}$$

4. Form effective stiffness matrix

$$K = K = K+a0M+a1C$$

5. Triangularise $K: K = LDL^T$

B. For Each Time Step

1. Calculate effective load at time $t+\theta\Delta t$

$$P(t+\theta\Delta t) = Pt+\theta(R(t+\Delta t)-Rt)+ M(a0xt+a2\dot{x}t+2\ddot{x}t)+C(a1xt+2\dot{x}t+a3\ddot{x}t)$$

2. Solve for displacements at time $t+\theta\Delta t$

$$LDL^T\, x(t+\theta\Delta t) = P(t+\theta\Delta t)$$

3. Calculate displacements, velocities and accelerations at time $t+\Delta t$:

$$\ddot{x}(t+\Delta t) = a4(x(t+\theta\Delta t)-xt) + a5\dot{x}t+a6\ddot{x}t$$

$$\dot{x}(t+\Delta t) = \dot{x}t + a7(\ddot{x}(t+\Delta t)+\ddot{x}t)$$

$$x(t+\Delta t) = xt + \Delta t\dot{x}t+a8(\ddot{x}(t+\Delta t)+2\ddot{x}t)$$

Newmark Method

The Newmark integration scheme is also an extension of the linear acceleration method. The following assumptions are used:-

$$\dot{x}(t+\Delta t) = \dot{x}t + (1-\delta)\ddot{x}t + \delta\ddot{x}(t+\Delta t)\ \Delta t \quad - 2.10$$

$$x(t+\Delta t) = xt + \dot{x}t\Delta t + (\tfrac{1}{2}-\alpha)\ddot{x}t+\alpha\ddot{x}(t+\Delta t)\ \Delta t^2 \quad - 2.11$$

Newmark proposed as an unconditionally stable scheme the constant average acceleration method, in which case $\delta = \frac{1}{2}$ and $\alpha = \frac{1}{4}$

As well as equations 2.10 and 2.11, for solutions of the displacements, velocities and accelerations at time $t+\Delta t$, the equilibrium equations at time $t+\Delta t$ are also considered.

$$M\ddot{x}(t+\Delta t) + C\dot{x}(t+\Delta t) + Kx(t+\Delta t) = P(t+\Delta t) \quad - 2.12$$

Solving from 2.11. for $\ddot{x}(t+\Delta t)$ in terms of $x(t+\Delta t)$, and then substituting for $\ddot{x}(t+\Delta t)$ into 2.10, we obtain equations for $\ddot{x}(t+\Delta t)$ and $\dot{x}(t+\Delta t)$ each in terms of the unknown displacements $x(t+\Delta t)$ only. These two relations for $\ddot{x}(t+\Delta t)$ and $\dot{x}(t+\Delta t)$ are substituted into 2.12 to solve for $x(t+\Delta t)$ after which $\ddot{x}(t+\Delta t)$ and $\dot{x}(t+\Delta t)$ can be calculated using 2.10 and 2.11.

The complete algorithm used in the integration is as follows:-

A. Initial Calculation

1. Form stiffness matrix K mass matrix M, and damping matrix C.

2. Initialise x_o, $\dot{x}_o$ and $\ddot{x}_o$

3. Select time step size Δt, parameters α and δ and calculate integration constants.

$\delta \geq 0.50$, $\alpha \geq 0.25(0.5+\delta)^2$

$$a0 = \frac{1}{\alpha\Delta t^2}, \quad a1 = \frac{\delta}{\alpha\Delta t}, \quad a2 = \frac{1}{\alpha\Delta t}, \quad a3 = \frac{1}{2\alpha} - 1,$$

$$a4 = \frac{\delta}{\alpha} - 1, \quad a5 = \frac{\Delta t}{2}\left(\frac{\delta}{\alpha} - 2\right), \quad a6 = \Delta t\,(1-\delta),$$

$$a7 = \delta\Delta t$$

4. Form effective stiffness matrix $\hat{K}$,

$\hat{K} = K + a0M + a1C$

5. Triangularise $\hat{K}$: $\hat{K} = LDL^T$

B. For Each Time Step

1. Calculate effective loads at time $t+\Delta t$

$\hat{P}(t+\Delta t) = P(t+\Delta t) + M(a0xt + a2\dot{x}t + a3\ddot{x}t) + C(a1xt + a4\dot{x}t + a5\ddot{x}t)$

2. Solve for displacements at time $t\Delta t$

$LDL^T x(t+\Delta t) = \hat{P}(t+\Delta t)$

3. Calculate accelerations and velocity at time $t\Delta t$

$$\ddot{x}(t+\Delta t) = a0(x(t+\Delta t)-xt)-a2\dot{x}t-a3\ddot{x}t$$

$$\dot{x}(t+\Delta t) = \dot{x}t+a6\ddot{x}t+a7\ddot{x}(t+\Delta t)$$

APPENDIX 2.3

Some Numerical Examples

Two well documented examples were analysed in order to verify that the numberical routines are functioning correctly.

The first example is a simple two degree of freedom system taken from Bathe and Wilson (1976). As can be seen from Fig. 2.3.1 the theoretical and numerical results bear close resemblence for both the Newmark and Wilson - θ routines.

The second example is a single degree of freedom system taken from Clough and Penzien (1975) and is used to illustrate the effect of specifying an elasto-plastic stiffness force/displacement relationship on the shape of the displacement time curve. As can be seen from Fig. 2.3.2 the permanent set resulting from the analysis is approximately 1.5 inches.

$$\begin{bmatrix} 2 & 0 \\ 0 & 1 \end{bmatrix} \begin{bmatrix} \ddot{x}_1 \\ \ddot{x}_2 \end{bmatrix} + \begin{bmatrix} 6 & -2 \\ -2 & 4 \end{bmatrix} \begin{bmatrix} x_1 \\ x_2 \end{bmatrix} = \begin{bmatrix} 0 \\ 10 \end{bmatrix}$$

TWO DEGREE OF FREEDOM SYSTEM - GOVERNING EQUILIBRIUM EQUATIONS

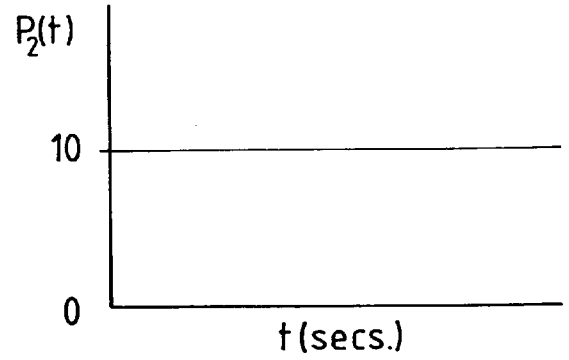

LOAD / TIME HISTORY

INITIAL CONDITIONS AT t=0 secs.

$$\ddot{x}_0 = \begin{bmatrix} 0 \\ 10 \end{bmatrix} \qquad \dot{x}_0 = \begin{bmatrix} 0 \\ 0 \end{bmatrix} \qquad x_0 = \begin{bmatrix} 0 \\ 0 \end{bmatrix}$$

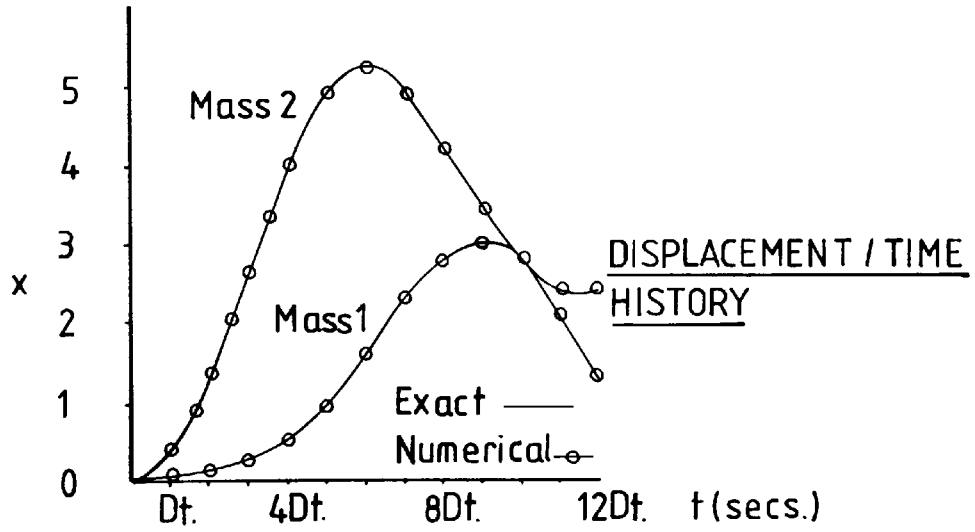

FIG. N°2.3.1 COMPARISON OF EXACT AND NUMERICAL SOLUTIONS FOR 2 D.O.F. SYSTEM (Numerical Methods in Finite Element Analysis - Bathe K.J., Wilson E.L.- Prentice-Hall, Inc.)

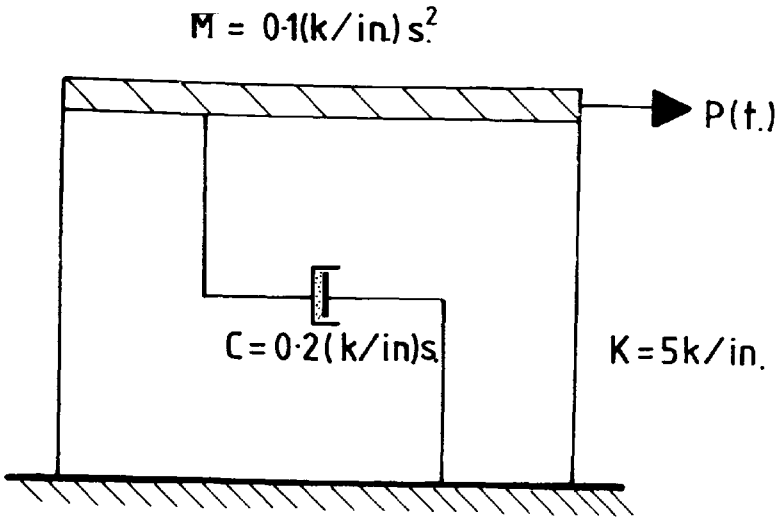

SINGLE DEGREE OF FREEDOM SYSTEM

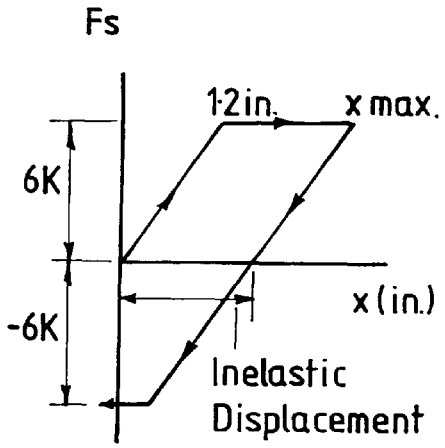

ELASTOPLASTIC STIFFNESS

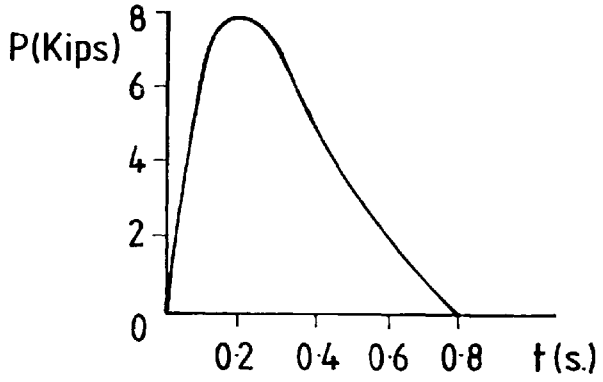

LOAD / TIME HISTORY

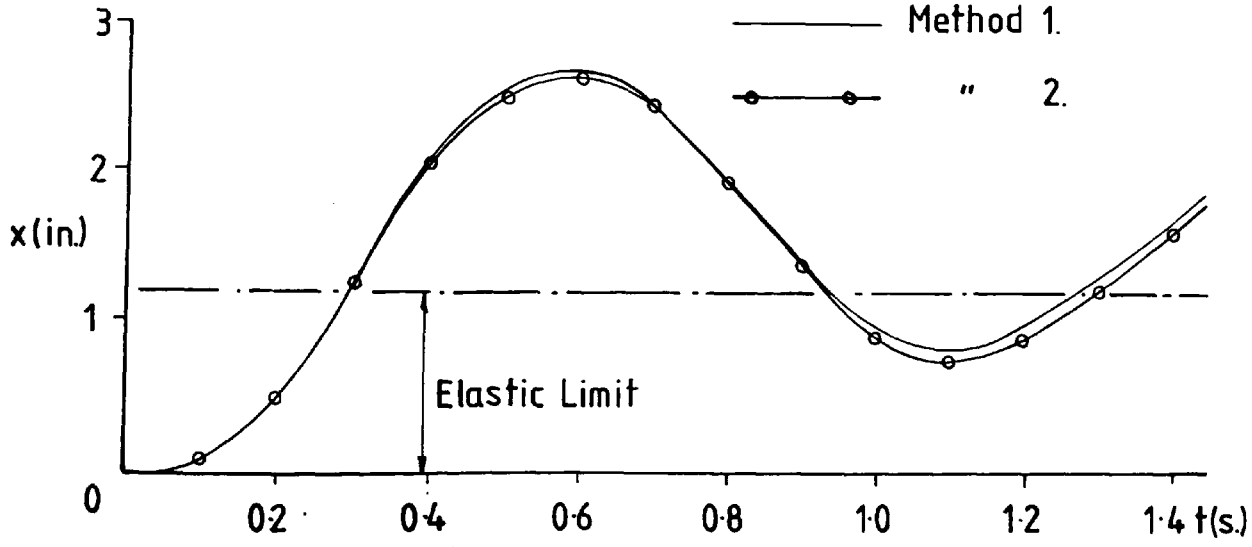

ELASTOPLASTIC - DISPLACEMENT / TIME HISTORY

FIG. N°232 ELASTOPLASTIC S.D.O.F. SYSTEM (Dynamics of Structures - Clough R.W., Penzien J. - McGraw-Hill)

CHAPTER 3

Pilot Study

3.1 Introduction

The pilot study was instigated for five main reasons:-

1. To develop apparatus suitable for use in dynamic testing.
2. To develop a system of instrumentation sensitive yet robust enough to transmit accurately dynamic signals without danger of breakdown.
3. To develop a monitoring and recording system suitable for use with the aforementioned instrumentation.
4. To conduct a series of small scale model tests on an instrumented model pile to verify that parts 1-3 have been successfully achieved. These tests would also be used to perfect experimental techniques for use in the semi-full scale tests.
5. To ascertain which of the study parameters are of significance in pile - soil interaction.

3.2 Apparatus

In order to study the distribution of load along a pile, suitable instrumentation had to be designed and tested and is described in the following sections.

3.2.1 Axial, Load Cell

A 'core' type load cell with screw thread and screw connectors (Fig. 3.1) was designed and manufactured for use in a 32 mm outside diameter tubular steel model pile. The strain

sensitive part of the cell was strain gauged using an eight gauge full bridge configuration (Fig. 3.2). This was similar to the arrangement used by Nicholls (1973) in tests to assess negative skin friction in model pile groups.

Further information on the strain bridge circuit is given in Section 3.4.5. while a breakdown of the strain gauging technique used is given in Bulletin B-130-6 W.S.M. Ltd. It has been shown by such workers as Fellenius and Haggen (1969), Housel (1966), Scanlan and Tomko (1969) that a strain gauged system is capable of monitoring both Static and Dynamic Signals provided the appropriate energising and recording equipment is used.

It was the original intention to adopt this method to monitor both types of signals, however, lack of funding made it impossible to obtain the correct type of strain bridge energiser to monitor the dynamic signals.

3.2.2 Performance of the Core Load Cell During Initial Impact Tests

Preliminary impact tests using the core load cell uncovered the following defects in the design:-

1. The screw type connectors used to connect the cells together tended to loosen due to vibration from successive blows causing loss of pile integrity.

2. The individual pile sections were free to move in a horizontal plane relative to each other. This twisting effect could lead to possible damage to any wiring running along the length of the model pile.

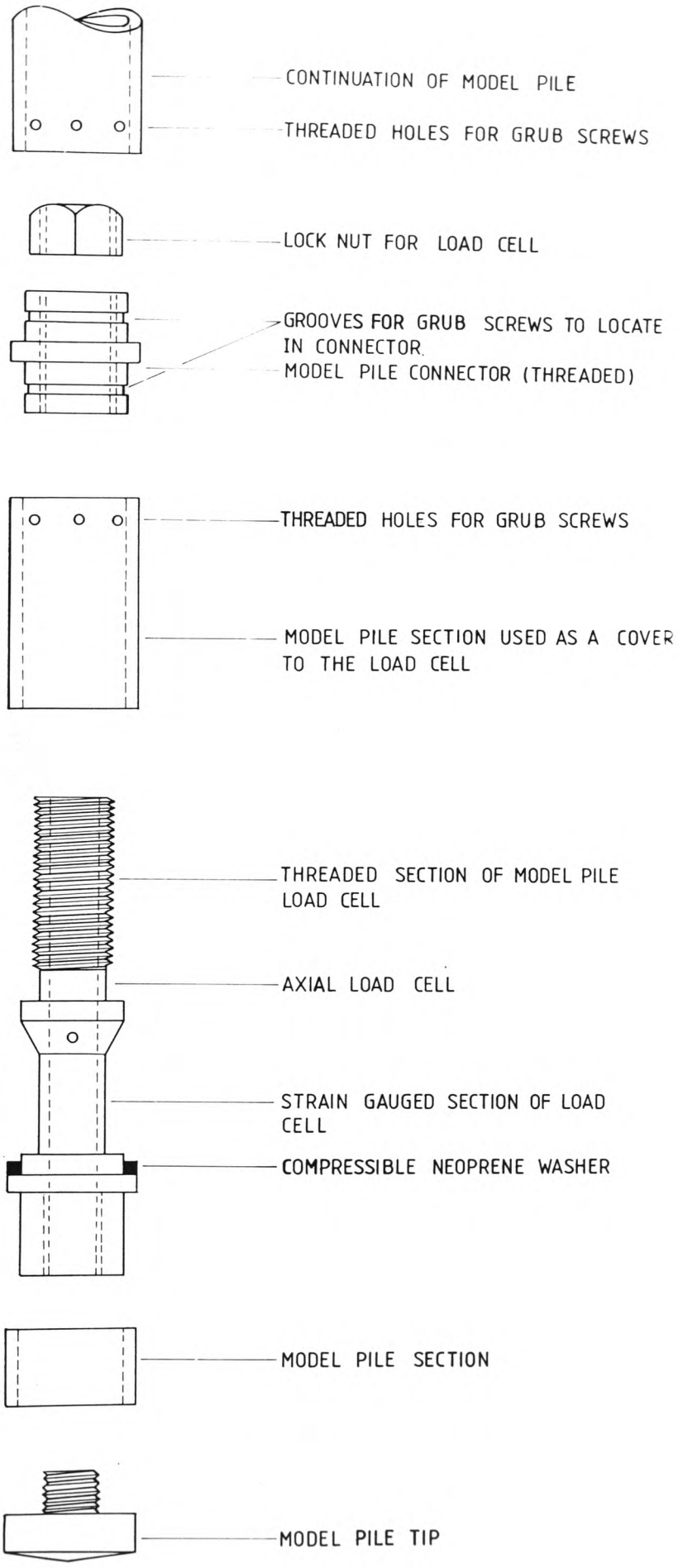

FIG 3.1 SHOWING SCREW TYPE AXIAL LOAD CELL

Wheastone Bridge Circuit

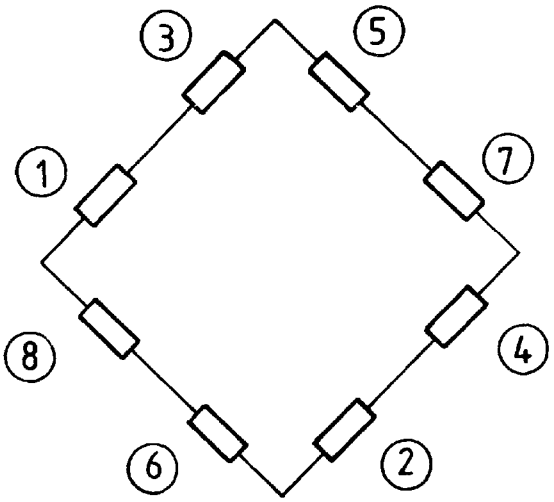

Strain Sensing Section of Core Load Cell
(Elevations)

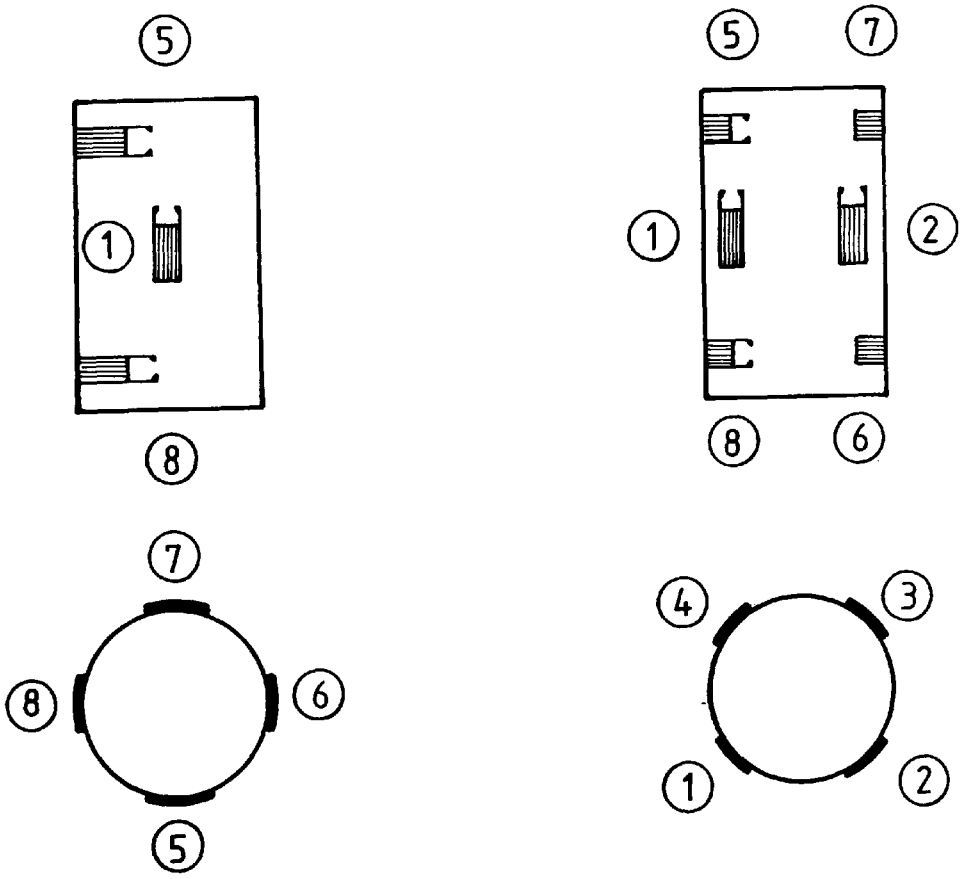

Dummy Lateral Gauges

Active Longitudinal Gauges

FIG 3.2 SHOWING STRAIN GAUGE CONFIGURATION FOR STATIC LOAD CELL

3.2.3 Redesigned Axial Load Cell

It was therefore decided to use the basic design of the load cell but change the screw connectors to keyed taper connectors (Fig. 3.3) to eliminate slackness and horizontal movement between joints.

The mode of operation of the taper connector is the same as the 'bayonet' connector used in the Piling Industry whereby each blow drives the male and female parts of the connectors together giving rise to a very tight push fit.

To verify that a load cell of this type would eliminate slackness a prototype was manufactured for use with a 60 mm outside diameter tubular steel section.

The larger section was chosen because it would be easier to study the effect of impact on the joint and would also verify that a taper connector of this kind would be suitable for use in the semi-full scale tests.

A simple impact test was performed using a "High Speed" camera running at 400 frames per second to record the effects on a typical joint.

The pile section was hand held and the camera focused on the joint to be filmed. The pile was then struck with a wooden mallet a total of seven times and the results recorded. The pile movement was not constrained in any vertical plane and was also able to rebound after each blow.

Analysis of the film showed that the joint remained 'intact' not only on the actual impact but also during the rebound when the joint was in tension.

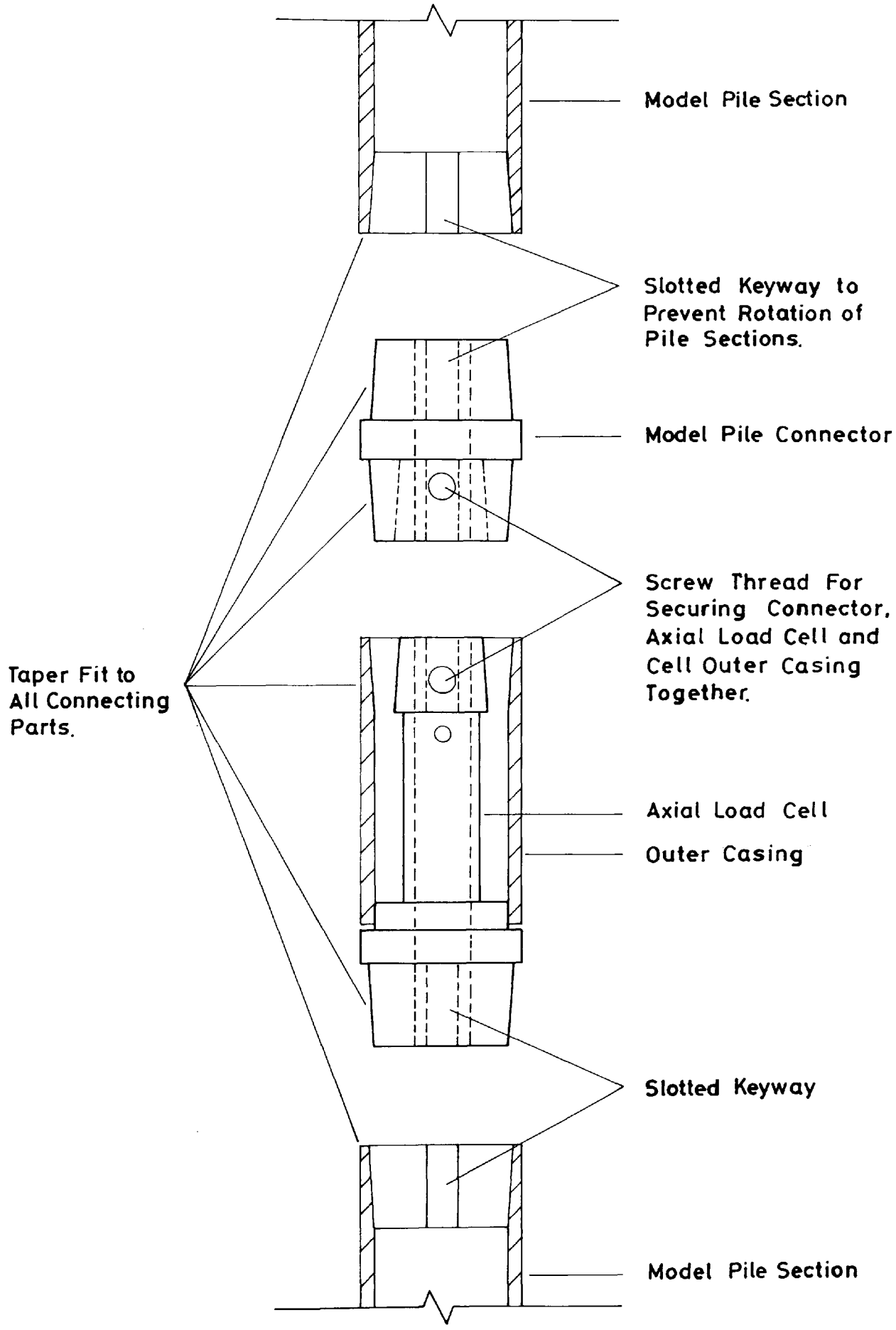

FIG. 3.3 SHOWING PART SECTIONAL EXPLODED VIEW OF AXIAL LOAD CELL

3.2.4 Axial Dynamic Load Cell

Satisfactory monitoring and recording equipment made the use of piezoelectric transducers more practical for measuring dynamic signals than using an equivalent strain gauged system.

In order to test that this type of system was capable of performing to the criteria laid down in the introduction, piezoelectric equipment already available in the department but not ideally suited for this purpose was used.

A suitable housing for the piezoelectric force transducer was designed and constructed for use in a 38 mm diameter model pile and is shown in Fig. 3.4. The larger diameter was made necessary in order to accommodate the force transducer in the pile shaft.

3.2.5 Disconnection of Load Cells

Due to the type of joint employed a non destructive means of separation had to be designed to disassemble the model pile after each test.

As can be seen from Fig. 3.5 the apparatus consists of two clamps each separated into two halves.

The inside of the clamps were machined to a radius equal to that of the model pile. Each of the two halves were then connected together by countersunk Allen screws.

The upper clamp had two threaded holes drilled on an opposite diameter and in a plane vertical to the half clamp connectors. The method then employed to disconnect a joint was as follows:-

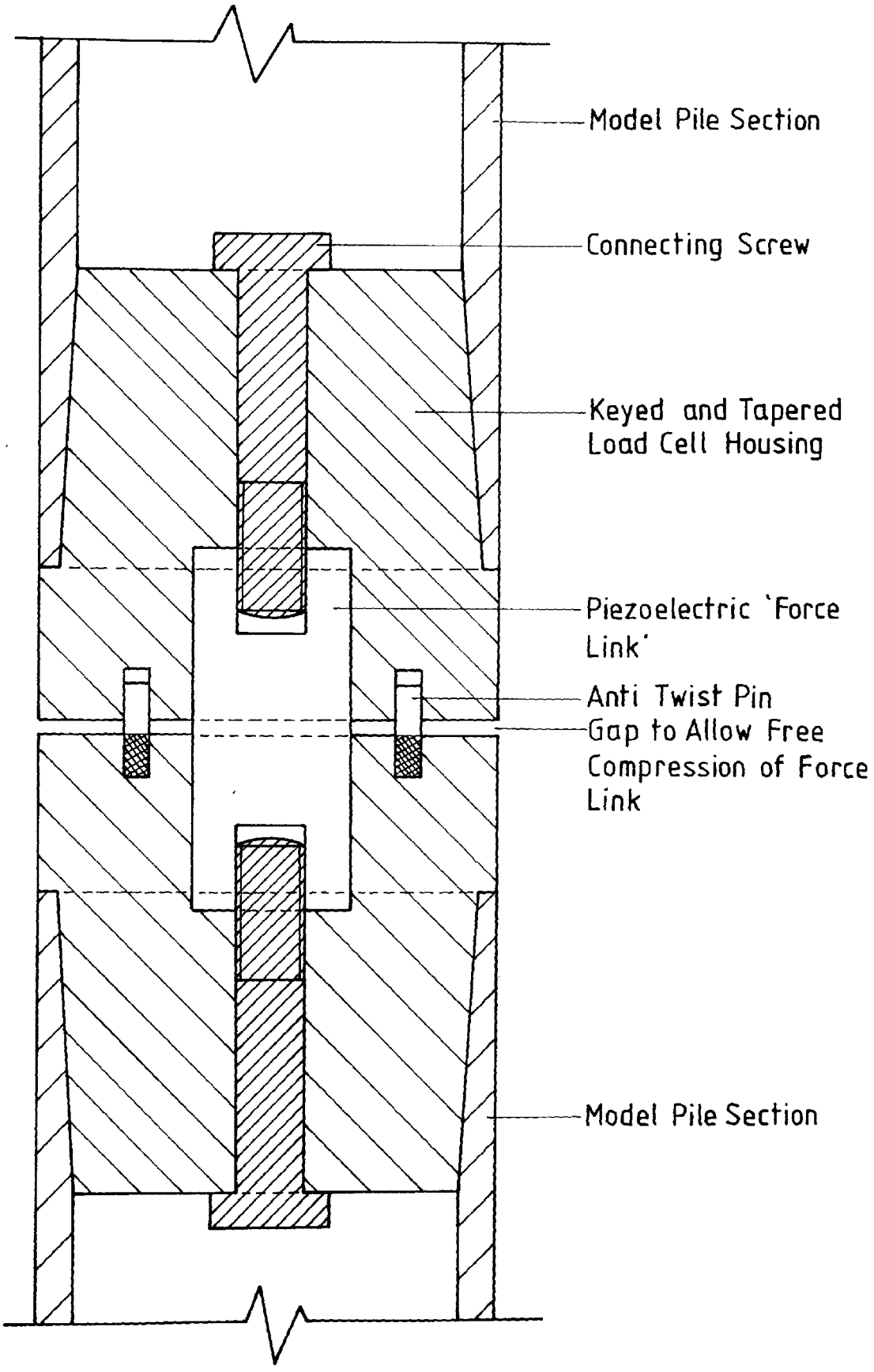

FIG 3.4 SHOWING FORCE LINK HOUSING (DYNAMIC AXIAL FORCE TRANSDUCER)

Allen Screws Used to Seperate The Upper and Lower Clamps When Connected at Model Pile Joints.

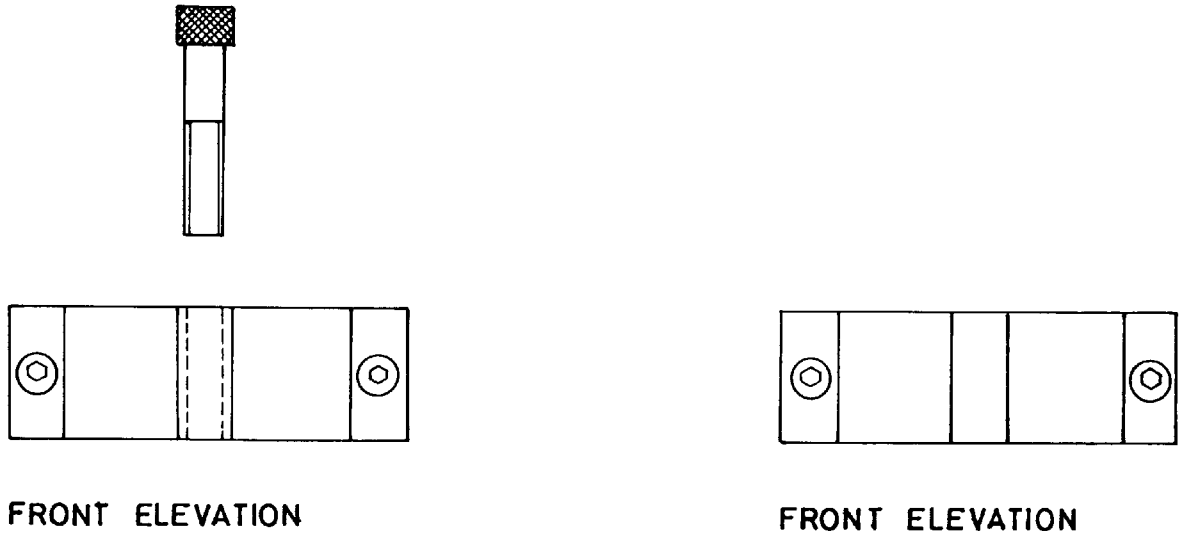

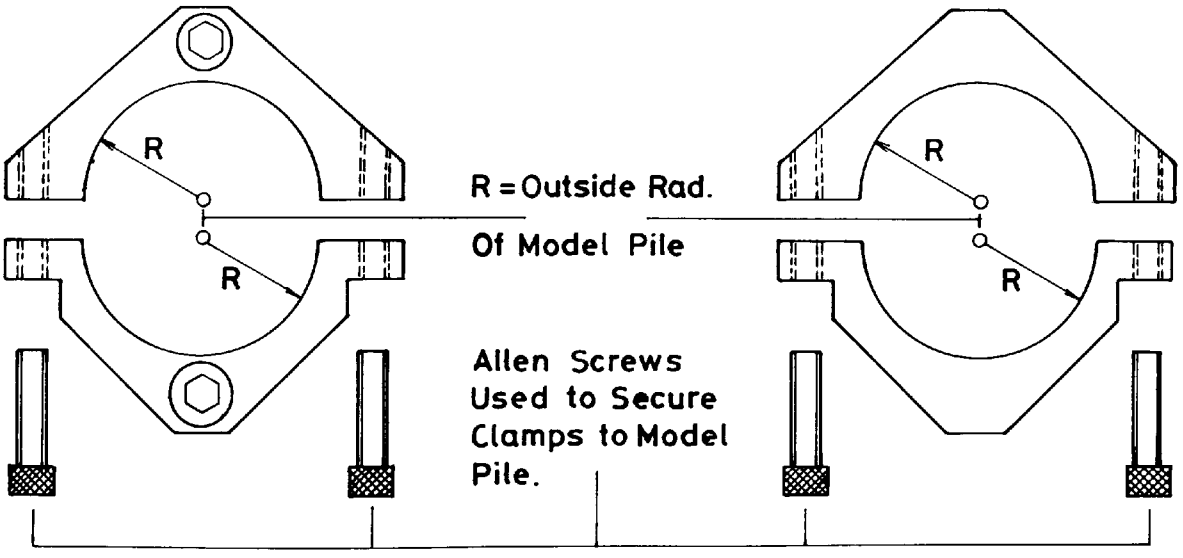

Upper Clamp

Lower Clamp

FIG. 3.5 SHOWING APPARATUS USED TO DISCONNECT MODEL PILE SECTIONS

1. The lower clamp was placed just below a joint and the half clamp connectors were firmly tightened to secure the lower clamp to the model pile.

2. The upper clamp was then placed above the joint and secured as in (1).

3. The two Allen screws in the upper clamp were then tightened sequentially to bear on the lower clamp.

In this way the joint was pushed apart gradually and separated without damage to the instrumentation.

A prototype was constructed and proved effective when used to separate the joints on the 60 mm diameter load cell.

The method decided upon proved to be a simple and effective means of separating the taper joints without damaging any instrumentation.

3.3 The Model Pile

3.3.1 Construction

The model pile section finally decided upon for the pilot tests, was a 38 mm diameter seamless tubular steel section of approximate wall thickness 3.0 mm. The overall length of the model pile including load cells and pile point was 600 mm.

3.3.2 Model Pile Sections

Section 1 consists of a pile shoe turned out of mild steel with a point angle of 30 degrees and threaded to fit a 52 mm section of the tubular steel model pile. A sealing agent

was then applied to the threaded surface to ensure that once tightened the shoe would not loosen due to vibration. The other end of the section was then keyed and tapered to fit section 2.

Section 2 consists of two halves turned out of mild steel, both halves being tapered and keyed to fit section 1 and section 3. These two halves when fitted together house the piezoelectric force transducer (Fig. 3.4).

Section 3 consists of a 55 mm length of tubular steel model pile tapered and keyed at both ends to fit section 2 and 4.

Section 4 consists of 3 subsections:-

Subsection (a) consists of a static axial load cell tapered and keyed at the bottom end to fit section 3 and tapered and keyed at the top end to fit subsection c.

Subsection (b) consists of a 63 mm length of tubular steel model pile tapered at the top end to fit subsection c. This section seals the axial load cell and also ensures that load is transmitted through the core of the load cell only.

Subsection (c) consists of a machined section of mild steel keyed and tapered at both ends and used to connect subsections (a) and (b) together.

Section 5 consists of a length of 360 mm tubular steel model pile keyed and tapered at one end to fit subsection (c) of section 4.

A complete assembly of the model pile is shown diagramatically in Fig. 3.6 and pictorially in Plate 3.1.

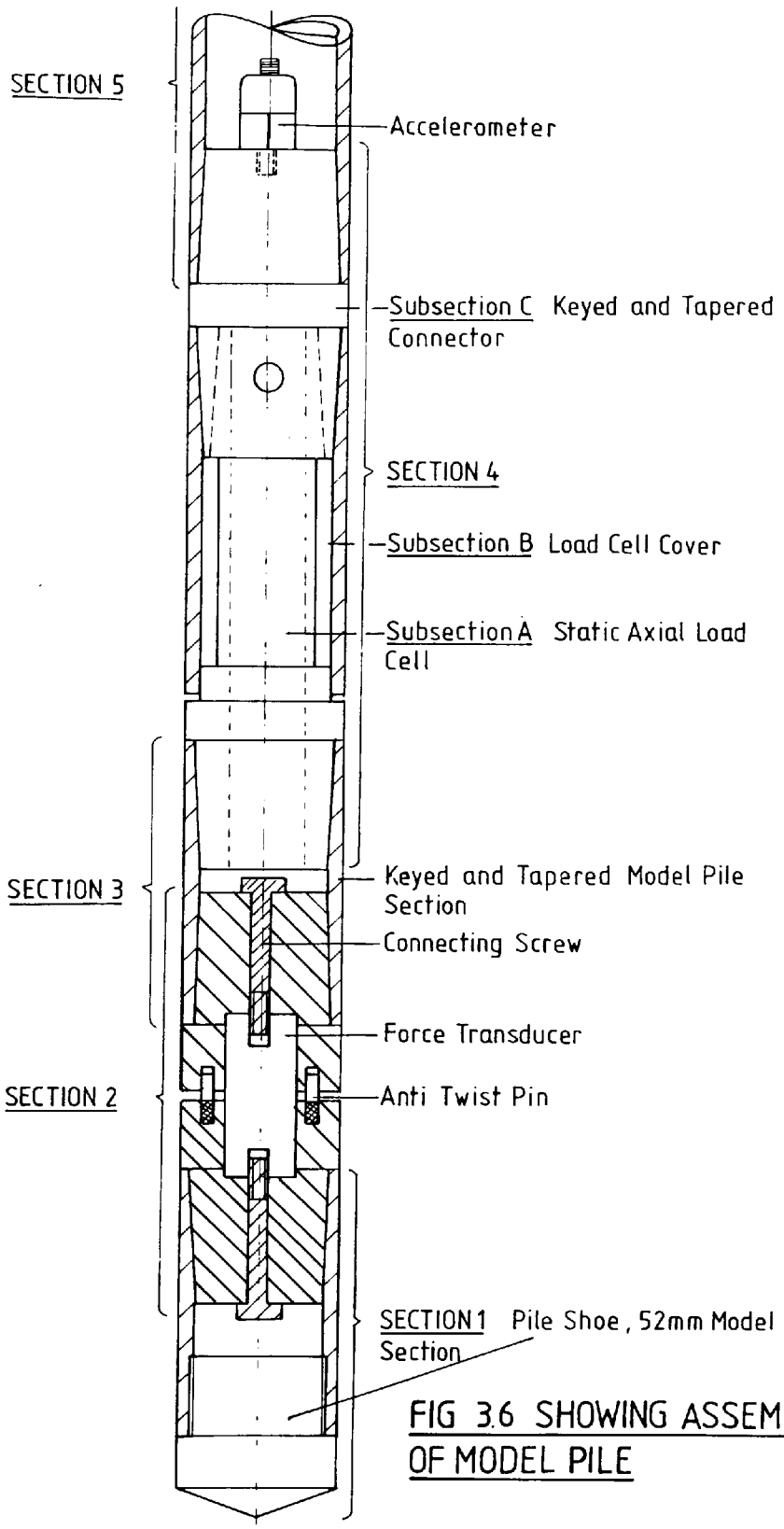

FIG 3.6 SHOWING ASSEMBLY OF MODEL PILE

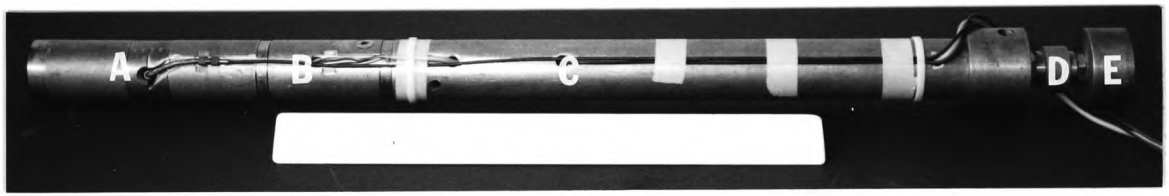

KEY:

A. Dynamic Axial Load Cell

B. Static Axial Load Cell

C. Accelerometer Mounted Internally On Central Axis

D. Dynamic Force Transducer

E. Model Pile Cap

PLATE 3.1 Assembled Model Pile and Pile Cap

After assembly of the model pile a slot was milled up the outside to accommodate the instrumentation wiring. The wiring was then secured to the body of the pile.

As can be seen from Fig. 3.6 a piezoelectric accelerometer is fitted to the top of subsection (c) of section 3 to record acceleration/time.

3.3.3 Model Pile Cap

The model pile cap was required to protect the load cell and also to increase the duration of the force time signal by providing a wooden cushion. The model pile cap can be subdivided into two sections:-

Section 1 consists of a length of 50 mm diameter mild steel rod machined at its lower end to fit tightly over the top of the model pile. The top has a central hole threaded to allow placement of a piezoelectric force transducer.

Section 2 again consists of a length of 50 mm diameter mild steel rod and differs from section 1 in the following respects only:-

(i) The top end is threaded centrally to allow a 12.5 mm diameter mild steel rod used to locate the drop weight to be screwed into it.

(ii) A 12.5 mm wooden disc is glued to the top to act as a pile cushion.

3.3.4 Model Pile Driving Rig

The model pile driving rig was designed and manufactured to

fit into a large triaxial apparatus with a 10 Kn loading frame. As can be seen from Fig. 3.7 the driving rig is hand operated and consists of:-

A cross piece in which a central boss is incorporated with an internal diameter of 40 mm to allow the model pile to pass through freely. Also included in the boss are three holes set at 120 degrees to each other at a central radius of 58 mm. The top plate is correspondingly threaded so that the three 12.5 mm diameter mild steel bars locate in the bottom and top plates as shown in Fig. 3.7.

The internal radius of the bars is 52 mm so as to allow the drop weight to fall freely but be fully restrained in the vertical plane.

3.4 Instrumentation

3.4.1 Piezoelectric Transducers (Dynamic System)

3.4.2 Principles

Piezoelectric instrumentation is based on the piezoelectric effect discovered by the Curie brothers in 1880. They found that certain crystals become electrically charged when stressed mechanically. Quartz crystals are usually employed in such instruments because they are excellent piezoelectric materials, have a high mechanical strength and can be employed over a wide range of temperature.

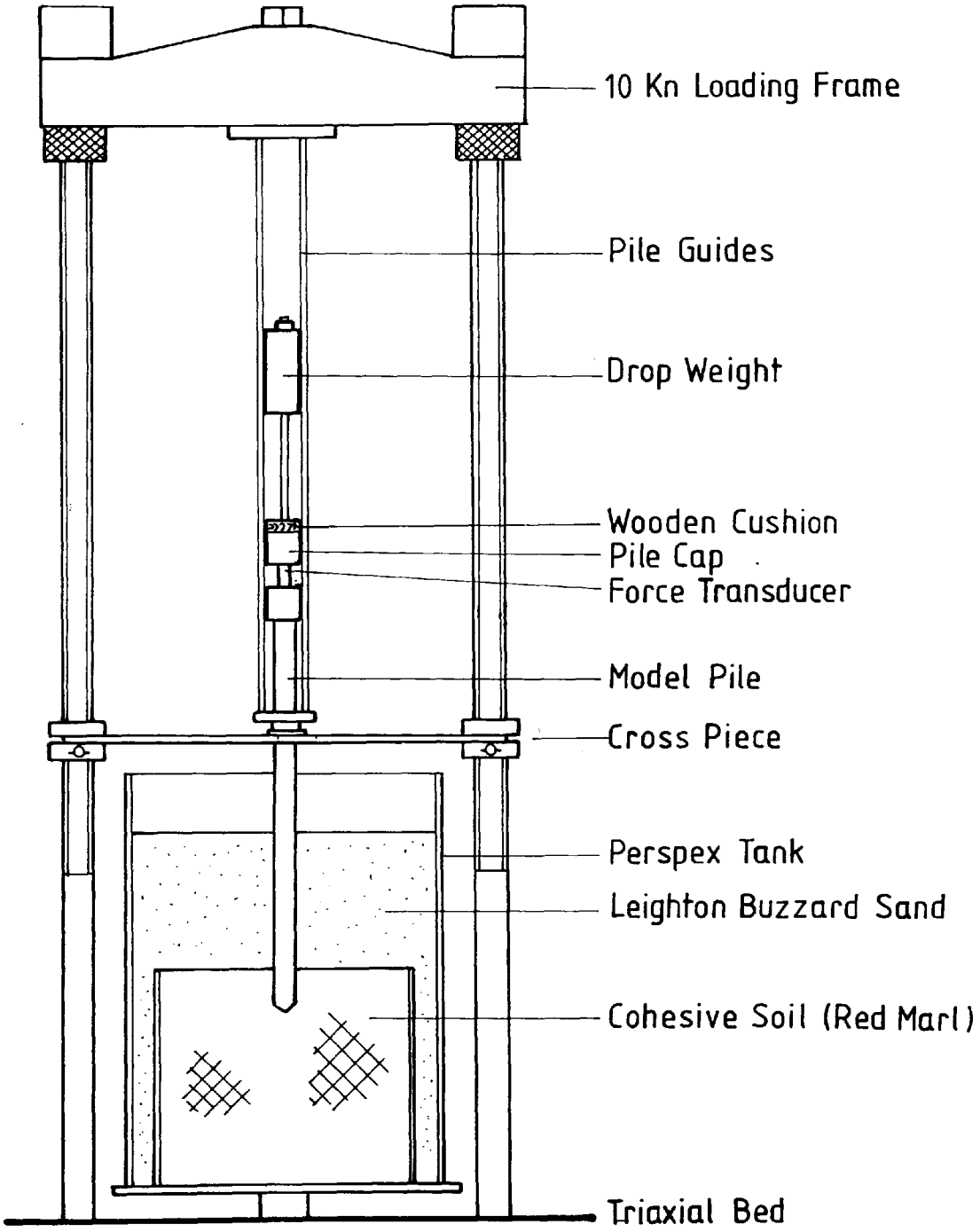

FIG 3.7 MODEL PILE DRIVING RIG

3.4.3 Force Transducers

For the pilot study two piezoelectric transducers were used. These consisted of:-

1. A Bruel and Kjaer type 8201 with a maximum capacity of 10 Kn and used at the top of the model pile.

2. A Kistler type 9311A with a maximum capacity of 5 Kn and used along with a previously designed housing at the model pile toe.

3.4.4 Accelerometer

One accelerometer was used in the pilot study and was positioned on the static load cell at the base of the model pile (Fig. 3.6). The accelerometer was a DJB type A02/T and was check calibrated prior to testing.

3.4.5 Strain Gauged Load Cell (Static System)

An eight gauge full bridge circuit was used for the model pile tests. These were mounted on the core part of the axial load cell referred to in section 3.2.1. Figure 3.2 shows the wheastone bridge configuration adopted. This type of bridge has the following advantages:-

1. The full bridge circuit has double the sensitivity over a half bridge circuit and 2.6 times the sensitivity over a quarter bridge circuit.

2. Temperature compensation is automatically effected.

3. The full bridge circuit is wired in such a way as to minimise the effects of lateral strain and possible eccentric loading.

3.5 Monitoring

The specifications and operational features of the monitoring equipment used are readily available from the manufacturers, therefore, only a brief description of the equipment is included here.

3.5.1 Conditioning Amplifiers

The charge amplifiers used in the model tests were as follows:-

1. A Kistler type 5007
2. A Bruel and Kjaer type 2626
3. A Bruel and Kjaer type 2635

All the charge amplifiers were of the low noise type enabling long transducer connection cables to be used without affecting the charge sensitivity of the transducers. The amplifiers feature precision conditioning networks for 'dial-in' on the amplifier of exact transducer charge sensitivities. These condition the sensitivity of the transducer and amplifier combination giving unified output ratings.

3.5.2 Narrow Band Spectrum Analyser (Bruel and Kjaer 2031)

This is an instrument designed for the narrow band frequency analysis of continuous and transient data coming from

vibrational and other signal sources.

The maximum frequency measurable with this instrument is 20 KH_z. The analyser operates by Fourier Transforming records of 1024 samples of the input signal into the frequency domain.

Amplitudes are displayed in decibels (DB's) which may be converted into voltages and hence force, by referring to the transducer charge sensitivity.

The analyser may be used in conjunction with a conditioning amplifier alone, for 'single shot' analysis or used with previously recorded data for analysis at a later stage.

3.6 Recording

3.6.1 Tape Recorder

The recorder used to store dynamic signals was a Racal Store 4 DS which has the capacity of storing four signals simultaneously.

Signal electronics and switchable dual standard intermediate and wideband 1FM. The store 4 DS has 7 recording and replay speeds ranging from 15/16 to 60 inches/second.

3.6.2 Chart Recorder

A Bruel and Kjaer, X-Y plotter type 2305 was used to obtain 'hard copy' prints of the dynamic signals when connected to the Real Time Analyser. A typical instrumentation set up for monitoring and recording dynamic signals is shown schematically in Fig. 3.8.

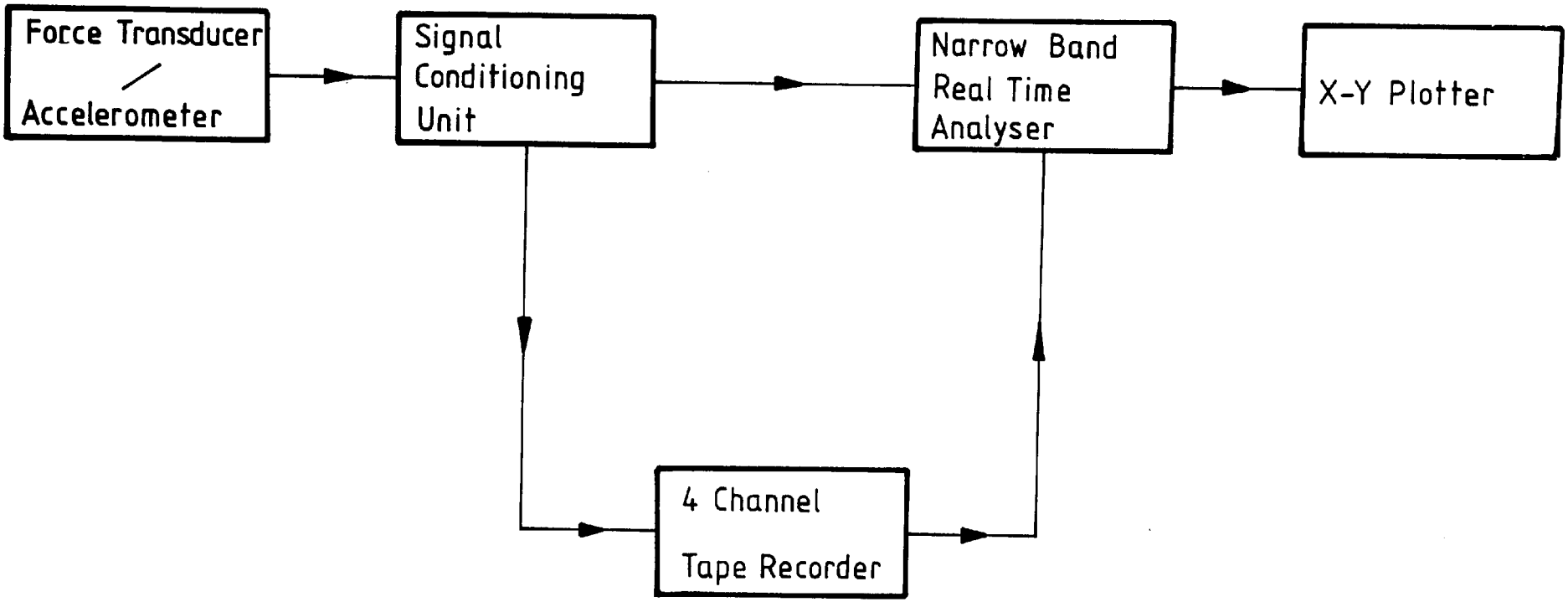

FIG 3.8 SCHEMATIC DIAGRAM OF A TYPICAL INSTRUMENT SET UP FOR DYNAMIC MEASUREMENTS

3.6.3 Static Monitoring and Recording

During the calibration of the screwed type axial load cell monitoring and recording was achieved by a Mycalex Data Logger interfaced with a P.E.T. microcomputer.

However for subsequent work, the role of the data logger was taken over by an Orion 3530 system.

3.7 Calibration

3.7.1 Strain Gauge Axial Load Cell

The pile was mounted in a 10 Kn triaxial loading frame with lateral support provided to prevent buckling. Load was applied through a proving ring in increments of 0.1 mm (522 N) to a limit of 1350 Newtons and then unloaded in corresponding increments. Before any readings were taken the pile was loaded and unloaded a total of 5 times. The calibration procedure was repeated a total of 10 times for the screw type connector load cell and 5 times for the taper connector load cell.

Whereas the calibration graph of load/micro volts was substantially linear for both the loading and unloading cycles of the screw type load cell, linearity for the taper load cell was only displayed in the loading phase (Fig. 3.9). This non linearity displayed in unloading was thought to be due to the type of joint used.

Although it was shown in section 3.2.5 that a taper connector was more than adequate at resisting dynamic forces without separating, it appears that when these connectors are used

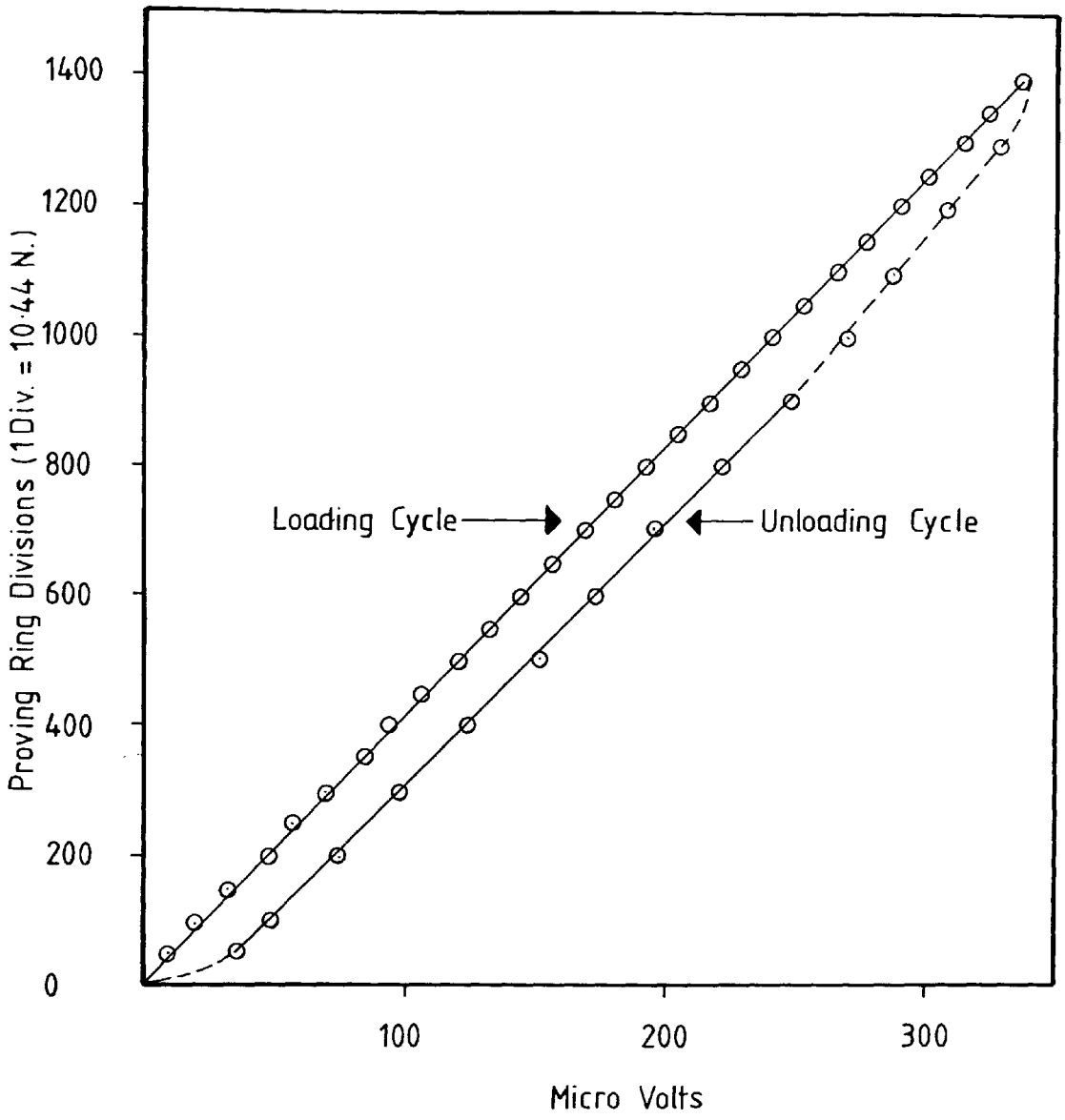

FIG. N° 3.9 SHOWING CALIBRATION GRAPH FOR THE TAPER CONNECTOR LOAD CELL

for a static load cell there is a 'lock up' of stresses occurring on the upper portion of the unloading cycle gradually reducing and returning to zero with a jump at the end of the unloading cycle.

It is hoped that by modifying the joints to the type shown in Chapter 4, section 4.5.1 that the problem of non linearity will be solved and that the joint will have the same resistance to impact that the taper connector had.

3.8 Preliminary Tests on the Dynamic Systems (end bearing only)

3.8.1 Check on Narrow Band Spectrum Analyser

Prior to any impact tests it was thought prudent to perform checks on the Analyser to ensure that the output from the Analyser was indeed a true representation of the force records obtained from the Transducers. These tests are described in the next two sections.

3.8.2 Voltage Check on Spectrum Analyser

The calculated voltage obtained from the Analyser was compared against the direct voltage output given by a recently overhauled four channel oscilloscope. The instrumentation was set up so that an impulse signal could be output to the Analyser and the Oscilloscope simultaneously.

Results of decibels read directly from the analyser and converted to voltage were the same as volts read directly from the Oscilloscope.

3.8.3 Quasistatic Load Test

A quasistatic load test was conducted by connecting the top and bottom load cells to two channels of the Oscilloscope and applying a gradually increasing load at the pile top with the pile tip bearing on a concrete surface. As would be expected the observed output from the Oscilloscope was identical for the two load cells both in shape and magnitude and served as a necessary check on the satifactory functioning of the transducers.

3.8.4 Dynamic Tests

The following preliminary impact tests were conducted on the model pile to ensure that the dynamic system was functioning satisfactorily.

1. Impact tests performed by dropping a 1.73 kg weight from various heights on to the model pile. For these tests the pile tip was bearing on a surface consisting of a thin layer of rubber overlaying concrete tiles. The rubber was provided in order that any possibility of overloading the bottom transducer would be avoided (max force 5 Kn). These tests were used primarily to enable the author to get a 'feel' for the system as a whole.

   The mild steel rod used to locate the drop weight was graduated in increments of 25 mm starting with a drop of 12.5 mm. An additional drop height of 20 mm was added in order to perform the second set of impact tests. Each impulse was recorded on the Real

Time Analyser as a trace of decibels against Time.

2. Impact tests performed by dropping a 1.73 kg weight from a set height of 20 mm with the pile tip bearing down on different surfaces.

3.8.5 Test Procedure

The procedure used for dynamic tests type (1) and (2) was as follows:-

1. The pile was impacted regularly with the drop weight until a consistent signal was obtained (i.e. repeatibility of testing).

2. When step 1 had been achieved the next three to six readings (depending on the repeatibility of the signals) were recorded and a hard copy trace of one of the signals obtained.

The initial tests were 'hand held' and simply intended to check that the system was functioning satisfactorily and that the pile configuration did not have a perceptible influence on the results.

3.8.6 Impact Tests (1)

Drop heights ranging from 20 mm to 95 mm were used and the results tabulated in Fig. 3.10. A graph of peak force against drop height is shown in Fig. 3.11. The figure highlights two basic facts:-

1. The relationship between peak force and drop height was roughly linear for the drop heights used.

DROP HEIGHT (mm)	FORCE TRANSDUCER OUTPUT (N)		
	TOP TRANSDUCER	BOTTOM TRANSDUCER	
		INITIAL PEAK	SECONDARY PEAK
12.5	1862)) 1862) 1862) 1862	389)) 380) 383) 380)	631)) 631) 631) 631)
25.0	2630)) 2691) 2671) 2691)	678)) 647) 662) 662)	1074)) 1074) 1074) 1074)
50.0	4466)) 4466) 4466) 4466)	1416)) 1416) 1416) 1416)	1742)) 1702) 1715) 1702)
75.0	6165)) 6165) 6165) 6165)	2182)) 2182) 2182) 2182)	2420)) 2420) 2420) 2420)

Fig. No. 3.10 Table showing calculated peak force against drop height for impact test (1)

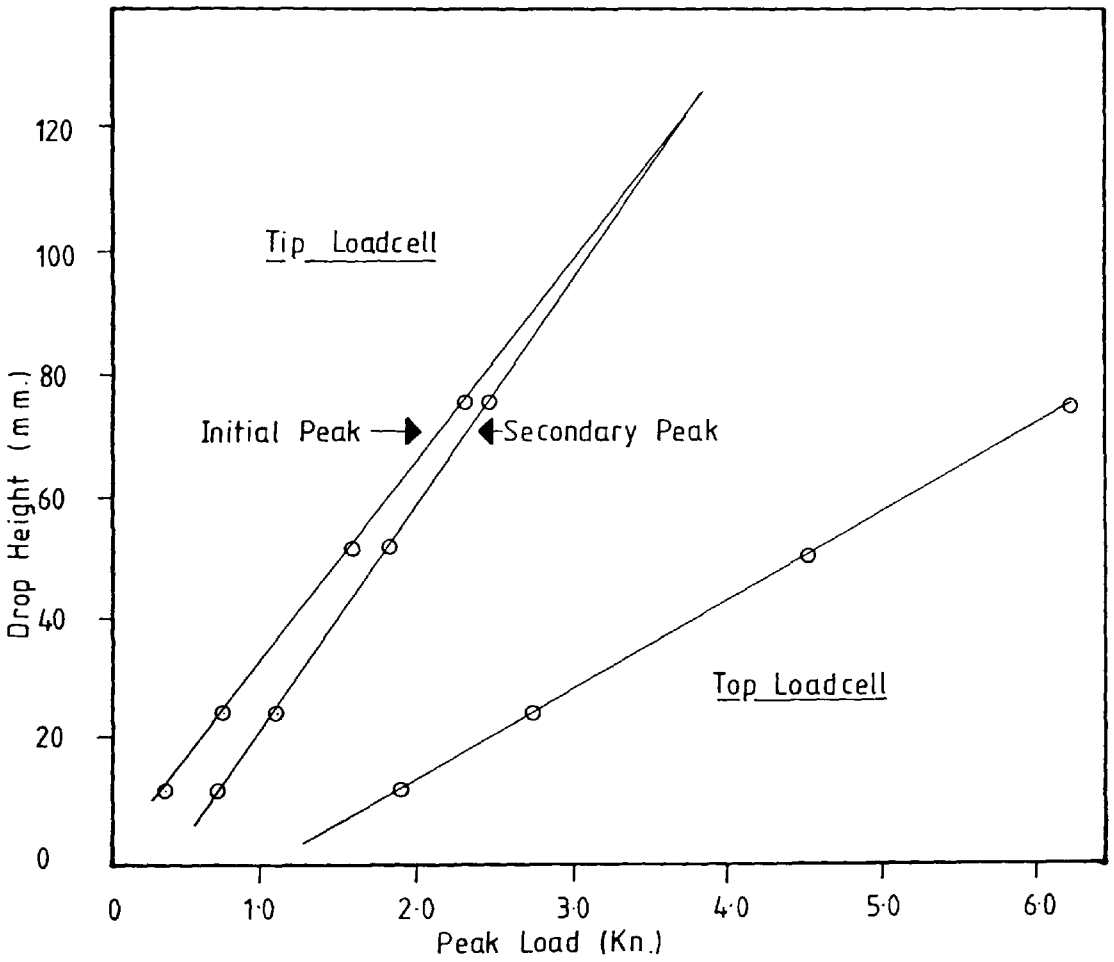

FIG. N° 3.11 SHOWING GRAPH OF DROP HEIGHT AGAINST PEAK LOAD

2. The peak force of the top transducer was considerably higher than the tip transducer.

Also it was observed that the characteristic triangular peak signal of the transducers when 'unconnected' remained the same for the top transducer but changed significantly for the tip transducer (Fig. 3.12). Interpretation of the signals are conducted in the following sections.

3.8.7 Effect of Construction of Tip Load Cell on Output signal for Impact Tests (1)

As can be seen from Fig. 3.4 the construction of the load cell makes it necessary to pretension the transducer in order to connect one section of pile to another. Also antitwist pins are inserted in the bottom half of the transducer housing to prevent one section of pile moving in a horizontal plane relative to another.

In order to ascertain if the above mentioned construction had a significant effect on the output signal the following procedure was adopted:-

1. Two arbritary drop heights of 20 mm and 82 mm were used for the experiment.

2. In turn the following steps were taken:-
   (a) The antitwist pins were removed (i.e. no possibility of resistance to compression of the load cell) and impact tests performed.

   (b) The holding screws were then removed from the cell (i.e. no pretension) and impact tests again performed.

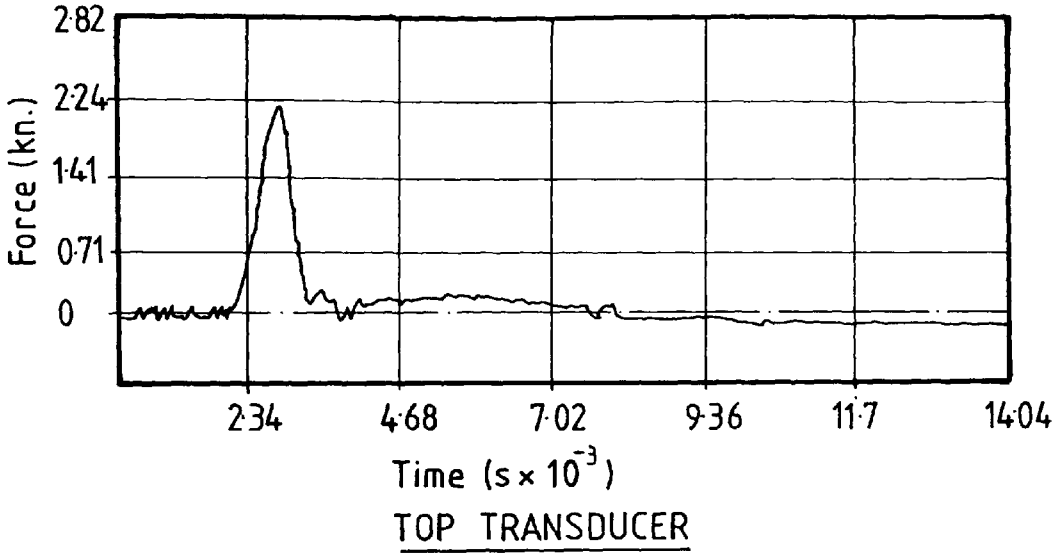

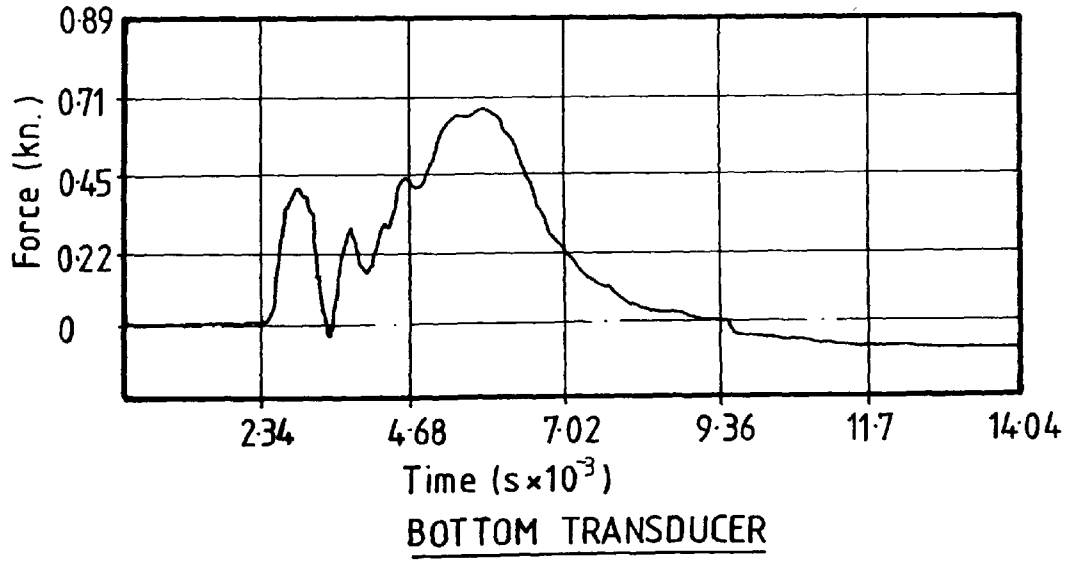

FIG. Nº 3.12 SHOWING THE VARIATION OF OUTPUT SIGNALS FOR THE TOP AND BOTTOM TRANSDUCERS

The results are shown in Fig. 3.13 and show that the peak force does not vary significantly for any combination of disassembly used.

It can also be seen from Fig. 3.13 that the overall form of the signal is not affected by the transducer housing.

It was therfore decided to perform a second set of impact tests to establish the effect of the bearing surface on the output signal of the bottom transducer.

3.8.8 Signal Changes with Varying Bearing Surfaces

Five different bearing surfaces were chosen namely, concrete, steel, wood, clay and rubber. The testing procedure was as described in section 3.8.5.

As can be seen from Fig. 3.14 the type and magnitude of the force/time signal for the bottom transducer varies significantly for different bearing surfaces. The top transducer however remains much the same in both magnitude and shape for the surfaces tested (Fig. 3.15).

Evidence from the results was an increase in peak force for the lower transducer with respect to the top transducer for inflexible surfaces such as concrete and steel. For flexible surfaces capable of substantial deformation such as rubber or clay the reverse was true.

In an effort to quantify and rationalise these results the experiments were conducted under more rigorous conditions.

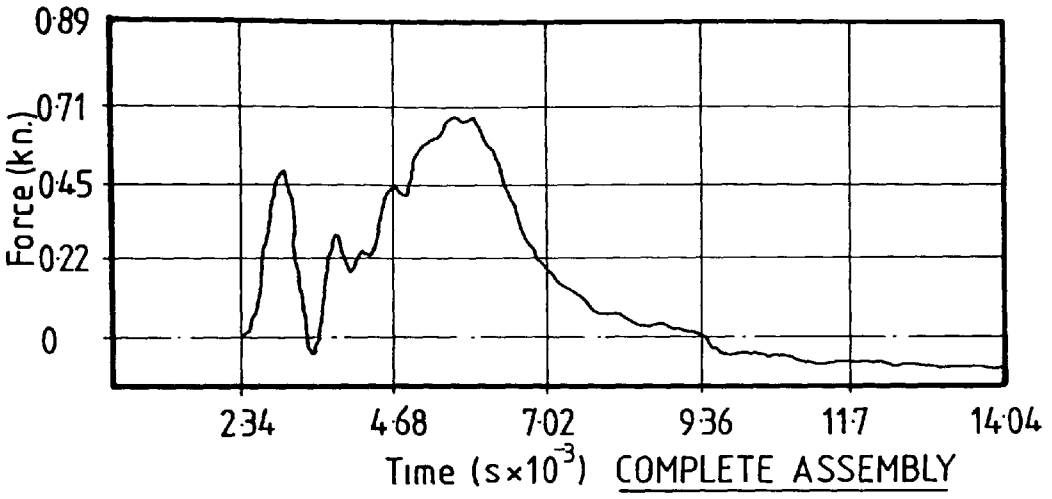

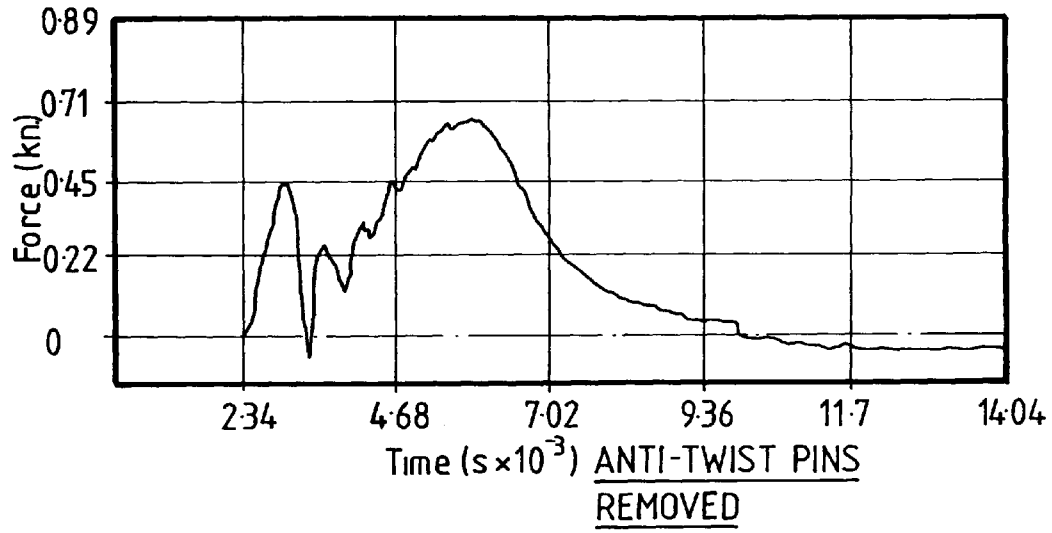

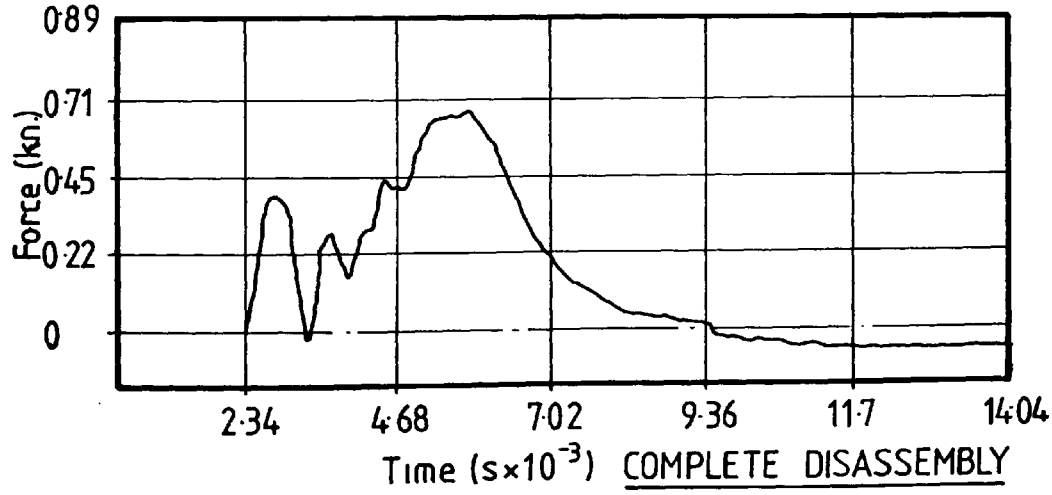

FIG. Nº 3.13 SHOWING THE VARIATION IN THE OUTPUT SIGNAL AS THE TRANSDUCER HOUSING IS DISASSEMBLED

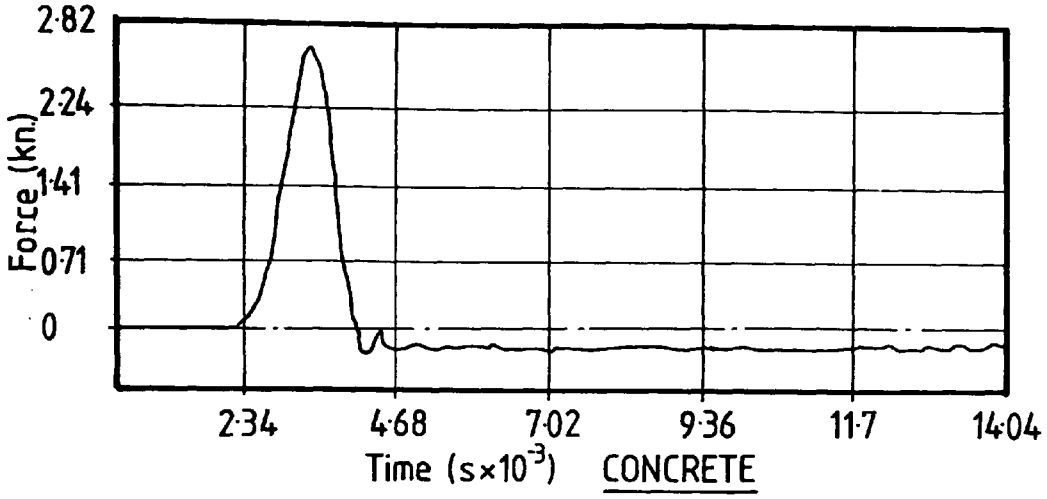

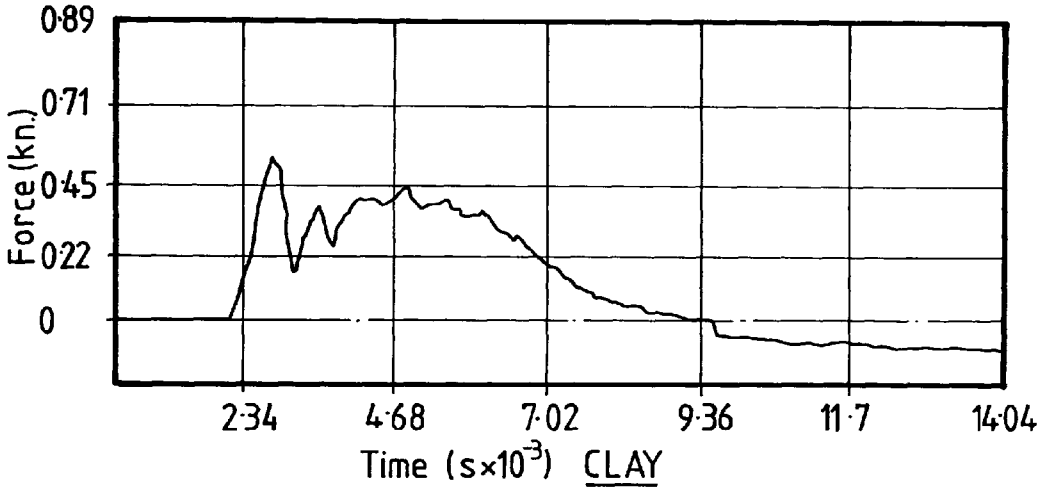

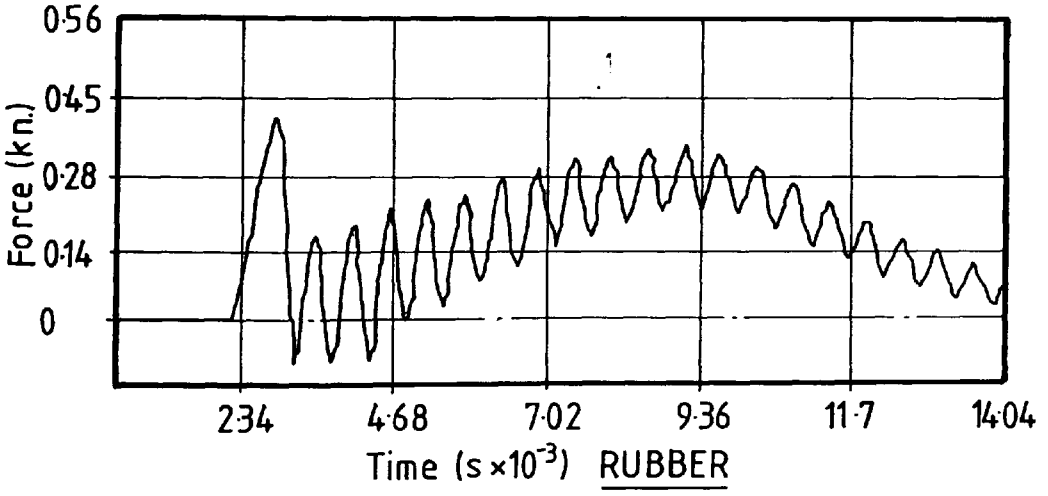

FIG. N° 3.14 SHOWING THE VARIATION IN THE OUTPUT SIGNALS FOR DIFFERENT BEARING SURFACES (TIP TRANSDUCER)

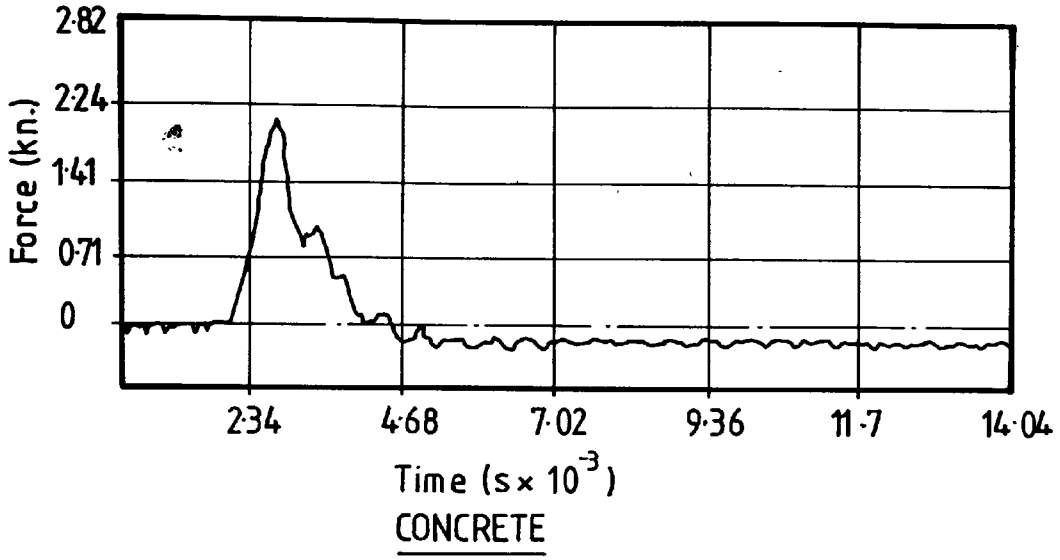

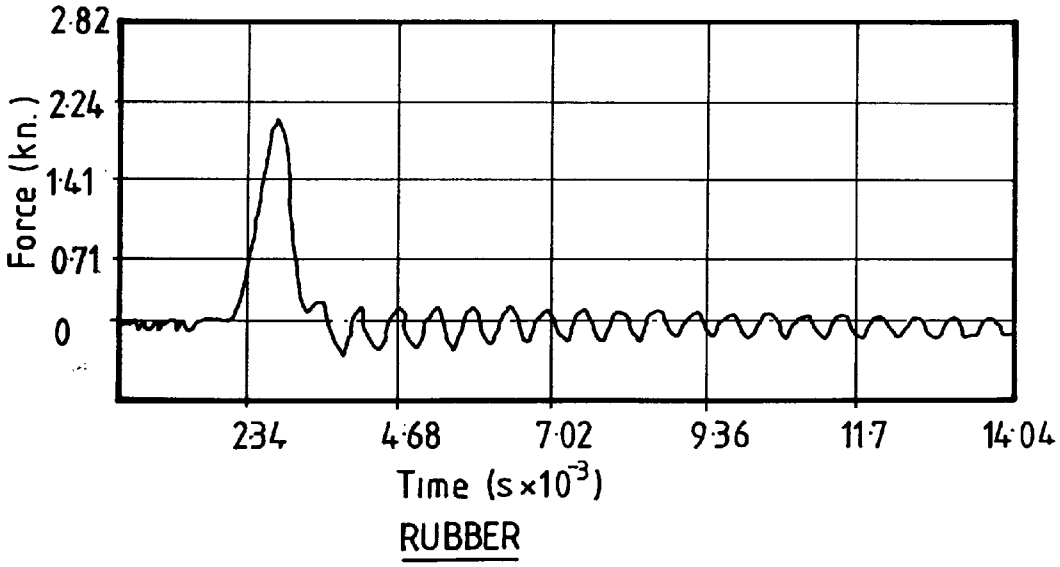

FIG. Nº 3.15 SHOWING THE VARIATION IN THE OUTPUT SIGNALS FOR DIFFERENT BEARING SURFACES (TOP TRANSDUCER)

3.8.9 Rigorous Test Procedure

A typical test set up is shown in Plate 3.2 and was conducted as follows:-

1. The model pile was set up in a 10 Kn triaxial loading frame so that it was perpendicular to the bearing surface in all planes.

2. The ram was dropped on to the model pile from a set height of 20 mm for a total of 10 consecutive blows, the force time signal for each blow being recorded and documented.

3. Steps (1) and (2) were then repeated a total of 10 times (5 in the case of sand) on different areas of the same material.

4. The results were then averaged and a graph of peak force/blow number drawn (Fig. 3.16).

In the case of Leighton Buzzard Sand the process was a little different. The sand was contained in a Standard California Bearing Ratio (CBR) mould, the surface of which was levelled off prior to each test. The variation in sand density, initial penetration due to self weight and final penetration after driving are shown in Fig. 3.17.

3.8.10 Discussion of Test Results

3.8.11 Effect of Pile Penetration on the Peak Force against Blow Number Curve Shape

As can be seen from Fig. 3.16 apart from surface such as sand and rubber the resistance of which remains much the

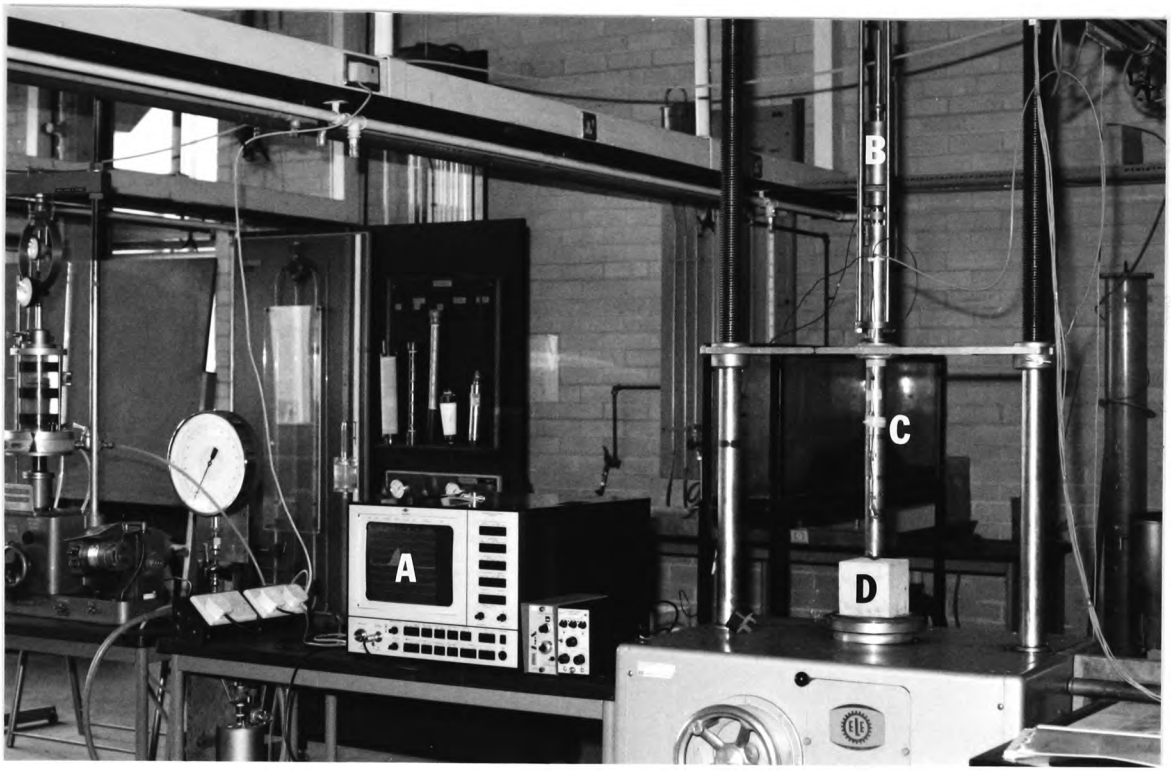

KEY:

A. Monitoring Equipment

B. Driving Rig

C. Model Pile

D. Bearing Surface

PLATE 3.2 Showing Typical Test Set-Up for Impact Tests on Various Bearing Surfaces

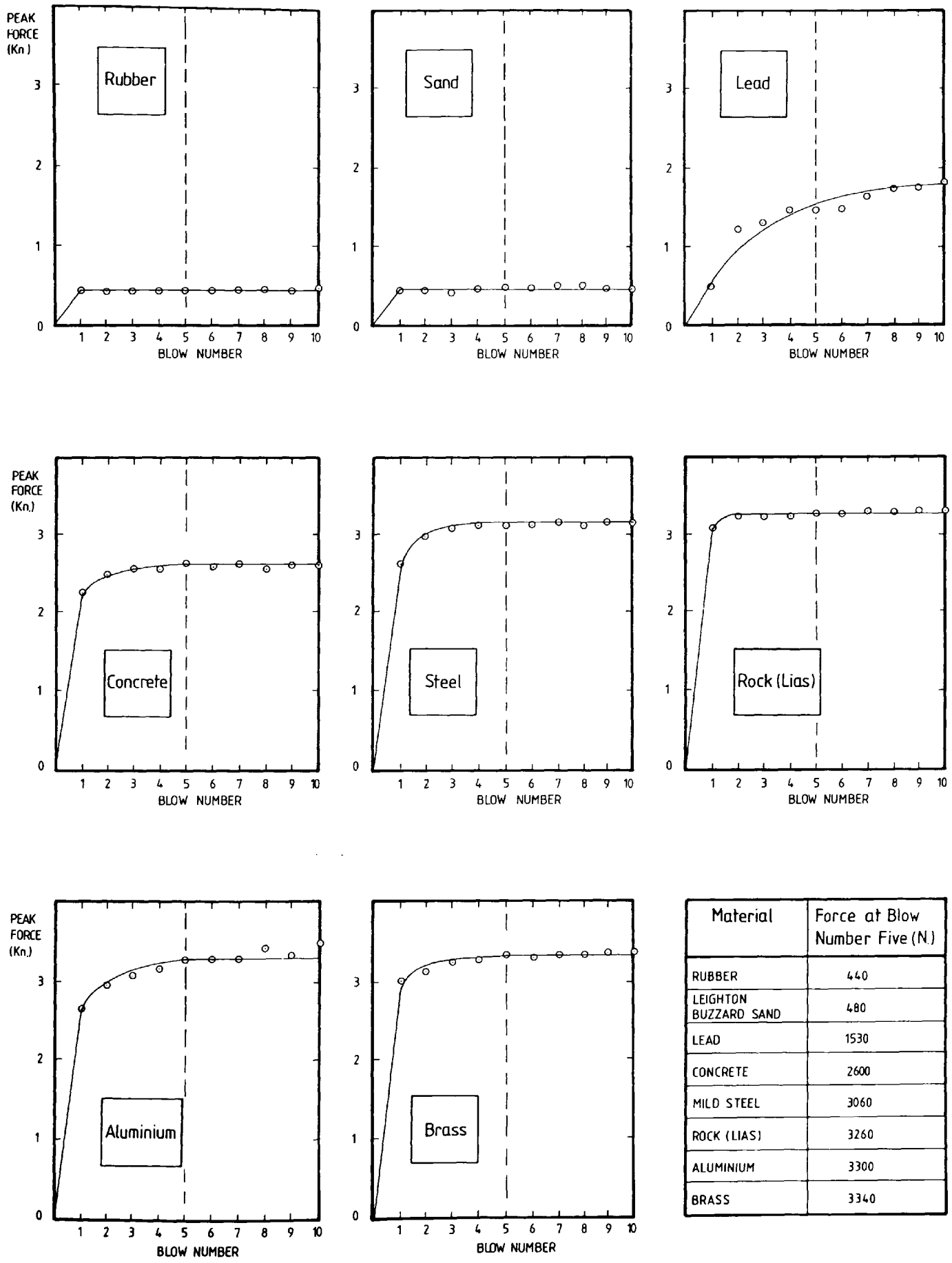

Material	Force at Blow Number Five (N.)
RUBBER	440
LEIGHTON BUZZARD SAND	480
LEAD	1530
CONCRETE	2600
MILD STEEL	3060
ROCK (LIAS)	3260
ALUMINIUM	3300
BRASS	3340

FIG 3.16 SHOWING GRAPHS OF PEAK DYNAMIC FORCE / BLOW NUMBER FOR DIFFERENT END BEARING SURFACES (38mm. DIAMETER MODEL PILE)

TEST N°	1	2	3	4	5
Initial Penetration (m.m.)	40	42	40	45	43
Final Penetration (m.m.)	61	61	60	68	71
Average Density (Kg./cu.m)	1510	1520	1520	1500	1490

FIG. N° 3.17 SAND DATA (Rigorous Test Procedure)

same over the 10 blows an increase in peak force was observed up until a maximum value was reached.

The average maximum force of the tip transducer for rubber and sand was 68% less than the input force but generally higher than the input force when bearing on surfaces such as rock or concrete.

These effects can be readily explained using one dimensional wave theory, as shown by Bredenberg and Broms (1981). Referring to Fig. 3.18 the forces acting at the pile point are:-

fs (t) = point resistance
fi (t) = force of the initial stress wave
fr (t) = force of the reflected stress wave

At equilibrium of the pile point
fs (t) = fi (t) + fr (t)

If the reflected stress wave is compressive which is the case for hard surfaces such as concrete and steel the superposition of initial and reflected waves yields a greater point resistance than the input force would suggest.

However, if the bearing surface is capable of substantial deformation such as sand then the converse is true, (reflected wave being tensile).

Similar findings have been reported by Goble and Rausche (1972) with respect to increased tip force and also by Dismuke (1979) who reported on field tests on H section steel piles.

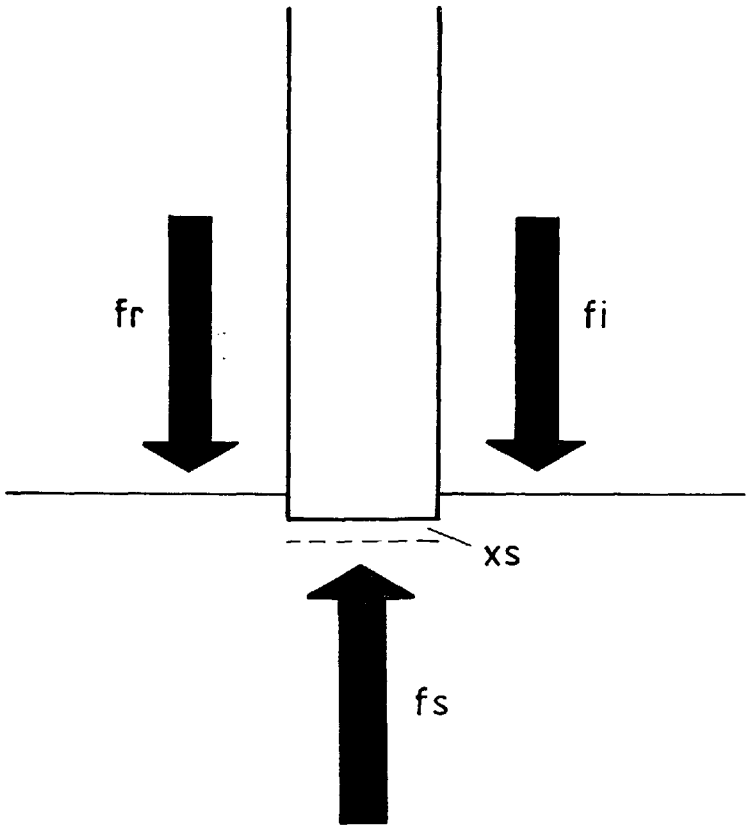

$fs(t) = fi(t) + fr(t)$

fs = Point Resistance
fi = Force of the Initial Stress Wave
fr = Force of the Reflected Sress Wave
xs = Point Displacement

FIG. Nº. 3.18 FORCES AT A PILE POINT
(After Bredenberg & Broms (1982))

The only graph in which a peak force had not been obtained was in the case of lead and was due to the fact that the pile had not reached an equilibrium position within the ten blows.

Bredenberg and Broms (1982) stated that 'The actual dynamic point force relationship for a single blow depends to a large extent on the contact between the pile point and the rock'. From this it would be logical to assume that the greater the surface area of the pile point in contact with the bearing surface the greater the force.

3.8.12 Type and Magnitude of Force/Time Records

(a) Top Transducer (Input Signal)

The shape of signal obtained for the bearing surface was characterised by a singular triangular peak with an average maximum value of 2.04 Kn.

The signal was not affected greatly by any bearing surface for the small drop heights used. Goble and Rausche (1972) state that 'the pile top stresses at the time of impact depend on Ram impact velocities only'.

Using one dimensional wave theory the time taken to reach peak force at the pile top is 2L/C (Timoshenko and Goodier) (1970) where L = pile length

C = value of longitudinal wave propogation

Thus working on a value for C of 5190 m/s and given a model pile length of 630 mm the time taken to reach peak force is 0.242 milli-seconds, i.e. 26 times longer than theory suggests.

Bredenburg and Broms (1982) suggests that distortion of the wave front as it travels down the pile changes the rise time of the force signal. Also the short length of model pile involved will cause quatitative analysis of the signals to be suspect.

However subsequent sections will show that a much more favourable correlation with wave theory is achieved when the pile is fully restrained in a soil medium.

3.8.13 Relationship between Peak Force and Modulus of Elasticity (E) of the Bearing Surface

A correlation between one of the bearing surface properties such as density, modulus of elasticity, longitudinal wave speed was attempted.

The only one that proved useful was a correlation between modulus of Elasticity and peak dynamic force. Referring to Fig. 3.16 the peak force at blow number 5 was chosen to plot against the material E values because apart from lead all the other bearing surfaces had reached a set value at this time. The subsequent graph shows clearly a relationship between peak force and modulus of elasticity and is characterised by the polynomial:

$Y = 460 \times 103.07x - 2.36x^2 + 0.03x^3 - 0.0026x^4$ and is shown in Fig. 3.19. It must be stressed that this relationship is only valid for the particular length and configuration of pile used but the phenomenon may be worthy of further research at a later date.

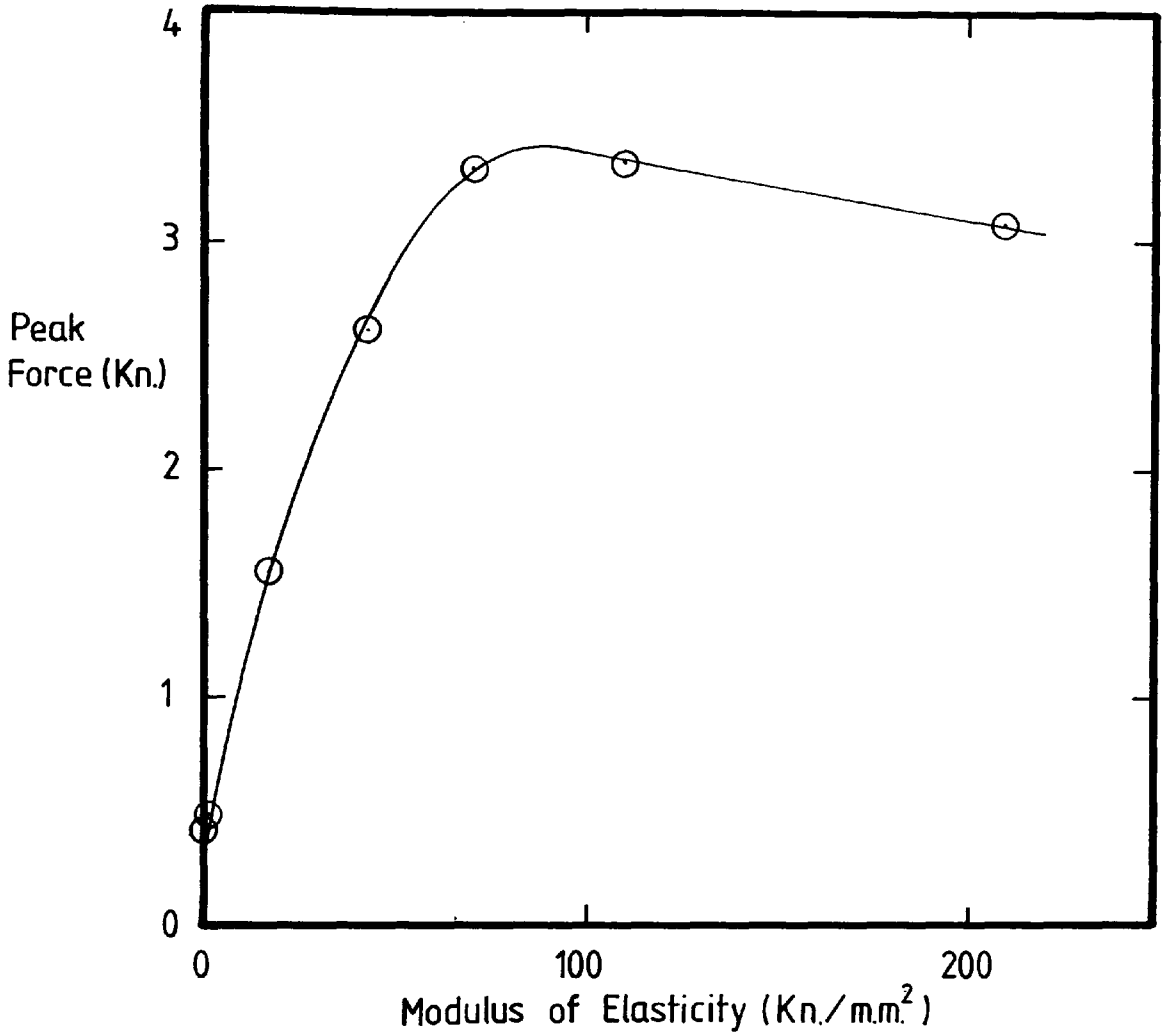

FIG 3.19 SHOWING RELATIONSHIP BETWEEN MODULUS OF ELASTICITY FOR DIFFERENT END BEARING SURFACES AGAINST PEAK DYNAMIC FORCE FOR MODEL PILE

3.8.14 Methods of obtaining Modulus of Elasticity Values for the Bearing Surfaces

A brief description of the method of determining the E values is included at this point for completness.

(a) Metals (except lead)

The E values for the metals were obtained by standard tensile tests on the material specimens and carried out in an Instron 1251 machine.

(b) Rock (Lias)

The E value for the rock was an average value obtained from a number of straingauged specimens stressed in an E.L.E. "Rocktester". These experiments were conducted as part of research carried out at the polytechnic by Grimes (1986) and concerned with rock weathering along the 'Heritage Coast'.

Leighton Buzzard Sand

The E value for Leighton Buzzard Sand was obtained by Werscning (1985) using the relationships given by Cooke (1974) and Barkan (1962).

i.e. $$v = \frac{fsd}{2G} \log e \frac{r}{nd} \qquad \text{---- (1)}$$

where fs = transfer stress
v = shaft displacement

$$E = 2(1 + v)G \qquad \text{---- (2)}$$

where $v = 0.3$

By back analysis, equation (1) yielded a value for G of 10 Mn/m^2,

therefore $E = 2(1 + 0.3)10$

$E = 21.3\ Mn/m^2$

i.e. $0.0213\ Kn/mm^2$

3.8.15 Effect of Overall Pile Construction on Output Signals

A mild steel rod of 25 mm diameter and the same overall length as the model pile was used.

The two transducers were positioned along the axis of the rod and in the same spatial position as in the model pile. The results of impact tests (conducted as in impact test (2)) are shown in Figs. 3.20 and 3.21 for the top and bottom transducers.

3.8.16 Comparison of Output Signals for the Solid Bar and and Model Pile

1. Top Transducer

As can be seen from Figs. 3.15 and 3.20 the two signals for each surface compare favourably in both shape and magnitude.

2. Bottom Transducer

Figs. 3.14 and 3.21 show that comparison of the bottom signals are somewhat more difficult.

For surfaces such as concrete the signals compare favourably in both shape and magnitude.

For the more flexible surfaces such as clay and rubber, while the overall shapes are the same the magnitudes of the peak forces differs slightly, the lower transducer on the pile displaying the higher peaks.

This effect cannot be explained fully but may be due to eccentricity of loading and stress concentration within the pile.

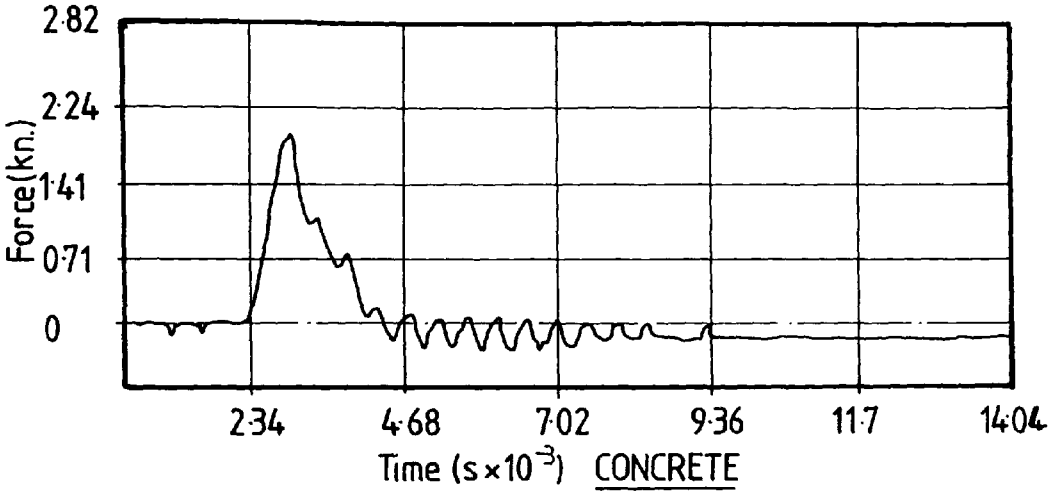

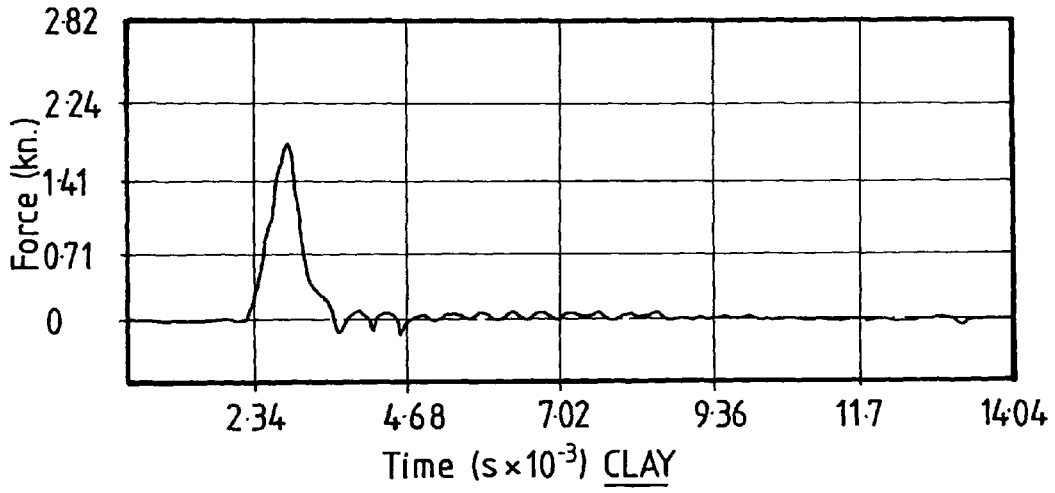

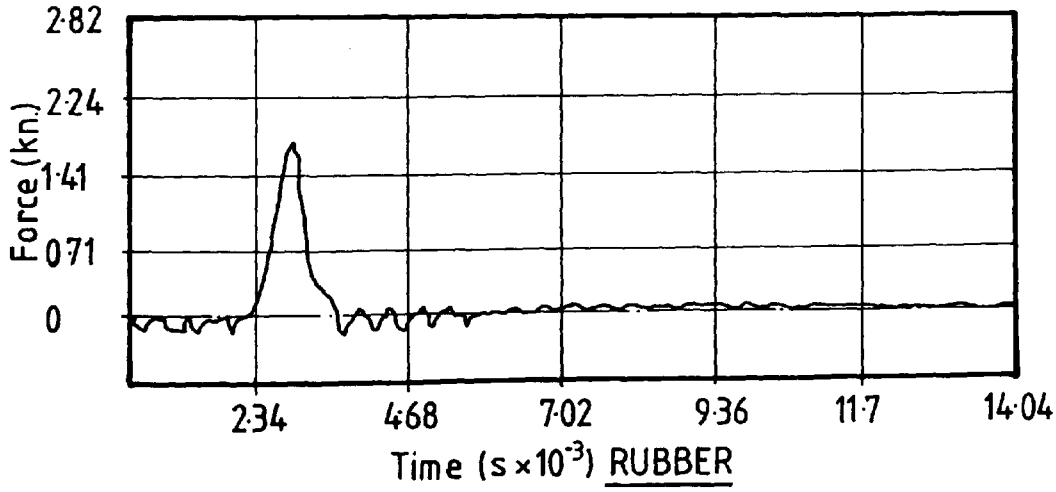

FIG. Nº 3.20 SHOWING THE VARIATION IN THE OUTPUT SIGNALS FOR DIFFERENT BEARING SURFACES (TOP TRANSDUCER), SOLID BAR

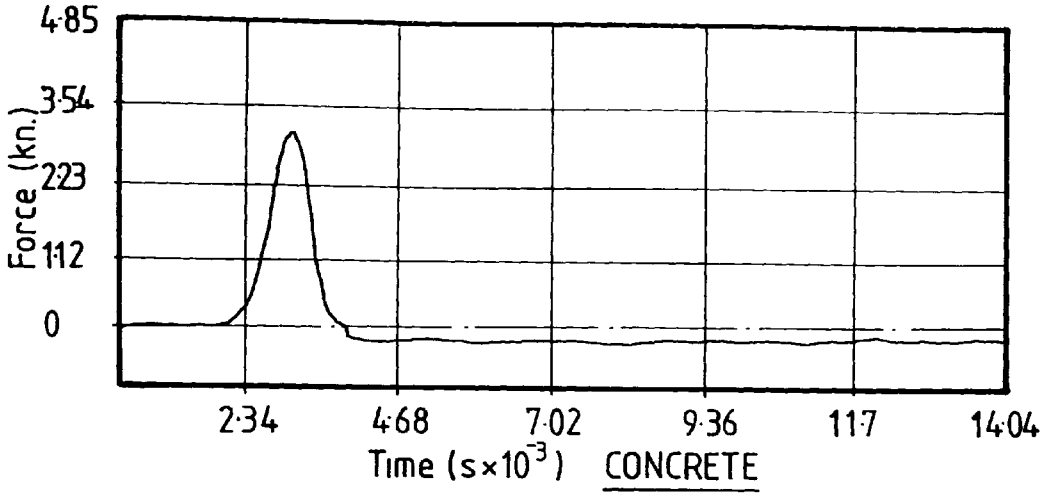

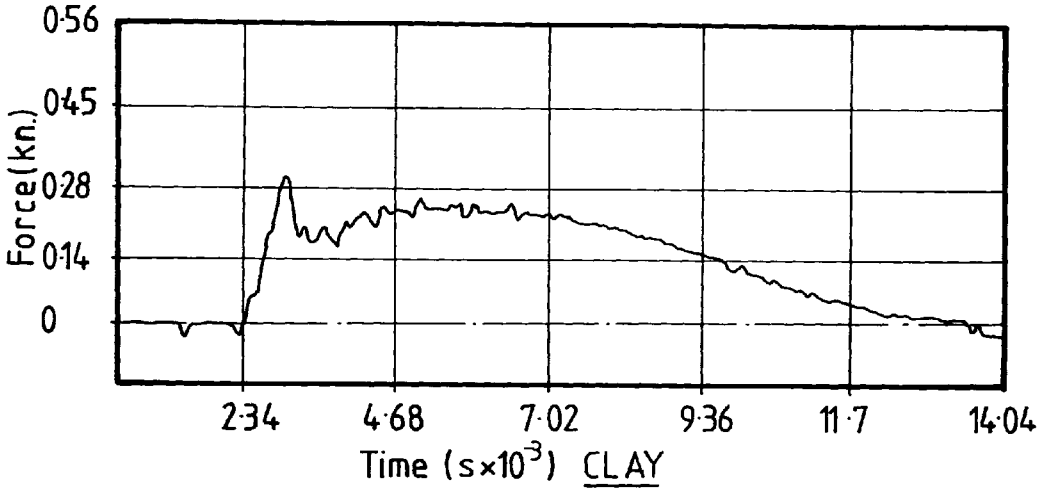

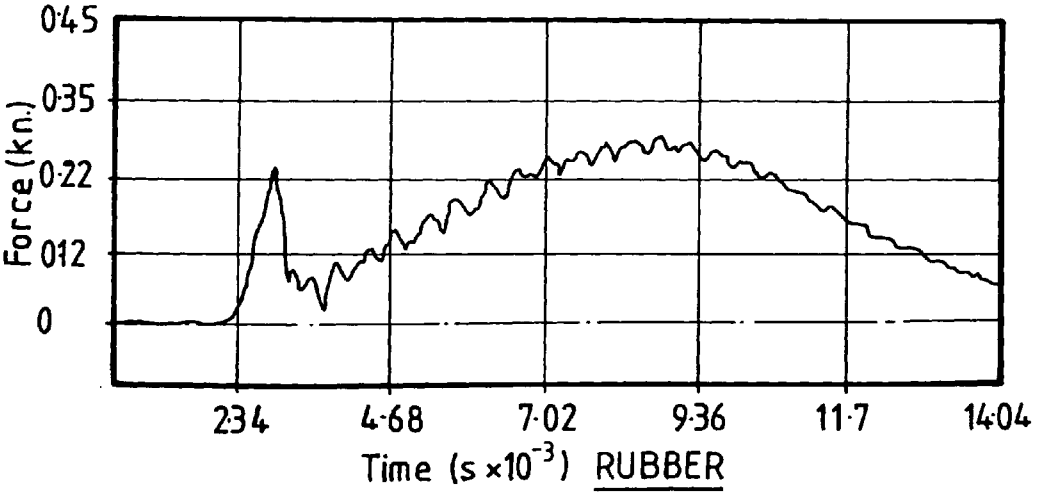

FIG. Nº 3.21 SHOWING THE VARIATION IN THE OUTPUT SIGNALS FOR DIFFERENT BEARING SURFACES (TIP TRANSDUCER), SOLID BAR

3.8.17 Effect of Gross Angular Tilt on the Output Signal

In order to study the effects of pile misalignment of the output signals impact tests were again performed with the pile bearing on a concrete surface. The 1.73 Kg mass was dropped from a height of 12.5 mm with the pile being inclined at various tilt angles in relation to the vertical.

Results are shown in Figs. 3.22 and 3.23 for angles of inclination from the vertical of 0°, 10° and 20°.

As can be seen from the figures the magnitude of peak force is affected adversely with a drop of 6.4 per cent for the top and 16.03 per cent for the bottom. The type of signal however remains unaffected.

The worst angle of tilt likely to be encountered during the model tests in 2° and therefore the effects of tilt will be negligable.

3.8.18 Conclusions drawn from Preliminary Dynamic Tests

As a result of the preliminary tests the following conclusions were drawn:-

(1) The magnitude of the signals are consistent with one dimensional wave theory (Timoshenko and Goodier) with the bottom transducer recording a greater peak force than the top transducer for bearing surfaces such as concrete.

(2) The peak force at the pile top is dependant on ram impact velocity only (Goble and Rausche(1972)).

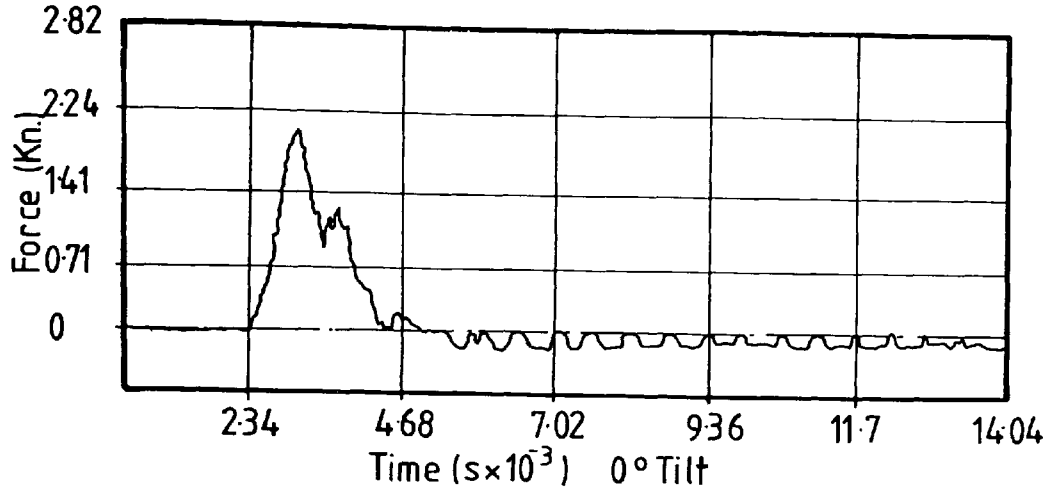

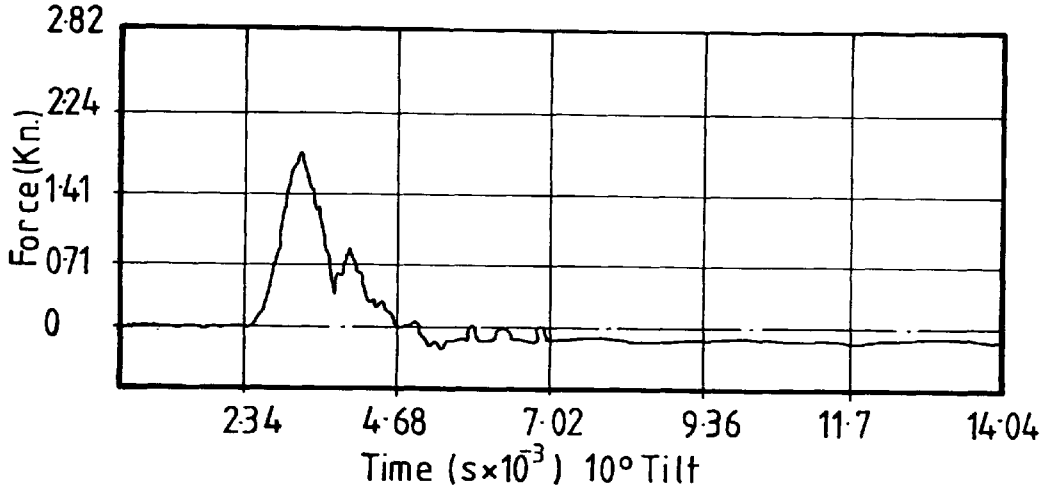

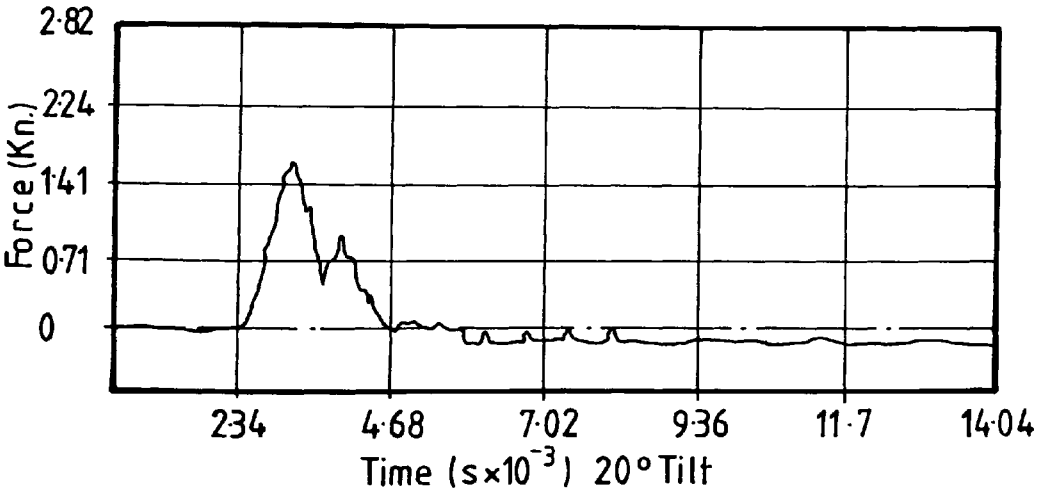

FIG. N° 3.22 SHOWING THE VARIATION IN THE OUTPUT SIGNALS FOR DIFFERENT ANGLES OF AXIAL TILT (TOP TRANSDUCER)

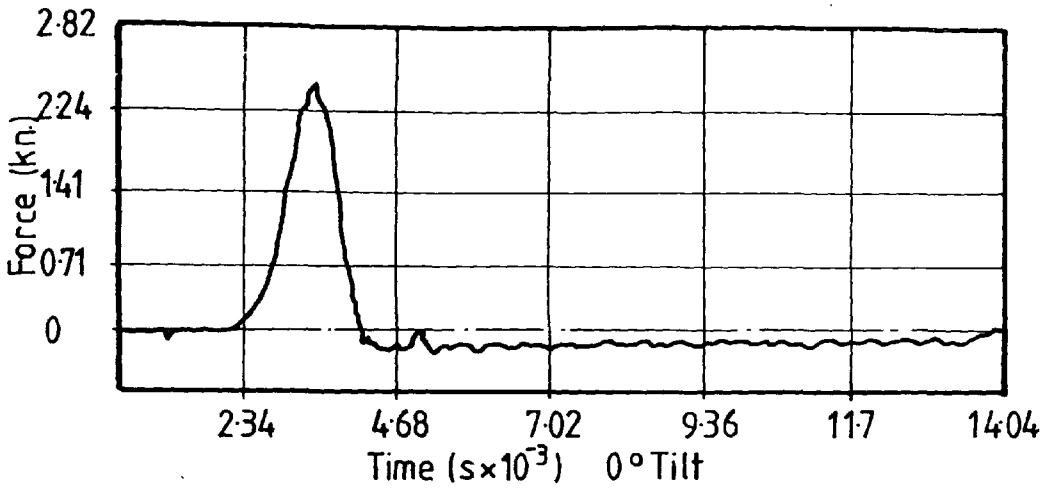

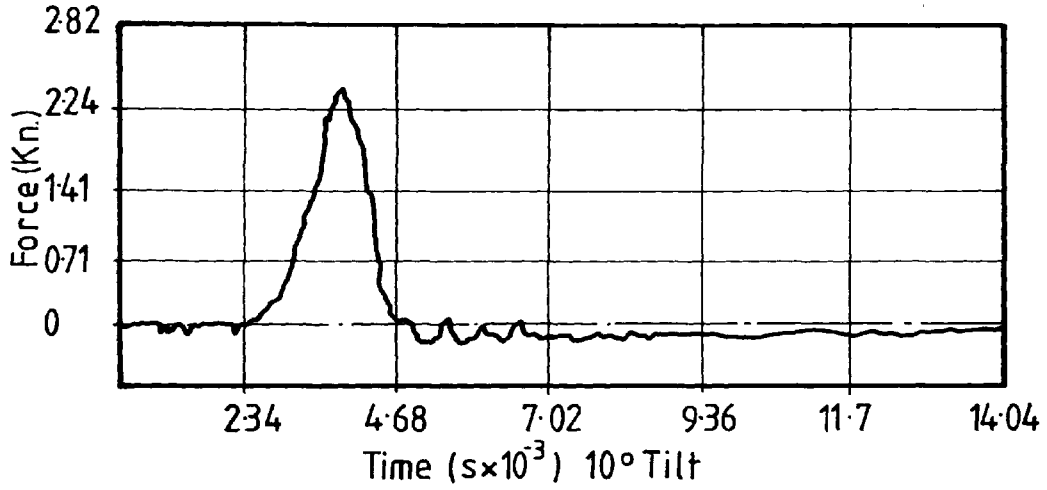

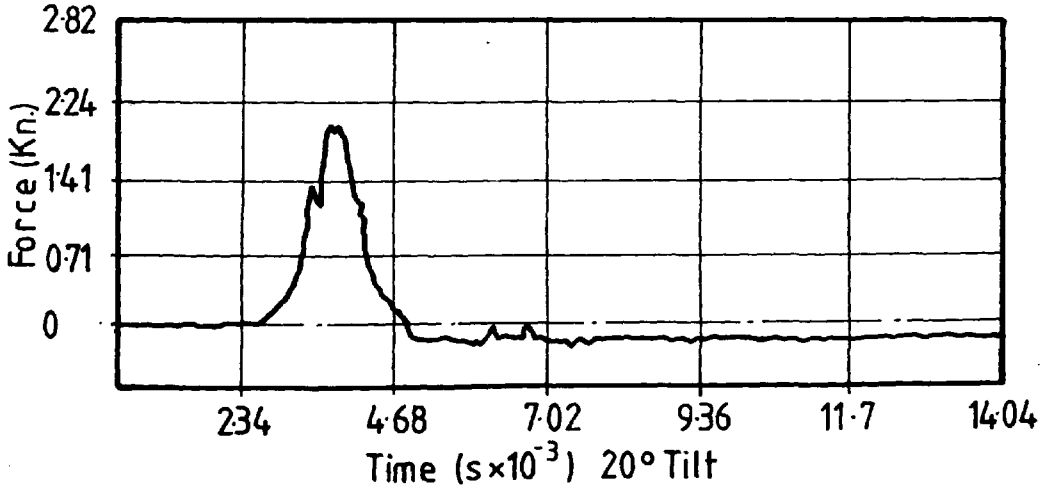

FIG. N° 3.23 SHOWING THE VARIATION IN THE OUTPUT SIGNALS FOR DIFFERENT ANGLES OF AXIAL TILT (TIP TRANSDUCER)

3.9 Experimental Procedure (Small Scale Tests)

Some small scale pile experiments were conducted in sand and sand/clay mediums and are described in the foregoing sections.

3.9.1 Soil Placement and Preparation

3.9.2 (i) Sand only

Prior to sand placement the perspex tank and base used in the experiments were placed on a fork lift for ease of movement. The procedure for placement was then as follows:-

(1) Known masses of sand were placed in the tank by pouring the sand carefully from a small scoop. Care was taken to ensure that the maximum height of drop of the sand was less than 50 mm.

(2) This process was repeated until the tank was filled and the top levelled off.

3.9.3 (ii) Sand over Clay

Red Marl Preparation

The clay used was a local red marl (Mercia Mudstone) the properties of which are fully documented (Werscheing, 1986) and given in Appendix 6.1. Having obtained the marl from site it was then dried and crushed to a fine powder. It was decided to aim for an undrained apparent cohesion (Cu) value of 50 Kn/m^2 for the model tests. The necessary moisture content needed to yield the undrained apparent cohesion (Cu) value was obtained from a graph of moisture content/log undrained apparent cohesion(Cu) value (Werscheing, 1986) and was approximately 18.5 per cent.

A plastic U.P.V.C. pipe of internal diameter 38 cm x 31 cm high was cut and secured to the bottom of the tank to contain the marl (Fig. 3.7). One side of the pipe was cut from top to bottom and fixed with fasteners in order that the pipe could be separated from the marl after each test.

3.9.4 Mixing Procedure

Working on a compacted density of 2100 Kg/m^3 the amount of marl to be mixed was approximately 80 Kg. It was decided to mix 100 Kg. so that there would be enough marl to perform three tests allowing for wastage due to moisture content and triaxial tests.

It was decided to start with a moisture content of 18.5% initially and to use a pocket penetrometer to determine an approximate value of cchesion (Fig. 3.24).

Having decided upon what moisture content to use the mixing process was as follows:-

(1) A known amount of marl and water was placed in a 10 Kg Hobart mixer and the timer set for five minutes.

(2) On completion of the mix the approximate undrained apparent cohesion value (Cu) was determined using a pocket penetrometer.

(3) The mixed batch was then placed on a large mixing tray and covered with polythene to prevent moisture loss.

(4) The procedure was repeated until approximately 100 Kg. was mixed.

(5) The marl was then remixed ensuring that different

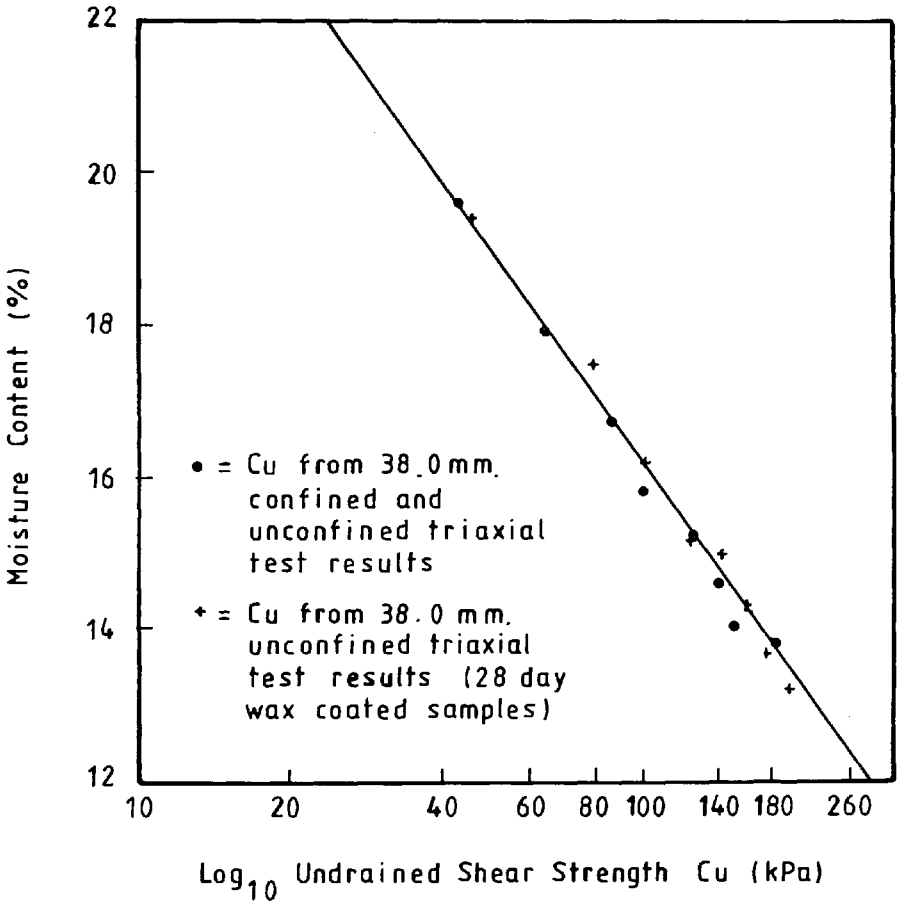

FIG N° 3 24 VARIATION IN UNDRAINED SHEAR STRENGTH OF CLAY WITH MOISTURE CONTENT (After Wersching (1986))

batches were combined together to give a more even moisture content.

(6) The remixed marl was then placed in a bin lined with polythene and covered with a damp cloth then sealed with polythene and allowed to condition for three days.

3.9.5 Marl Placement and Compaction

The pipe used to contain the marl was lined with polythene in order to cut down on the amount of moisture migration from the marl to the sand.

Placement of the marl was as follows:-

(1) A known amount of marl (approximately 10 Kg) was placed in the pipe and a Kango hammer used to compact the marl to as near a zero air voids situation as possible.

(2) This process was repeated until the pipe was full.

(3) The surface was levelled off and a Vinyl spray used, again to prevent moisture migration to the sand. Sand was pressed into the surface of the clay while the spray was still wet in order to form a bond between the sand and the marl.

Sand was then placed over the marl as previously described. The maximum time that a prepared specimen was left standing prior to a test was eighteen hours.

3.9.6 Insitu Density Measurements of Sand

A method for determining the insitu density of dry sand using a mixture of Kaffir D plaster and sand and developed at the

Polytechnic by Werscheing (1983) was used to determine the insitu density of the sand at selected points in the sand only profile tests.

The selected points were as follows:-

(1) Directly under the model pile at a vertical depth of five centimetres from the pile tip after completion of a test.

(2) At the rim of the tank on the same level as (1).

(3) At the rim of the tank at a depth of ten centimetres from the top surface. These results along with moisture content, and triaxial results are shown in Fig. 3.25. The results for the two tests indicate a decrease in density immediately below the pile tip. This phenomenon is also reported by Robinsky and Morrison (1964) with respect to loose sand.

3.9.7 Trial Dynamic Test

A trial dynamic test was conducted using the apparatus shown in Figure No. 3.7 to determine the optimum recorder levels for the tape recorder and charge amplifiers. A blow rate of 12 blows/minute was used and the pile driven into the tank of sand. Driving was not continuous as non-recorded output signals were checked against recorded and replayed signals for authenticity. After it was determined that the recorded and replayed signals were a true representation of the actual signals and that recorder levels were not exceeded, the pile was driven to a set penetration. The dynamic records for the last blow were used as input data to check

Test No.	Test Description	Average Density Kg/m³	Density according to Sand/ Specimen 1	Specimen 2	Specimen 3	Av. Density of Marl Kg/m³	Cu Value of Marl Kn/m²	Value of Ø° of Marl	Av. M/L of Marl (Av. of 9 specimens)
1	Sand Only 12 blows/min	1547.0	1546.4	1555.2	1512.8	--	--	--	--
2	Sand Only 20 blows/min	1527.0	1511.2	1491.0	1488.1	--	--	--	--
3	Sand over Marl 12 blows/min	1544.5	--	--	--	2125.7	48.0	0	18.65
4	Sand over Marl 20 blows/min	1530.99	--	--	--	2138.02	62.5	0	18.34
5	Sand over Marl 40 blows/min	1527.37	--	--	--	2120.58	40.0	0	19.06

FIG. 3.25

a theoretical analysis derived in Chapter 2. Prior to driving into clay a similar procedure was adopted in order to again ensure that recorder levels were not exceeded.

3.9.8 Dynamic Driving in Sand and Sand/Marl Soil Profiles

These tests, using the small scale pile were conducted primarily to gather information for use in the larger scale tests. However some interesting trends were observed and are discussed in the following sections.

The method employed in the tests were as follows:-

(1) The prepared sand or sand/marl specimen was mounted on a 10 Kn triaxial machine and the settlement in the sand layer noted.

(2) The model pile was placed in the frame as shown in Fig. 3.6 and allowed to settle in the sand under its own weight.

(3) The drop weight was then connected and the pile again allowed to settle. The total settlement due to self weight and ram did not exceed 45 mm.

(4) The rest of the driving assembly was then carefully placed around the pile again as shown in Fig. 3.7.

(5) The model pile was then pushed into the soil to a depth of 50 mm.

(6) The upper and lower transducers together with the accelerometer were then connected, the tape recorder switched on and driving commenced.

(7) The number of blows/50 mm were recorded and logged. The total penetration after driving was approximately 390 mm, with 120 mm being in the marl.

The driving rates used in the experiments were as follows:-

(a) Sand Only - 12 blows/min., 20 blows/min.
Sand over marl - " , " , 40 blows/min.

3.9.9 Constant Rate of Penetration Tests for determing Ultimate Bearing Capacity in Model Tests Whitaker (1957)

In this test a rate of penetration between 0.75 mm/min and 1.5 mm/min depending upon the type of soil has been found suitable.

Fig. 3.26 which represents five penetration curves are typical for end bearing piles (Whitaker (1963)). The point at which the substantially linear portion of the graph occurs (ultimate bearing capacity) is difficult to interpret and so Whitaker stated "that it is usually satisfactory to take the force required to cause a penetration equal to 10 per cent of the diameter of the pile base as the ultimate bearing capacity".

3.9.10 Procedure

After the model pile was dynamically driven to a depth of 390 mm the driving assembly and ram were carefully removed. The crosshead on the triaxial frame was then lowered and a 2500 N maximum load proving ring fitted.

Fitted on the proving ring was a linear potentiometer

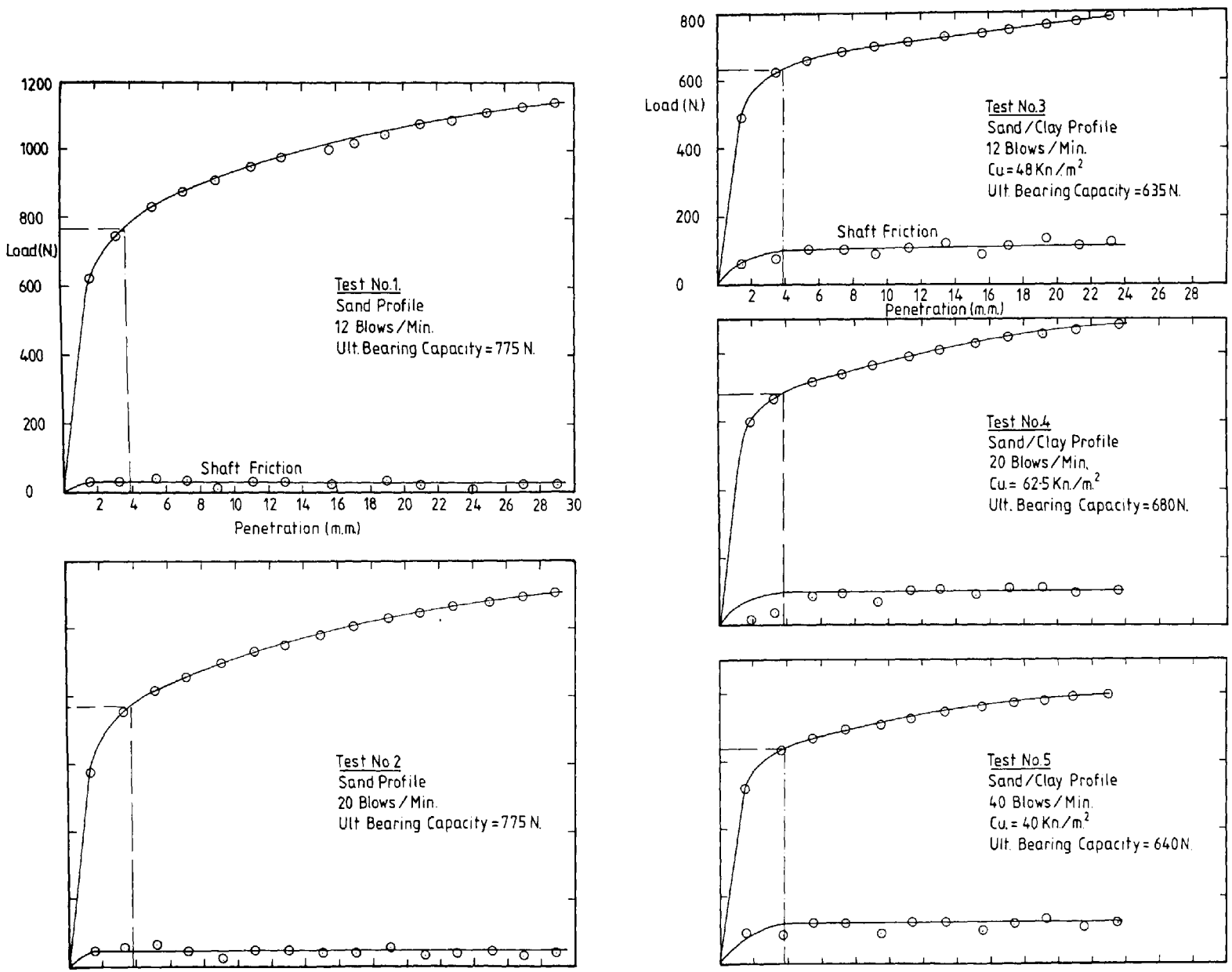

FIGURE No 3.26 CONSTANT RATE OF PENETRATION GRAPHS FOR MODEL TESTS

which had been previously calibrated enabling change in voltage to be converted to load. The proving ring was then positioned over the top of the pile and a C.R.P. test conducted using the triaxial motor running at a speed of 1.0 mm/min.

The top load was monitored via the proving ring while the toe load was monitored using the static axial load cell referred to in Section 3.2.3. The tank movement was monitored using a previously calibrated linear potentiometer of 75 mm maximum stroke. An adjustment was made at each deflection to allow for the compression of the proving ring.

An Orion 3510 data logging system interfaced with a P.E.T. microcomputer was used for overall monitoring and voltage conversion to load and displacement. The test results both from the dynamic and static experiments will be discussed in the foregoing sections.

3.9.11 Sand Dragdown into the Marl

After completion of the C.R.P. test the sand was drained to allow the pile entering the clay to be examined. Plate 3.3 shows a ring or plug of sand of average thickness 3 mm which has been pushed into the clay with the pile.

This dragdown of sand extended to 1.5 diameters from the clay surface. Also evident is a substantial plug of sand which precedes the pile point and is shown in Plate 3.4. The dragdown effect is similar to that suggested by Tomlinson (1971) in which he maintains that sand may be pulled down into an uderlying clay layer by as much as three diameters.

KEY:

A. Sand Ring Dragged Down Into The Clay

PLATE 3.3 Showing Ring of Sand Pushed into the Clay due to Driving

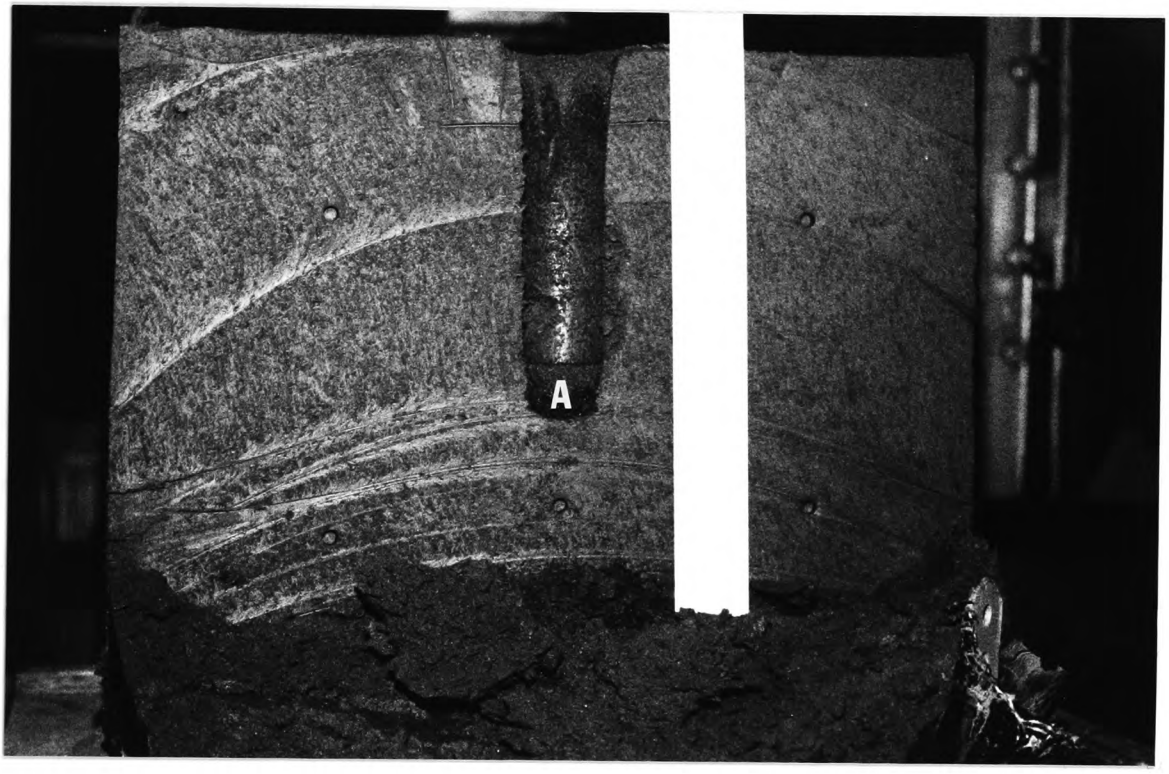

KEY:

A. Sand Plug

PLATE 3.4 Showing Sand Plug below the Pile Toe

The granular barrier between the pile wall and the clay formed by driving may substantially reduce cohesion over this portion of the pile shaft. In order to study these effects the marl was cut down the centre with a "cheese wire".

3.9.12 Shear And Moisture Content Samples

After the clay mass had been cut five core samples were taken, two for unconfined compression tests and three for immediate undrained triaxial tests at confining preasures of 344.5, 689 and 1019.72 Kn/m^2. These values were choosen because the axial stress as estimated from the C.R.P. graphs was 660 Kn/m^2 and hence reproducing a similar situation in the triaxial apparatus.

Moisture content samples were taken at four random points after completion of a test and combined with the triaxial and unconfined samples to give nine values of moisture content. The average moisture content together with the values are shown in Fig. 3.25.

3.9.13 Ultimate Bearing Capacity for Model Tests

As can be seen from Fig. 3.26 the type of load deflection curve obtained does not vary significantly in all of the tests.

The ultimate bearing capacity for the sand only profile is slightly greater (16%) than the average bearing capacity for the sand/clay profile tests.

The slight differences are not significant with the decrease in bearing capacity being attributed to the decrease in shear strength caused by remoulding of the clay (Cummings et

al (1950), Orje and Broms (1967). Another factor may be the dragdown of sand into the clay causing a loss of adhesion.

Also evident is that the driving rates used has little or no effect of the ultimate bearing capacity and is similar to the findings of (Jolly 1963). Jolly stated "that although driving increases the skin friction there is a subsequent decrease in end bearing so that the maximum difference between bearing capacity for statically and dynamically driven piles is 5%".

3.10 Dynamic Driving Results from Small Scale Tests

3.10.1 Top Transducer (Input Signal)

3.10.2 Type of Signal

As is to be expected the type of force time signal for the two soil profiles used is very similar (Fig. 3.27). The only deviation being that the magnitude of the peak force varies somewhat and is to some extent dependant on the soil resistance. This phenomenon has been explained in Section 3.8.11.

3.10.3 Magnitude of Peak Force

Evident from the preceeding sections and highlighted in Fig. 3.28 is that the peak force is dependant on ram impact velocity. However, this statement must be qualified to some extent. The magnitude of the peak force is also dependant on the area of the pile point in contact with the bearing surface (Bredenberg and Broms (1981)).

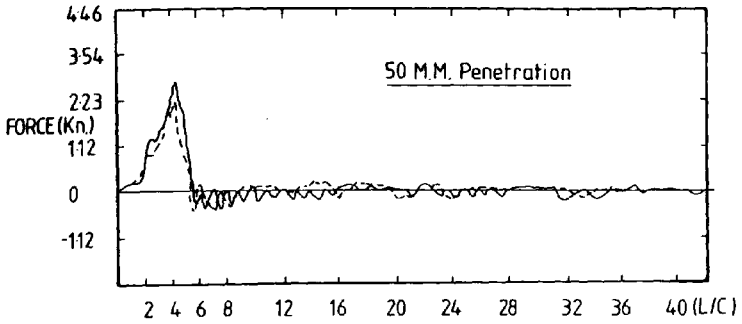

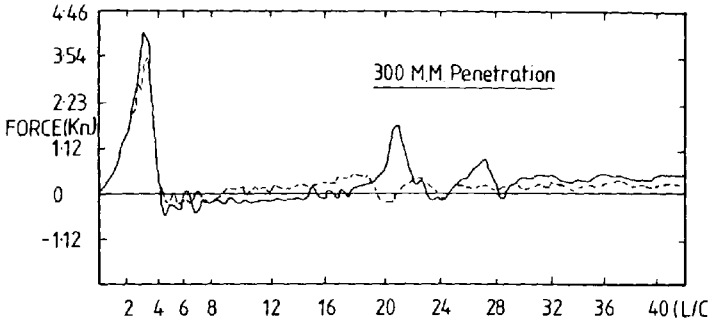

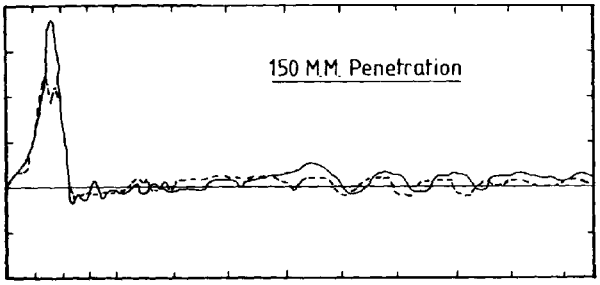

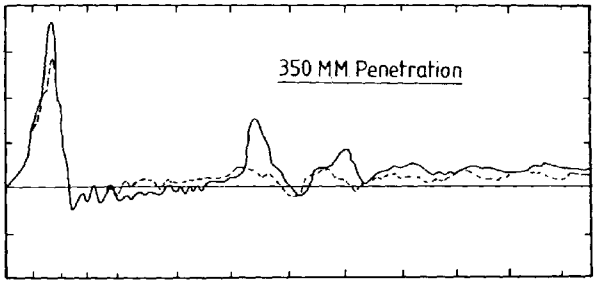

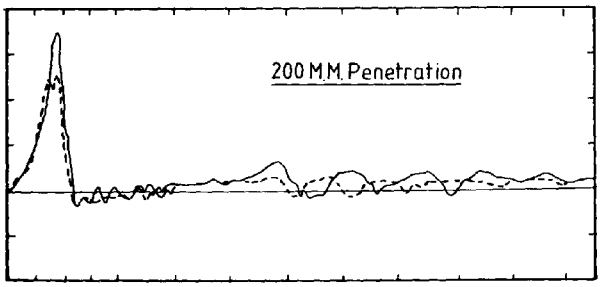

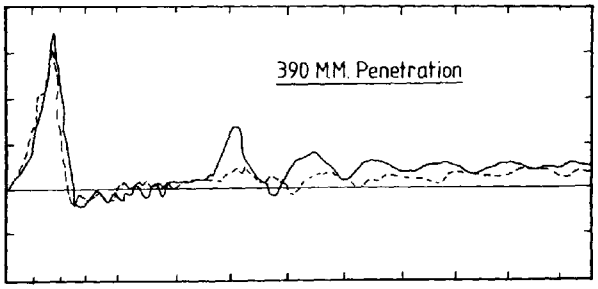

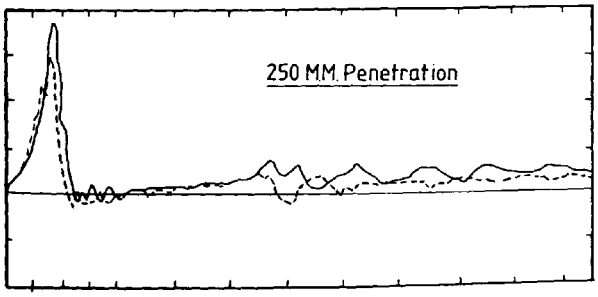

KEY :- – – – SAND PROFILE (TEST 1.)
——— SAND / MARL PROFILE (TEST 4.)
L/C = 0·1214 × 10⁻⁴ SECONDS

VARIATION WITH DEPTH OF FORCE / TIME SIGNALS (Toe Transducer) FOR DIFFERENT SOIL PROFILES

FIGURE No. 3.27

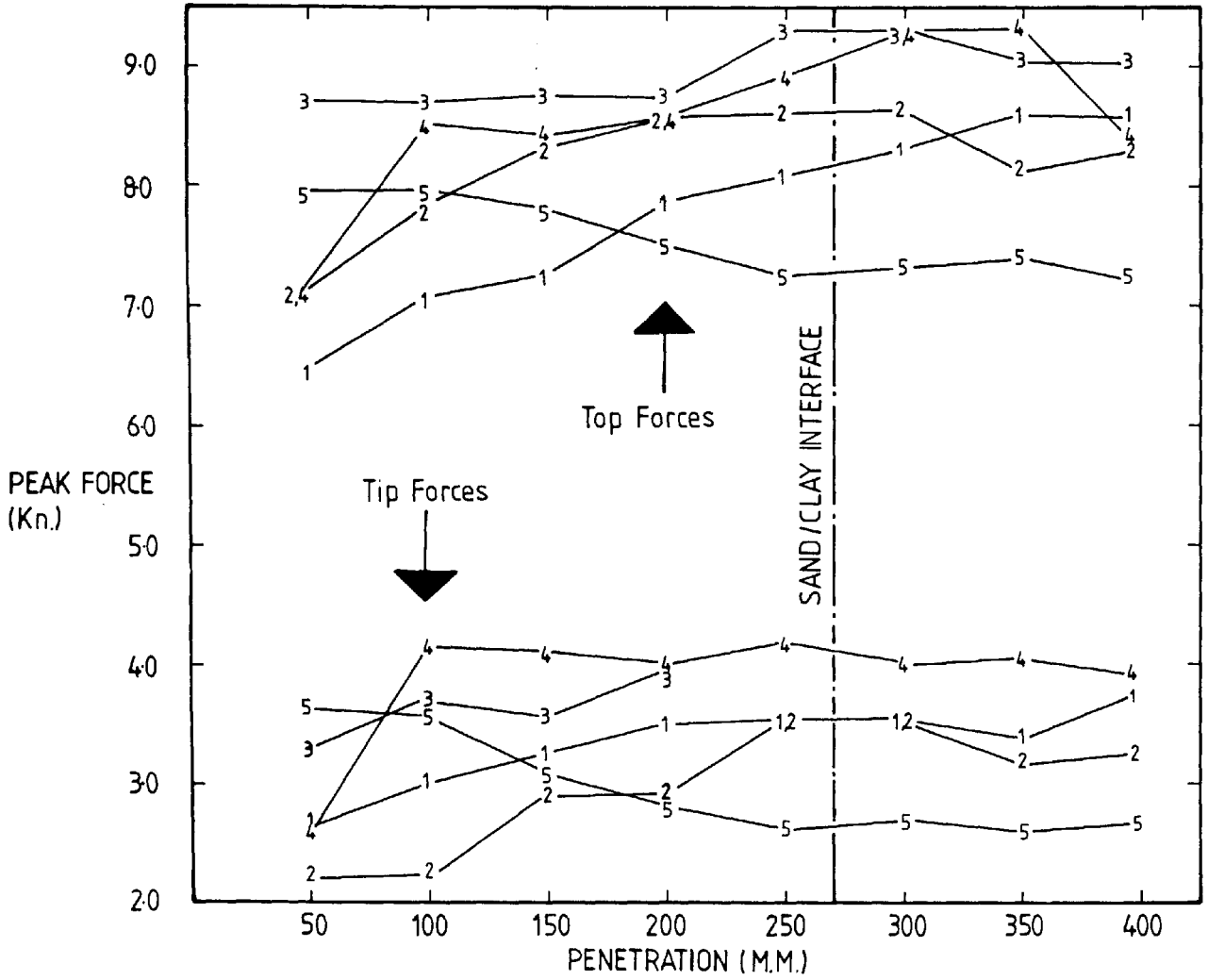

TEST No.	SOIL PROFILE	BLOW RATE
1	Sand Only	12 / Min.
2	" "	20 "
3	Sand/Clay	12 "
4	" "	20 "
5	" "	40 "

PEAK FORCE / PENETRATION FOR TOP AND BOTTOM TRANSDUCERS (MODEL TESTS)
FIGURE No. 3.28

3.10.4 Toe Transducer (Bottom Signal)

The type of signals obtained from the toe transducers varied with the different soil profiles used (Fig. 3.27) the main features of which were:-

3.10.5 (1) For Sand Only

The force time signal for the sand only profile was characterised by a single triangular peak and subsequent insignificant reverberations (Fig. 3.27).

The magnitude of the peak force was somewhat less than for the sand/clay tests and was again due to the greater resistance of the clay bearing surface. The type of signal did not alter significantly for any pile penetration.

3.10.6 (2) For Sand/Clay

For initial penetration up to the sand clay/interface the force/time signal was similar to the signals in the sand only profile, the only difference being that the peak force was somewhat higher. This was reflected in the graph of penetration/number of blows (Fig. 3.29) in which the number of blows needed to drive the pile to the sand/clay interface level was significantly greater for all the sand/clay profile tests.

As the pile penetrated the clay however a secondry peak of appreciable magnitude built up (Fig. 3.27). It is not exactly known why this occurred but it may be due to the change in end fixety encountered with the pile end bearing in clay.

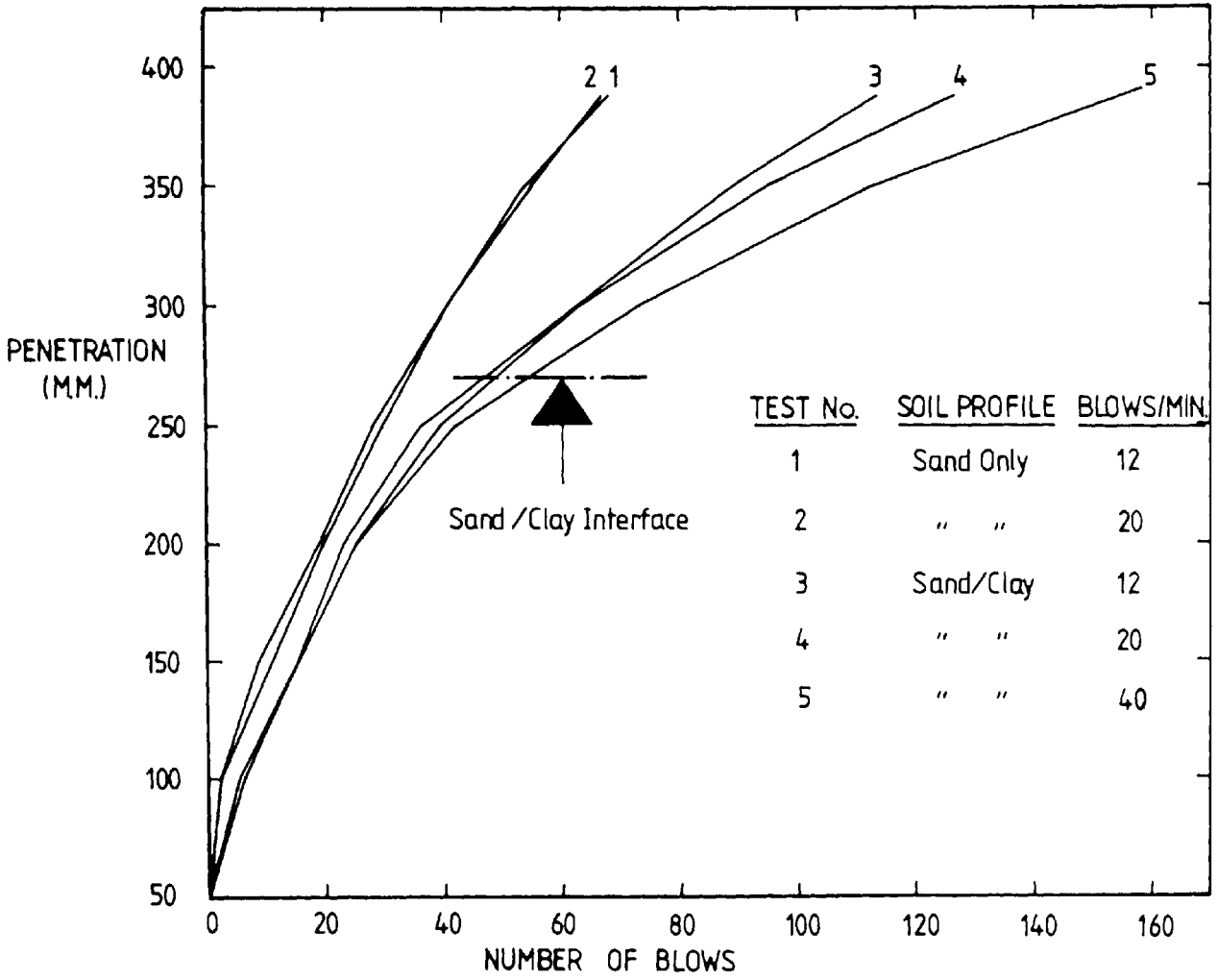

FIGURE No 3.29 GRAPH OF PENETRATION / BLOW No. FOR MODEL TESTS

3.10.7 Graph of Penetration/Blow Number

(1) Sand Only Profile

Fig. 3.27 shows clearly that there is no appreciable variation in the blow number/penetration curves for the two blow rates used.

3.10.8 Sand/Clay Profile

The blow number/penetration curves for tests three, four and five demonstrate that it is harder to drive the model pile in the sand/clay profile than in the sand alone. This would be expected when the pile is penetrating the clay however the phenomenon is visible from the onset of driving and at a depth of 250 mm (40 mm above the sand/clay interface) it takes on average 10 blows extra to drive it to the same depth.

The average number of blows to reach a final penetration of 90 mm for these tests was 133 compared with 67 for the sand only profile.

If conclusions were drawn by looking strictly at Fig. 3.29 alone it would suggest that the slower the driving rate the easier it is to achieve penetration. However if the difference in the values of cohesion for tests three and four are taken into account (Fig. 3.25) in which the cohesion value for test four is significantly greater than the value for test three the resistance to penetration would be expected to increase.

The cohesion value in test five however is the lowest encountered in the tests and recourse to Fig. 3.28 must be

taken to explain the increased driving resistance. Fig. 3.28 shows that in the case of test five after a penetration of 200 mm the input force is much less than for the other tests. This may have been due to friction between the ram and the ram guide. Further recourse to the acceleration/time records for selected tests (Fig. 3.30) show that the acceleration/time records for test five is somewhat different to the other tests with an appreciable difference in peak acceleration. Thus it would be expected that the blow count would increase for this test.

3.10.9 Conclusions from Pilot Study

The conclusions are broken down into two main areas:-

(1) Performance of Load Cells and Instrumentation

(a) Load Cell Connectors

The taper connectors used, performed satisfactorily during all phases of the pilot study however a number of defects in the design were in evidence and were:-

(i) Although the connectors were resistant to seperation due to impact, retrieval of the pile after a test, expecially when end bearing in clay, was difficult because the connectors were not sufficiently resistant to tension to allow the pile to be pulled out.

(ii) The taper connectors hampered the function of the static load cell where the unloading cycle was not exactly linear. This was not a major drawback in the pilot study but it was expected to perform a pull-out test in the semi-full scale experiments and hence a modified joint will have

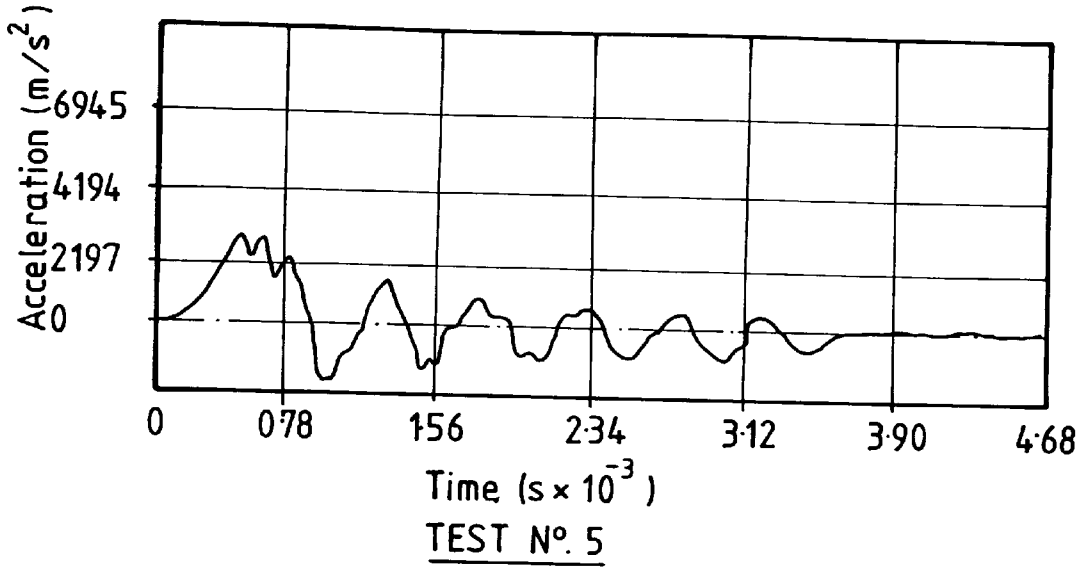

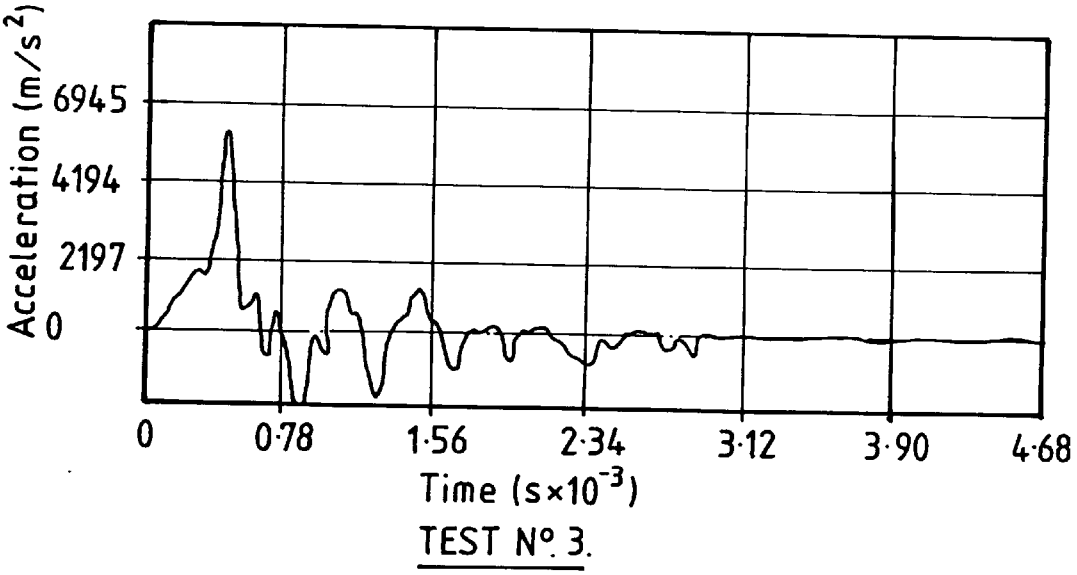

FIG. Nº. 3.30 VARIATION IN ACCELERATION / TIME PLOTS BETWEEN TEST Nº 3 AND 5

to be employed. A different joint incorporating some of the features of the taper type connector and the screw thread connector has been designed and is discussed in Chapter 4.

(b) Instrumentation

Except for one instance where a faulty connection to the tape recorder resulted in a loss of signal (test 3) the dynamic and static systems functioned satisfactorily.

(2) Test Results

From the experimental results it is evident that there is no appreciable difference in the bearing capacity or penetration/blow by varying the driving rates. The driving rates used in the pilot study are the fastest possibly attainable using the semi-full scale pile driving rig. However, there is an appreciable difference in pile performance in the two different soil profiles used and so the semi-full scale tests will be used to highlight these differences while keeping the driving rate constant.

CHAPTER 4

Semi-Full Scale Equipment

4.1 Introduction

It was found that a pile 60 mm O.D. and with a driven length of 1.956 m could be installed in the sand tanks available in the Geotechnics laboratory. With such a pile it was possible to expand the instrumentation to obtain a more accurate record of the consequence of the driving operation. This also meant that a pile driving rig had to be designed that could be operated by some mechanical system.

The main criteria on which the design of the driving rig was based was as follows:-

1. The cost of manufacture and also purchase of specialist parts should not be prohibitive.

2. The design should be as simple as possible yet sophisticated enough to fulfill all the experimental requirements. These requirements were:-
   (a) Variable drop height for the ram.
   (b) Variable driving rates.
   (c) Close control of the overall driving operation.
   (d) Constant drop height of the ram in order to deliver the same energy for each blow.

3. The rig should fit onto existing equipment and be easily erected and dismantled.

With these considerations in mind a pneumatically controlled rig was designed based on the Laboratory Proctor Compaction

Apparatus. Complete working drawings of the rig are included and are shown in Figures 4.1 to 4.6.

4.2 Description of the Driving Rig

The rig can be divided into the following sub-assemblies:-

4.2.1 (1) Main Driving Frame

As can be observed from Figures 4.1 and 4.2 the main driving frame consists of :-

(a) A mild steel base plate of dimensions 1219 x 299 x 16 mm (48" x 9" x 5/8") thick. The base plate is drilled and tapped as shown in Fig. 4.2 to accomodate the central column, yoke guides, levelling screws and clamps. At the front of the column is a section of 16 mm (5/8") thick mild steel in which is machined a 63.5 mm (2½") diameter hole to allow the model pile to pass through and two 19 mm diameter holes on either side of the central hole to accomodate the ram guides. A 60 degree arc is cut out of this section to allow any wiring associated with the model pile to pass through freely.

(b) The main column consists of a 102 x 51 mm (4" x 2") channel section welded at the bottom to a 171 x 51 mm (6 3/4" x 2") plate which locates on the base plate.

A similar plate is welded on top of the column to accomodate the top plate.

(c) The top plate has a 63.5 mm (2½") diameter hole machined in it to allow the drop weight to pass

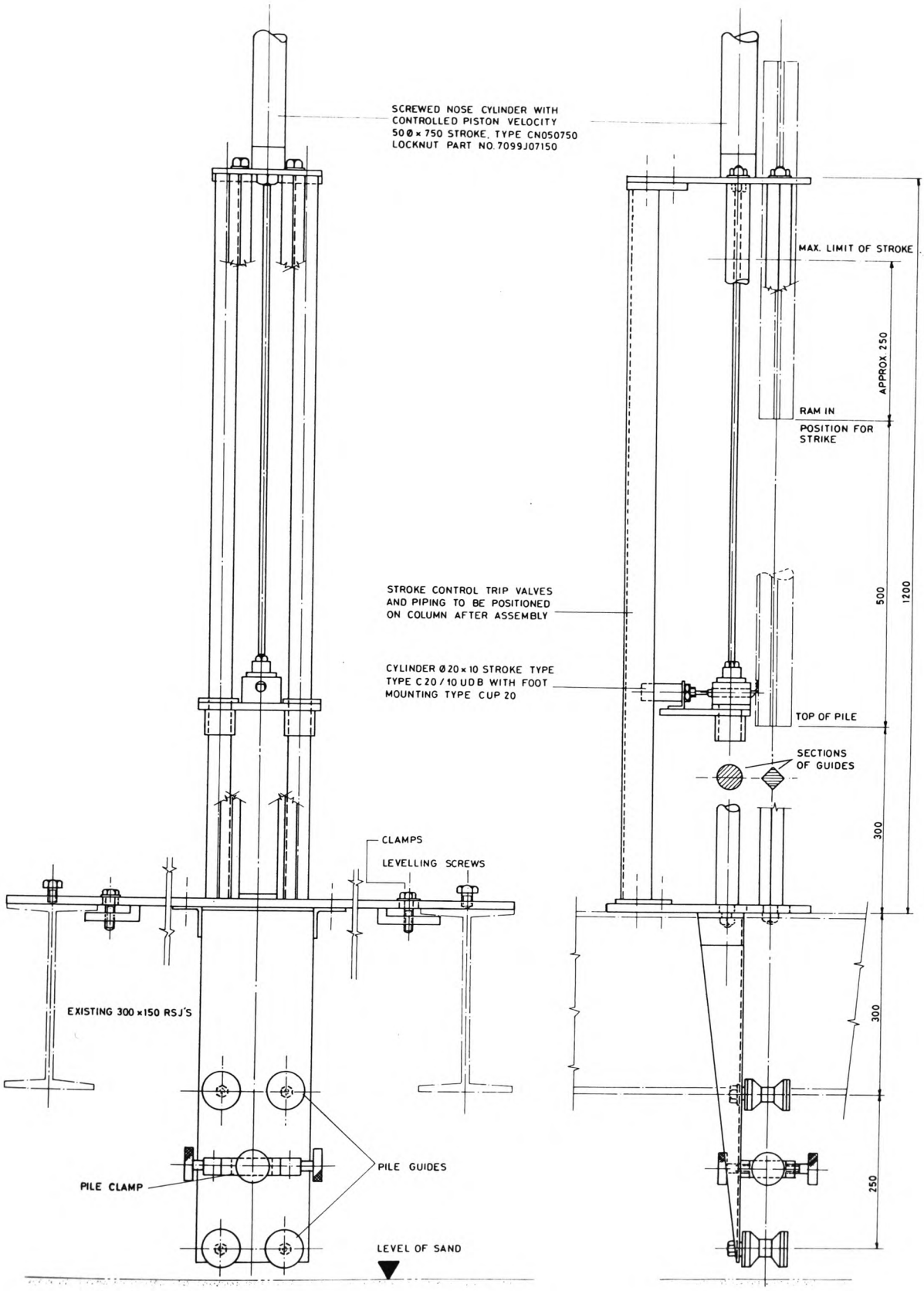

MODEL PILE DRIVING RIG

SCALE 1:4

NOTE ALL DIMENSIONS IN MILLIMETRES

Designed & Drawn by G.C.Lake

FIG. Nº. 4.1.

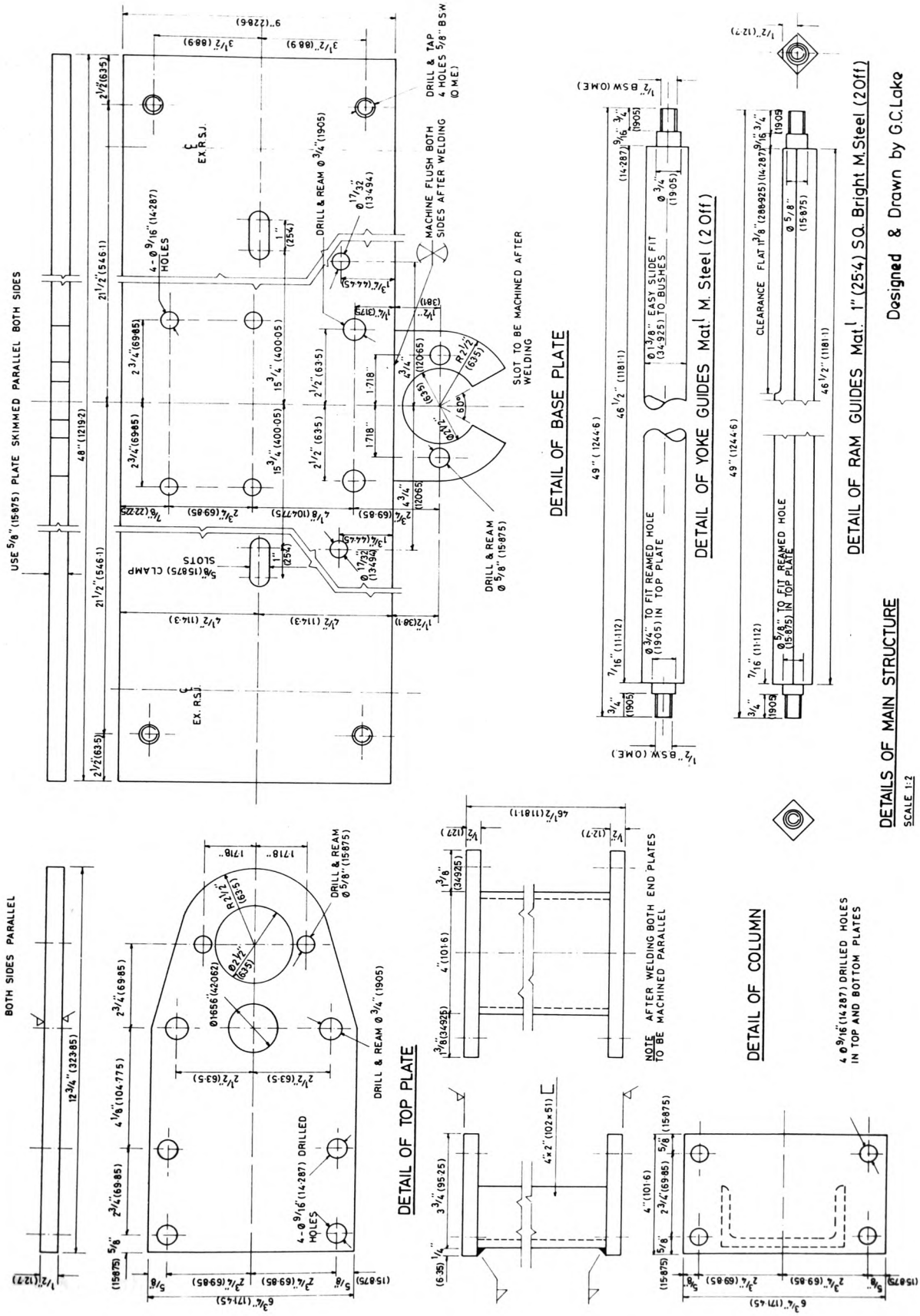
USE 5/8" (15875) PLATE SKIMMED PARALLEL BOTH SIDES
DRILL & TAP 4 HOLES 5/8" BS.W (O.M.E.)
MACHINE FLUSH BOTH SIDES AFTER WELDING
DRILL & REAM Ø 3/4" (1905)
4 - Ø 9/16" (14287) HOLES
SLOT TO BE MACHINED AFTER WELDING
DRILL & REAM Ø 5/8" (15875)
5/8" (15875) CLAMP SLOTS
DETAIL OF BASE PLATE
DETAIL OF YOKE GUIDES Mat.l M. Steel (2 Off)
Ø 1 3/8" EASY SLIDE FIT (34925) TO BUSHES
Ø 3/4" TO FIT REAMED HOLE (1905) IN TOP PLATE
CLEARANCE FLAT 1" (288925) (14287) 9/16" 3/4"
Ø 5/8" (15875)
DETAIL OF RAM GUIDES Mat.l 1" (254) SQ. Bright M.Steel (2Off)
Designed & Drawn by G.C.Lake
DETAILS OF MAIN STRUCTURE
SCALE 1:2
BOTH SIDES PARALLEL
DRILL & REAM Ø 5/8" (15875)
DRILL & REAM Ø 3/4" (1905)
4 - Ø 9/16" (14287) DRILLED HOLES
DETAIL OF TOP PLATE
NOTE AFTER WELDING BOTH END PLATES TO BE MACHINED PARALLEL
DETAIL OF COLUMN
4 Ø 9/16" (14287) DRILLED HOLES IN TOP AND BOTTOM PLATES

FIG. Nº 4.2.

freely through. Also situated in the top plate are holes to locate the yoke guides, ram guides and main pneumatic cylinder.

4.2.2 (2) Driving Assembly

The driving assembly can be split into two sub-sections:-

(a) Drop Weight (Ram)

The drop weight consists of a 670 mm (26") length of 60 mm (2 3/8") diameter mild steel rod. The weight is cored out at the top to provide stability.

Grooves are machined down the complete length with V-shaped sections milled out of the weight on either side of a diameter at right angles to the grooves (Fig. 4.3). The ram is constrained to move in a vertical direction only by means of the ram guides which fit into the V-shaped sections in the ram.

(b) Yoke Assembly

As can be seen from Fig. 4.4 the yoke assembly consists of:-

(i) The yoke plate.
(ii) Guide bushes.
(iii) Plunger.
(iv) Plunger block.
(v) Piston rod connector (i.e. the yoke is connected to the main cylinder).

Fig. 4.5 shows a full assembly and also the position of the miniature pneumatic cylinder (lock cylinder) on the yoke.

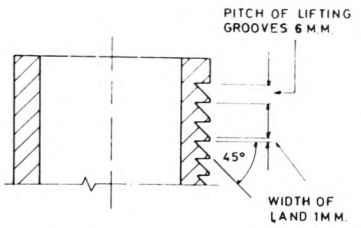

Section 'A-A' Through Grooves

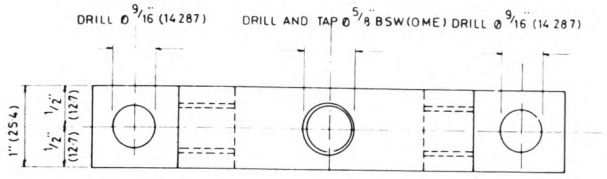

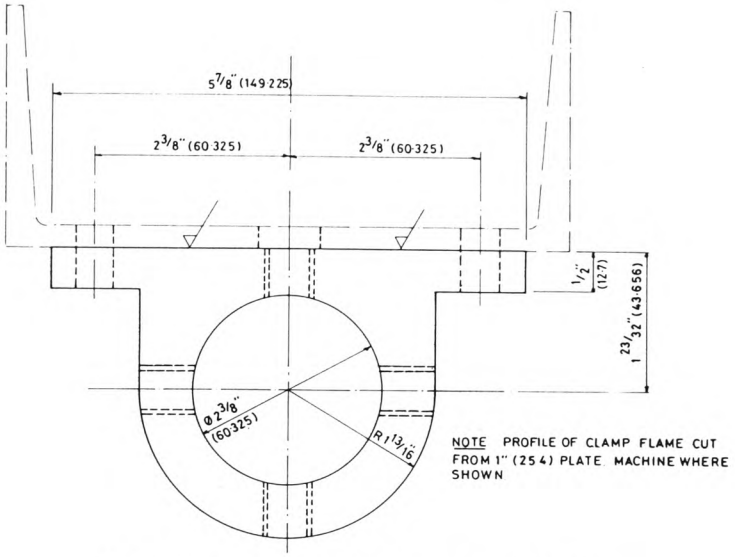

DETAIL OF MODEL PILE CLAMP Mat.! Mild Steel

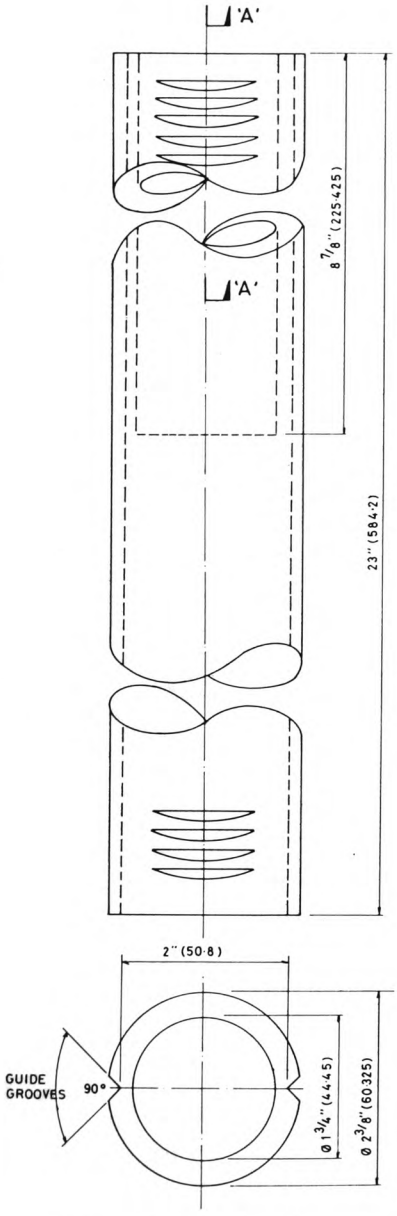

DETAIL OF RAM Mat.! E.N.8 (Mass 10 Kg)

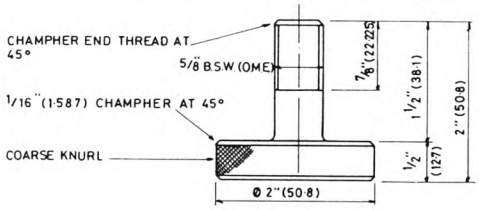

DETAIL OF CLAMP SCREW (4 Off) Mat.! M. Steel

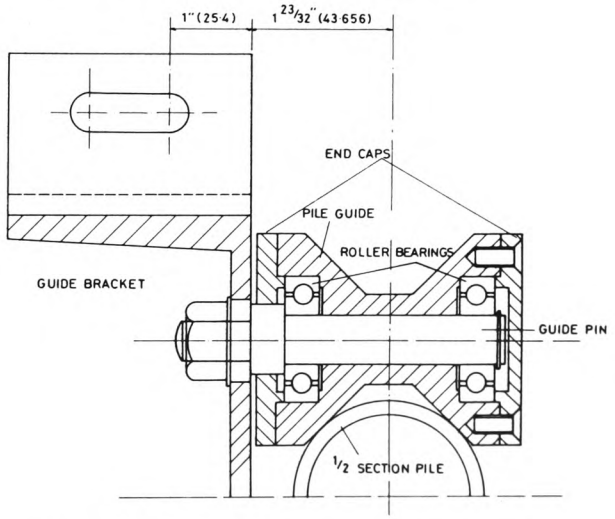

DETAIL SHOWING ASSEMBLY OF A PILE GUIDE

MISCELLANEOUS DETAILS

SCALE 1:1

Designed & Drawn by G.C.Lake

FIG. Nº 4.3

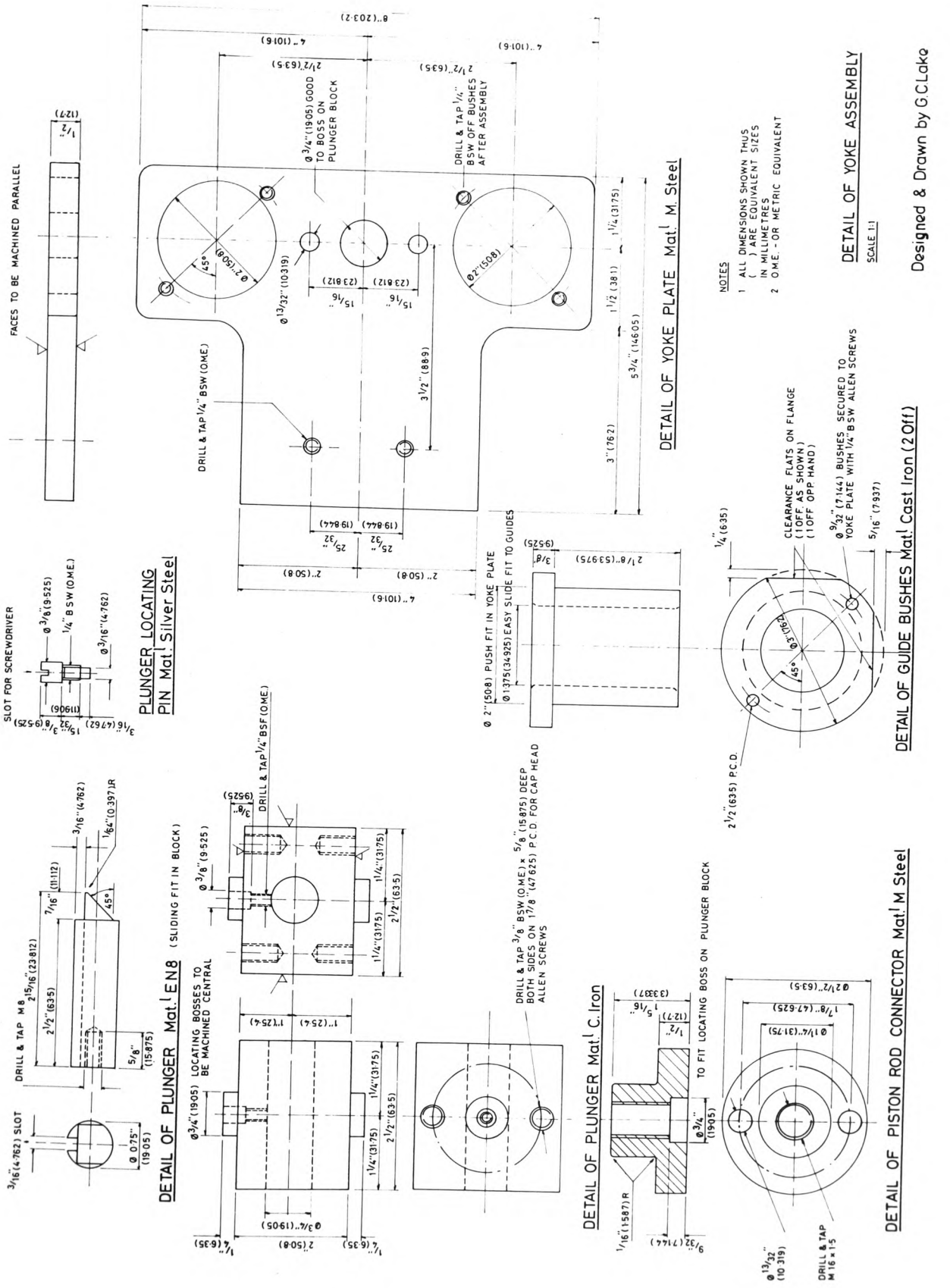
DETAIL OF YOKE ASSEMBLY
SCALE 1:1
Designed & Drawn by G.C.Lake
NOTES
1 ALL DIMENSIONS SHOWN THUS ( ) ARE EQUIVALENT SIZES IN MILLIMETRES
2 O.M.E. - OR METRIC EQUIVALENT
DETAIL OF YOKE PLATE Mat.l M. Steel
FACES TO BE MACHINED PARALLEL
DRILL & TAP 1/4" BSW (O.M.E.)
DRILL & TAP 1/4" BSW OFF BUSHES AFTER ASSEMBLY
Ø 3/4" (1905) GOOD TO BOSS ON PLUNGER BLOCK
PLUNGER LOCATING PIN Mat.l Silver Steel
SLOT FOR SCREWDRIVER
DETAIL OF GUIDE BUSHES Mat.l Cast Iron (2 Off)
Ø 2" (50.8) PUSH FIT IN YOKE PLATE
Ø 1.375 (34.925) EASY SLIDE FIT TO GUIDES
CLEARANCE FLATS ON FLANGE (1 OFF AS SHOWN) (1 OFF OPP HAND)
Ø 9/32" (7.144) BUSHES SECURED TO YOKE PLATE WITH 1/4" BSW ALLEN SCREWS
DETAIL OF PLUNGER Mat.l E N 8 (SLIDING FIT IN BLOCK)
DRILL & TAP M 8
LOCATING BOSSES TO BE MACHINED CENTRAL
DRILL & TAP 1/4" BSF (O.M.E.)
DRILL & TAP 3/8" BSW (O.M.E.) x 5/8" (15.875) DEEP BOTH SIDES ON 1 7/8" (47.625) P.C.D. FOR CAP HEAD ALLEN SCREWS
DETAIL OF PLUNGER Mat.l C. Iron
TO FIT LOCATING BOSS ON PLUNGER BLOCK
DETAIL OF PISTON ROD CONNECTOR Mat.l M Steel
DRILL & TAP M 16 x 1.5

FIG. Nº 4.4

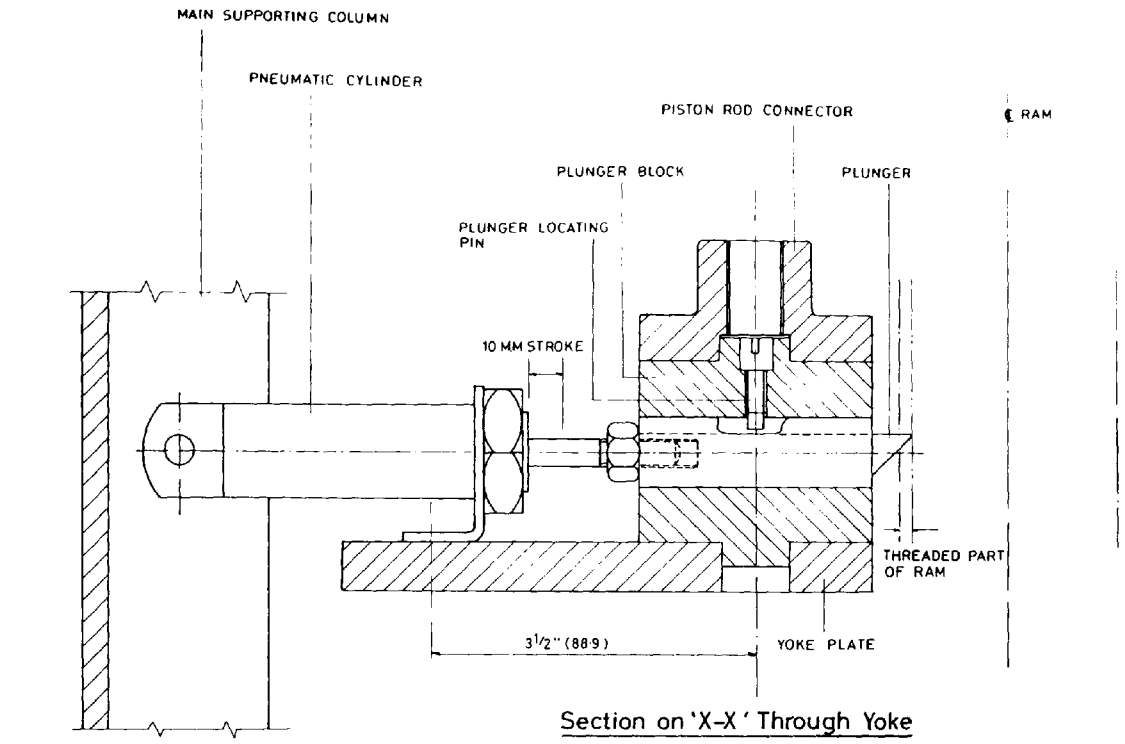

Section on 'X-X' Through Yoke

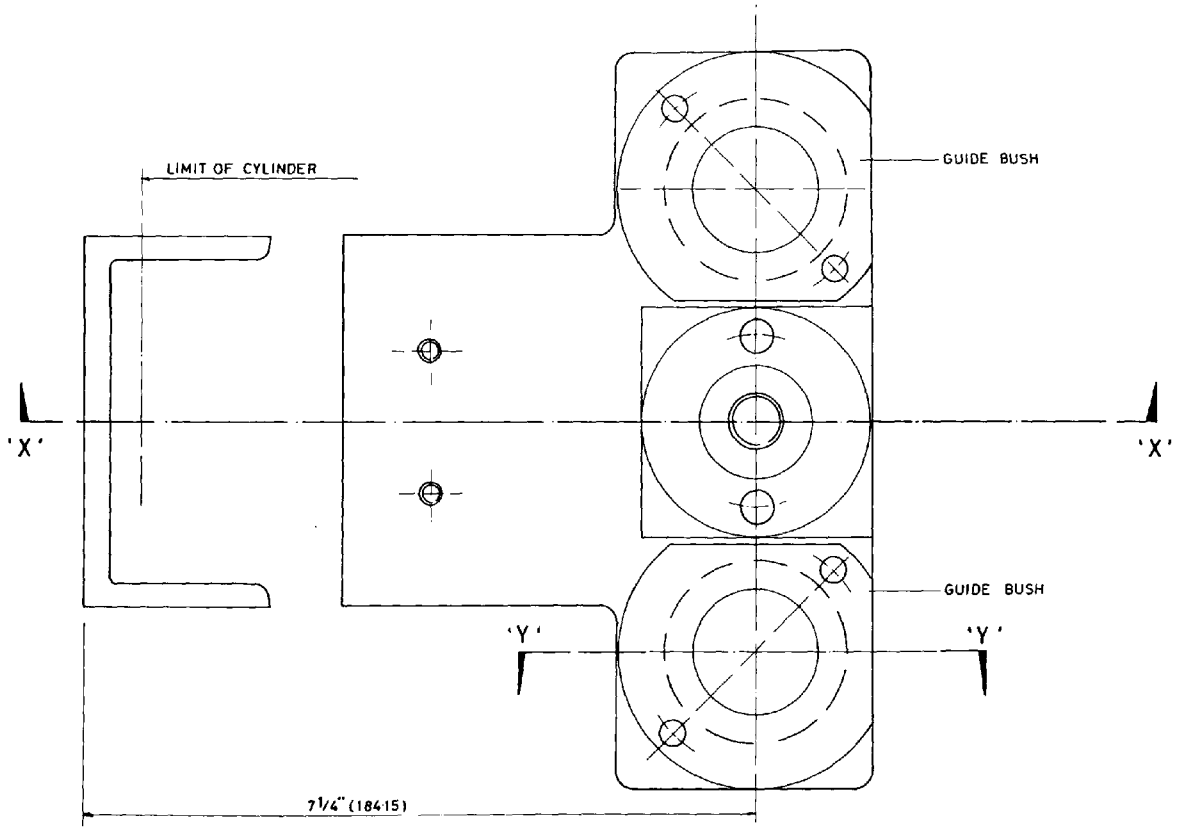

PLAN OF ASSEMBLED YOKE

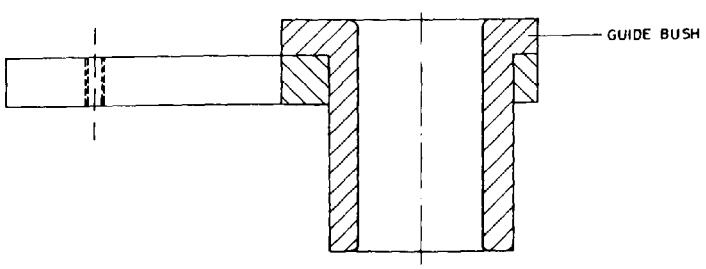

Section on 'Y-Y' Through Bush

FIG. Nº. 4.5

DETAIL SHOWING FULL YOKE ASSEMBLY

SCALE 1:1

Dosigned & Drawn by G.C.Lake

4.2.3 (3) Guide Bracket

The guide bracket is manufactured from a 178 x 76 mm (7" x 3") channel section and shaped as shown in Fig. 4.4. On it are bolted four pile guides each pair set 254 mm (10") apart and positioned to constrain the pile in a vertical direction. Bolted onto the guide bracket halfway between the pile guides is a pile clamp (Fig. 4.6) which is used to clamp the pile in position when a new section is added. In this way the pile sections already driven are not disturbed.

4.2.4 (4) Pneumatic Control Gear

A schematic representation of the pneumatic circuit used to operate and control the system along with a listing of the main parts are shown in Fig. 4.7. A complete cycle of the circuit is also shown in Fig. 4.7.

The main operating features of the system are as follows:-

(1) Button valve No. 4 manually starts the cycle.

(2) When On/Off valve No. 9 is turned off the cycle will end with the main cylinder forward and the lock cylinder retracted. This allows the drop weight to be removed and a new pile section added.

(3) When the pile is driven to a set limit, valve No. 6 closes and stops the cycle as in (2). This ensures that the pile wiring does not become entangled in the pile guides.

(4) If the guard valve is opened, valves 7 and 8 will shut, air is exhausted from the system and all valves are isolated. This is incorporated as a safety measure.

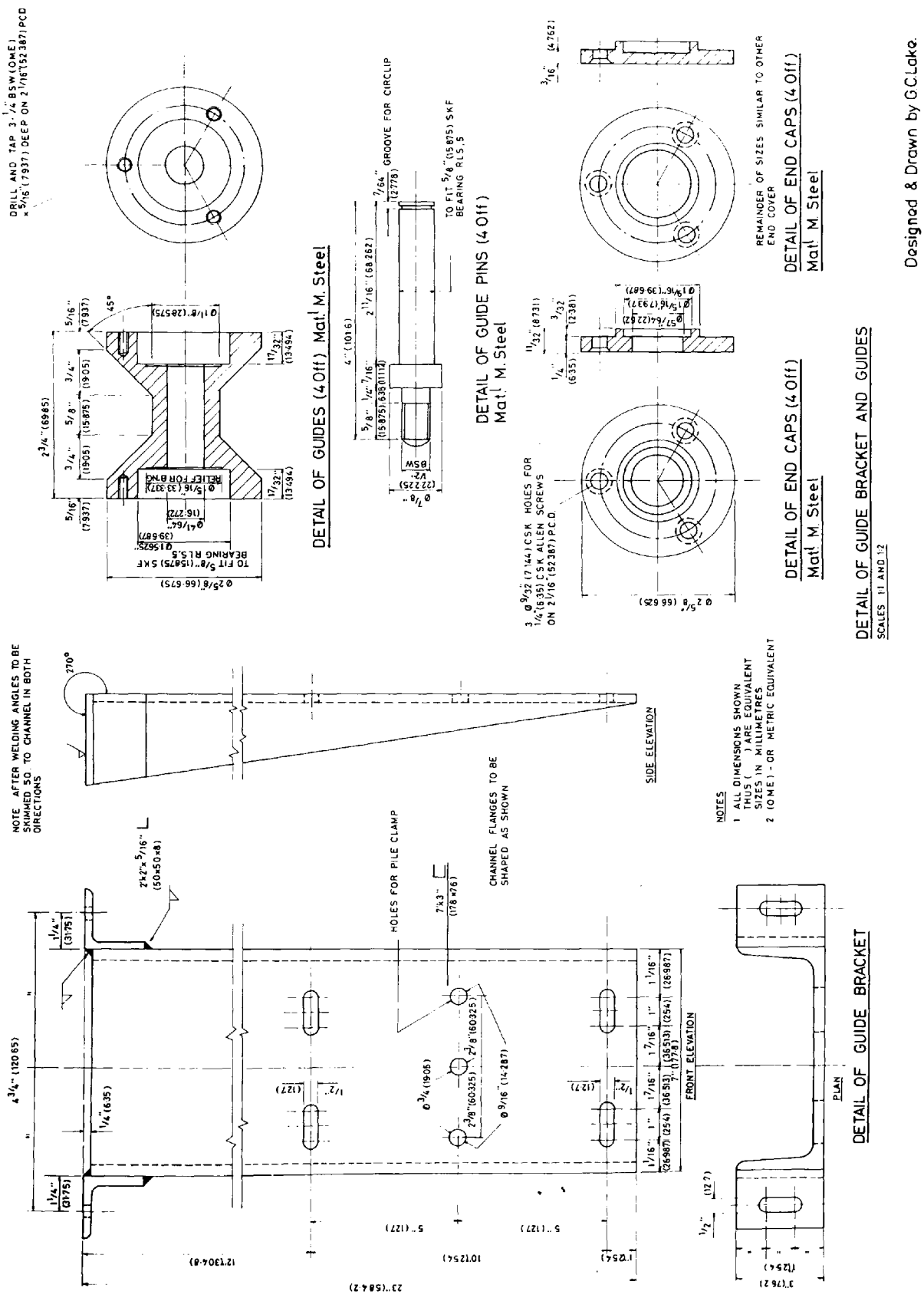
DETAIL OF GUIDE BRACKET AND GUIDES
SCALES 1/1 AND 1/2
DETAIL OF GUIDES (4 Off) Mat' M. Steel
DETAIL OF GUIDE PINS (4 Off) Mat' M. Steel
DETAIL OF END CAPS (4 Off) Mat' M Steel
DETAIL OF END CAPS (4 Off) Mat' M Steel
DETAIL OF GUIDE BRACKET
Designed & Drawn by G.C.Lake.
NOTE AFTER WELDING ANGLES TO BE SKIMMED SO TO CHANNEL IN BOTH DIRECTIONS
NOTES
1 ALL DIMENSIONS SHOWN THUS ( ) ARE EQUIVALENT SIZES IN MILLIMETRES
2 (O.M.E.) - OR METRIC EQUIVALENT
HOLES FOR PILE CLAMP
CHANNEL FLANGES TO BE SHAPED AS SHOWN
SIDE ELEVATION
FRONT ELEVATION
PLAN
REMAINDER OF SIZES SIMILAR TO OTHER END COVER
TO FIT 5/8" (15.875) SKF BEARING RLS.5
GROOVE FOR CIRCLIP
DRILL AND TAP 3 - 1/4 BSW (O.M.E.) x 5/16" (7.937) DEEP ON 2 1/16" (52.387) PCD

FIG. Nº 4.6.

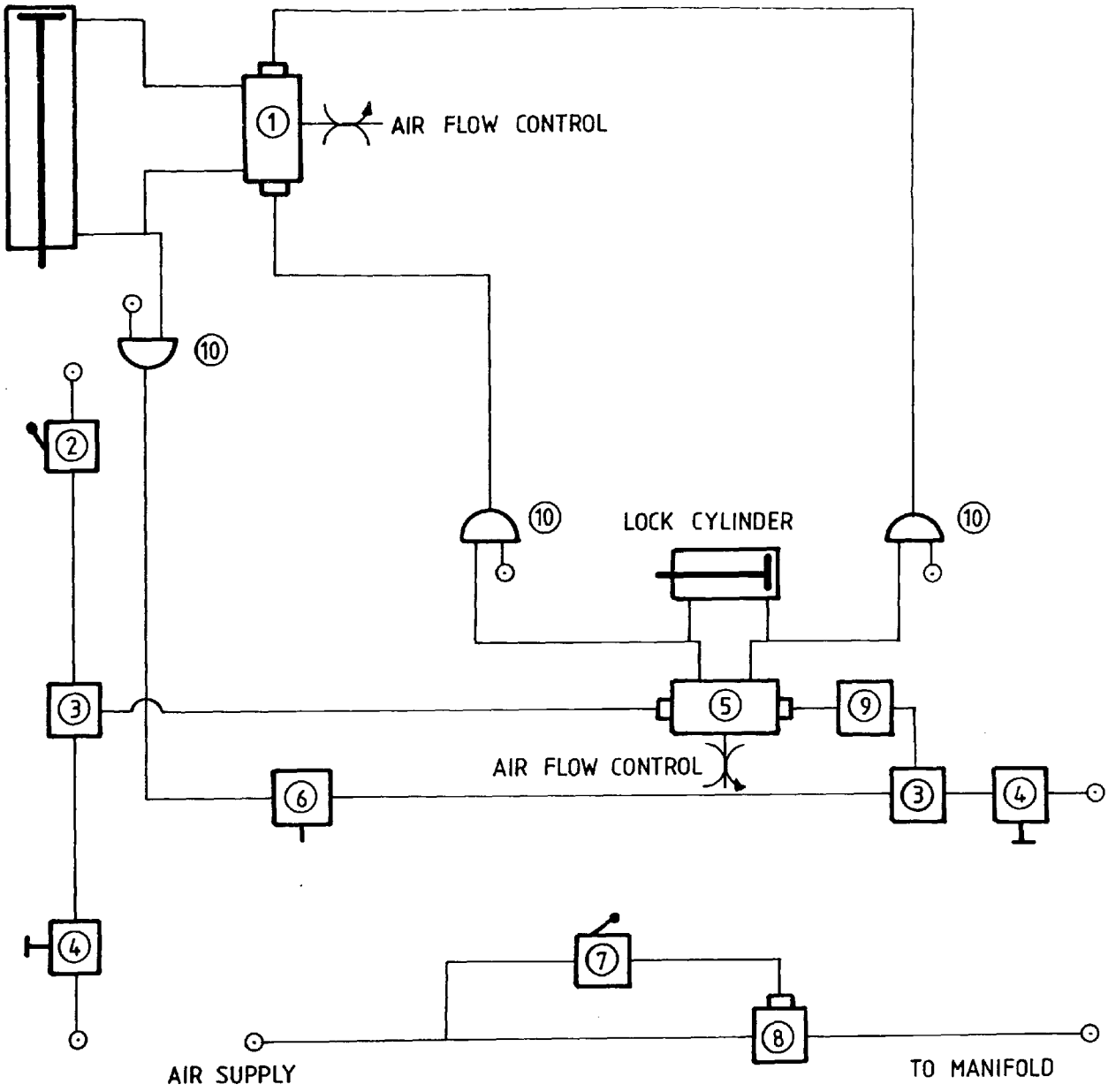

LEGEND

1. Main Cylinder Valve
2. Drop Weight Valve
3. Shuttle Valves
4. Push Button Valve
5. Lock Weight Valve
6. Pile Limit Valve
7. Guard Valve
8. Main Air Supply Valve
9. On/Off Valve
10. Not Units

PNEUMATIC CYCLE

1 Lock Cylinder Engages
2 Main Cylinder Retracts
3 Lock Cylinder Disengages
4 Main Cylinder Forward
(Recycles From 1)

FIG. 4.7 SCHEMATIC DIAGRAM OF PNEUMATICS FOR MODEL PILE DRIVING RIG

(5) Flow control valves are included on the main cylinder valve to allow regulation of the air flow in the main cylinder. In this way the rate of stroke of the main piston can be readily controlled. The maximum number of cycles per minute being 30. A counter is added to the system which is used as a blow counter and is activated on each cycle.

As can be seen from Fig. 4.5 the lock cylinder is connected to a plunger which locates in a plunger block. This ensures that the lock cylinder is not damaged in any way by the weight of the ram.

The complete pneumatic circuit was 'bench tested' to ensure that the system operated correctly.

4.3 Driving Operation

The operation commences with the first pile section in place ready for driving. The ram is positioned over the pile with the lock cylinder locating in the lowest groove in the ram. The system is started and the main cylinder retracts, the ram is lifted by the up stroke of the main cylinder until a preset trip disengages the lock cylinder on the yoke. The ram falls and driving commences. The main cylinder recycles and at the bottom of the stroke the lock cylinder relocates the ram.

The drop height remains constant because the lock cylinder engages the ram at a different point each blow. The cycle is repeated until valve No. 6 is closed at which time driving ceases.

A new section is added and the process repeated.

4.4 Modification to the Driving Rig

After manufacture a number of alterations were made to the rig and are listed below:-

(1) A window was cut in the guide bracket above the top set of pile guides in order that new pile sections could be fully secured.

(2) The 60 degree slot machined in the base plate was enlarged in order to ensure that the wiring in the pile passed through freely.

(3) The clearance flats on the ram guides were extended due to a miscalculation.

(4) The ram length was extended to 670 mm again due to a dimension miscalculation.

4.5 Semi-Full Scale Pile

The 60 mm diameter pile was chosen for the following main reasons:-

(1) The diameter and length should be large enough to be representative of true pile behaviour.

(2) The pile should be small enough so that boundary effects from the testing tank would not influence the experimental results.

The suitability of the model pile for use in the sand tank is discussed in Section 4.6.1.

Cooke (1973) suggested that for a typical size pile the l/d

ratio should be greater than 20 and less than 40. The actual l/d ratio of the embedded section of the model pile was 33.

Vesic (1965) suggested that in order to obtain representative results from a model study the diameter of pile should be greater than 1.5 inches.

It can be seen therefore that the model pile is of adequate size and length in order to represent full scale pile behaviour.

A diagrammatic representation of the model pile showing the position of the static and dynamic axial load cells along with the driving sequence is shown in Fig. 4.8.

4.5.1 Static Axial Load Cell

As was discussed in Chapter 3, Section 3.7.1 deficiencies were discovered in the design of the load cell. Although the taper connectors proved to be efficient in resisting separation due to impact loads the design had an adverse effect on the linearity of the static calibration. Fig. 4.9 shows the design modifications decided upon to remedy this deficiency. The basic features are as follows:-

(1) The taper connectors are replaced by tight fitting parallel connectors. These connectors each have a groove machined out of a diameter. Eight countersunk Allen grub screws are screwed through the pile wall to locate in the groove such that any slackness in the joint is eliminated by the action of tightening the screws. One of these screws locates in a hole drilled into the groove to stop any possibility of the joint turning.

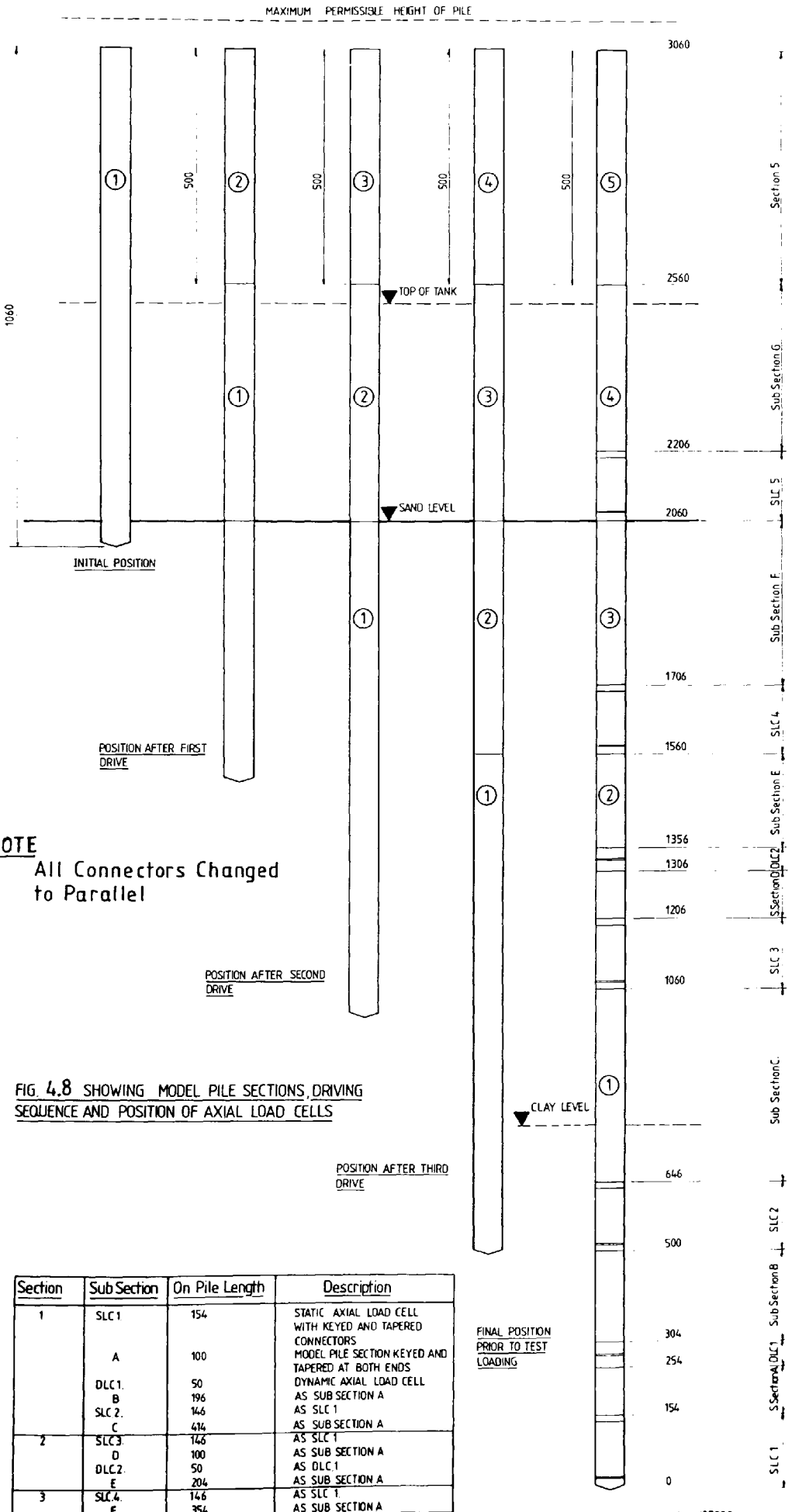

NOTE

All Connectors Changed to Parallel

FIG. 4.8 SHOWING MODEL PILE SECTIONS, DRIVING SEQUENCE AND POSITION OF AXIAL LOAD CELLS

Section	Sub Section	On Pile Length	Description
1	SLC 1	154	STATIC AXIAL LOAD CELL WITH KEYED AND TAPERED CONNECTORS
	A	100	MODEL PILE SECTION KEYED AND TAPERED AT BOTH ENDS
	DLC 1	50	DYNAMIC AXIAL LOAD CELL
	B	196	AS SUB SECTION A
	SLC 2	146	AS SLC 1
	C	414	AS SUB SECTION A
2	SLC 3	146	AS SLC 1
	D	100	AS SUB SECTION A
	DLC 2	50	AS DLC 1
	E	204	AS SUB SECTION A
3	SLC 4	146	AS SLC 1
	F	354	AS SUB SECTION A
4	SLC 5	146	AS SLC 1
	G	354	AS SUB SECTION A
5	—	500	" " " "

NOTE ALL DIMENSIONS IN MILLIMETRES

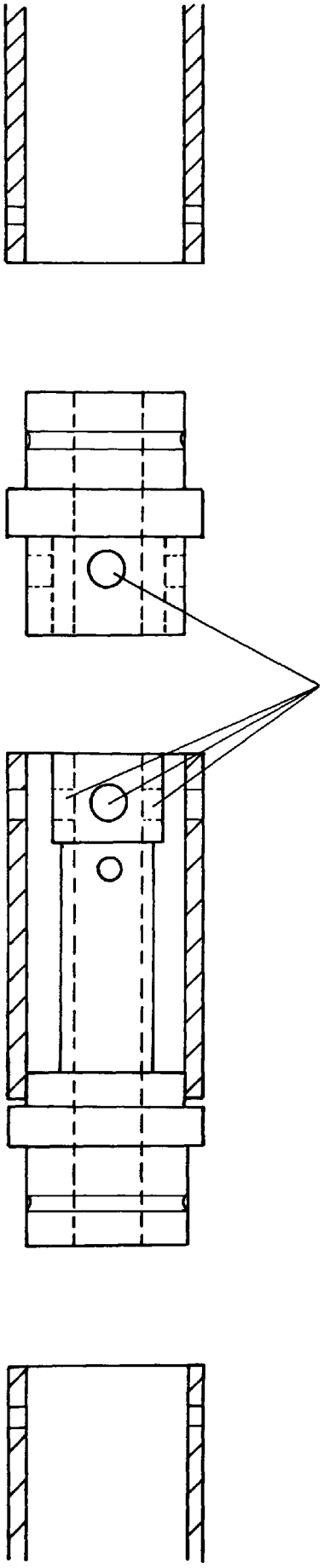

FIG N° 4 9 DESIGN MODIFICATIONS TO AXIAL LOAD CELL

2. The taper connector connecting the two halves of the load cell together are replaced by another parallel joint. These are secured together along with the load cell cover by four Countersunk Allen screws drilled and tapped to pin the three components together.

4.5.2 Pile Cap

Fig. 4.10 shows the model pile cap used and consists of two sections. The top section is machined on its lower side to enable a Kistler Piezo electric load washer type (9051) to fit snugly into it to just under half its width. The lower side is also threaded centrally to allow a connecting bolt to be secured. A 3/4" ply disc is glued to the top of the section to act as a pile cushion and to prevent "ringing" between the hammer and cap. A hole is also drilled and tapped in the top section in order that a 6 mm diameter bar may be inserted horizontally. This is used to secure the displacement transducer described in Section 4.5.4.

The lower section has a corresponding machined portion to allow the other half of the load washer to be located. When the two sections are connected there is a gap of 2 mm to allow free compression of the load washer. The connecting bolt passes freely through the centre of the load washer and screws into the top half. The bolt is then tightened using a torque wrench to a pressure of 60 psi., in order to connect the two sections and also to pre-compress the load washer. The end of the bolt is drilled and tapped to allow a B & K type (4334) piezoelectric accelerometer to be mounted. Plate 4.1 shows a picture of the assembled pile cap.

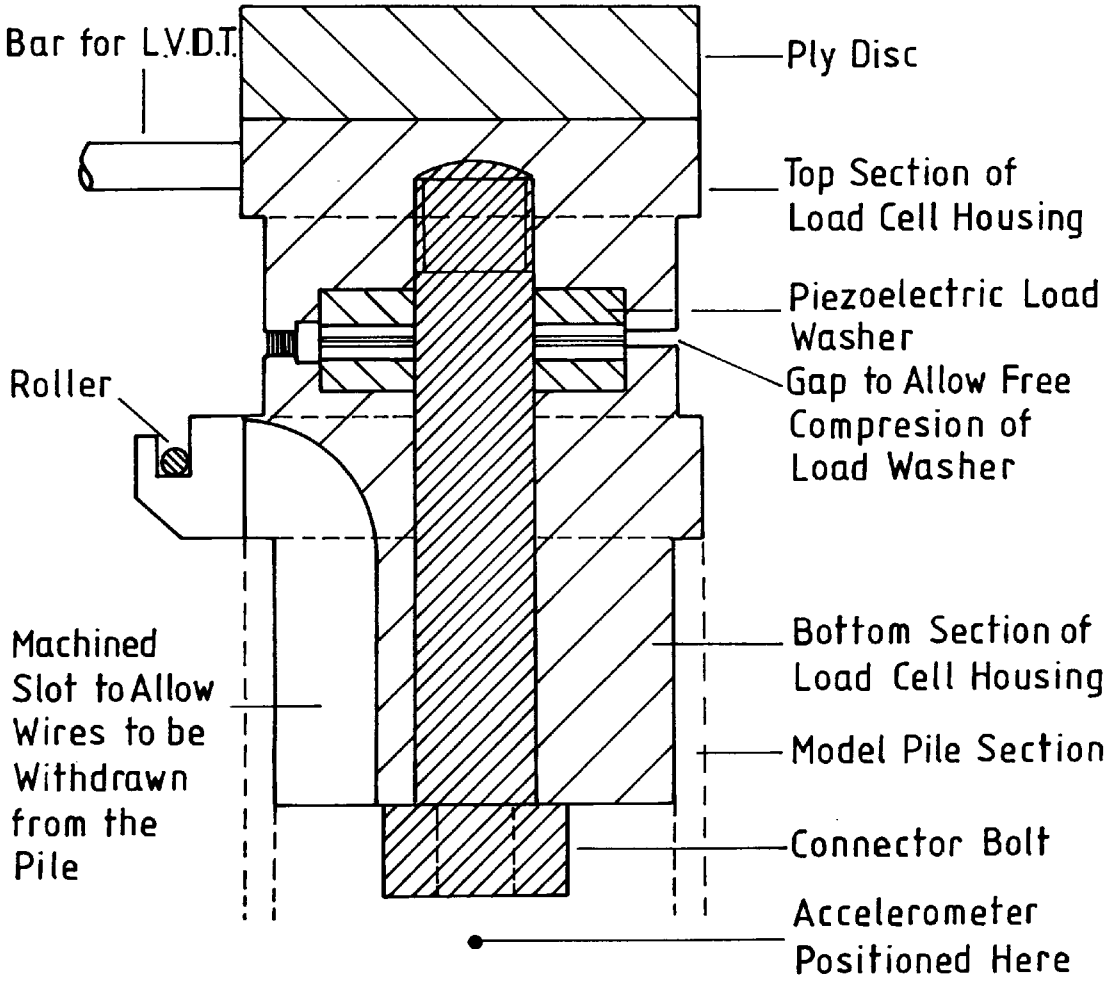

FIG. N°. 4.10 ASSEMBLY OF MODEL PILE CAP (Sectional View)

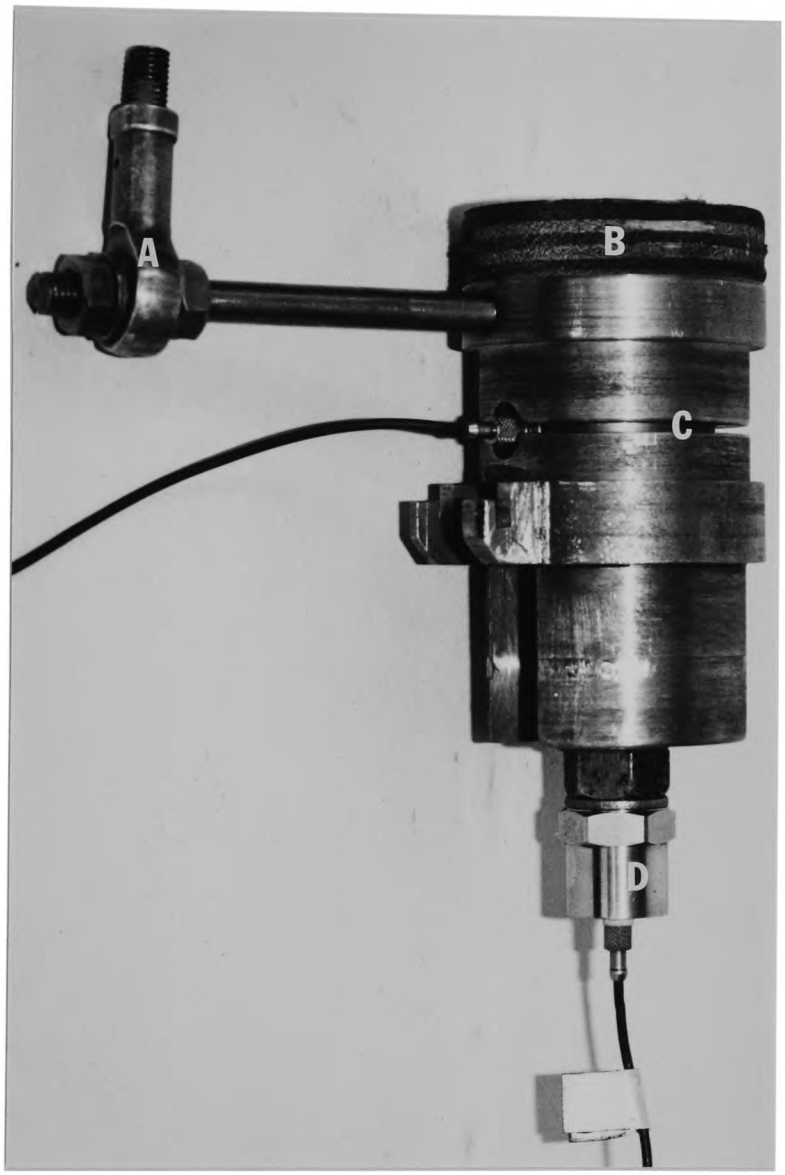

KEY:

A. Universal Coupling

B. Ply Disc

C. Piezoelectric Force Washer

D. Accelerometer

PLATE 4.1 Showing Assembled Pile Cap

4.5.3 Dynamic Axial Load Cell

As with the static axial load cell the taper connectors were replaced by parallel connectors. The joints were easier to manufacture and had the advantage that a pull-out test could be performed on the pile as well as the envisaged CRP and MTL tests. Fig. 4.11 shows the design of the load cell. A hollow bolt is used to connect the two halves of the load cell together and also to pre-compress the load washer. A double locknut is used to secure the bolt. The bolt was then tightened using a torque wrench to a pressure of 60 psi. Due to the size of the load washer used the coaxial cable connector protruded out of the side of the pile. A cover was designed and manufactured to protect the cable and is shown in Plate 4.2.

4.5.4 Penetration Measurement

A means of measuring the amount of penetration of the pile head was needed that would fulfill two main tasks:-

1) To provide a record of displacement for each blow during driving operations and also to provide a trace of displacement/time for individual blows.

2) To provide a record of displacement against load for the loading and pull-out tests.

4.5.5 Linear Variable Differential Transformer (L.V.D.T.)

It was decided to use an A.C. powered L.V.D.T. of maximum stroke 600 mm. When fed through a conditioner, output from the L.V.D.T. was direct current and capable of driving an

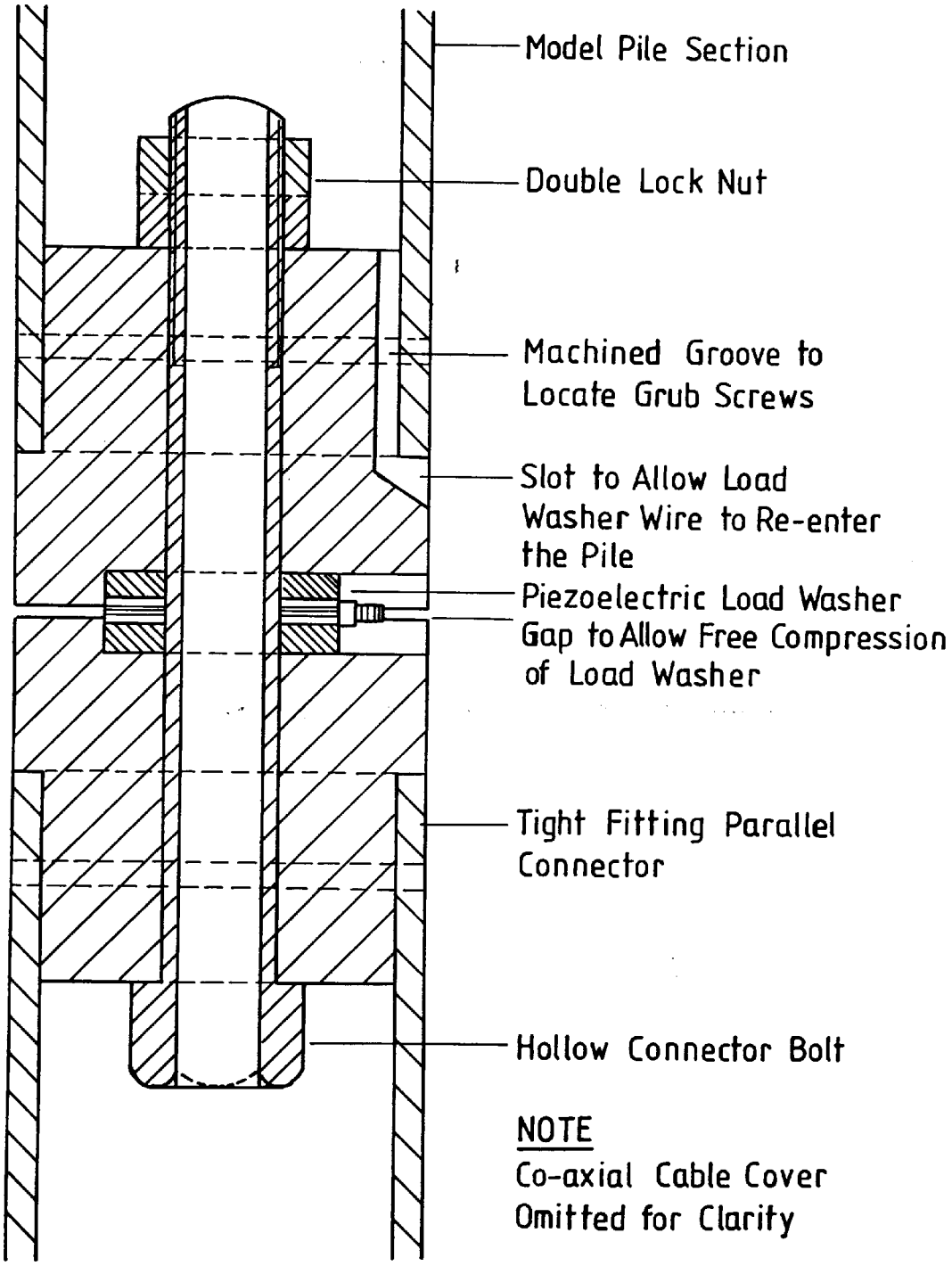

FIG.Nº 4.11 DYNAMIC AXIAL LOAD CELL

PLATE 4.2 Showing Co-axial Cable Cover

Ultra Violet recorder while being scanned by the Orion for use in the static tests.

The advantage of a L.V.D.T. is its fast response and light body, thus reducing inertia effects on the pile head. The L.V.D.T. and conditioner used were manufactured by Sangamo Transducers Ltd., (type AC/300 and C90 respecively). The Ultra Violet recorder used was a Bell and Howell type 5/137.

Plate 4.3 shows the L.V.D.T. in position on the driving rig. Also illustrated is the universal coupling which connects the L.V.D.T. to the pile cap and enables deviation from the vertical to take place without damaging the transducer.

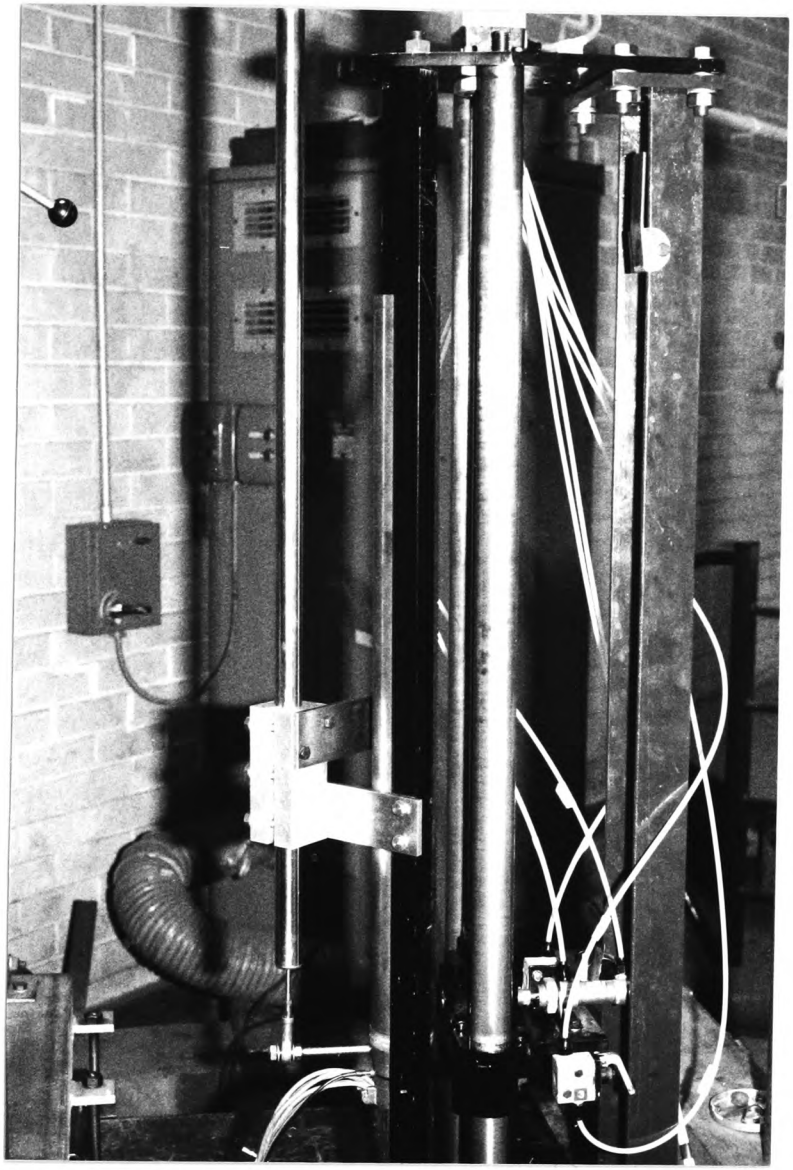

PLATE 4.3 Showing L.V.D.T. in Position on Driving Rig

4.6 Static Testing Equipment

The equipment used for the loading and Pull Out tests along with the sand tanks has been comprehensively described by Kay (1980) and is shown in Figure 4.12 and Figure 4.13. As can be seen from Figure 4.13 a 50 Kn Dartec hydraulic jack is used to carry out the static tests. In order that the static tests could be performed after driving the following procedure was adopted:-

1. The base plate of the driving rig was placed at right angles across the reaction frame (Fig. 4.13) and levelled.

2. The complete rig was then assembled and a dummy pile section fitted.

3. The ram and dummy section were then aligned with each other and the roller bearings adjusted to touch the pile.

4. The dummy section was then clamped in position.

5. The rig was then dismantled to base plate level with the dummy section of pile left in place.

6. The hydraulic jack was then placed on its mounts and levelled.

7. The base plate was then moved until the vertical alignment of pile and jack coincided.

8. The base plate was then levelled once more and then clamped in position for the duration of the tests.

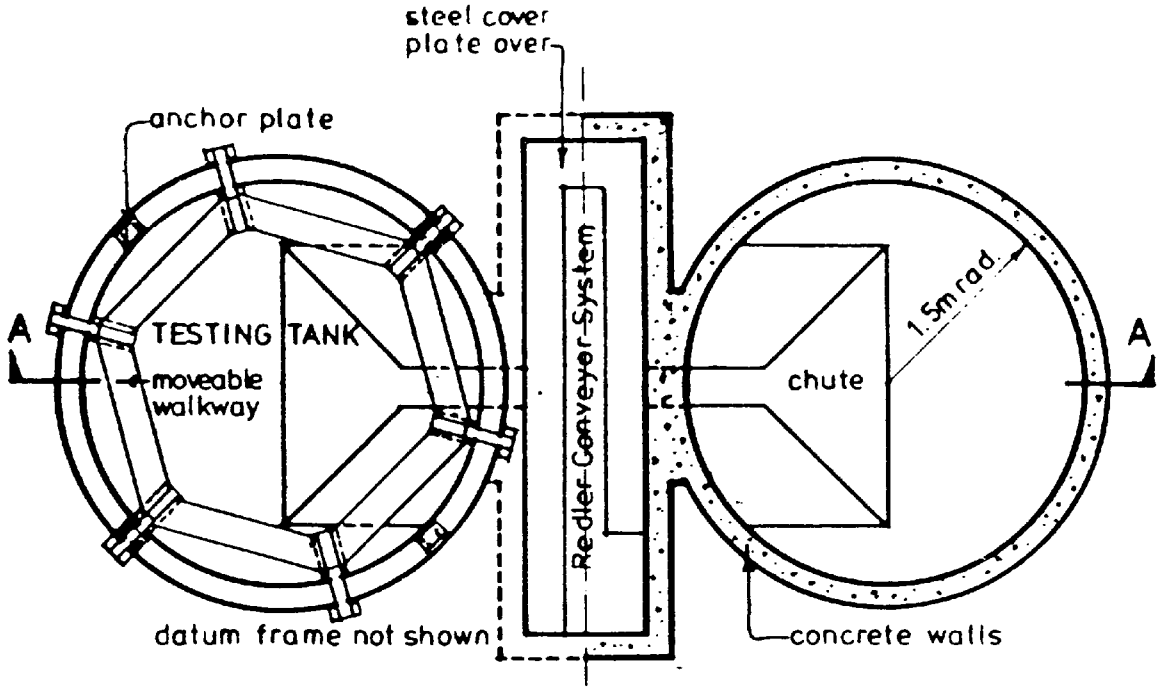

HALF PLANS

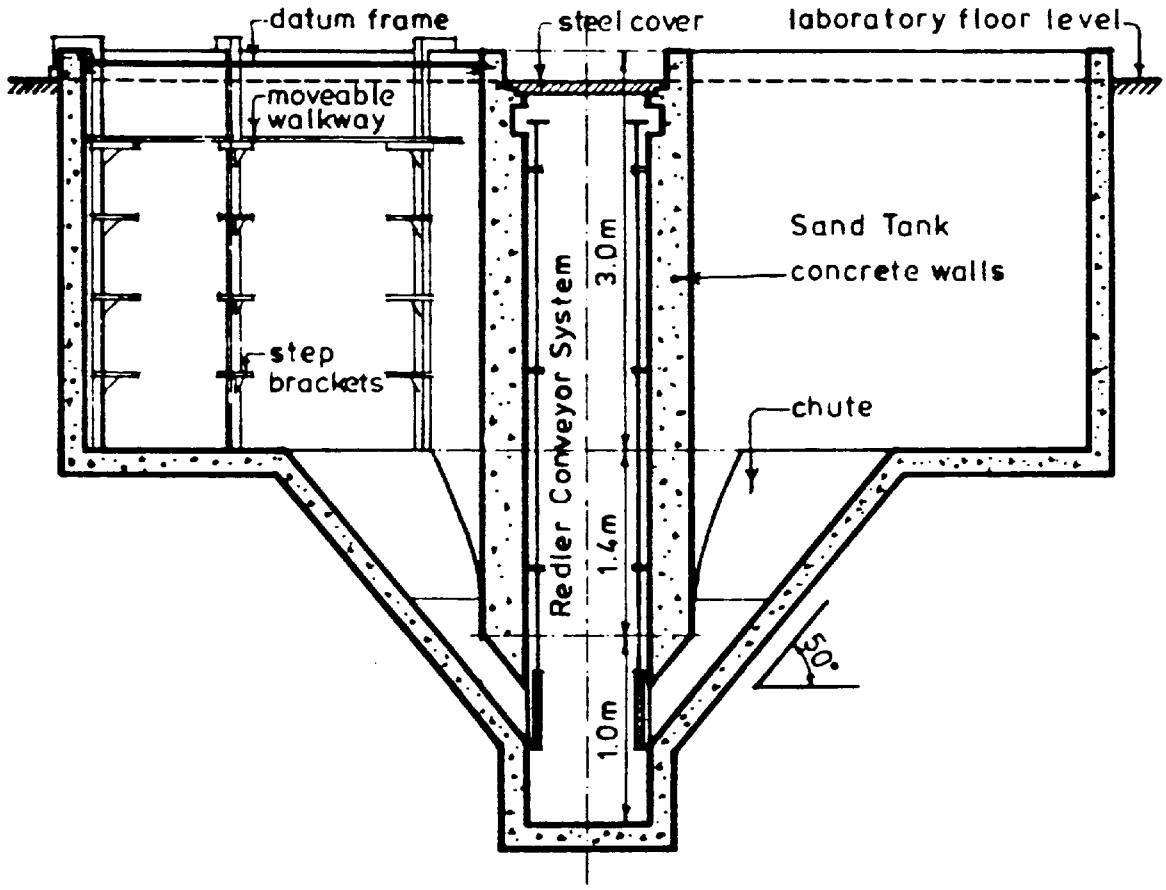

SECTION A-A

FIGURE 4.12

SAND TANKS AND REDLER CONVEYOR SYSTEM
(After Kay (1980))

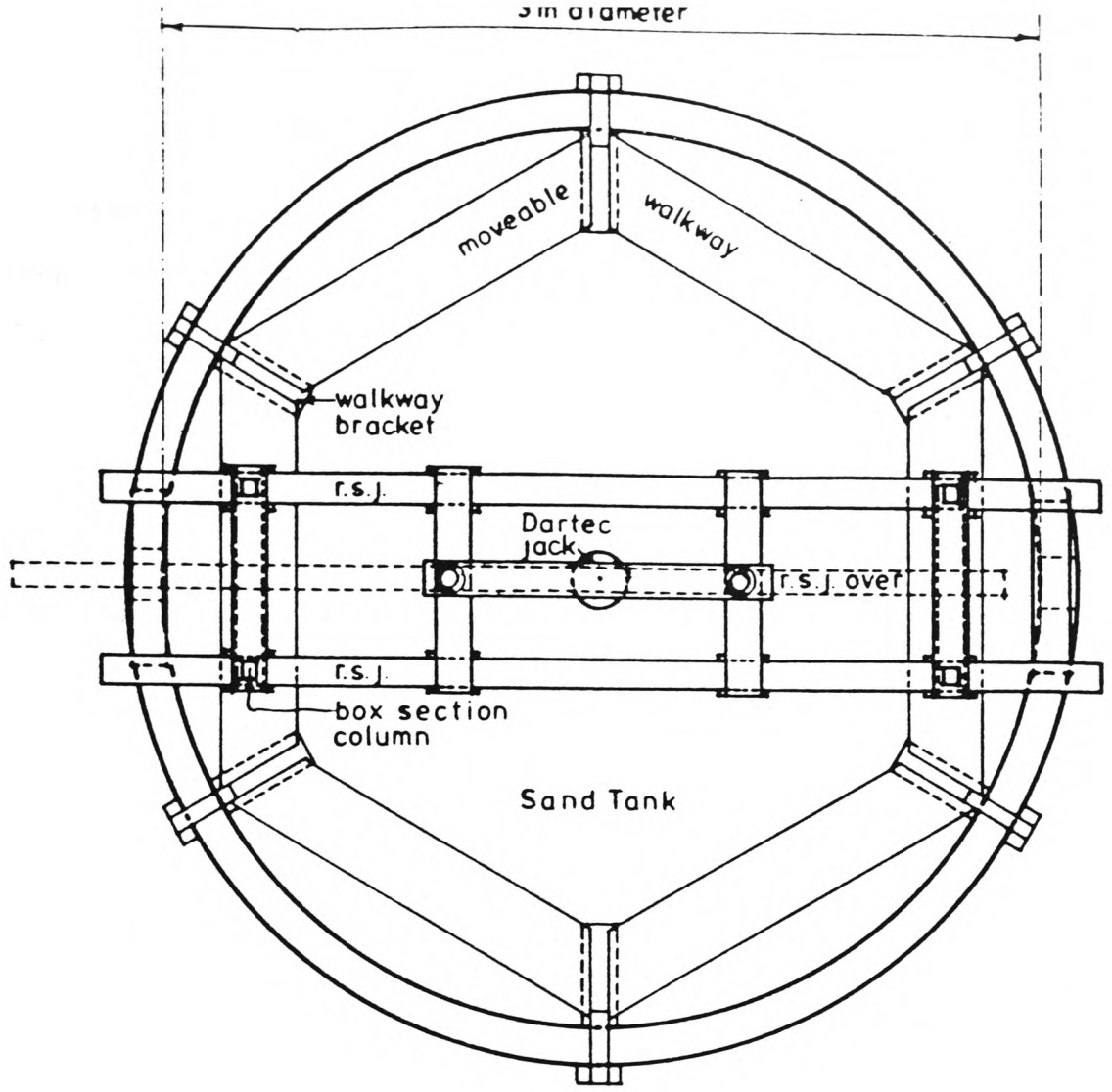

FIGURE 4.13

LOADING FRAME AND GANTRY (After Kay (1980))

4.6.1 Sand Tanks

The sand tanks used consist of a pair of 3 m diameter by 3 m deep concrete silos connected by a Redler conveyer which moves sand from one tank to another. Tests are performed in one tank only the other tank being used as a sand store. The tanks are shown diagramatically in Figure 4.12.

As discussed in Section 4.5 one of the reasons for choosing a 60 mm diameter model pile was to ensure that boundary effects to the tank walls would not arise. Meyerhof (1959) on his tests with a driven pile in loose sand concluded that the compacted zone could be up to six times the shaft diameter while the compacted zone below the pile would extend to five diameters.

Kishida (1963) in model tests in loose sand indicated that the compacted zone was approximately equal to eight pile diameters.

Robinsky and Morrison (1964) using radiography in small laboratory model tests also showed that for medium dense sand visible movement of the soil extended up to 5.5 diameters horizontally and up to 4.5 diameters below the pile point.

Therefore in the case of the sand only tests it can be seen that the surrounding tank has no effect on the experimental values with a radial clearance between pile and tank wall of approximately 50 diameters and minimum vertical clearance between pile tip and tank base of 8 diameters.

Cummings et al (1950) in field tests on driven pile groups in soft clays observed that at a distance of approximately 2 pile diameters the clay within a group was disturbed only a small amount.

Cooke and Price (1973) found considerable disturbance for a distance of approximately one pile diameter around the pile shaft, while Cooke, Price and Tarr (1979) showed significant soil disturbance up to 4 diameters when driving a 163 mm diameter pile in normally consolidated London clay.

Orrje and Broms (1967) found that immediately after driving 100 and 250 mm diameter concrete piles with normally consolidated clay there was a zone of disturbance in relation to shear strength of 1.5 diameters.

Data from Soderberg (1962) and Seed and Reese (1951) indicated that driving created excess porewater pressures which extended to about 5 diameters from the pile surface.

Koisumi and Ito (1967) in laboratory tests on 30 cm diameter model piles showed that excess porewater pressure extended approximately 7 diameters from the pile wall with little change thereafter.

For driven piles however the zone of increased porewater pressure extends to a distance of approximately 16 diameters (Lo and Stermac (1965), Bjerrum and Johannessen (1960), Milligan et al (1962)).

Therefore in the case of the sand over clay tests although the margins of safety are closer than the sand only tests

(radial distance between pile and clay container being 16.5 diameters) the clay container is still of suitable dimensions for the experiments.

4.6.2 Containment of Marl

As has been previously mentioned it was hoped to simulate a two strata system with Red Marl as the lower strata.

The depth of the red marl layer was to be 1.2 m and therefore the amount of marl needed to fill the tank (diameter 3 m) would be prohibitive. A rough calculation based on a bulk density of 2100 kg/m^3 and excluding the conveyer outlet yielded 1800 kg.

Obviously mixing, storage and placement of such a large amount of marl would be impossible in the limited confines of a laboratory.

To this end a circular wooden former of dimension 1.2 x 0.49 metres radius was constructed (Wersching (1986)). The former was contained in a Braithwaite tank resting on the pit floor so that the centre of the former was on the central axis of the model pile.

The dimensions of the former was decided upon after due consideration was given to edge and base effects (Section 4.6.1).

4.6.3 Reaction Frame and Gantry

Figure 4.13 shows the reaction frame which consists of two 300 mm x 150 mm R.S.J's bolted to the tank wall. On it are clamped two box sections with threaded rods positioned

centrally to allow the dartec jack to be mounted. A gantry is positioned directly over it to allow easy installation of heavy equipment.

4.6.4 Dartec Jack and Waveform Generator

The static loading equipment consists of a dartec hydraulic jack with a maximum stroke of 150 mm. A load cell of capacity 50 Kn and accuracy of 1% is fitted to the jack. A frequency generator (Type Exact TY 336 M.T.F.G.) along with a control unit is used to drive the jack in either displacement or load control. The frequency generator is interfaced with a P.E.T. microcomputer in order that the jack may be linked along with other instrumentation in one control program (Section 4.8).

The complete layout of the monitoring equipment is shown in Plate 4.4.

4.7 Soil Instrumentation

4.7.1 Introduction

The following sections detail the instrumentation used to monitor the changes in insitu and surface conditions of the soil due to pile driving and subsequent test loading. Only the type of instrumentation used are discussed in these sections, the means of placement, positioning and calibration are described and discussed in Chapter 5.

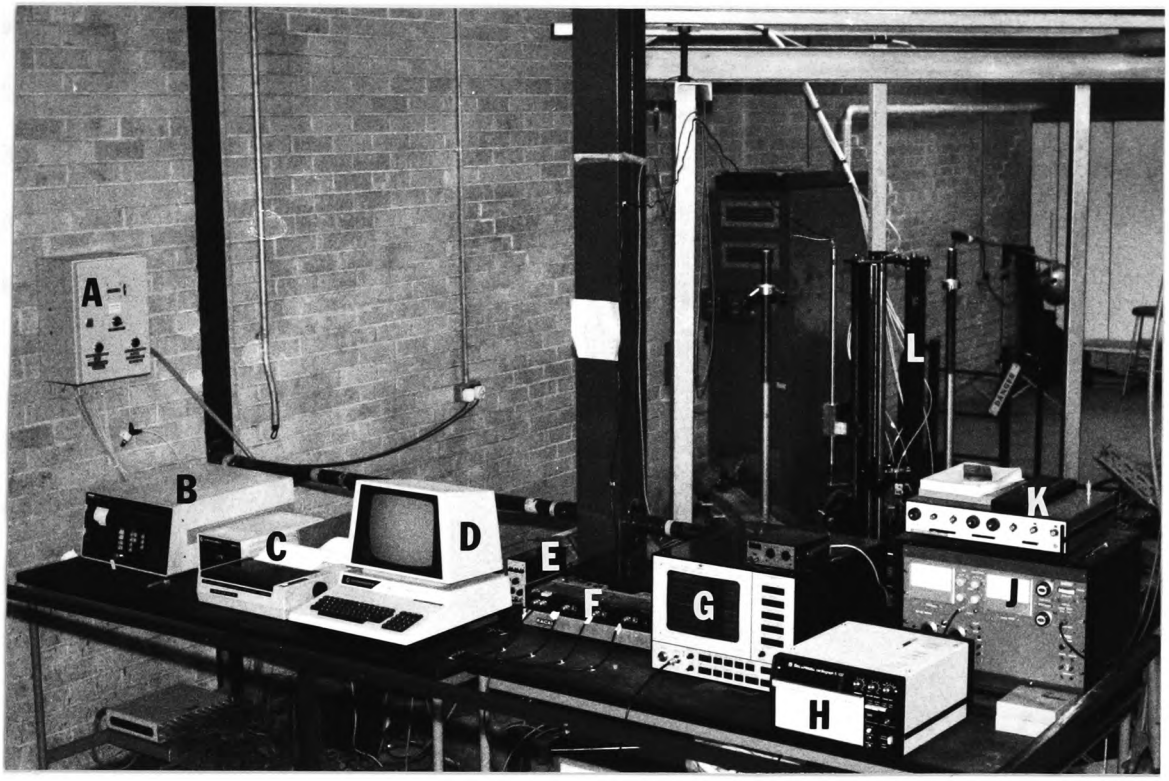

KEY:

A. Pneumatic Control Box
B. Orion 3530A Data Logging System
C. Output and Storage
D. PET Microcomputer
E. Charge Amplifiers
F. RACAL Store 4DS Recorder
G. Real Time Analyser
H. U.V. Recorder
J. Dartec Control Box
K. M.T.F.G.
L. Model Pile Driving Rig

PLATE 4.4 Showing Layout of Control, Monitoring and Recording Equipment

4.7.2 Insitu Displacements

Gravity Sensing Electrolytic Transducers (Inclinometers)

The use of inclinometers to measure insitu displacements around driven piles has been reported by Cooke and Price (1973) and used in the field (Cooke, Price, Tarr (1979)) to measure vertical displacements at five levels around a 168 mm diameter pile jacked into London Clay.

Wersching (1986) has also used inclinometers to measure insitu displacements due to a 110 mm tubular steel pile jacked into a homogeneous mass of dry sand under controlled laboratory conditions.

Inclinometers are designed to provide an output voltage proportional to angle of tilt and a phase indicative of tilt direction when connected in an appropriate bridge circuit and exited with an A.C. voltage. They consist of a tubular glass envelope partially filled with an electrolytic fluid with metal electrodes in contact with the electrolyte.

The two types of inclinometers used were supplied by the Fredericks Company U.S.A. (type 7650, type 7660) and are shown in Plate 4.5.

In order to provide protection for the inclinometers while embedded in the soil a clear perspex tube was used to encase the inclinometers after they had been wired up. Finally the ends of the tube were sealed with epoxy resin to provide a robust cover for the inclinometers (Plate 4.5).

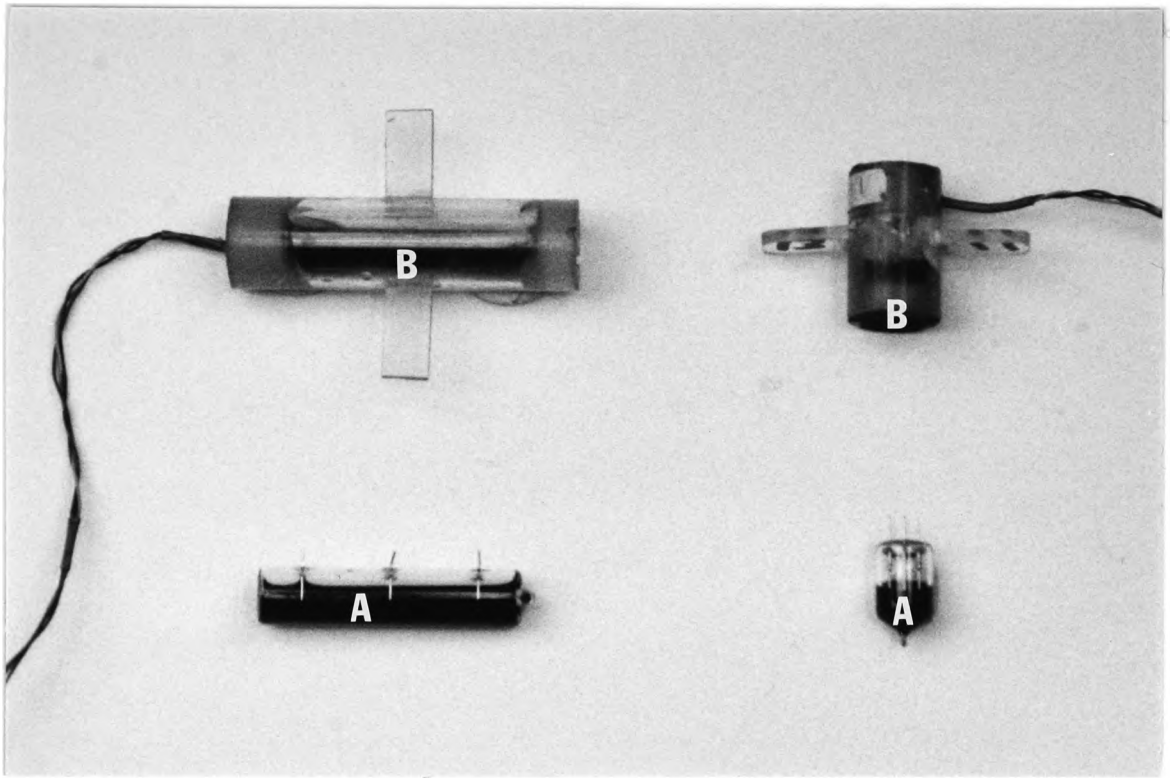

KEY:

A. Electrolytic Level (Inclinometer)

B. Inclinometer Encased in a Perspex Tube for Protection

PLATE 4.5 Showing Cased and Uncased Electrolytic Levels (Inclinometers)

4.7.3 Inclinometer Bridge Conditioner

This unit comprised a power supply/converter producing a Sine wave output at a frequency of 400 Hz (nom) at 5 volts R.M.S. and with a current capacity of 325 m.a. This waveform is fed via bridge completion resistors (1k, 5%) to 28 transducer connector sockets on the rear panel.

The full scale output was approximately 2 volts R.M.S.

4.7.4 Density Measurements

The insitu density of the sand at selected predetermined points was measured using hydrated sand plaster mixtures as described in Chapter 3.

4.7.5 Pressure Transducers

Nottingham pressure transducers which consist of a circular straingauge diaphragm in a steel housing were used in the semi full scale experiments. Their suitability for use in the experiments with regard to soil type and load cell aspect ratio has been fully discussed by Werscheing (1986).

4.7.6 Linear Potentiometers

A number of small linear potentiometers connected to a datum frame mounted below the reaction frame were used in the experiments.

The potentiometers were used for two purposes:-

1. In order to measure surface changes due to driving.

(2) To record insitu displacements of the electrolytic levels (Chapter 5).

Again this instrumentation is fully described by Werscheing (1986).

4.8 Monitoring Equipment

The same equipment was used to monitor dynamic signals as was used for the pilot experiments and is fully described in Chapter 3. Hence only the static monitoring system is described here.

4.8.1 Orion Data Logging System

The static axial load cells, inclinometers, pressure transducers, shear transducer and potentiometers were monitored using an Orion 3530A data logging system. This system is programmable, capable of monitoring 100 channels of information and also acting as a stand alone measuring system. It has an internal voltage source of 2 volts when used as a strain bridge energiser and is capable of accepting both A.C. and D.C. inputs.

However for the purpose of these tests it was more convenient to use the Orion as a 'Volt Meter' and interface with a P.E.T. microcomputer to provide logging control.

A schematic representation of the static monitoring and recording systems is shown in Figure 4.14.

In the case of the strain gauged axial load cells a higher energising voltage was needed than that supplied by the Orion 3530A (see Chapter 5).

4.8.2 Static Control Program

In order to interface the P.E.T. with the Orion and use it as a control a basic program to enable the P.E.T. to receive and interpret characters from the Orion was written by the manufacturers Solatron.

Basically the program output channel number and voltage in blocks of four to the P.E.T. screen.

From this initial program a much more sophisticated control program was written (Wersching (1986)) which centered on an Option Menu.

This option menu consists of the following:-

(1) Initial drive increment

(2) Drive increment

(3) C.R.P. Test

(4) M.T.L. Test

(5) Pull Out Test

(6) Initialisation

(7) Disc change routine

The program is controlled by a displacement criteria which when exceeded stops logging, retracts the jack and returns to the option menu for a further test.

All scanned data is stored on disc with a partial output to a C.B.M. 3401 printer for each scan.

Output data to the printer is converted to the desired units via calibration factors listed in the program.

The Exact TY 336 M.T.F.G. waveform generator is interfaced with the P.E.T. to allow the jack to be controlled by the program again using the displacement criteria.

Options (1) to (6) are self explanatory as is option (7).

The initialisation option is used prior to testing and scans all channels a total of 10 times, averages them and uses them as zero values.

The original control programme developed by Werscheing (1986) had to be altered to accommodate the dynamic driving technique and the changes in the instrumentation. The main alterations are listed below:-

(1) Due to the nature of driving the driven length of each 500 mm section could vary by as much as $\pm$30 mm. Therefore if the driving increment specified in the program was not exceeded a manual stop had to be incorporated that automatically allowed for the difference in calculated and actual driven length when calculating the next driving increment before returning to the option menu.

(2) The task definitions as used in the original program defining the number of channels to be scanned, time between scans, whether voltages are A.C. or D.C. were altered in order to accommodate the authors' instrumentation.

(3) As a subsequence of (2) the rest of the program was altered to allow for the different channel functions along with the incorporation of the various calibration factors.

CHAPTER 5

Calibration and Experimental Procedure - Semi-Full Scale Pile

5.1 Calibration

5.1.2 Introduction

In order to calibrate the various types of instrumentation described in Chapter 4 use was made of the static monitoring system described in Chapters 3 and 4.

The static control program (Chapter 4, Section 4.8.2) suitably altered and simplified for each different calibration procedure was also used. The data storage and output routines were as previously described in chapter 4.

The foregoing sections describe the basic calibration procedures and the changes needed for each particular type of instrumentation.

5.1.3 Static Axial Load Cell

The calibration set up for the static axial load cells is shown in Plate 5.1.

Load was applied by means of an Instron 1251 as shown in Plate 5.2. Special sections of the tube used to construct the model pile were machined to fit over each end of a load cell. These were intended to simulate as far as possible the loading conditions encountered in the fully assembled model pile. As can be seen from Plate 5.1 logging of the data was achieved by an Orion interfaced with a P.E.T. microcomputer. An external power source of ≈ 3 volts was

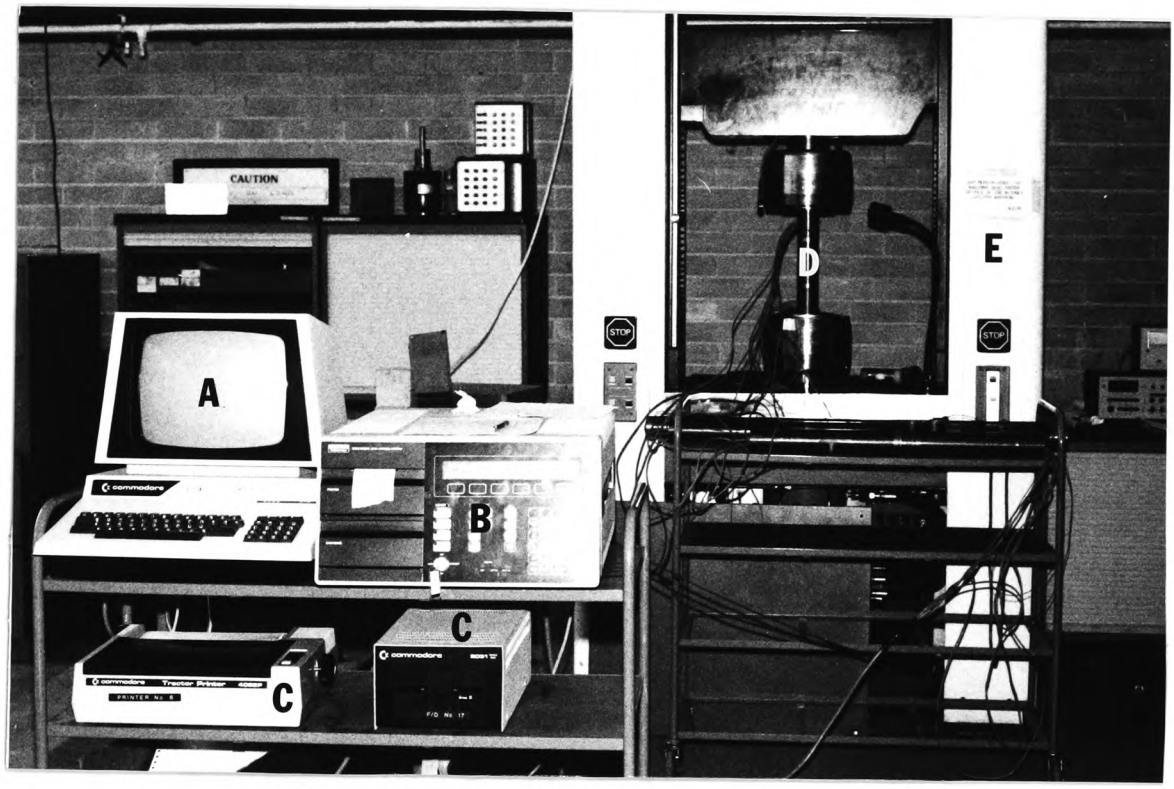

KEY:

A. PET Microcomputer

B. Orion 3530A Data Logging System

C. Data Storage and Output

D. Load Cell under Calibration

E. Instron 1251

PLATE 5.1 Showing Calibration Set-Up for the Axial Load Cells

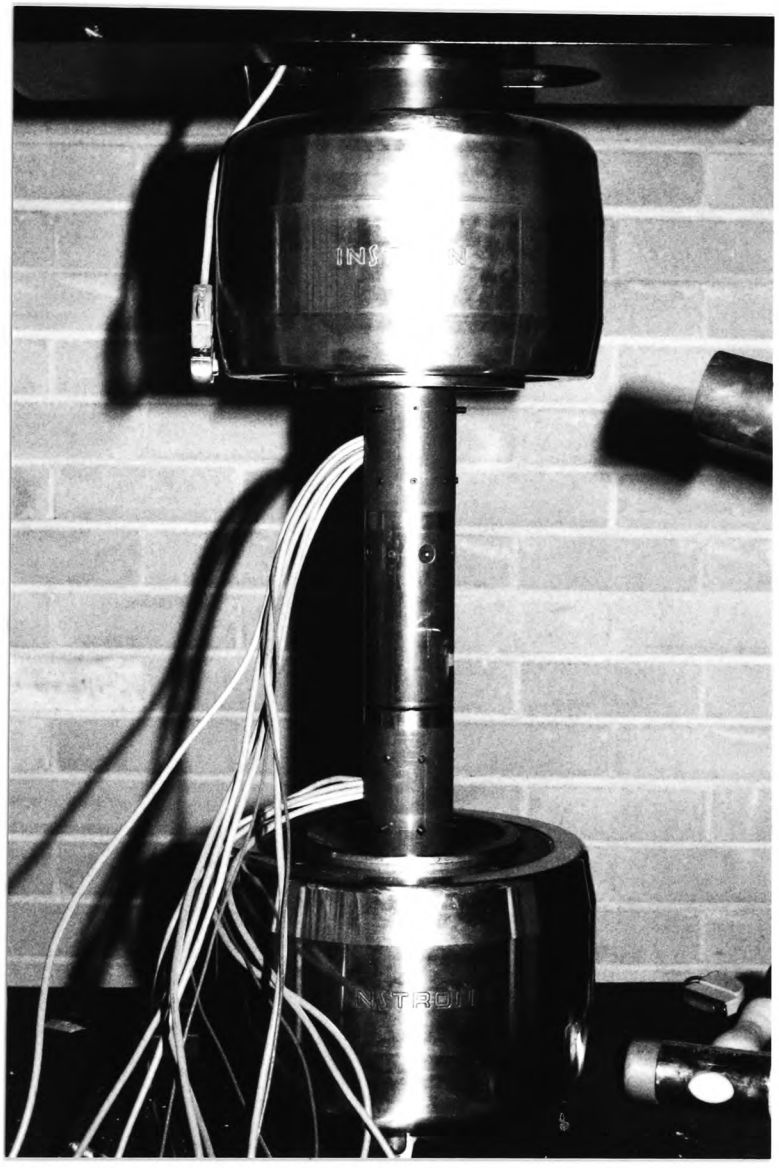

PLATE 5.2 Showing Close-Up of Axial Load Cell under Calibration

used to energise the load cell as opposed to the internal Orion power source of 2 volts.

The external power source was used because a greater energising voltage was needed to compensate for the increased wall thickness of the load cell made necessary by the method of driving. The stability of the external power source has been fully discussed and documented by Wersching (1986).

In order to determine what maximum load to calibrate the load cells to, an estimate of the static bearing capacity of the pile was made using the well known relationship:

$$Qu = Qb + Qs$$

where Qu = ultimate bearing capacity

Qb = ultimate base resistance

Qs = ultimate shaft resistance.

Using Terzaghi's equation for a circular foundation and neglecting the breadth term gives:-

$$Qb = po.(nq-1).Ab$$

po = effective stress of base load

nq = bearing capacity coefficient

Ab = area of base

Using the relationship suggested by Meyerhof (1953):

$$Qs = Ks.po.\tan\delta.As$$

Ks = constant depending on soil type

δ = angle of wall friction

As = surface area of embedded shaft

These relationships hold for sand but it was envisaged that the pile would also be driven into an underlying clay stratum. Therefore the estimated bearing capacity equation was

modified to:

$$Qu = Qb(clay) + Qs(clay) + Qs(sand)$$

Qb clay is given by:-

$Qb = Nc \times Cb \times Ab$ (Meyerhof 1951)

Nc = bearing capacity factor (9.0)

Cb = undisturbed shear strength of soil at base pile

Qs clay is given by:-

$Qs = \alpha \times \bar{c} \times As$

α = adhesion factor = 0.45

$\bar{c}$ = average undisturbed shear strength of the soil adjoining the pile.

The calculated values for Qu were 5.0 and 9.0 Kn respectively.

Using an appropriate safety factor it was therefore decided to calibrate the pile to a maximum load of 15 Kn in increments of 3 Kn.

Prior to a calibration run the load cell was loaded and unloaded a total of 10 times. This was to ensure that any possible lock up of stresses due to manufacture and assembly was as far as possible avoided. Each load cell, apart from the toe load cell was calibrated in both compression and tension. The calibration procedure for tension was identical to the compressive calibration except that the load cell was calibrated to 5.0 Kn in increments of 1.25 Kn.

5.1.4 Procedure

After the initial loading and unloading sequences the calibration procedure was as follows:-

(1) The pile was loaded in 3 Kn increments up to the maximum value of 15 Kn.

(2) The pile was then unloaded, again in increments of 3 Kn back to zero.

(3) The load cell was then turned through 360 degrees in 90 degree increments and the process repeated each time.

This gave a total of 4 complete loading cycles and ensured that any errors arising from unevenness of the bearing surface would be minimised.

The data from each calibration was stored on disc for later use in a polyfit program to determine the calibration constants. Full details of the data storage methods are given by Wersching (1986).

Fig. 5.1 shows the calibration graphs for tension and compression and highlight three important facts:-

(1) The calibration of the load cells were linear in both the compressive and tensile regions for the ranges tested.

(2) The calibration factors for the tensile and compressive phases of loading differed from each other by a maximum of 3 per cent ranging down to a minimum of 0.002 per cent.

(3) Each calibration graph displayed a zero offset which was due to the initial out of balance voltage of the bridge circuit and therefore of no concern.

5.1.5 Inclinometers

Plate 5.3 shows a typical set up for calibrating an inclinometer. The apparatus consists of three

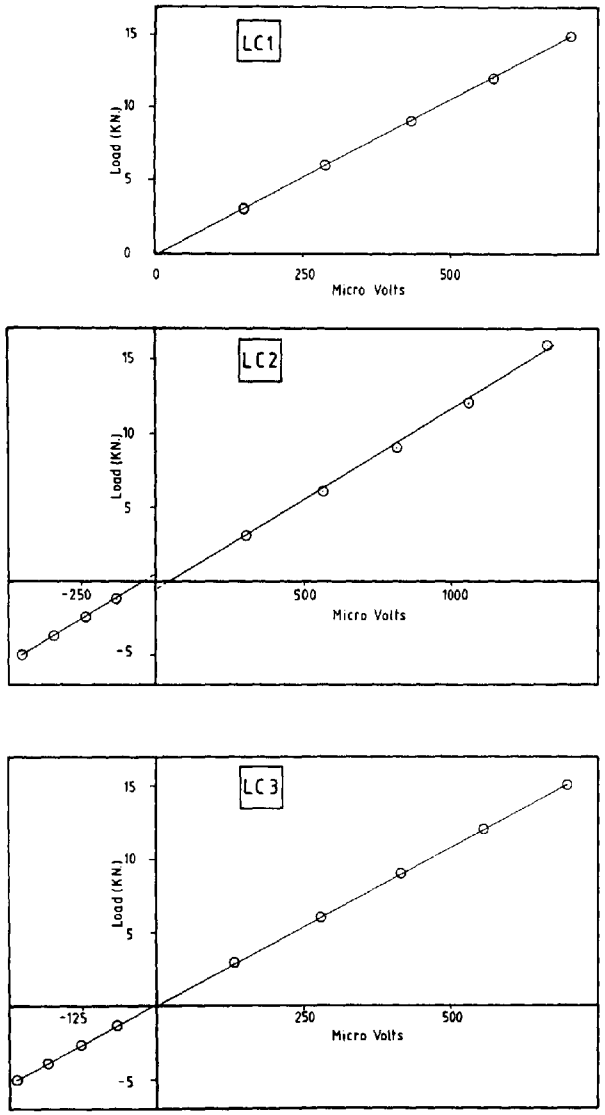

FIG N° 5.1 SHOWING CALIBRATION GRAPHS FOR THE STATIC AXIAL LOAD CELLS (SEMI-FULL SCALE PILE)

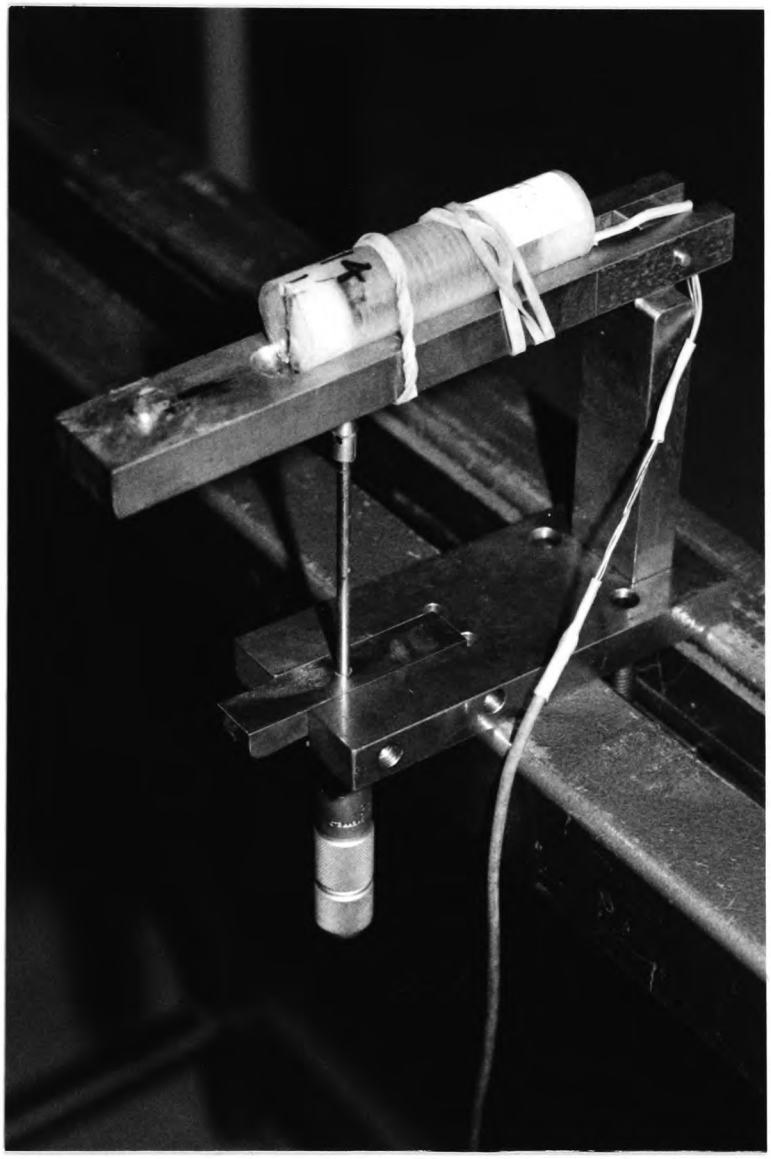

PLATE 5.3 Showing Typical Calibration Set-Up for an Inclinometer

major parts:-

(a) A base plate which incorporates an apeture for positioning a depth gauge (micrometer) with a vertical column at the plates rear.

(b) A hinged top plate which is grooved to allow the inclinometer to be mounted securely.

(c) A depth gauge with a conical brass point to support the hinged top plate.

The calibration procedure was then as follows:-

(1) The inclinometer was mounted in the calibration frame with its axis vertical.

(2) Using the control program previously described and with visual reference to the P.E.T. screen a null voltage was obtained by adjusting the micrometer barrel. This ensured that the inclinometer was truly horizontal before commencing calibration.

(3) Readings were then taken at 2 mm intervals up to an elevation of 18 mm.

(4) The process was then repeated until the inclinometer was again horizontal.

(5) Steps 3 and 4 were then repeated but this time for depression.

As in Section 5.1.4 the data was stored on disc for later use in a polyfit program to determine the calibration constants.

The calibration procedure for the inclinometers is a brief description only, for full details see Werscheing (1986).

5.1.6 Pressure Transducers

As with the inclinometers full calibration details are given by Werscching (1986) with a brief description included here for the interest of the reader.

The calibration procedure for a transducer was as follows:-

(1) The transducer was placed in a circular ply housing of depth equal to that of the transducer.

(2) The housing and transducer was then mounted in a Roe pressure cell. (The outside diameter of the ply housing being equal to the internal diameter of the Roe cell).

(3) The cell was then sealed and filled with water.

(4) Air pressure was then applied in increments of 5 Kn/m^2 up to a limit of 30 Kn/m^2.

(5) The process was then repeated from 30 Kn/m^2 down to zero.

Again as in the other calibration procedures, data was stored on disc for use in a polyfit program to determine the calibration constants.

5.1.7 Shear Transducers

The shear transducers used were designed by Werscching (1986) and are a variation of the miniature normal and shear transducers used by him in a 110 mm diameter tubular steel pile to determine pile interface stresses.

Full calibration details are given by Werscching (1986) together with the method of manufacture, strain bridge configurations, etc.

5.1.8 Linear Variable Differential Transformer (L.V.D.T.)

The long stroke of the L.V.D.T. (600 mm plus) made normal calibration techniques such as used in the smaller stroke displacement transducers (max. stroke 75 mm) impractical. To this end the bed of a precision milling machine with a travel of 650 mm was used.

The basic procedure was as follows:-

(1) The L.V.D.T. was secured to the bed of the milling machine.

(2) The bed was then moved in 50 mm increments up to 600 mm.

(3) The process was then repeated from 600 mm down to zero.

(4) The results were then averaged and a calibration graph drawn.

5.2 Soil Placement and As Placed Properties of the Sand

5.2.1 Sand Placement

The Redler conveyor used to lift sand from one tank to another inevitably caused a great deal of dust to be produced while placing the sand. Kay (1980) devised a system for minimising the dust problem during placing which consisted of various lengths of flexible hosing running from the conveyor outlet to the sand surface.

Sand was deposited through an 85 mm diameter tube located in a larger 150 mm diameter tube. A dust extraction unit connected to the outer tube then removed the dust between the two tubes before it reached the atmosphere.

This method was only partially successful as the extraction unit was not powerful enough to cope with the volume of dust. Since that time the original dust extraction unit has been replaced by a large Nilfisk industrial vacuum cleaner with a further Nilfisk cleaner being trained on the outlet of the flexible pipe to 'catch' any remaining dust escaping into the atmoshpere. This combined with careful operator control of the flexible pipe has succeeded in reducing the dust problem to an acceptable level.

The method of sand placement thereafter was as follows:-

(1) Sand was deposited in the tank using the flexible pipe previously mentioned. A sweeping motion was employed during pouring which distributed the sand evenly and ensured that secondary placement was kept to a minimum. This was necessary in order to limit the possibility of local density variations. During placing care was taken to ensure an even drop height of between 150 - 250 mm.

(2) When a 250 mm deep layer had been placed the surface was smoothed over using level boards and the horizontal level corrected using a spirit level as a proprietry step to placing instrumentation.

(3) This process was repeated for each 250 mm layer with the length of the flexible tube being adjusted to accommodate the decreased drop height. A total of 10, 250 mm layers, were placed in this way with care being taken not to pour sand directly onto any instrumentation in order to prevent disturbance.

5.2.2 Density Checks during Placing

In an attempt to monitor the as placed density of the sand from layer to layer the following methods were adopted.

(1) Two standard CBR moulds were placed in each layer and the sand allowed to fill the moulds using the same procedure as in the actual pouring. The moulds were then retrieved and the densities determined.

(2) To monitor the relative density of the placed sand a small version of the Mackintosh Prospector Probe has been developed, Kay (1980) and is used in two predetermined positions in each layer at a radius of 960 mm from the pile central axis.

(3) Sand/plaster mixtures as described in Chapter 3, Section 3.9.6 were also placed at levels indicated in Figure No. 5.2 and served as a further check on the as placed densities.

The results of the minimac probes are shown graphically in Figure No. 5.3 whilst the CBR mould density determination and sand/plaster densitys are presented in Chapter 6.32.

As a further check of insitu density and also to verify the sand/plaster mixture results two CBR moulds were left in place during a test at the second layer of density samples (Fig. No. 5.2) and retrieved after the experiment was completed.

It should be noted that the procedure for placement of the sand was the same for all tests even though no instrumentation was placed in the sand below the sand/clay interface for test 3. This was made necessary to ensure continuity of placement over the complete series of tests.

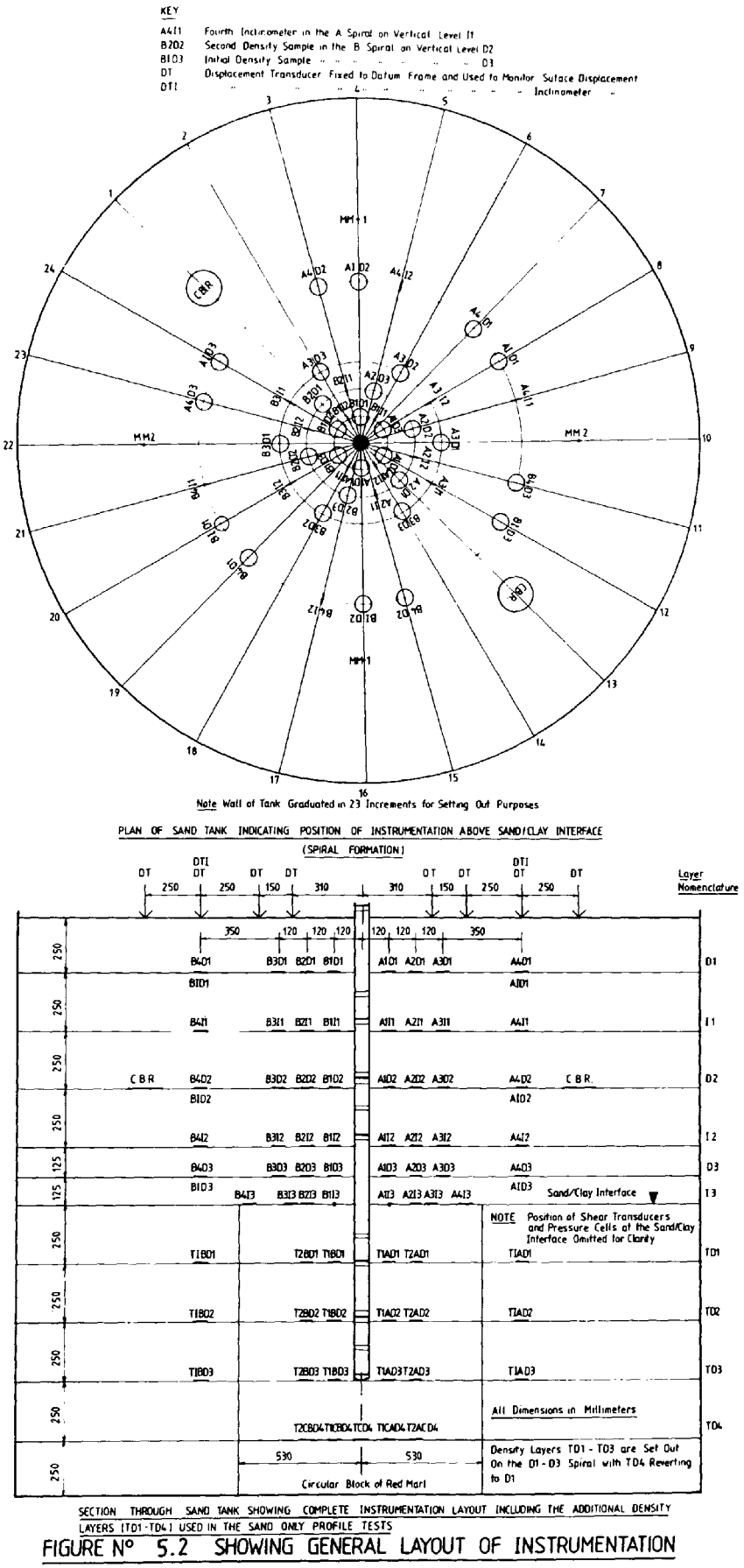

PLAN OF SAND TANK INDICATING POSITION OF INSTRUMENTATION ABOVE SAND/CLAY INTERFACE

(SPIRAL FORMATION)

SECTION THROUGH SAND TANK SHOWING COMPLETE INSTRUMENTATION LAYOUT INCLUDING THE ADDITIONAL DENSITY LAYERS (TD1-TD4) USED IN THE SAND ONLY PROFILE TESTS

FIGURE N° 5.2 SHOWING GENERAL LAYOUT OF INSTRUMENTATION

The results of the minimac probe shown in Figure No. 5.3 highlights two important points:-

(1) The formation of a 50 mm 'crust' which was relatively denser than the overall mass of sand at the surface of each layer caused by secondry placement and levelling.

(2) Apart from the 'crust' mentioned in (1) the placement technique produces a fairly homogeneous mass of sand.

5.2.3 Red Marl - Mixing

The basic procedure for preparation and mixing is as described in Chapter 3, Section 3.9.5. A larger volume Hobart mixer of capacity 15 Kg was used because of the increased volume needed to fill the circular former.

After mixing the marl to a moisture content of 18 per cent, it was stored in bins and sealed to prevent moisture loss, again as described in Chapter 3, Section 3.9. The bins were then stored in a temperature controlled room and allowed to condition for 3 months.

5.2.4 Red Marl Placement

The circular wooden former was graduated in increments of 150 mm with sub increments of 50 mm. The former was then lined with two separate layers of Visqueen polythene sheeting, the edges being sealed with Sylglas tape.

Prior to placing the marl three moisture content samples were taken from each bin to ensure that there had been no moisture loss and that there was no significant difference in moisture contents from bin to bin.

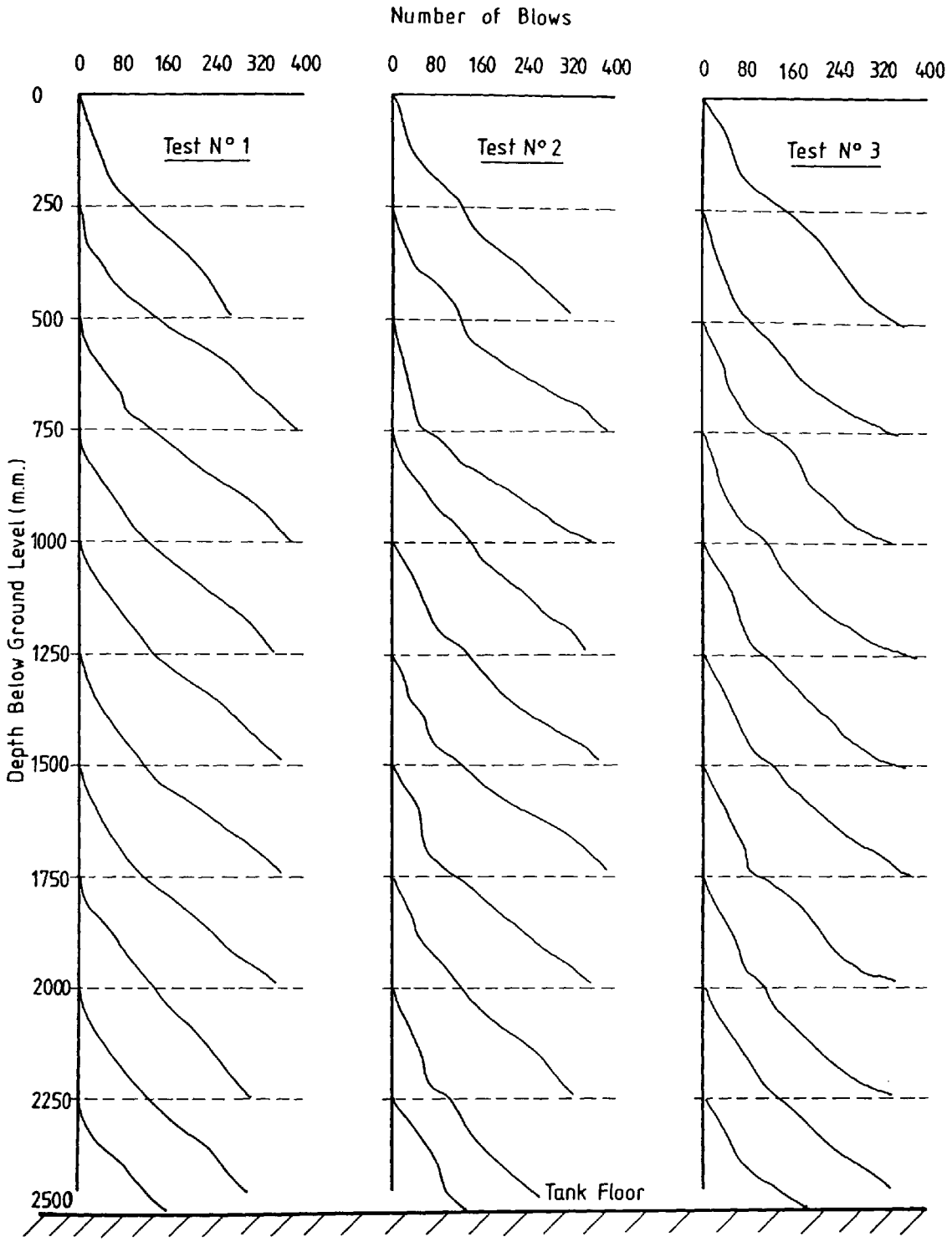

FIG. N°. 5.3 MINI-MAC. PROBE TEST RESULTS

The moisture contents showed that there was no significant difference in moisture content from bin to bin with an average moisture content of 18.1 per cent and maximum and minimum values of 18.6 per cent and 17.4 per cent respectively.

After removing the marl from the bins it was placed in the former to such a depth that when compacted a 50 mm layer had been placed. The marl was compacted as described in Chapter 3, using a Kango Hammer in a kneeding action while using as random a pattern as possible in an effort to prevent predetermined formations in the marl. This process was repeated until a 150 mm layer had been placed.

On completion of each 150 mm layer four core samples of the placed marl were taken using standard U $1\frac{1}{2}$" tubes at 90 degree intervals on a 300 mm radius. The coring was staggered at each 150 mm layer so as not to take cores from the same place each time. After the cores were taken the resulting holes were first 'beaten down' using a hand rammer and then filled before commencing with the next layer.

5.2.5 As Placed Properties of the Marl

The core samples taken were used to determine the as placed moisture content, bulk density, void ratio, degree of saturation and apparent cohesion.

The apparent cohesion was determined by using the unconfined compression apparatus and averaging the values obtained from the two samples.

The procedure for obtaining the remaining marl properties were as follows:-

(1) The samples were cut from the two remaining cores at 50 mm intervals.

(2) The samples were then weighed.

(3) The volume of the samples were then determined by immersion in a beaker of water mounted on a balance and recording the change in weight.

(4) These samples were then oven-dried.

(5) The properties were then determined using basic soil mechanics incorporated in a simple computer program.

The graphical results are shown in Figure No. 5.4 and show the relative uniformity of the placement technique.

5.2.6 Prevention of Moisture Loss at the Sand/Clay Interface

The basic method for sealing the surface of the clay is described in Chapter 3 and consists of spraying the surface with a vinyl waterproof membrane. After the complete surface has been sprayed the membrane was allowed to dry. At this stage the instrumentation was set out and placed as described in Section 5.3.5. Finally a further coat of vinyl was applied over the surface after a light dusting of sand had been applied. This was to ensure that slip between the sand and red marl due to the vinyl coat would be kept to a minimum.

The success of the method in preventing moisture migration was shown when the final test was completed and the sand emptied. The time lapse between placing and emptying was 6 days and in that time moisture had migrated a vertical distance of 11 mm. The average moisture content of the sand was 0.005 per cent.

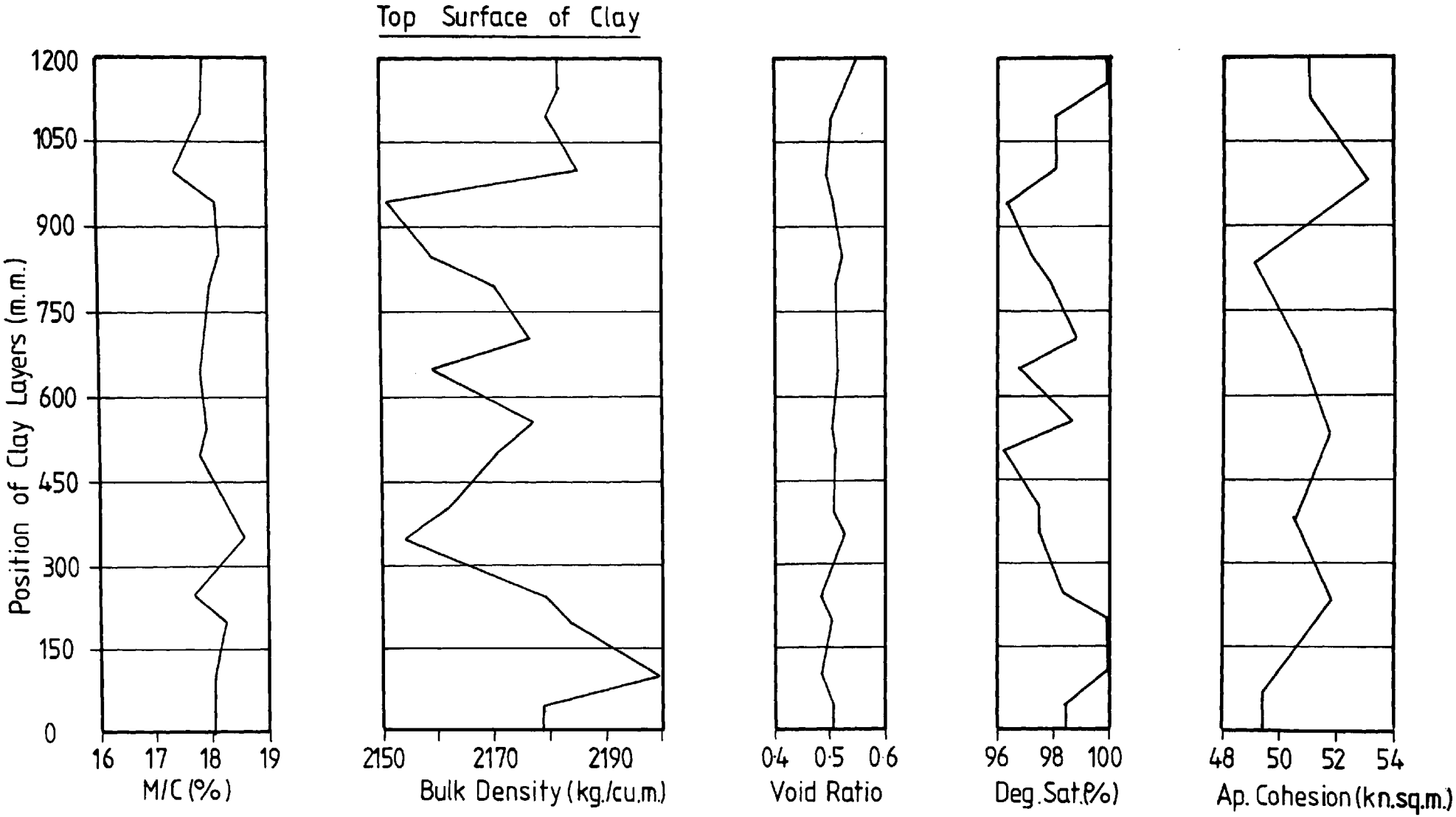

FIG. N° 5.4 SHOWING 'AS PLACED' PROPERTIES OF THE RED MARL

5.3 Instrumentation (Setting Out Details)

5.3.1 General Setting Out Details

As can be seen from Figure No. 5.2 the instrumentation is based on two spiral arms per layer radiating from the centre outwards in opposite directions. In this way any local soil effects which may yield spurious results will be kept to a minimum.

In order to locate the centre of the spiral (model pile vertical axis) a dummy section of pile was inserted in the pile guides. This section has two cross wires soldered to the top end in order to determine the pile vertical axis. A plum bob was then lowered from the cross wires to determine the centre of the spiral at each sand layer.

When the centre point of the spiral was located setting out was achieved merely by referring to Figure No. 5.2 and using a rule aligned with the graduation markings on the tank wall.

The position of each piece of instrumentation was marked using a 'cotton bud' prior to placement.

A similar procedure was used on the clay surface except a felt pen was used instead of the cotton bud for marking.

The instrumentation set up for the sand/clay interface is shown in Figure No. 5.5.

5.3.2 Inclinometers

5.3.3 Procedure for the Placement of the Inclinometers

The placement procedure falls into two main areas:-

(1) Sand.

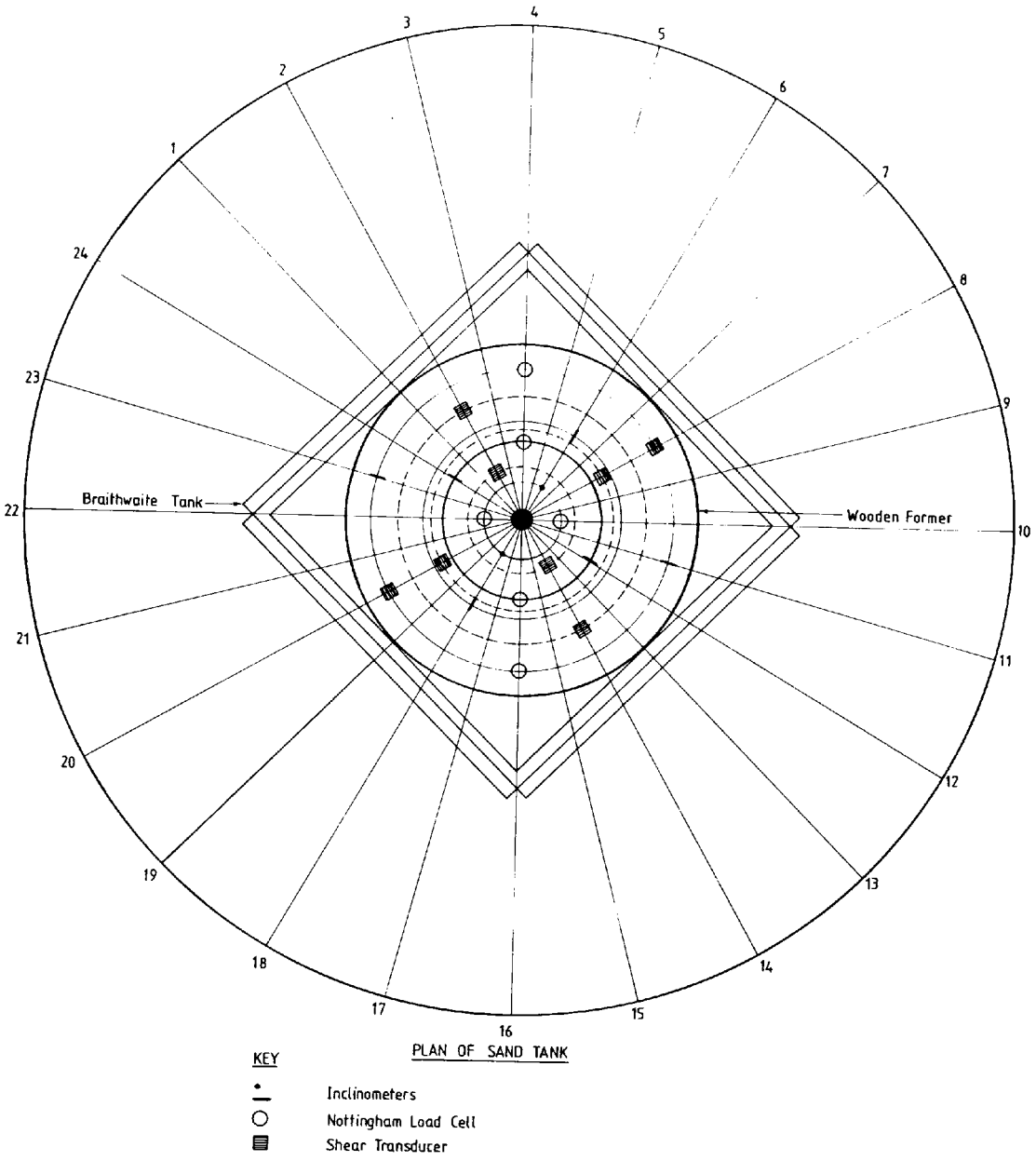

FIG N° 5.5 SHOWING THE INSTRUMENTATION LAYOUT AT THE SAND/CLAY INTERFACE

(2) Clay.

5.3.4 Placement in Sand

Once the surface has been levelled and set out as previously described the procedure for placing an inclinometer was as follows:-

(1) The Orion was set to monitor the inclinometer channel in local control.

(2) The inclinometer was placed in position with its longitudinal axis perpendicular to the model pile wall (Figs. 5.2, 5.5).

(3) The inclinometer was then set in the vertical plane in which it was calibrated by using a small plumb bob arrangement and aligning it with a slit cut in the front of the inclinometer casing.

(4) The inclinometer was then tilted along its longitudinal axis until 0.8 volts was displayed on the Orion (the tilt being adjacent end up with respect to the model pile). The inclinometer was tilted in this way to ensure that the rotation produced by driving would not cause it to pass through its electrical zero. This would cause problems in determining whether rotations were positive or negative in the integration program. This process was repeated commencing with the inclinometer nearest to the pile and working outwards along the spiral.

The placement of the outermost inclinometer in each spiral is somewhat different because each inclinometer has a hinged attachment (Plate 5.4) which is connected to a linear

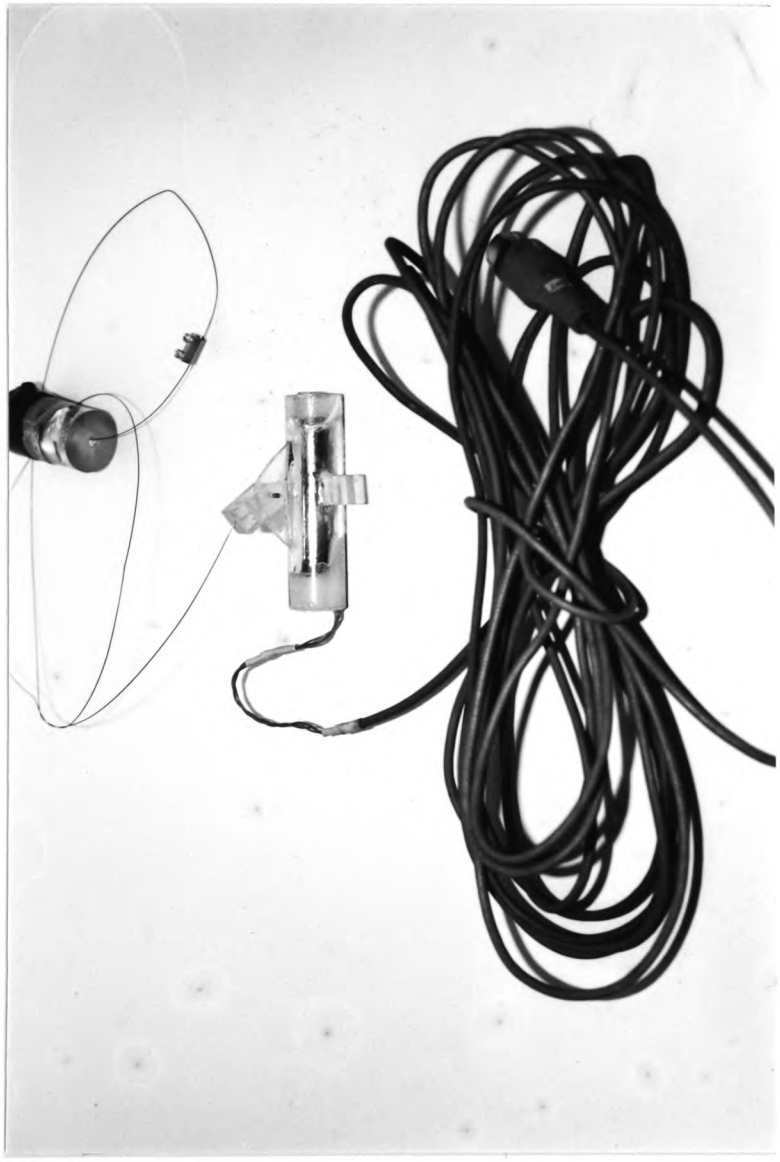

PLATE 5.4 Showing Hinged Attachment on Inclinometer to Measure Gross Vertical Displacements

potentiometer mounted on the datum frame via piano wire.

In this way any vertical movement of the outermost inclinometers may be detected even if no change in the horizontal attitude of the inclinometer has taken place.

Thus incorporation of these displacements in the integration programme means that gross displacements may be displayed as opposed to relative ones. (Wersching (1986)).

5.3.5 Placement in Clay

The placement of an inclinometer in clay follows the same procedure as in sand except for the following differences.

(1) A section of the clay surface was removed so that the inclinometer fitted into the resulting slot up to half its depth.

(2) Prior to fitting the inclinometer in place the slot was treated with vinyl spray to prevent moisture loss.

(3) After the inclinometer had been set up as previously described a final coat of vinyl spray was applied as a further safety measure against moisture loss.

5.3.6 Density Samples

The placement of the density samples is also previously described in Chapter 3. The only additional feature being that the hollow tubes used to hydrate the samples are secured to the side walls in order to prevent them moving during placing.

5.3.7 Pressure Transducers

The procedure for placing the pressure transducers was simply to lay them on the prepared surface in their correct positions in the case of the sand only tests. In the case of the sand/clay tests the procedure follows the same lines as those laid down in the placement of inclinometers in clay except that all of the transducer housing was embedded in the clay.

5.3.8 Shear Transducers

The shear transducers were only used in the sand/clay tests and their method of placement differs with that of the inclinometers in clay only to the extent that the whole of the transducer is placed in the clay.

Plate No. 5.5 shows the sand/clay interface with all instrumentation in place.

5.4 Experimental Procedure (Semi Full Scale)

The experiemntal procedure for the semi full scale tests may be divided into two areas:-

(1) Dynamic driving operations.

(2) Pile loading and pull out tests.

5.4.1 Dynamic Installation (General)

Prior to driving the following procedures were carried out:-

(a) The model pile cap was positioned on the first pile section and secured in place.

(b) The first section was then placed in position in the driving rig.

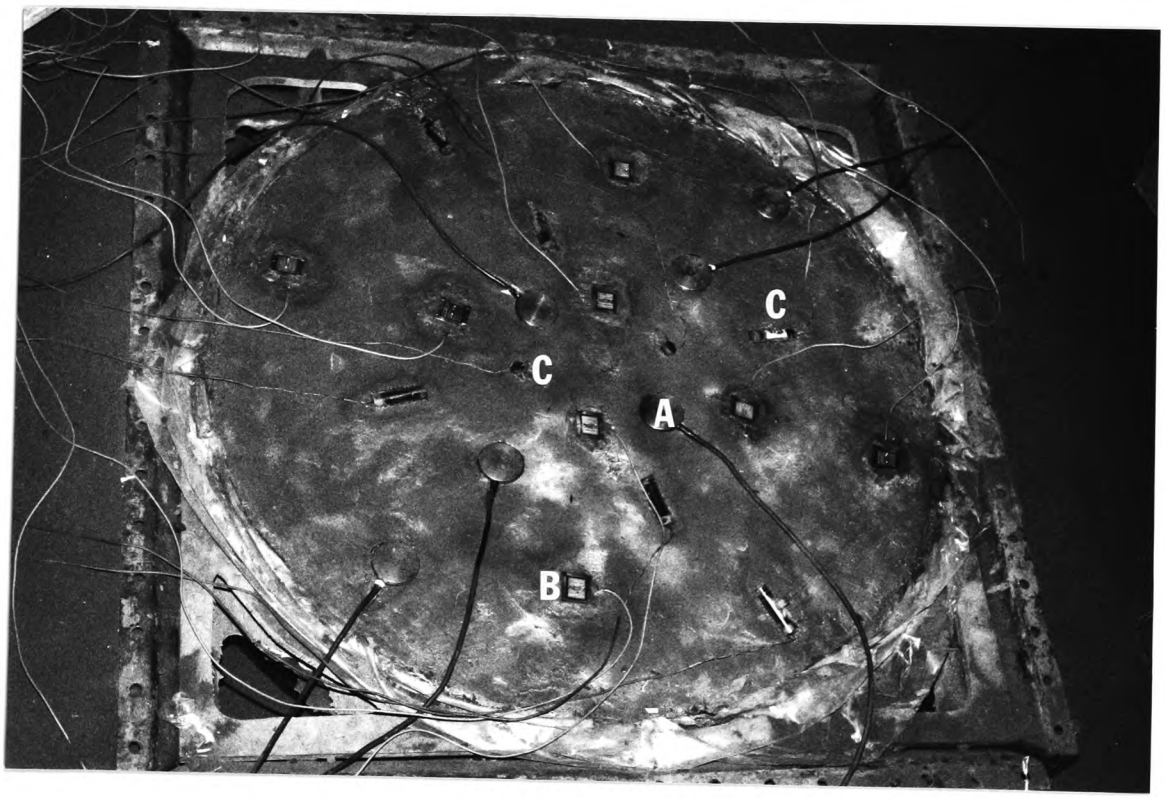

KEY:

A. Nottingham Pressure Transducers

B. Shear Transducers

C. Inclinometers

PLATE 5.5 Showing Instrumentation at the Sand/Clay Interface

(c) The model pile was then pushed into the sand until the top of the cap reached a predetermined position on the driving rig. This was made necessary so that any level irregularities in the sand surface would be compensated for and the pile would be driven from the same position each time.

(d) The L.V.D.T. was then connected to the pile cap as discussed in Chapter 4.

(e) The sand/plaster mixtures used to determine initial densities were hydrated.

(f) Data logging was then commenced using the control program discussed in Chapter 4, Section 4.8.2. Initially the program was used to scan the instrumentation used for static tests a total of 10 times and average these values for use as a datum in the test.

(g) After intialisation the driving option of the static monitoring program is chosen which scans all channels until a preset driving increment is reached (or the program is manually stopped).

5.4.2 Pile Driving

The means of pile driving is fully described in Chapter 4, Section 4.3 and will not be reiterated in this Chapter.

Driving commences with the static monitoring program already in operation. The transient signals are stored and monitored as described in Chapter 3, Section 3.6 with a continual check on the operations of the transducers being kept by outputing one of the signals to the Analyser.

Before driving the complete increment, the driving process is stopped and the U.V. recorder zeroed so that a record of displacement/time for the last few blows of each driving increment may be recorded. The U.V. recorder was then started and driving recommenced to complete the increment. The L.V.D.T. was also connected to a D.P.M. voltmeter so that the change in voltage due to each blow would be recorded to yield a complete driving record.

At the end of each driving increment the model pile clamps are secured to prevent any movement of the already driven section while positioning the next section. The procedure was to tighten screws on opposite diameters in order that the pile should not be pushed out of its alignment by the clamping process. The model pile cap was then removed and positioned on the next section.

After securing the next section the process was repeated until the pile was fully driven.

When the pile was fully driven the model pile cap was removed and the driving rig disassembled to base plate level and a dummy section added to the pile ready for the static tests.

5.4.3 Pile Loading and Pull Out Tests

5.4.4 Constant Rate of Penetration Test (C.R.P.)

Plate 5.6 shows a typical set up for the C.R.P. test with the Dartec Jack mounted in position over the model pile.

A brief history of the C.R.P. test along with recommended penetration rates is given in Chapter 3, Section 3.9.9 and will not be reiterated here.

As can be seen from Plate 5.6 a special pile cap is used which enables all static tests (including Pull Out tests) to be performed without further changing of caps. A recess in the centre of the cap allows a 25 mm diameter steel ball bearing to be inserted between the jack and cap to ensure that load is applied in a vertical direction only.

When the jack has been levelled the L.V.D.T. is clamped to the jack frame and the central rod screwed to the pile cap (Plate 5.6).

When these preparations have been completed the pile clamping screws are released and the appropriate control program option chosen. The jack then drives the pile a total distance of 30 mm at a rate of 1.524 mm/min. Scanning of all channels is continuous with a complete scan taking approximately one minute.

Data recording and output are as described in Chapter 4.

5.4.5 Maintained Load Test (M.T.L.)

It is well known that the displacement of an individual pile recorded by the C.R.P. test does not equate with the settlement of that pile under sustained loading. Thus for the purpose of determination of settlement acceptance criteria at design loads and also higher loads the maintained load test is more suitable.

For the purpose of this test the design load was taken as the load obtained from the C.R.P. test when penetration had reached 10 per cent of the pile diameter divided by a safety factor of 2.5.

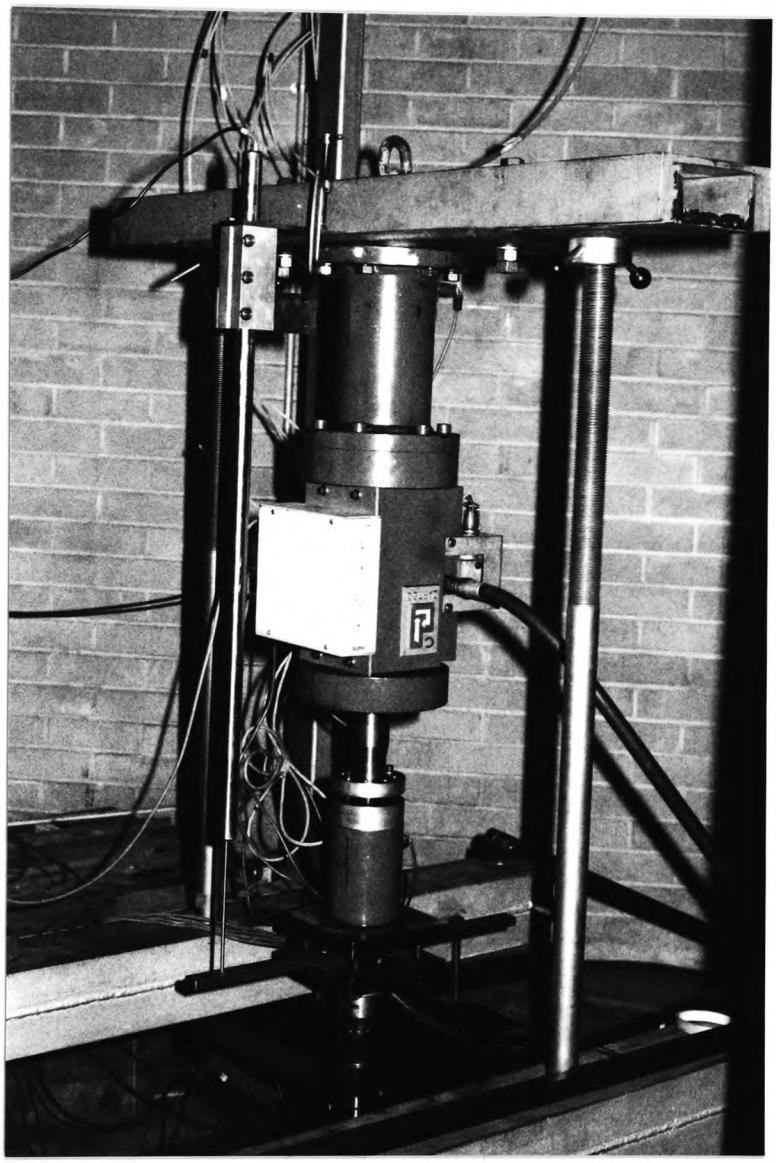

PLATE 5.6 Showing Typical Test Set-Up for Penetration and Pull Out Tests

The loading program and minimum holding times for the test are given in Fig. 5.6.

Load Percentage of Design Load	Minimum Time of Holding (min)
33	10
67	10
100	10
0	10
100	10
133	10
167	10
200	10
233	10
267	10
0	10

FIGURE 5.6

The cessation of movement criteria adopted was that used in the ICE Piling and Model Procedures and Specification (1977) i.e. 0.25 mm/hr providing the rate of settlement is reducing.

As a further check three consecutive readings were taken and each reading checked against the movement before commencing with the next loading increment.

It was soon found that the minimum holding time was not always necessary especially in the case of the sand only profile where the cessation of movement is easy to establish as there is no discernible consoldiation stage and protracted settlement periods are not manifest until failure is approached.

The method employed to perform the tests was as follows:-

(1) The Dartec control box was adjusted so that the jack was registering zero load.

(2) The control lead which interfaced the Dartec control box to the P.E.T was disconnected (manual control

of jack).

(4) The procedure for setting up and levelling the jack prior to a test was the same as for the C.R.P test.

(5) The control program was started using the M.T.L. option and the load increments dialled in manually using the Dartec control box.

(6) The procedure for testing along with percentage load increments and cessation of settlement criteria are as previously described.

(7) After the test was completed all density samples were hydrated before commencing with the Pull Out test.

5.4.6 Pull Out Test

In this test the Dartec jack was carefully lowered using pulley and adjustment nuts so that there was no play in the ball bearing situated between the cap and jack.

Bolts were then placed up through the pile cap and screwed into locating holes in the Dartec jack (Plate 5.6).

The test procedure was then the same as for the C.R.P. test except that the control program retracted the pile a total distance of 30 mm at a rate of 1.524 mm/min.

When the pile had been retracted 30 mm the disc file was closed and the program ended.

It should be noted at this stage that prior to the commencement of the C.R.P., M.T.L. and pull out tests the correct phase on the MTFLG generator must be chosen, i.e. 90 degrees for penetration tests and 180 degrees for pull out tests.

5.5 Instrumentation Retrieval

After each test the procedure for retrieving the instrumentation in sand was as follows:-

(1) After starting the Redler Conveyor a careful watch on the sand surface was kept by an operator situated in the tank above the sump.

(2) When a density sample appeared on the surface it was picked up, sealed in a plastic bag and stored for later analysis. In the case of an inclinometer it was removed from the tank and stored for later use.

In this way 98 per cent of the density samples were retrieved and all but one of the inclinometers.

CHAPTER 6

Discussion of Test Results

6.1 Pile Driving and Dynamic Measurements

6.1.1 General Considerations

The inclusion of the dynamic and static axial load cells in the model pile made a segmental construction the only practical means of assembly. Consequently due to stress wave reflections at joints and discontinuities a quantative analysis of the driving forces was extremely difficult.

One example of this is in the proportionality which exists between the input force and velocity multiplied by $EA/_C$ prior to the stress wave returning to the pile top at time $2L/_C$. This relationship is used extensively in piling (Rausche and Goble (1972)) to validate the shape and magnitude of the force/time relationship from hammer to pile. Ideally to conduct such a comparison the pile should be of single cross section with no joints. However a comparison has been attempted using an average cross-sectional area and is shown in Section 6.2.

Also while every effort was made to ensure that joint fits were perfect, minute differences in the mating surfaces may have caused uneven loading on the dynamic load cells especially when considering the short duration and high value of the impulse loads. The effects of such joints on the overall shape and magnitude of the force/time signals were discussed in Chapter 3. The study showed that distortion of the signal shape was negligible although a numerical increase in peak

force was observed for the enclosed load cell when compared to a similar blow on an 'unconfined' load cell.

It is well to note therefore that although such distortions are small and negligible their effects are present and may alter the natural shape of the signals slightly. It was also noted at an early stage in the research project that due to the short length of model pile, a wave equation analysis to predict bearing capacity was impractical. The latter observations were confirmed by informal discussions with research staff at Queen Mary College, London, who were at the time, having difficulties in mathematically modelling a pile of slightly longer length than the one used by the Author.

To complicate matters further, reference to the displacement time plots in Section 6.7 show that separation of the hammer and pile occurs at an average time of 10 milliseconds, i.e. the hammer and pile are still in contact after the stress wave has returned to the pile top from the tip. This again complicates matters considerably when using a wave equation type analysis. Therefore in the following sections while every effort is made to fit theoretical considerations with experimental results, comparison was not always possible.

6.1.2 Design Criteria for Measuring and Recording Systems

Likins (1982) has laid down a number of criteria for compatability of the measuring instrumentation and pile. These are summarised as follows:-

(1) Accelerometers

The accelerometers must be installed along the central axis of the pile and be linear to at least 1000 g's and 10000 Hz.

(2) Force Transducers

The impedence ($EA/_C$) of the transducer shall be between 50 and 200 per cent of the impedence of the pile at its top.

(3) Measurements

Recorded information should be stored on magnetic tape or equivalent such that components of up to 10000 Hz frequency are accurately stored.

6.1.3 Suitability of the Measuring and Recording Systems

The Author's measuring and recording systems compared favourably with the latter criteria and are summarised as follows:-

(1) Accelerometer

The accelerometer used was mounted along the central axis of the pile and had a linear range of 20 Khz.

(2) Force Transducers

The impedence of the force transducers were difficult to measure with the equipment at hand. All that can be said of the transducer is that the piezoelectric force washers have a stiffness of approximately 15 N/micro meter which when compared with the stiffness of the pile is greater than the figure of 50% quoted.

(3) Measurements

The recording system used was capable of recording and storing signals up to 20 Khz and was therefore more than adequate for the required task.

6.2 Validation of the Force/Time Signal from Hammer to Pile

6.2.1 (Input Signal)

As was explained in Section 6.1.1 a proportionality exists between velocity multiplied by $EA/_C$ and the input force prior to the stress wave returning to the pile top from the tip at time $2L/_C$. For a calculated wave speed of 5170 m/s the corresponding time for the wave to return to the pile head is 0.967×10^{-3} seconds.

Figure 6.1 shows that up to time $2L/_C$ the traces show close agreement with each other for the 3 tests.

At time $2L/_C$ the velocity increases and is indicative of easy driving conditions coupled with low end resistance (Authier and Fellenius (1980 (a)). This is indeed the case for test 3 (sand over clay profile) where the tip resistance has a maximum value of 1.5 KN.

The maximum values of end bearing obtained from a C.R.P. test for tests 1 and 2 are respectively 2.2 KN and 3 KN. These values are again numerically small but are nevertheless an average of 47 per cent of the total bearing capacity.

Therefore the overall low value of bearing capacity coupled with the fairly easy driving conditions (1 blow/11.4 mm for test 1 and 2, 1 blow/4.2 mm for test 3) produce the distinctive velocity traces shown in Fig. 6.1.

Also the velocity trace for the sand over clay test (Fig. 6.1) exhibits a distinct secondary (blip' about $2L/_C$ after the initial peak. Authier and Felleinius (1980 (b)) have shown that this is suggestive of a loose mechanical splice in the pile.

Inspection of the left in place model pile after the test was completed and the tank drained showed that the second connection joint situated 0.2 metres from the mid transducer had indeed slackened slightly, thus confirming the stated reason for the blip.

The close agreement between $VxEA/_C$ and force up to time $2L/_C$ helps to validate both the force/time records and also the acceleration/time records from which the velocity was obtained by integration. Finally the duration of the transient loading (approximately 1.8×10^{-3} seconds) compares well with the figure of 1.7×10^{-3} seconds quoted by Broms and Bredenberg (1982) for steel piles.

6.3 Evaluation of Force/Time Graphs in Relation to Longitudinal Wave Speeds

6.3.1 Introduction

In an effort to show that by using longitudinal wave speeds and superposition, the time to peak force and also secondary peaks can be predicted, the force/time signals obtained from the top, middle and bottom transducers were analysed

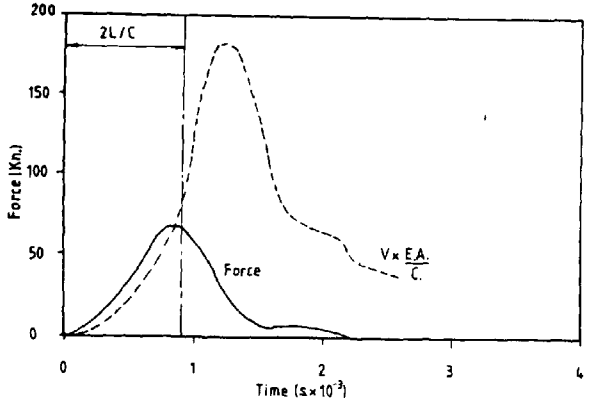

TEST 1 SAND ONLY PROFILE

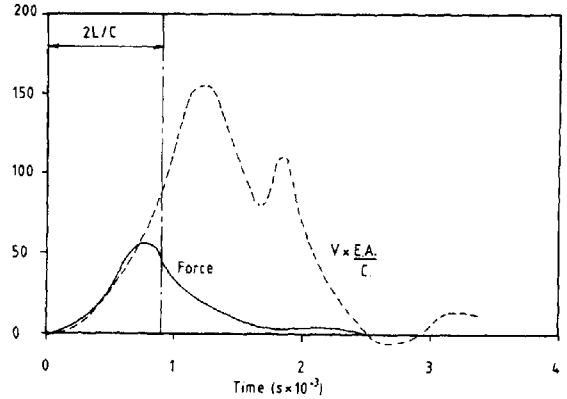

TEST 3. SAND OVER CLAY PROFILE

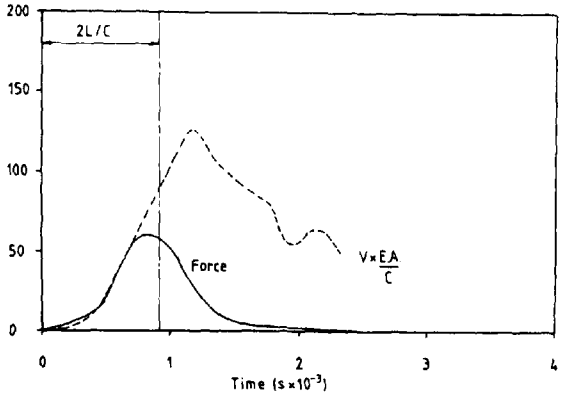

TEST 2 SAND ONLY PROFILE

FIG N° 6.1 SHOWING INPUT FORCE AND VELOCITY (× EA/C) TRACES FOR THE SEMI-FULL SCALE PILE

and the results shown in the following sections. Using a wave speed of 5170 m/sec. and a pile length of 2.0 metres various $L/_C$ ratios have been calculated and are shown below.

$\frac{L}{C}$	$\frac{1}{2}$	1	$\frac{3}{2}$	2	$\frac{5}{2}$	3	$\frac{7}{2}$	4	$\frac{9}{2}$	5
Time $Sx10^{-3}$	0.241	0.483	0.724	0.967	1.21	1.45	1.69	1.93	2.17	2.42

These calculated times were then compared with the experimental ones and conclusions drawn.

6.3.2 Top Transducer (Input Force)

For this pile the maximum force at the pile top was reached at a time of $2L/_C$ i.e. when the reflected wave returns from the pile point to the pile tip.

Subsequent stress peaks are reached and dispersed due to joint discontinuities and also dissipation to the surrounding soil. (Rausche and Goble (1972)). Hence any subsequent peaks will be lower than the initial one. The calculated time to the initial peak is 0.976×10^{-3} seconds which considering the make up of the pile with regard to the number of sections and change in cross sectional areas compared quite favourably to the theoretical time.

The shape and magnitude of the tip force/time graphs are shown in Figures 6.2 to 6.4 and will be discussed in detail in Section 6.4.

At a time of $4L/_C$ the stress wave returns to the pile top for a second time, however there is scant evidence of a peak in

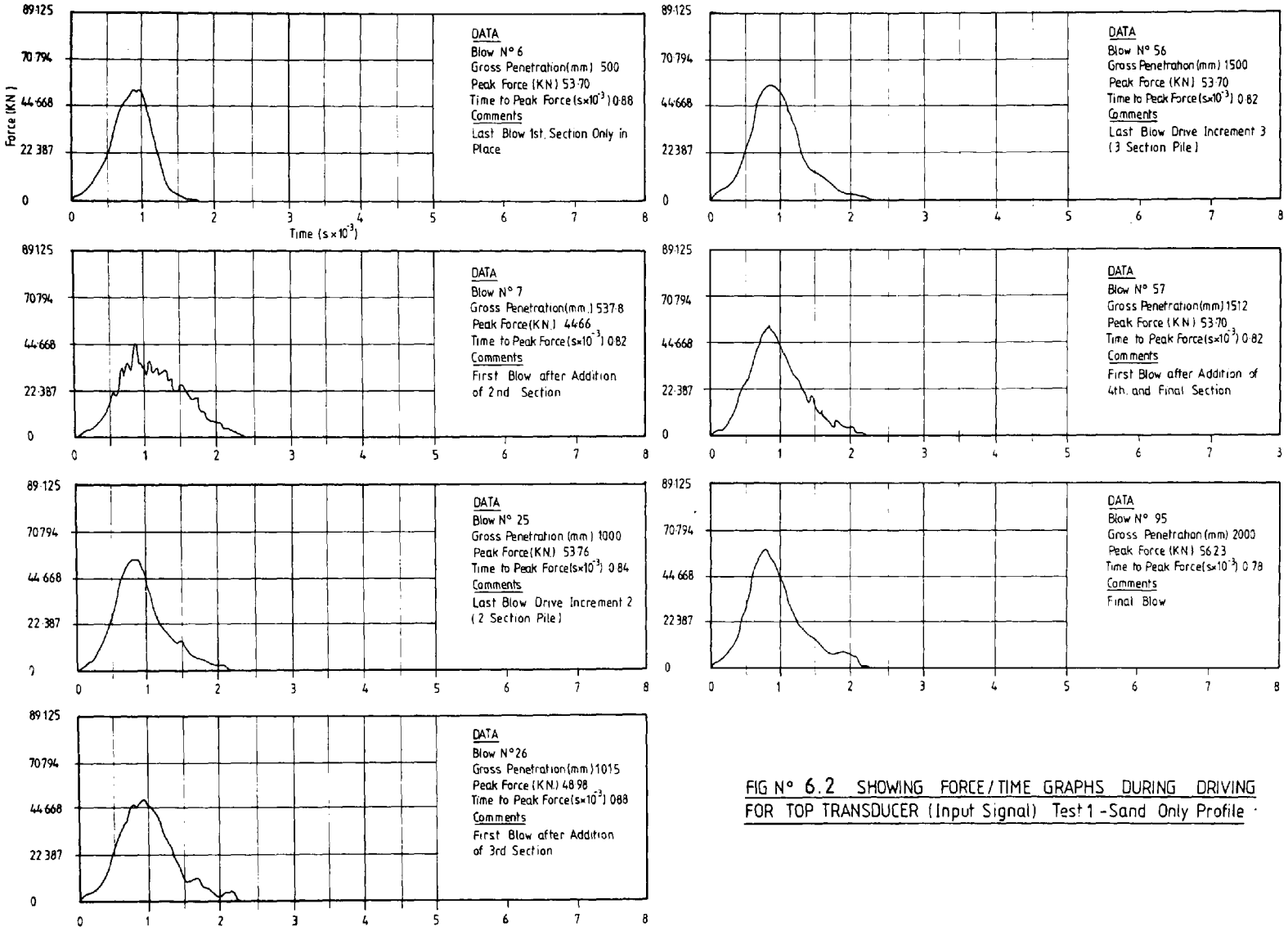

FIG N° 6.2 SHOWING FORCE/TIME GRAPHS DURING DRIVING FOR TOP TRANSDUCER (Input Signal) Test 1 - Sand Only Profile

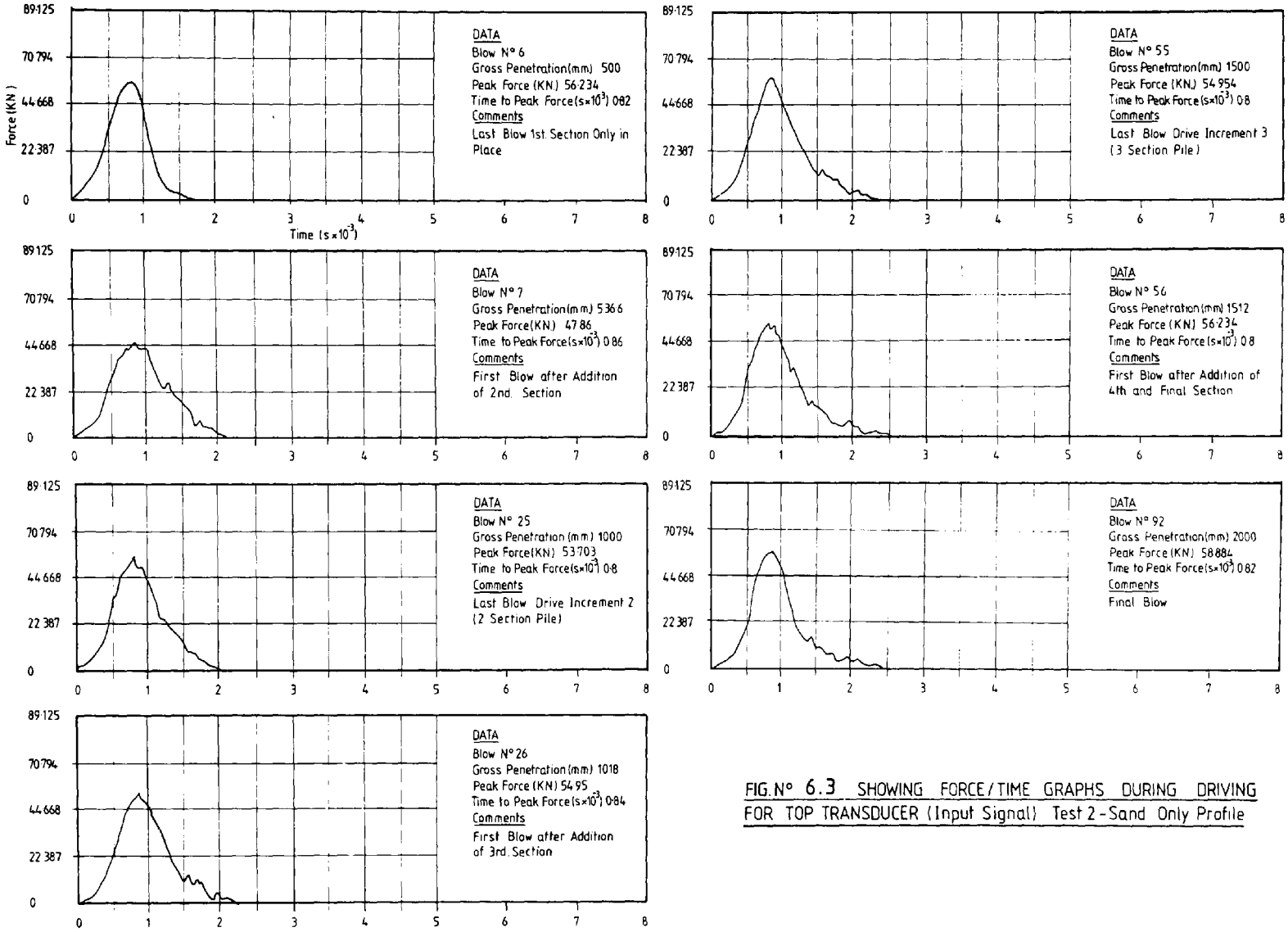

FIG. N° 6.3 SHOWING FORCE/TIME GRAPHS DURING DRIVING FOR TOP TRANSDUCER (Input Signal) Test 2 - Sand Only Profile

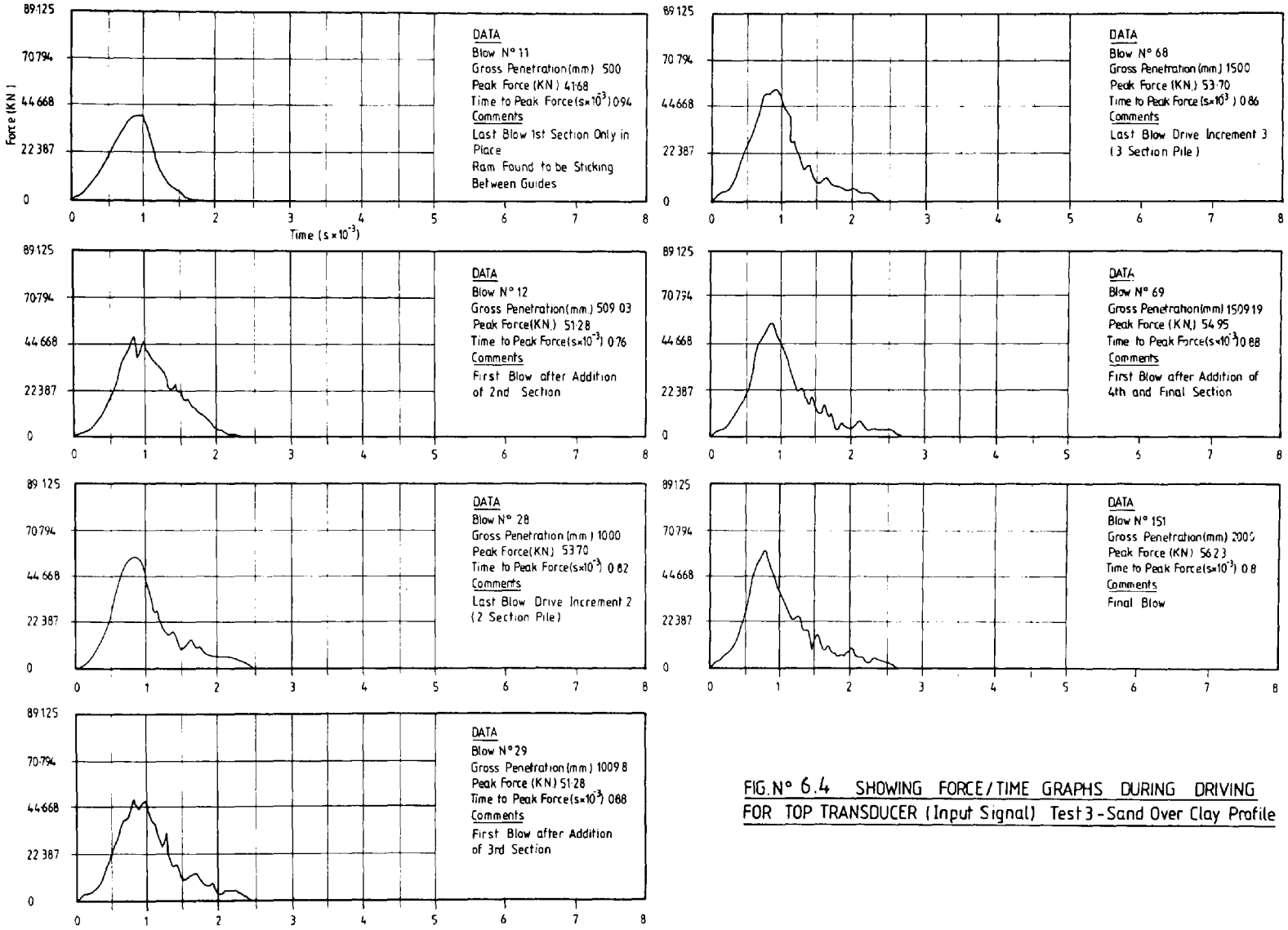

FIG. N° 6.4 SHOWING FORCE/TIME GRAPHS DURING DRIVING FOR TOP TRANSDUCER (Input Signal) Test 3 - Sand Over Clay Profile

the force/time graph at this point although some graphs do exhibit small peaks at the expected time.

6.3.3 Middle Transducer

The middle Transducer as is suggested is situated half way along the model pile and therefore the travelling stress wave will reach the transducer at times:-

$$\frac{1}{2}\frac{L}{C}, \frac{3}{2}\frac{L}{C}, \frac{5}{2}\frac{L}{C}, \frac{7}{2}\frac{L}{C} \text{ etc.}$$

Figures 6.5 to 6.7 show the force/time graphs for the middle transducer at various stages of installation. These signals are generally characterised by three distinct peaks in the compressive part of the signal. The time to these peaks correspond favourably to $\frac{1}{2}\frac{L}{C}, \frac{3}{2}\frac{L}{C}, \frac{5}{2}\frac{L}{C}$ and demonstrate quite clearly the effect that wave superposition has on internal pile forces.

The peak force was reached at a time of 0.7×10^{-3} seconds as compared to a theoretical time of 0.724×10^{-3} seconds ($\frac{3}{2}\frac{L}{C}$). This demonstrates that the maximum peak force is reached on the first return of the travelling wave from the pile point.

This again shows that subsequent peaks are smaller in magnitude due to losses discussed in the previous section.

As with the tip transducer signals the overall shape and magnitude of the middle transducer signal will be discussed in Section 6.4.

6.3.4 Bottom Transducer

Rausche and Goble (1972) stated that "the first non zero

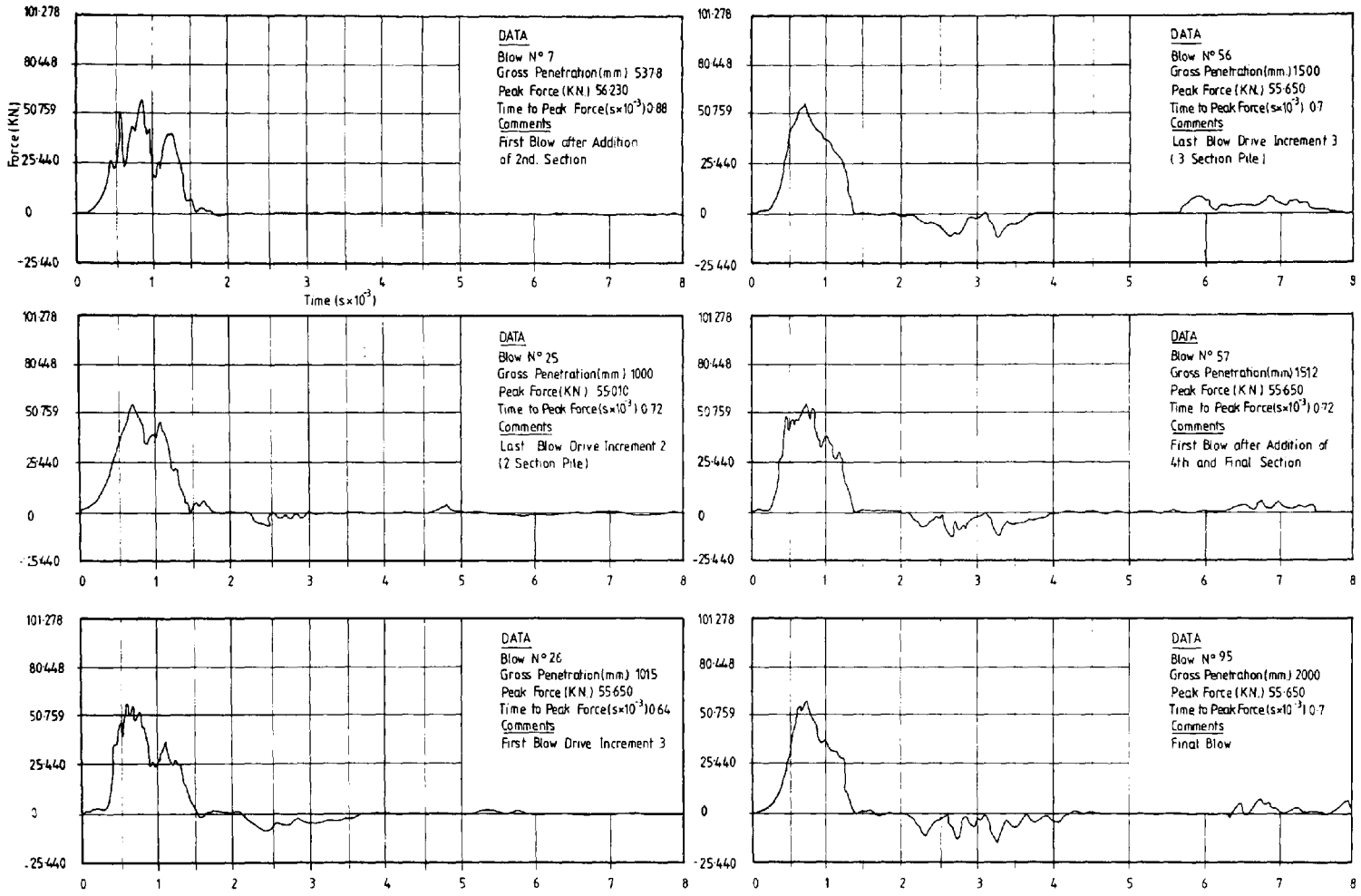

FIG N° 6.5 SHOWING FORCE/TIME GRAPHS DURING DRIVING FOR MIDDLE TRANSDUCER (Test 1 - Sand Only Profile)

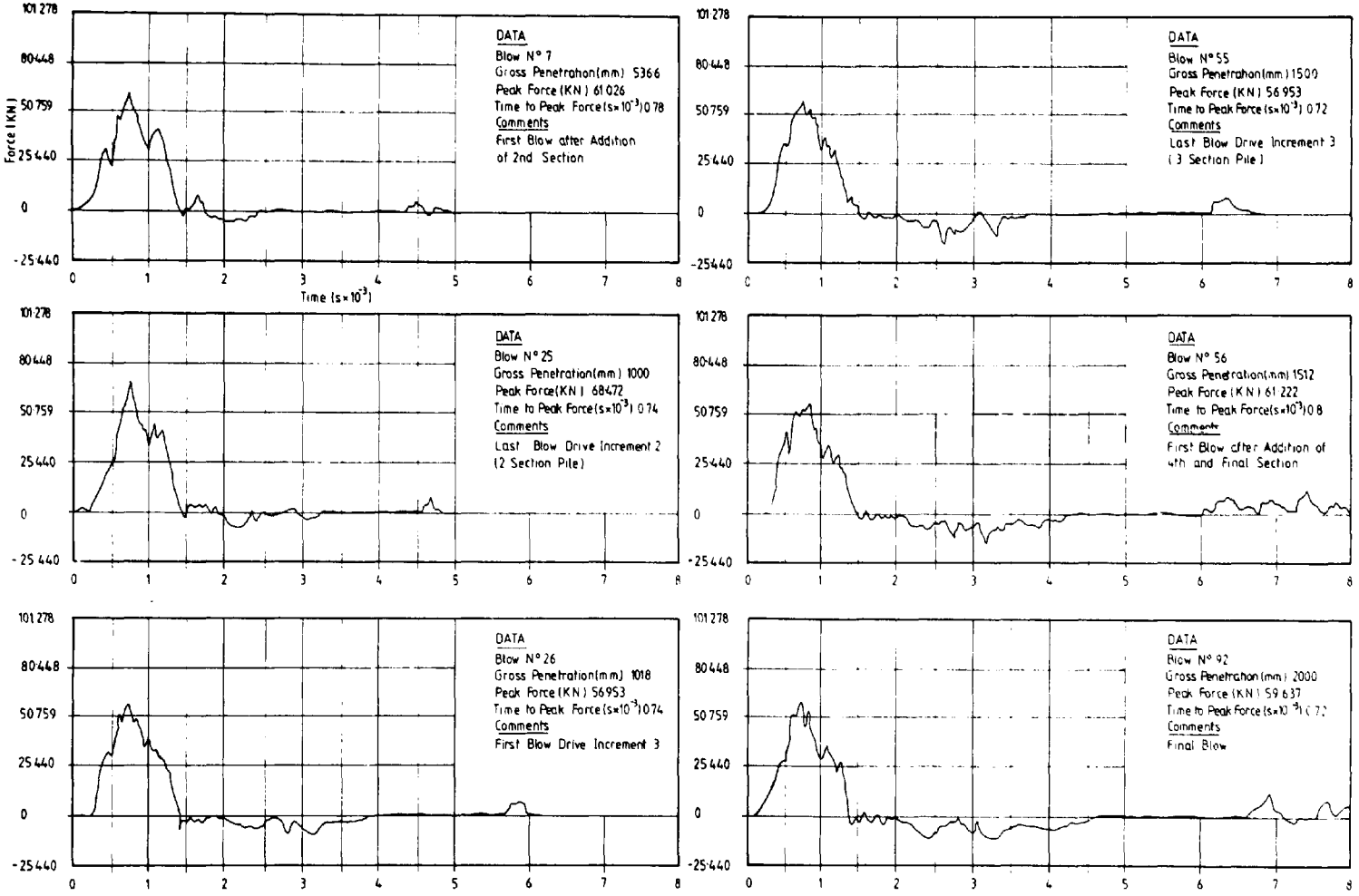

FIG N° 6.6 SHOWING FORCE/TIME GRAPHS DURING DRIVING FOR MIDDLE TRANSDUCER (Test 2 - Sand Only Profile)

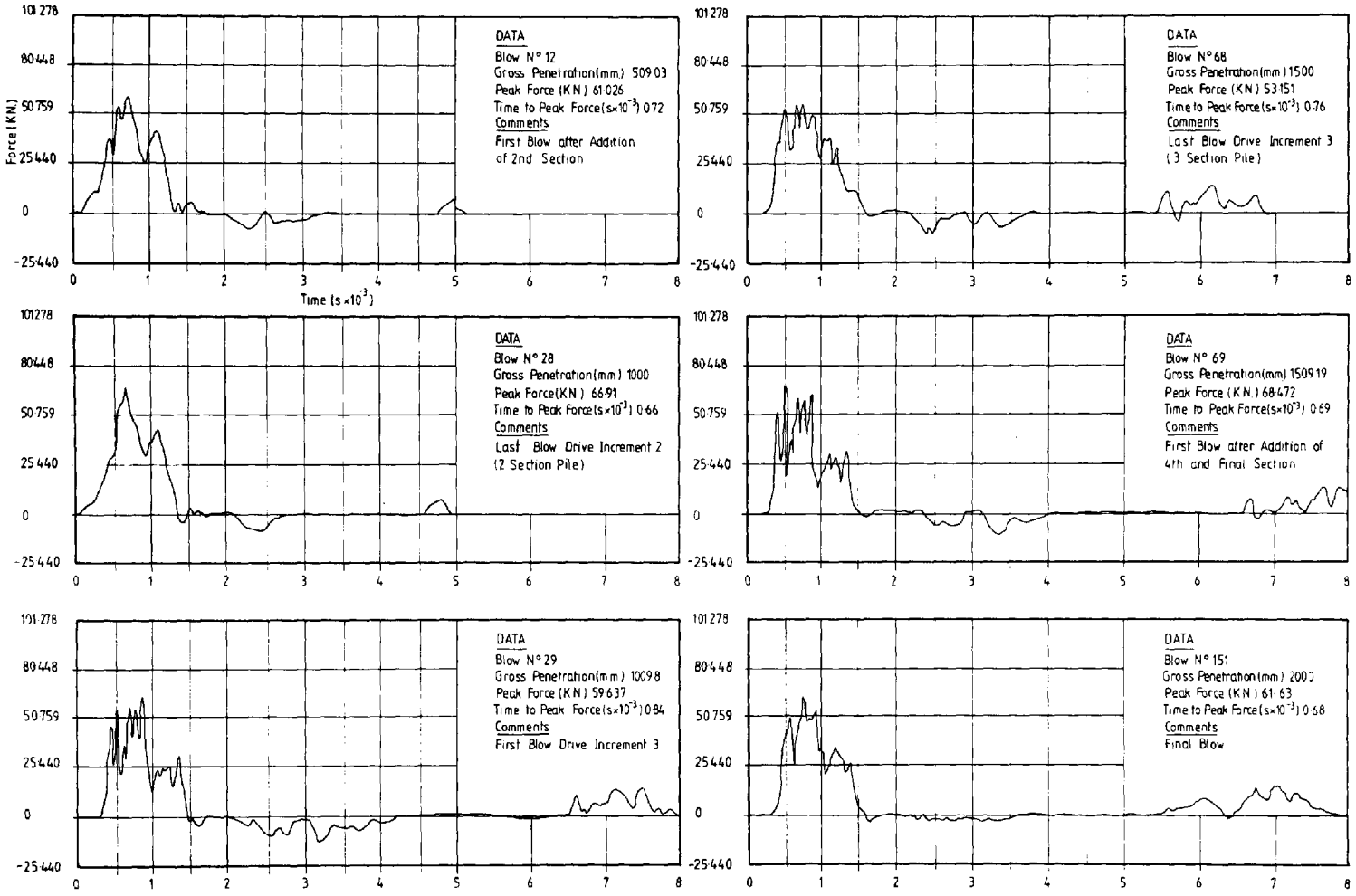

FIG N° 6.7 SHOWING FORCE/TIME GRAPHS DURING DRIVING FOR MIDDLE TRANSDUCER (Test 3 - Sand Over Clay Profile)

value at time $L/_C$ is twice the pile top stress at impact". Moreover in most practical cases the maximum bottom stress also occurs at this time since further stress peaks are reduced due to stress reflection along the pile and energy losses into the soil.

Recourse to Figures 6.8 to 6.10 shows the latter statements to be the case for the model pile. All signals are characterised by a single stress peak occurring at an average time of 0.5×10^{-3} seconds with no further peak of any significance thereafter. The theoretical time for one wave transmission $(\frac{L}{C})$ is 0.463×10^{-3} seconds and again compares favourably to the experimental time given.

It is interesting to note the very short rise time and duration of the force time signal when compared to those of the middle and top transducer and will again be discussed in depth in Section 6.4.

6.4 Effect of the Surrounding Soil on the Shape and Magnitude of the Force/Time Signals During Driving

Before discussing the shape and magnitude of the force time signals, recourse to work on pile point forces (Bredenberg and Broms (1981) already outlined in Chapter 3, Section 3, is necessary.

When the initial stress wave fi(t) reaches the pile point it starts to move. The force fs(t) on the point will increase with increasing displacement xS. At equilibrium

fs(t) = fi(t) + fr(t)

Where fi(t) and fr(t) are the initial and reflected stress waves, respectively. If the tip is free to move, fs will be equal to -fi.

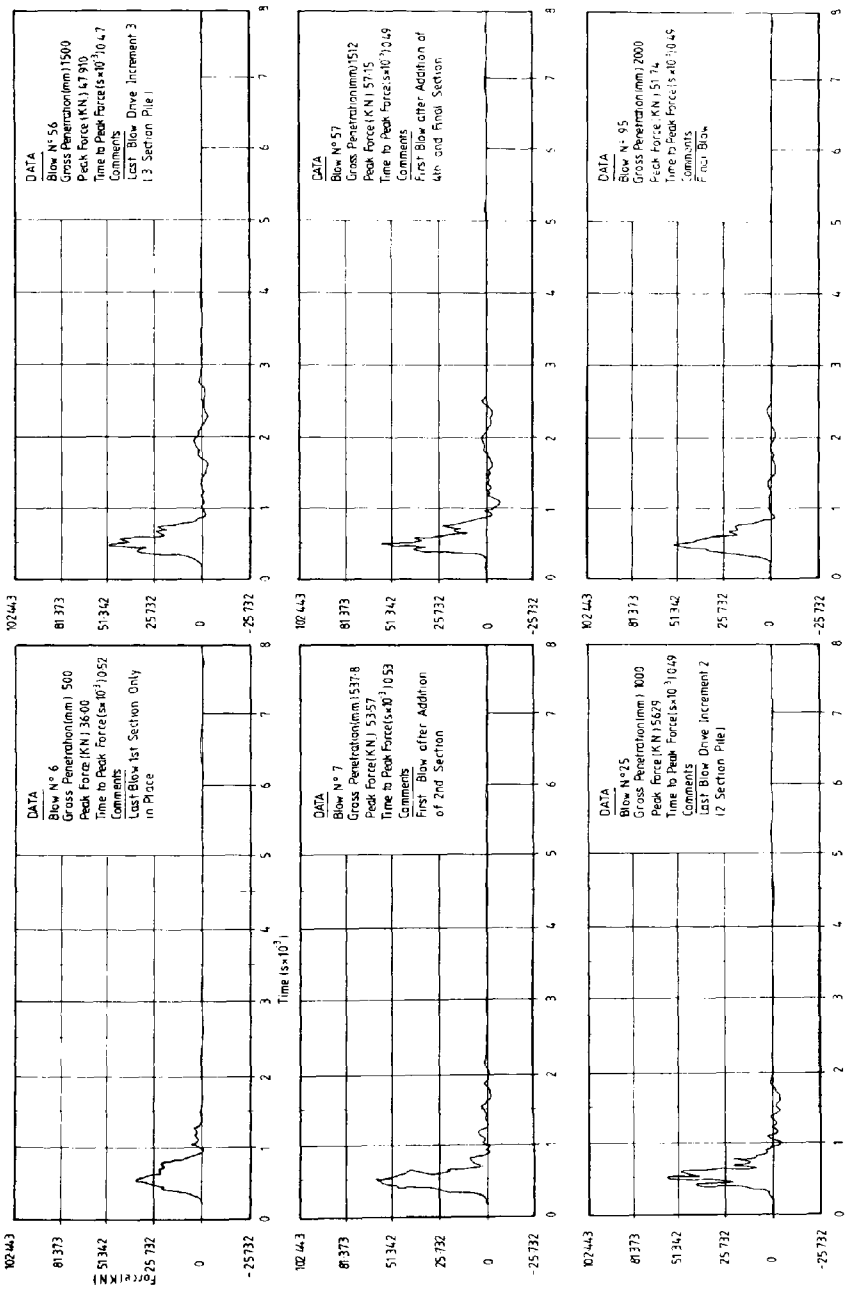

FIG N° 6.8 SHOWING FORCE/TIME GRAPHS DURING DRIVING FOR TOE TRANSDUCER Test 1 - Sand Only Profile

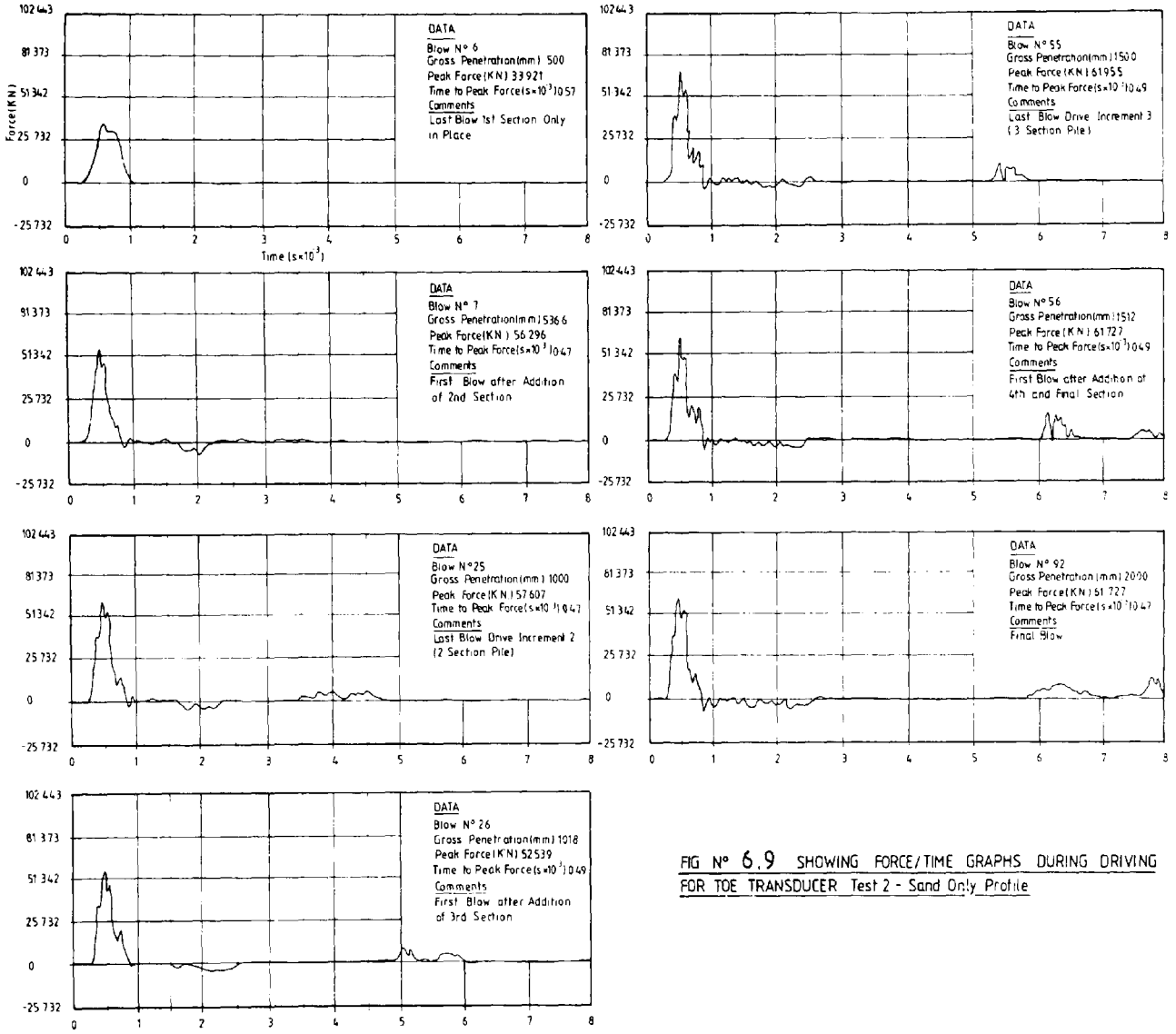

FIG N° 6.9 SHOWING FORCE/TIME GRAPHS DURING DRIVING FOR TOE TRANSDUCER Test 2 - Sand Only Profile

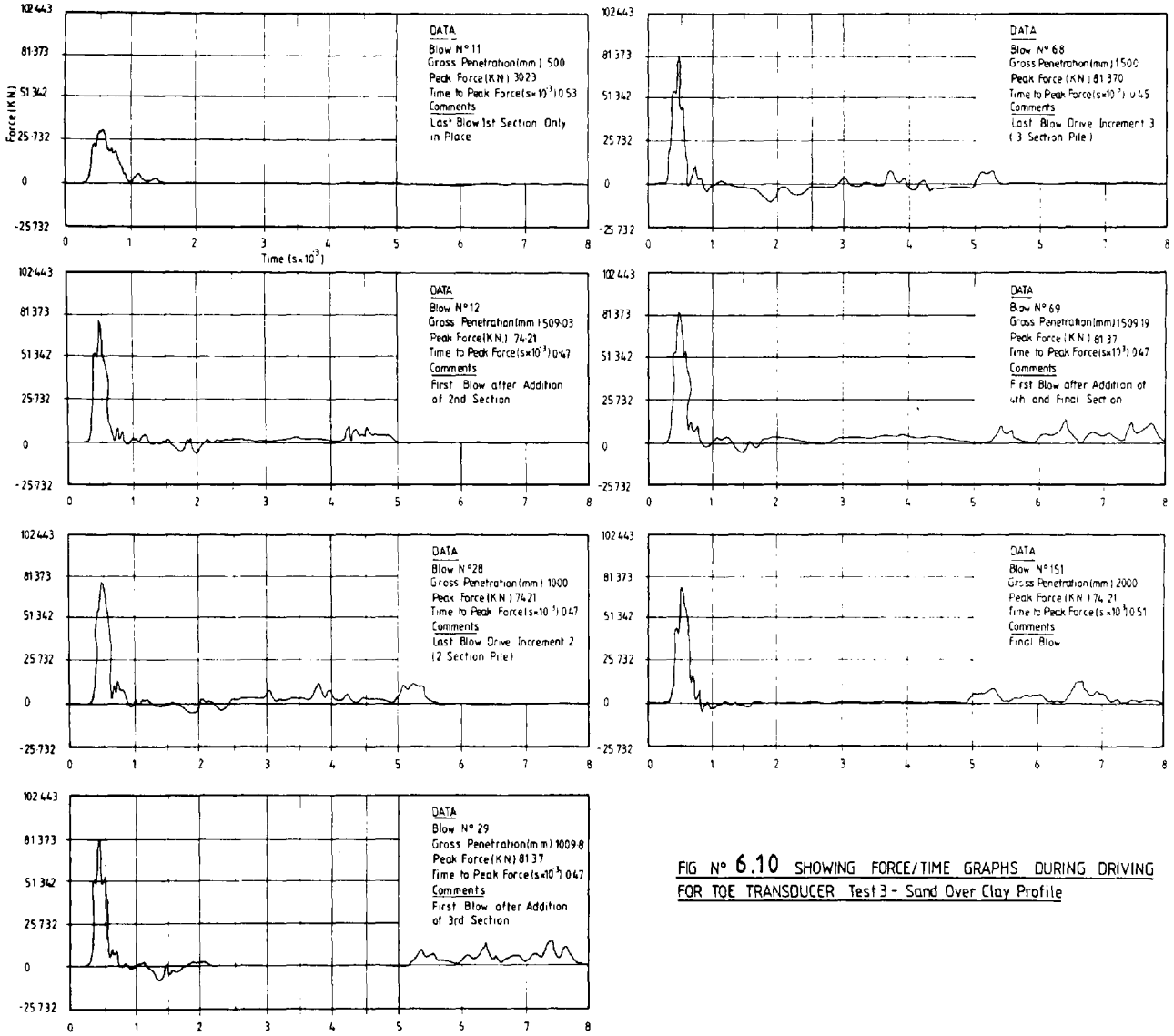

FIG N° 6.10 SHOWING FORCE/TIME GRAPHS DURING DRIVING FOR TOE TRANSDUCER Test 3 - Sand Over Clay Profile

In this case the initial compression wave will be reflected as a tension wave. However if the material below the pile tip is infinitely rigid then fr = fi and fs = 2fi. In this case the initial stress wave is reflected as a compression wave. In actual practice the force on the pile tip falls somewhere between these two extremes.

This is indeed the case with the author's experiments and will be discussed in the following sections.

6.4.1 Top Transducer

The average peak force taken from Fig. 6.2 to Fig. 6.4 show clearly that input force is dependant on ram impact velocity only with Tests 1-3 giving average peak forces of 52.104, 54.683, and 53.52 KN. respectively.

Even in the case of Test 3 (sand over clay profile) where the driving conditions are somewhat different than those of the sand only tests the average peak force is within 124 Newtons of the mean value of the first two tests.

The relatively low peak force displayed in the first driving increment of Test 3 can be accounted for due to the fact that after completion of the drive increment the ram was found to be sticking in the ram guides. After this was remedied the remaining traces corresponded to the expected norm. The slight variations in peak force from blow to blow is due in the main to the small changes in ram impact velocity caused by frictional variations from blow to blow between the ram and ram guides. Figure 6.11 show graphs of peak force/penetration for the three tests.

The plots were obtained by processing the raw data using a standard 'Polyfit' computer program. As can be seen from the results of test 1 and 2 the shape and magnitude of the curve is very similar in nature and characterised by a cubic distribution.

In the case of test 3 (sand over clay profile) the shape of the curve although again cubic in nature is somewhat different at small penetrations for the first two tests due to the lower peak forces obtained from the first drive increment. The reason for the lower peak forces obtained from the first drive increment have been explained previously. Apart from this difference the overall curve shape of test 3 follows those of tests 1 and test 2.

6.4.2 Middle Transducer

It has been explained in previous sections that the force time graphs for the middle transducer are formed from a combination of initial and reflected stress waves.

The average peak forces for the three tests were similar to each other (55.65, 60.71, 61.80 KN respectively) and were an average 11 per cent higher than the average top peak forces.

The shape of the force time signals are similar for the three tests with the only marked deviation from the norm occurring during the latter stages of Test 3. This deviation was characterised by a 'peaky' type of signal especially at the start of the later driving increments. This 'peaky' signal was caused by a joint slackness discussed in Section 6.2 giving rise to increased internal oscilations within the model pile. The total duration of the initial force/time

graph was on average 1.8×10^{-3} seconds with very little tension being displayed thereafter. Unfortunately the lack of tension may have been due to the construction of the load cell in which it was only possible to precompress the cell to a pressure of 414 N/M^2. Figure 6.11 shows that the shape of the averaged peak force/penetration curve is oscillating with a decaying motion and in all cases the peak forces converged on the plot for the top load cell as penetration increased. This indicates that as the pile penetrates, internal oscillations within the pile decrease and the shape and magnitude of each individual signal tends towards an even norm due to the damping effect of the surrounding soil.

It has been stated previously that there was a loss of integrity in the pile for test 3 and this is again shown by the peak force/penetration plot in Fig. 6.11. After the pile penetrates the sand clay interface, little or no oscillation is evident in the trace. This is caused by the unusually high peak forces at the beginning of the driving increments due to joint slackness cancelling out the other signals in the Polyfit averaging procedure. Thus it must be noted that these graphs show general trends and may not highlight slight eccentricity in the individual plots. These graphs are therefore intended as an overall view of the driving situation only.

6.4.3 Bottom Transducer

As has been described in Section 6.3.4 the rise time for the force/time signal is very steep with the force going from zero to a maximum in approximately 0.3×10^{-3} seconds. This

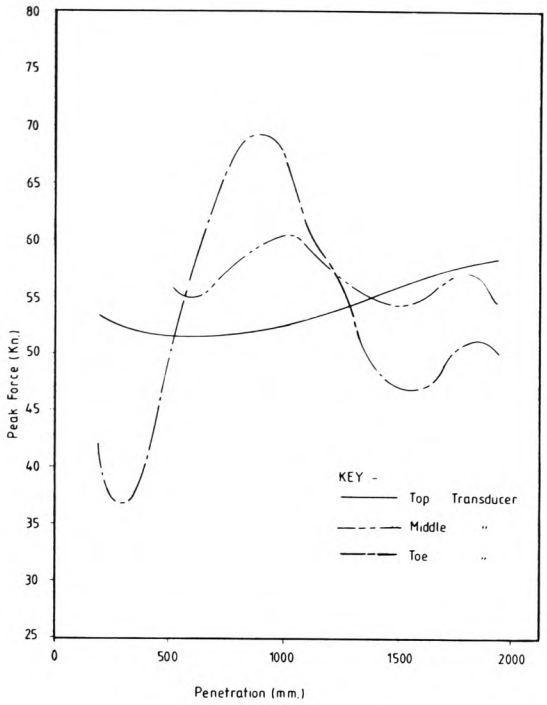

TEST 1 - SAND ONLY PROFILE

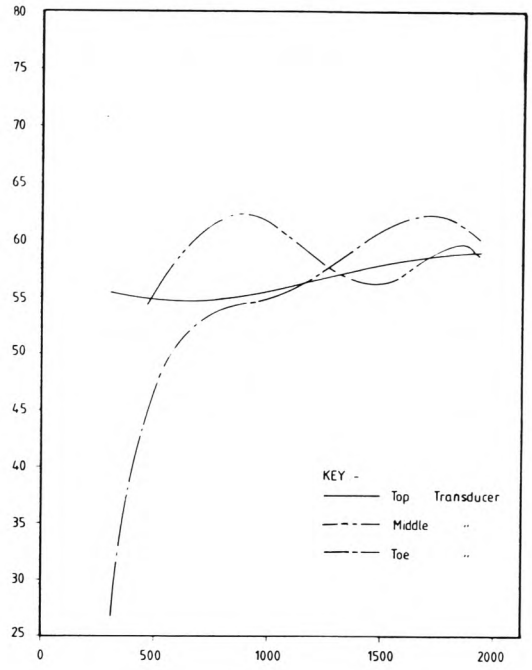

TEST 2 - SAND ONLY PROFILE

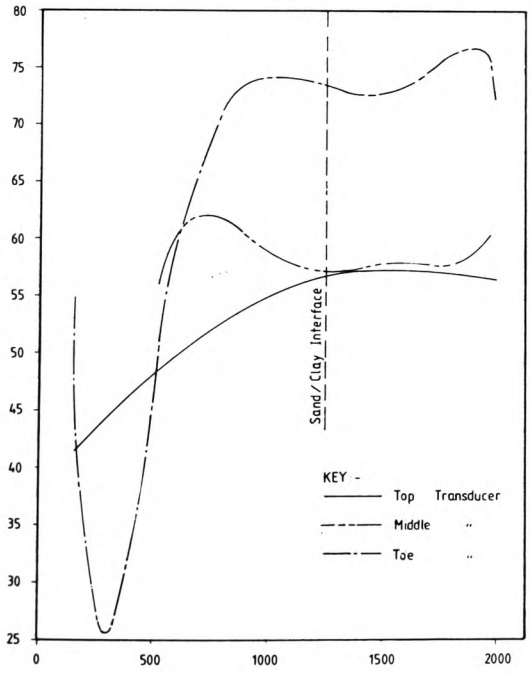

TEST 3 - SAND OVER CLAY PROFILE

FIG. N° 6.11 SHOWING PEAK DYNAMIC FORCE AGAINST PENETRATION FOR THE SEMI-FULL SCALE TESTS

is to be expected because of the close proximity of the load cell to the pile tip causing the initial and reflected stress waves to be almost coincidental with each other giving rise to a steepening of the travelling wave front. Also the short duration of the transient loading indicates that no second reflections from the pile top reaches the tip. This is again to be expected due to the segmented nature of the model pile causing losses due to reflections at joints.

Figure 6.8 to 6.10 shows force/time plots for the bottom transducer and indicate a build up of force and hence driving resistance as the pile penetrates. The peak forces for Tests 1 and 3 at a penetration of 500 mm were 36.0, 31.9 and 30.27 respectively and were considerably lower than the corresponding peak forces at the final penetration of 2.0 m. These final peak forces for tests 1-3 were 51.74, 61.73 and 74.21 KN respectively and were an average 87.4 per cent higher than the initial forces.

It should be noted that the peak force for Test 3 (sand over clay profile) was considerably higher than those of Test 1 and 2 even though the end bearing face for test 3 (obtained from a C.R.P. test) was approximately 60% less than that for test 1 and 2. This indicates that the pile receives most of its resistance (both dynamic and static) from skin friction in the Marl. Recourse to the graphs of stress transfer (Fig. 6.21-6.22) shows this to be the case with an increasing value of stress transfer towards the toe. The increased driving resistance is also highlighted in the number of blows it takes to drive the pile to the set depth of 2.0 m. In the case of Tests 1 and 2 (sand only profile)

the average number of blows were 93 while it took 153 blows for Test 3 (sand over clay profile).

Figure 6.11 also highlights the increased driving resistance with a considerable increase in peak force at the tip prior to the pile tip reaching the sand clay interface. In the case of test 1 and 2 however, although there is a considerable variation in the individual tip plots they all tend towards a value similar to both the middle and top transducer values as penetration increases.

6.5 Acceleration Time Plots

Figure 6.12 shows typical acceleration/time curves for the 3 tests and highlight a number of interesting features:-

1. The curve shape for test 1 and 2 (sand only profile) are indicative of a decaying motion characterised by a logarithmic decay.

2. In the case of test 3 (sand over clay profile) after the initial acceleration peak there are a number of higher value oscillations of extremely short duration before the wave shape reverts to a decaying motion.

A logical explanation for the phenomenon would be for the model pile to perform increased internal oscillations due to joint slackness giving rise to a 'ringing' effect.

This joint slackness has been shown to exist in previous sections.

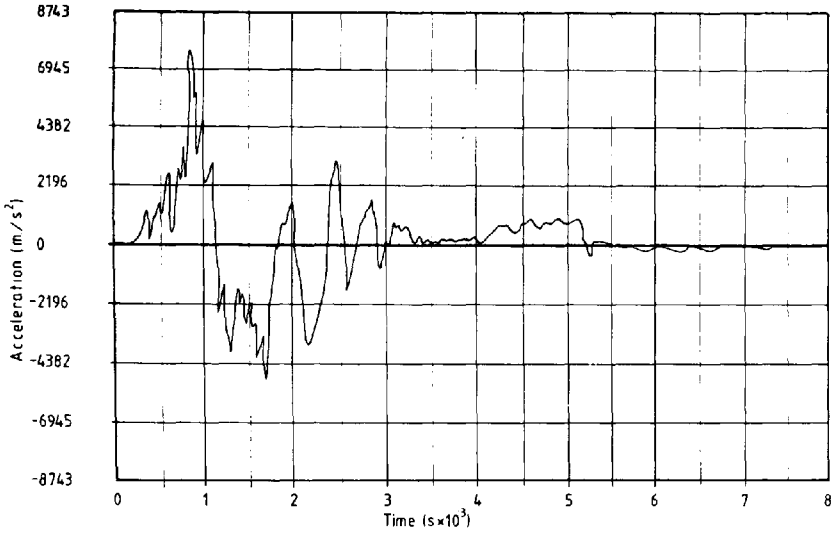

TEST 1 - SAND ONLY PROFILE

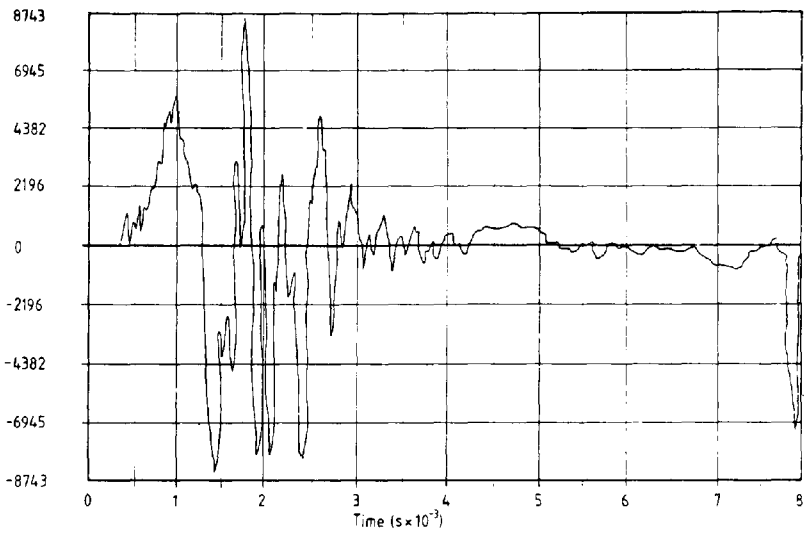

TEST 3 - SAND OVER CLAY PROFILE

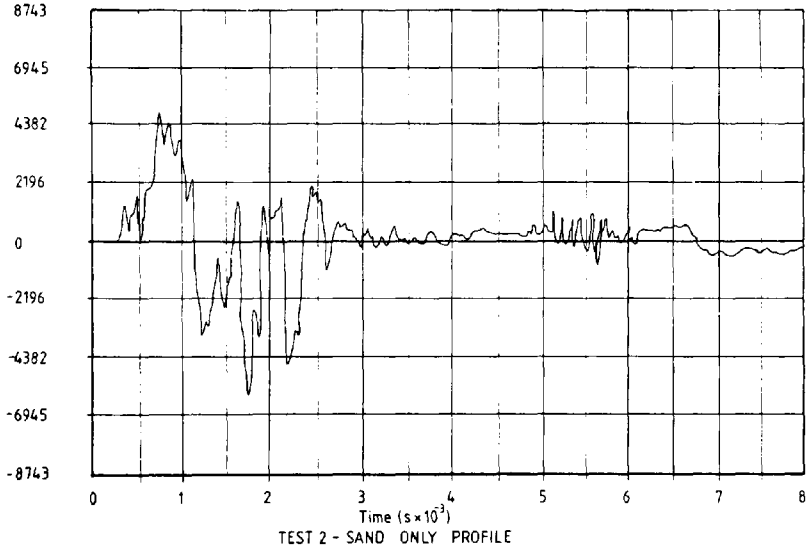

TEST 2 - SAND ONLY PROFILE

FIG. N° 6.12 SHOWING ACCELERATION / TIME GRAPHS FOR THE LAST BLOW OF EACH TEST

The acceleration/time signal for test 3 was therefore not a completely true representation of the actual pile motion. This is shown to be the case in Chapter 7 where the integrated displacement does not match accurately the actual displacement obtained from the L.V.D.T.

6.6 Driving System Performance

In order to assess the performance of the driving system designed by the Author the transferred energy from the hammer to pile was calculated and compared with the delivered energy. Using the measured top force and acceleration, the energy transferred to the pile top was determined by using the relationship:-

$$E(t) = \int_0^{\tau} F(t)V(t)$$

where τ is the impact duration.

In order to evaluate this function the input force/time curves and integrated acceleration/time curves were integrated numerically by a simple strip method, the two results multiplied together and then summed up.

The results of the numerical integration are shown graphically in Fig. 6.13.

The maximum values of the E(t) function for test 1, 2 and 3 were 59, 62, 56.5 KN respectively, compared with the delivered energy of 87.55 KN as calculated from the Kinetic energy Mgh.

The efficiency of the driving system for tests 1, 2 and 3 was therefore 67.39, 70.81 and 64.45 per cent respectively,

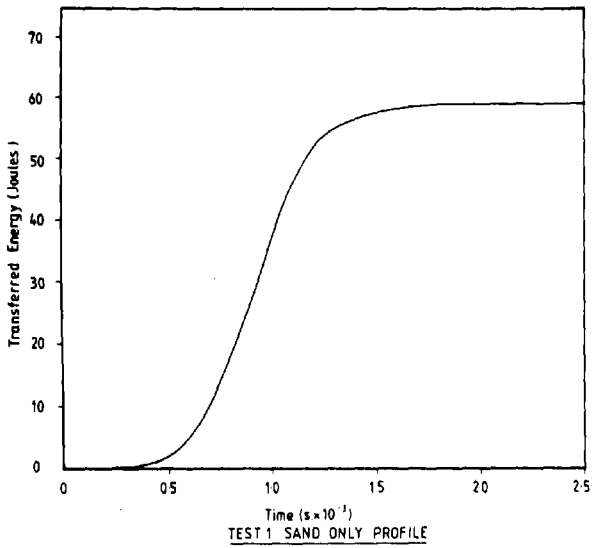

TEST 1 SAND ONLY PROFILE

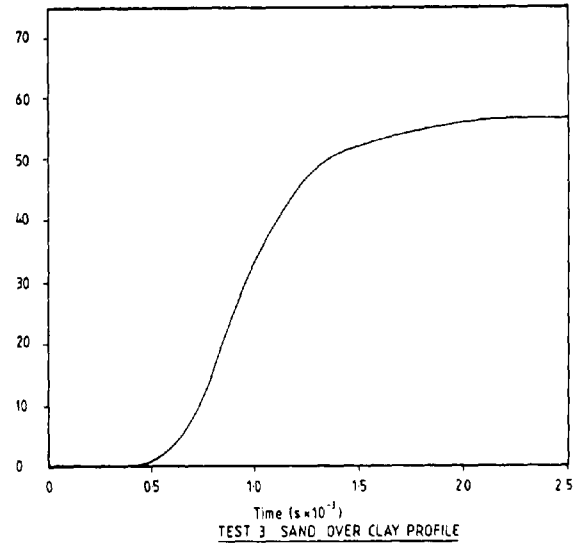

TEST 3 SAND OVER CLAY PROFILE

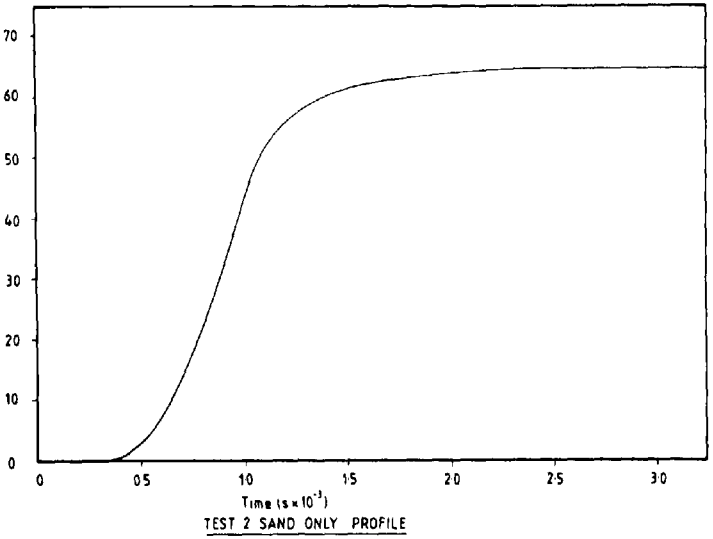

TEST 2 SAND ONLY PROFILE

FIG Nº 6.13 SHOWING TRANFERRED ENERGY / TIME CURVES FROM HAMMER TO PILE FOR THE SEMI-FULL SCALE TESTS

with an average value of 67.55 per cent.

The maximum value of the E(t) function was reached at a time of 2×10^{-3} seconds i.e. at the end of the impact duration.

It can be seen from the above results that the average efficiency of the driving system is high. This is in contrast with values of field efficiency quoted by Goble, Rausche and Likins (1980) which were as low as 10 per cent.

6.7 Penetration History of the Pile during Driving

6.7.1 Sand Only Profile

Figure 6.14 and 6.15 show individual displacement/time plots for the last blow of each drive increment (Test 1 and 2). These plots highlight a number of important events which take place between the hammer and pile which are not readily visible to the naked eye. These events are:-

(1) At a time of 0.025 seconds (penetration 500 mm) the hammer separates from the pile and a recovery of approximately 5 mm occurs (i.e. pile rebounds).

(2) The pile then oscillates about its new position in the soil for a further 0.03 seconds until restrike of the hammer occurs and the pile again penetrates.

(3) Subsequent to (2) the ram again separates from the pile and a further recovery of 2.5 mm takes place.

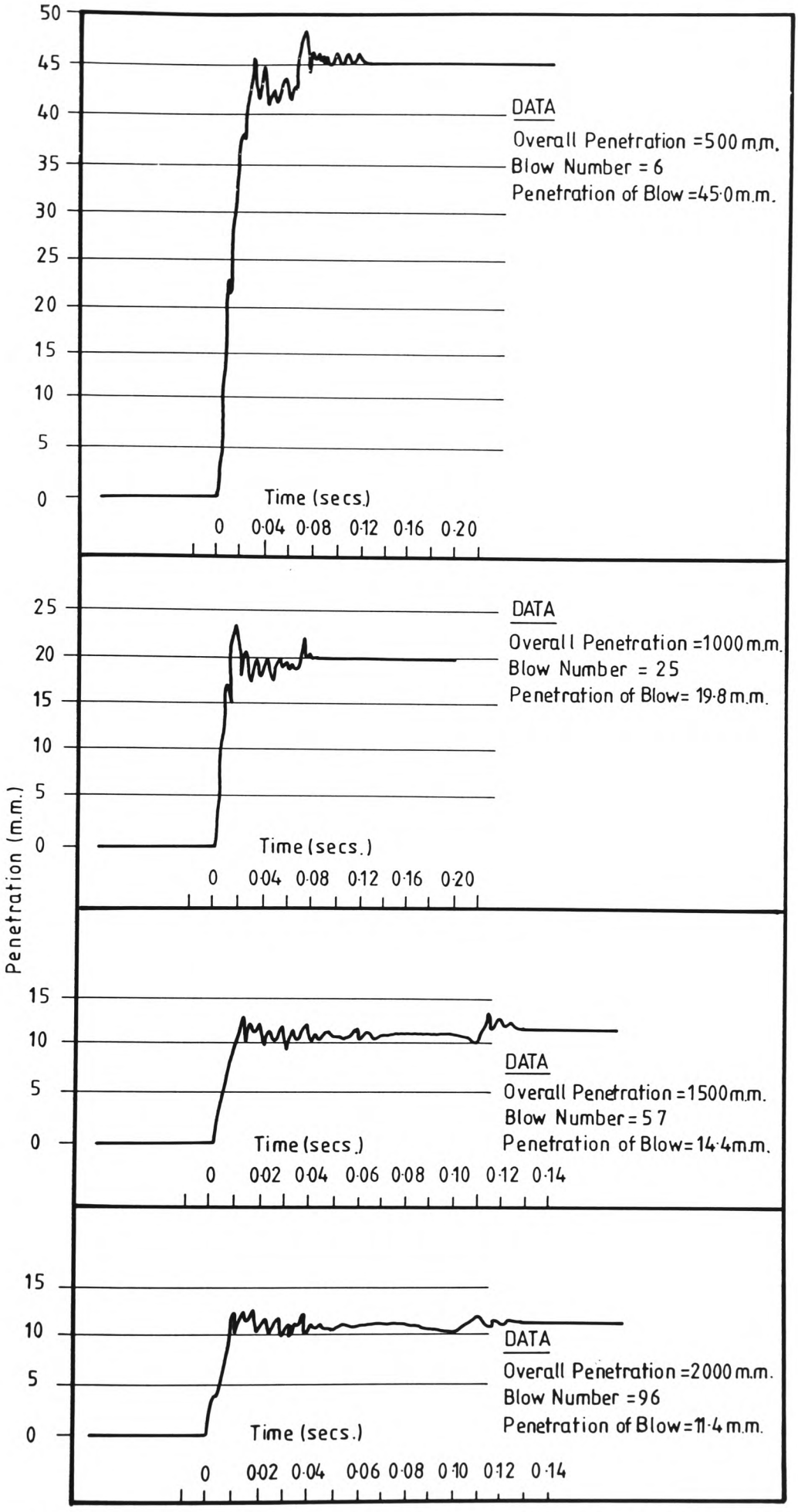

FIGURE Nº. 6.14 SHOWING DISPLACEMENT/TIME PLOTS FOR INCREASING PILE PENETRATIONS (Test 1.-Sand Only Profile)

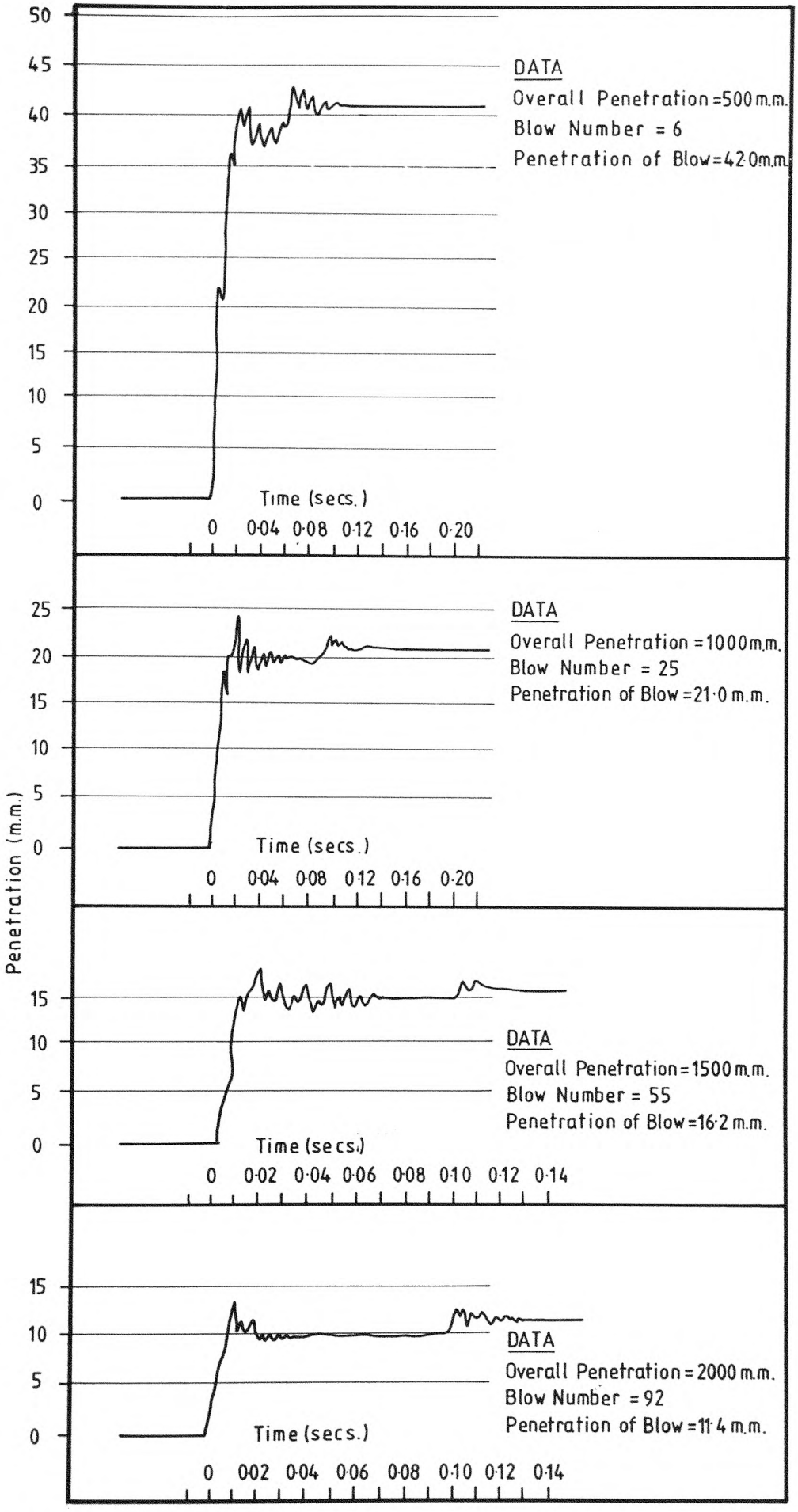

FIGURE N° 6.15 SHOWING DISPLACEMENT / TIME PLOTS FOR INCREASING PILE PENETRATIONS (Test 2: Sand Only Profile)

(4) Finally the pile oscillates about its new position until all oscillations are damped out by the surrounding soil with the complete event taking place in 0.125 seconds.

The final average penetration for the blow (Test 1 and 2) was 43.5 mm. The character of the curve remains much the same as penetration increases except for the following differences:-

(a) The initial recovery becomes less pronounced as penetration increases.

(b) The overall set of the blow decreased from the stated figure of 43.5 mm at a penetration of 500 mm to an average figure of 11.4 mm at a penetration of 2000 mm.

Recourse to Figure No. 6.16 which shows graphs of penetration against number of blows, indicates an even increase in penetration/number of blows after a penetration of 1200 mm, showing the uniformity of the soil profile and also the fact that refusal is not approached.

6.7.2 Sand Over Clay Profile

Apart from the displacement/time plots for the first drive increment where differences arise due to the ram sticking in the ram guides (Section 6.4.1) the plots for Tests 1, 2 and 3 are similar up to a penetration of 1000 mm (Fig. 6.17). From this penetration onwards the following differences between the plots for tests 1, 2 and 3 were evident:-

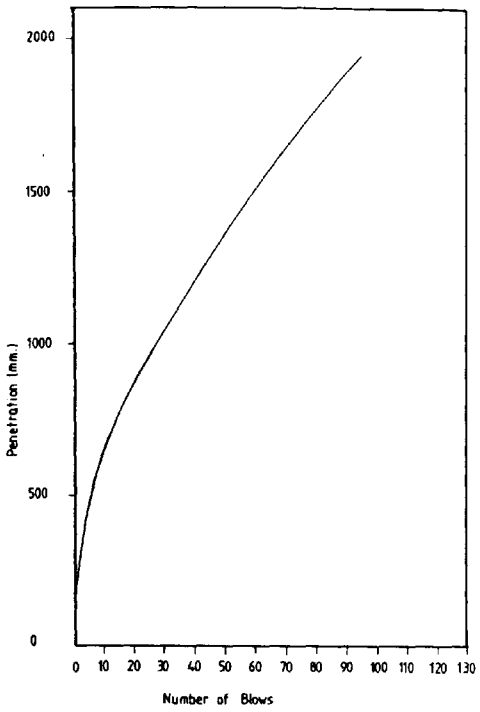

TEST 1 - SAND ONLY PROFILE

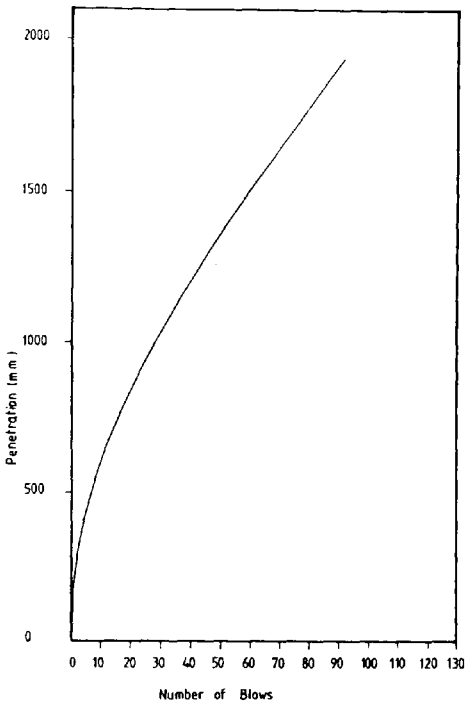

TEST 2 - SAND ONLY PROFILE

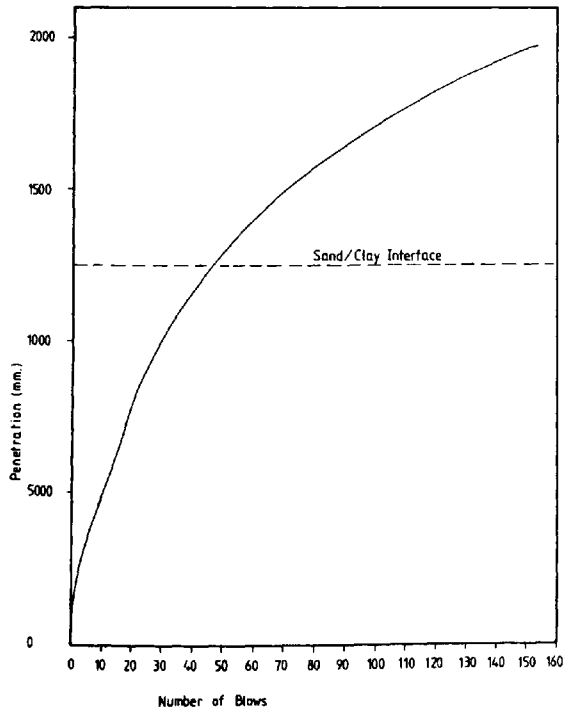

TEST 3 SAND OVER CLAY PROFILE

FIG N° 6.16 SHOWING PENETRATION / BLOW NUMBER GRAPHS FOR THE SEMI-FULL SCALE TESTS

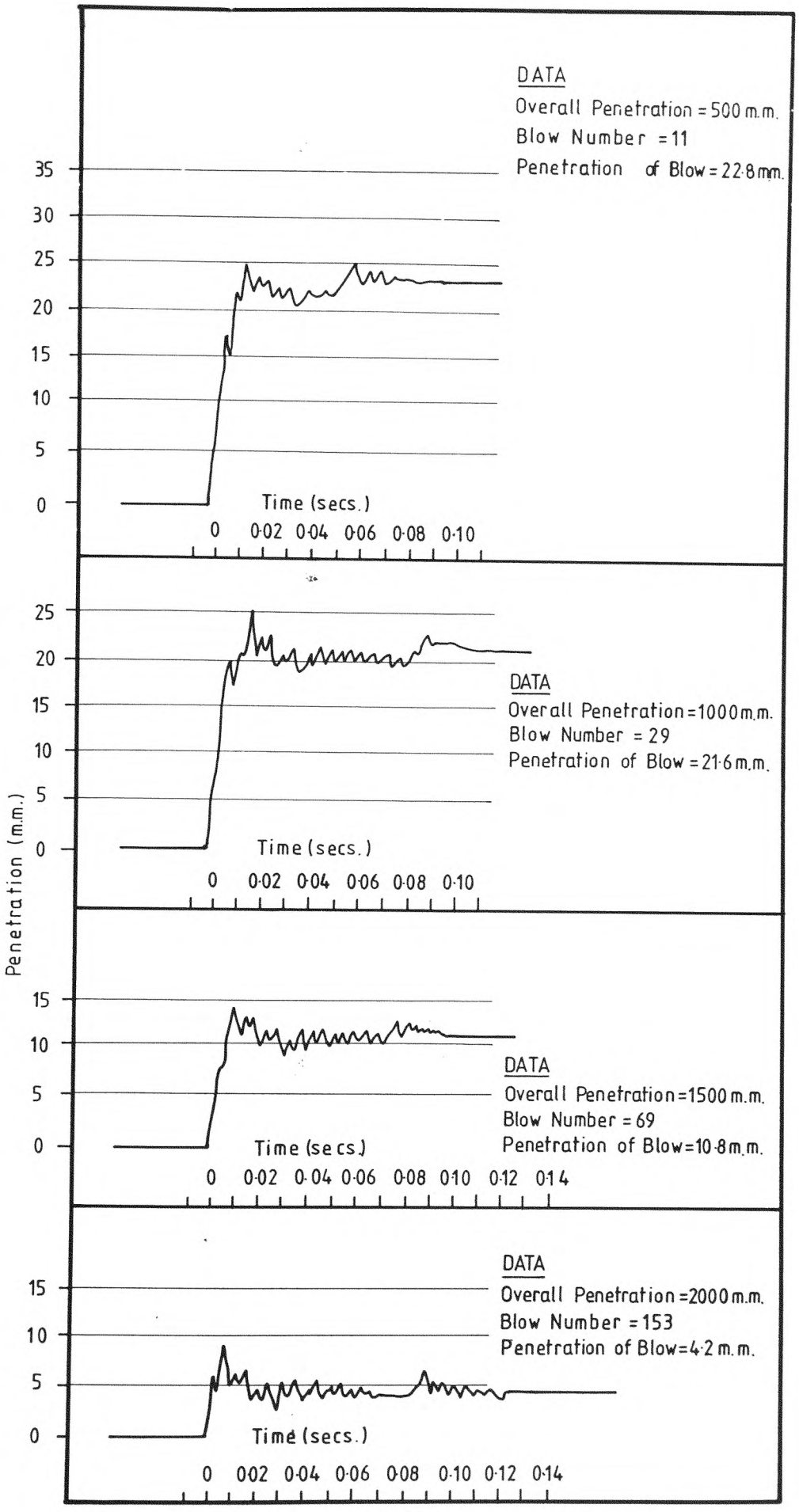

FIGURE Nº 6.17 SHOWING DISPLACEMENT / TIME PLOTS FOR INCREASING PILE PENETRATIONS (Test 3 Sand Over Clay Profile)

(1) The secondary oscillations of the pile were more pronounced in the case of Test 3 (again pointing to a loss of integrity).

(2) The restrike of the hammer on the pile was not as evident in Test 3 as it was in Tests 1 and 2.

(3) The penetration for each blow decreased rapidly as the pile penetrated the marl. Figure No. 6.16 (showing penetration/blow No.) highlights this point and shows that refusal of the pile is rapidly approached with increasing penetration into the marl.

An interesting feature of the curve is a 'Kink' at a penetration of 500 mm caused by the ram guides sticking. The unexpectedly low penetration per blow caused the curve shape to bend towards the horizontal in the latter stages of the first drive increment due to decreasing penetrations. Once the ram was realigned the penetration per blow increased causing a rise in curve gradient and hence the kink in the overall curve.

6.8 Relationship between Transient and Static Soil Response

Broms and Bredenberg (1982)have shown that if the load which corresponds to a certain displacement during driving and a static load test is FDYN/FSTAT, respectively, then three different cases can be recognised with respect to the FDYN/FSTAT ratio.

(1) FDYN/FSTAT < 1

This is the case when the ultimate bearing capacity of a pile increases with time after driving i.e. a friction pile in clays with high sensitivity ratios.

(2) FDYN/FSTAT ≃ 1

Piles driven into coarse sand.

(3) FDYN/STAT > 1

This case corresponds to a spring and dashpot soil response. It has been observed that the penetration resistance during driving of a pile into fine grained soils and shales can be considerably higher than the static penetration resistance and the long term bearing capacity.

The average ratio for the three tests was approximately 12 i.e. greater than 1 and is as would be expected.

This shows that the dynamic resistance at a given displacement can be smaller, equal to or greater than the corresponding static bearing capacity i.e. the peak force at impact bears no relationship to the pile resistance.

6.9 Static Test Results

6.10 Residual Stresses

Most methods of determining the load settlement behaviour of piles assume that the pile is stress free after driving and prior to test loading. This has been shown by many authors (Hunter and Davisson (1969), Hanna and Tan (1973), Gregerson, Aas and Di Biago (1973), Chan and Hanna (1979)) not to be the case. Sometimes large residual stresses are created due to the process of installation. Cooke, Price and Tarr (1979) found that base residual loads for a long pile in London Clay to be approximately 75% of the resistance to penetration at this level. Because of the above facts an effort was made to take into account residual loads when calculating load distribution along the pile. It has been pointed out in previous chapters that in order to minimise the risk of load cell breakdown due to high driving stresses the wall thickness in the strain sensing part of each load cell was increased slightly with a corresponding reduction in sensitivity. The Orion data logging system used was capable of measuring voltage changes of $\pm$ 0.5 microvolts and meant that the load cells were only capable of measuring to approximately 20 N with any accuracy. Prior to the tests the load cells were set to work continuously for 24 hours in order to ascertain possible errors due to 'zero drift'. From this exercise it was found that drift could be as much as 1 microvolt and therefore the measuring accuracy of the load cells was decreased to 40 N. Thus in most cases the monitoring system was working at the limit of its accuracy when measuring residual loads. In order to record the residual loads the

following procedure was adopted:-

(1) The first pile section which included load cells 1 and 2 was placed in the driving rig (Chapter 5, Section 5.4.1) and secured.

(2) The remaining sections were placed horizontally on a specially prepared pile support which straddled the reaction frame beams (Chapter 4, Section 4.6.3).

(3) The Orion data logging system was set to scan all instrumentation a total of 10 times, average these results and take these readings as the initial ones. (Chapter 4, Section 4.8.2).

6.10.1 Adjustment Due to Self Weight

To include self weight in the analysis the following procedure was adopted:-

(1) In the case of load cell one (pile tip) no allowance was made for the self weight of Section 1 because initialisation occurred with the pile vertical and bearing on the sand surface.

(2) In the case of the other load cells the self weight of the pile above the load cells was subtracted from any reading taken thereafter. It should be noted that in the case of load cell one, only the weight of Section 2 to 5 were subtracted from the load cell readings due to the reasons explained previously.

6.10.2 Procedure for Including Residual Loads

In all tests the process for including residual loads in the overall axial load distribution diagram along the pile was as follows:-

(1) After adjusting the data to include self weight a curve fitting procedure (Polyfit) was undertaken in order to smooth out any inaccuracies in the load cell readings. This procedure has already been fully described in Chapter 5, Section 5.1.4 and will not be reiterated here.

(2) These two sets of values (one from the residual curve and the other from the unadjusted curve) were then algabraically combined together. This meant that positive residual load was added and vise versa. The process of subtracting negative residual loads is possibly questionable since it probably takes only a very small load to bring the pile back to a zero state of load. However, for consistency of approach this procedure has been adopted.

(3) A further Polyfit procedure was then undertaken on the adjusted data to obtain the final load distribution curve.

This curve fitting procedure was made necessary due to the low values of some of the residual loads and also load fluctuations in the load cells at higher loads.

One example of this fluctuation was given by load cell No. 3 in Test 1 which at all stages of the test gave higher reading than load cell 4 which was nearer the pile top.

On subsequent tests the load cell behaved in the expected manner giving lower readings than load cell 4.

Check calibration after all the tests were completed yielded calibration values of within 5% of the original and so this initial overreading was probably due to an electrical malfunction.

6.11 Test Loading of Pile (Constant Rate of Penetration (CRP), Maintained Load Test (MTL), Pull Out Test)

6.11.1 General

The procedure for performing the above tests along with the testing sequence used is given in detail in Chapter 5, Section 5.4. Also given is the cessation of movement criterion used in the M.T.L. tests. A brief history of the C.R.P. test along with the criteria for determining ultimate load is given in Chapter 3, Section 3.9.9.

Thus only the results along with relevant comments will be presented here.

6.11.2 C.R.P. Test

6.11.3 Sand Only Profile

The curves of Load/Penetration presented in Figure 6.18 highlight a number of interesting points:-

(1) The shaft friction is built up from the earliest stages of loading to reach a maximum value which remains constant thereafter.

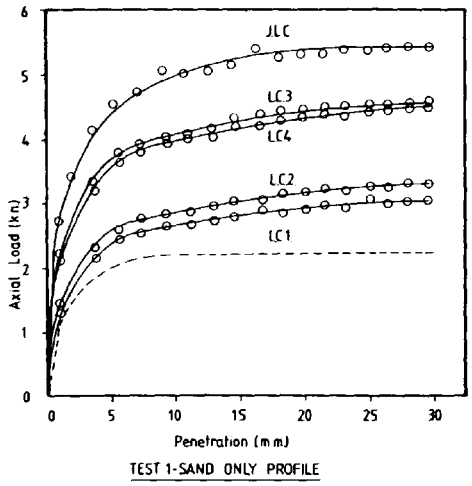

TEST 1-SAND ONLY PROFILE

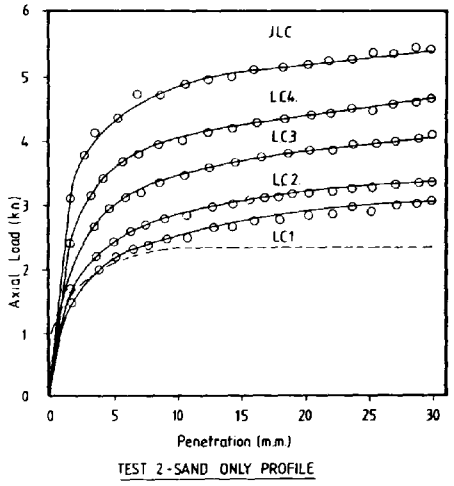

TEST 2-SAND ONLY PROFILE

KEY

——— Residual Loads not Included

—·—·— " " Included

- - - - - - Shaft Friction

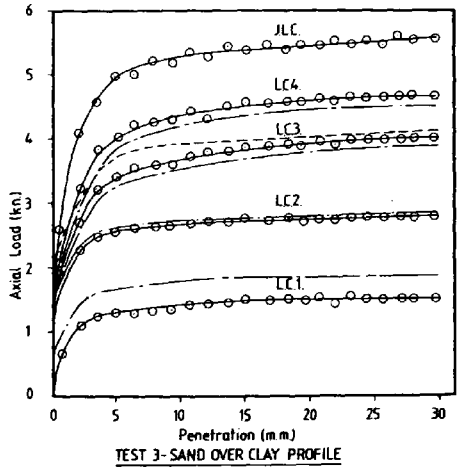

TEST 3-SAND OVER CLAY PROFILE

FIGURE N° 6.18 SHOWING DISTRIBUTION OF AXIAL LOAD IN THE PILE DURING C.R.P. TESTS

(2) End bearing resistance builds up simultaneously with shaft friction and remains the major load carrying component of load at all times.

(3) Once the shaft friction reaches a maximum the end bearing curve continues to rise indicating that most of the pile load is taken in end bearing.

These curves are typical for end bearing piles where the force tends to increase slightly with increasing penetration. (Whitaker 1976). Thus ultimate load was taken as the load reached at a penetration of 10% of the pile diameter. The failure loads determined from this criteria were 4.5 KN and 4.4 KN respectively for tests 1 and 2.

The build up of load along the pile is also shown in Figure 6.18. It should be noted that in the case of the sand only tests no adjusted curves (to include residual loads) have been plotted because only slight changes in the readings were evident. Thus the adjusted curves would only serve to add confusion to the figures. Adjusted curves have been added in the case of the sand/clay profile and will be discussed in the next section.

6.11.4 Sand/Clay Profile

The curves of Load/Penetration presented in Figure 6.18 again highlight a number of interesting points:-

(1) Shaft friction has built up at the earliest stages of loading and does not reach a maximum value but continues to rise slightly. The value is higher

than for the sand only tests.

(2) End bearing is built up simultaneously with shaft friction but does not remain the major load carrying component.

(3) Once the end bearing reaches a maximum the shaft friction continues to rise indicating that most of the pile load is taken in shaft friction.

These findings are different to the sand only profile tests and highlight the effects of the clay stratum on the load distribution throughout the pile. In the case of the sand/clay test the adjusted values (to include for residual loads) are shown.

It can be seen that after adjustments for residual loads the maximum vlue of end bearing was only 1.85 KN as opposed to 3.05 KN for test 1 and 3.0 KN for test 2.

The failure load for the sand/clay test was 5.1 KN.

6.11.5 M.T.L. Tests

In all tests the shape of the load/settlement curve corresponds to that of a pile in soft-form clay or loose sand (Tomlinson (1977)). The criteria for determining the ultimate load is the one given in CP4 (1954) in which failure load is the one which produces increasing settlement without further addition of load. Figure 6.19 presents the data from the three tests.

Unfortunately, due to the author's inexperience the ultimate load was not accurately determined in Test 1. A catastrophic failure was produced by increasing the load

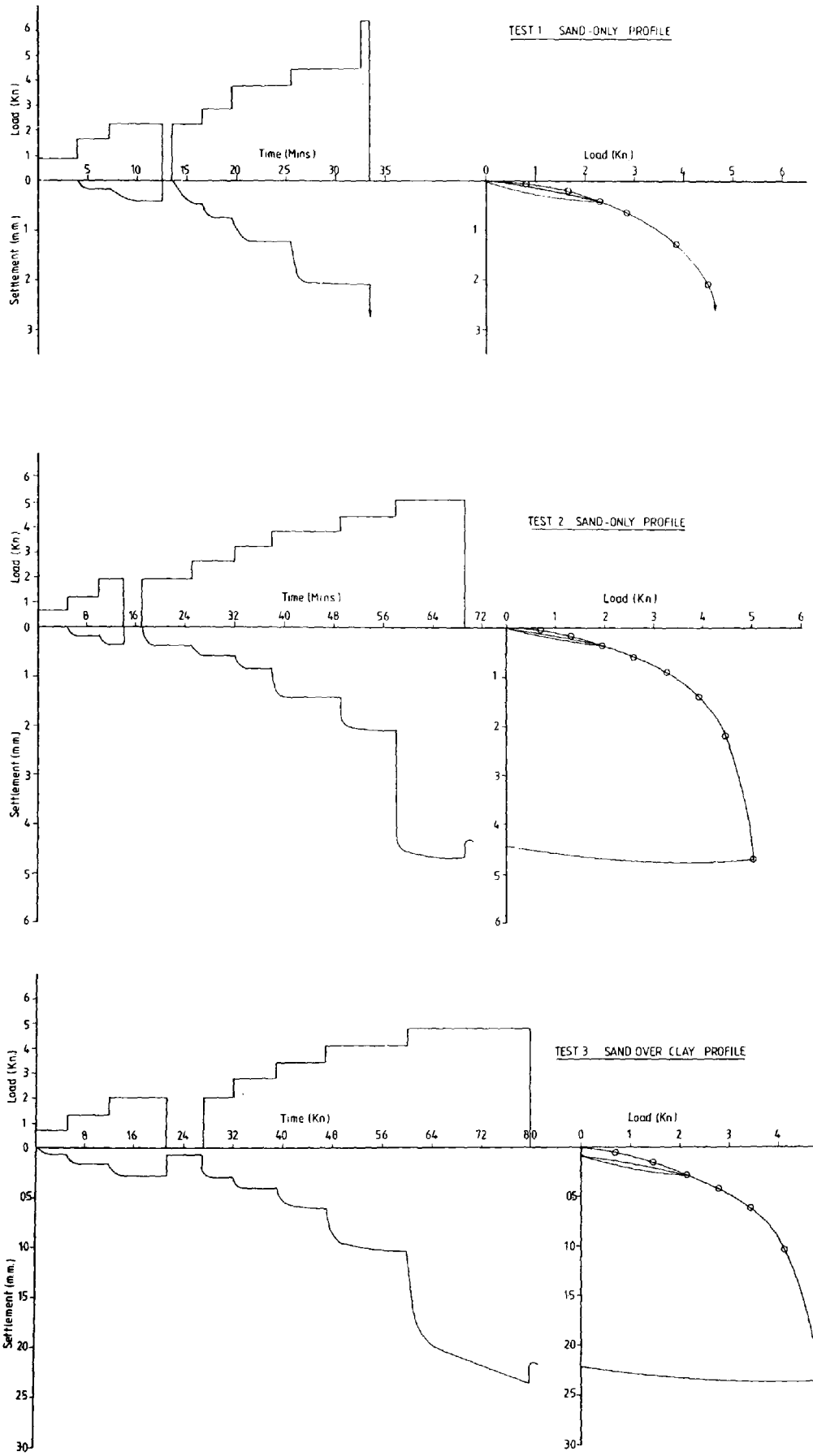

FIGURE Nº 6.19 SHOWING M.T.L. RESULTS FOR THE THREE TESTS

increment by an excessive amount. An approximate value only was obtained from this test.

The ultimate loads obtained from this test are compared with those obtained from the CRP test in the figure below.

Type of Loading	Test No.			Average % Difference
	1	2	3	
CRP	4.5	4.4	5.1	8%
MTL	4.75	5.0	4.85	

An interesting aspect of Figure 6.19 is that only half the settlement was needed to produce failure in the sand/clay test as was needed to produce failure in the sand only tests.

6.11.6 Pull Out Tests

Figure No. 6.20 shows graphs of pull out load/displacement for the 3 tests. Only the load displayed by the Dartec Jack load cell is shown because in all cases the axial load cells underestimated this load.

Load cell No. 5 (near to the ground surface) which was used as a check on the correct working of the load cells was on times reading as much as 50% less than the jack load cell. No explanation can be found for this phenomenon as the load cells behaved adequately under compressive loading and check calibrations after the tests were completed revealed a maximum deviation of 5% from the original calibration factors both for Tension and Compression.

As can be seen from Figure 6.20 in the case of the sand only tests a peak pull out load was obtained which gradually

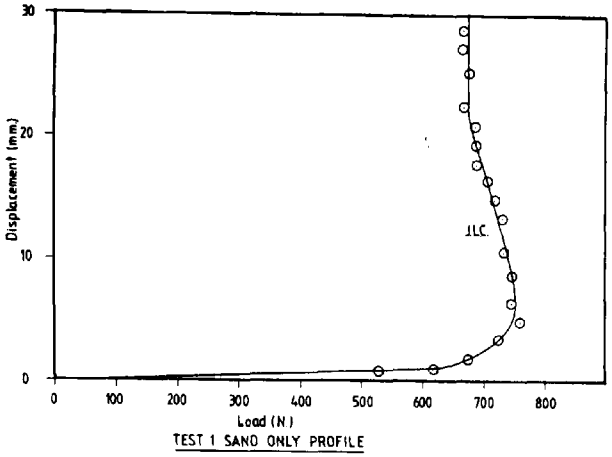

TEST 1 SAND ONLY PROFILE

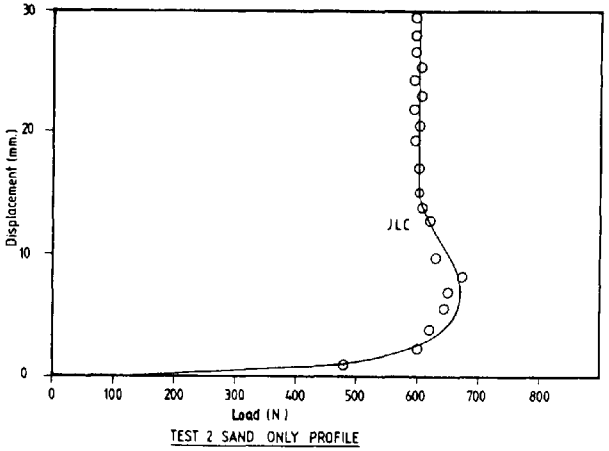

TEST 2 SAND ONLY PROFILE

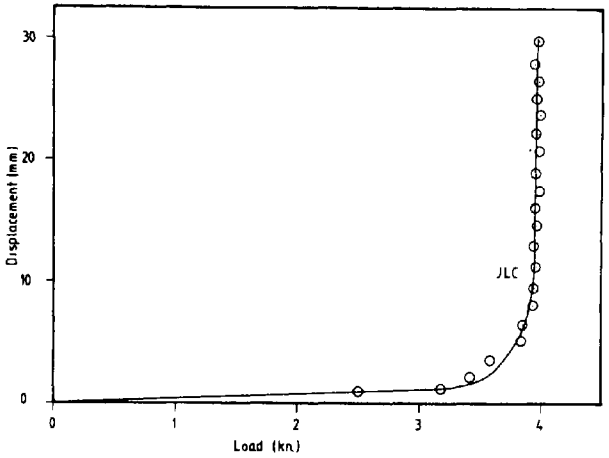

TEST 3 SAND OVER CLAY PROFILE

FIGURE N° 6.20 SHOWING PULL OUT TEST RESULTS FOR THE 60MM. DIAMETER MODEL PILE

reduced to a residual load which was unchanged for increasing displacements.

The peak load was reached at approximately 6 mm (i.e. 10% of pile diameter) and had values of 0.75 KN and 0.685 KN for test 1 and 2 respectively. In the case of Test 3 (Sand over Clay profile) no peak load was exhibited with the curve displaying a gradual rise to a maximum load of 3.8 KN at a displacement of 10 mm (16.7% of pile diameter).

The pull out value for the sand clay test is within 10% of the shaft friction load in pushing and is in agreement with the findings of Ireland (1957) with respect to driven piles in sand and Cooke and Price (1973) with respect to jacked piles in London Clay who both reported that the uplift failure load was approximately equal to the shaft friction in compression.

However, data summarised by Sowa (1970) and Downs and Chieurzzi (1966) indicated a considerable variation in the frictional resistance between tests and suggested a value of 2/3 the frictional resistance in pushing to be more reliable. They also recommended that the only reliable method to determine uplift resistance was from a pull out test in-situ. This statement was confirmed with the sand only tests where the resistance to uplift was only 1/3 of the skin friction in compression.

6.12 Residual Loads Prior to and After a C.R.P. Test

Hanna and Tan (1973) stated that residual stresses are created by relative movement between the pile and the soil after driving.

The residual loads in the case of the sand only tests immediately after driving but prior to a C.R.P. test are shown in Fig. 6.21 and 6.22. They are slightly negative near the pile top, increasing towards the centre and becoming slightly positive at the base. This distribution is probably due to a combination of the effect of the pile behaving as an elastic body and relative soil movements. This is shown to be the case when the recovery at the pile head (average value 0.635 mm) is compared to the elastic recovery of the soil. The soil recovery was obtained from graphs of insitu vertical displacement (Section 6.15.4, Fig. 6.29 and Fig. 6.30).

The elastic recovery obtained from these graphs yielded an average value of 0.01 mm. The actual recovery around the pile tip was not known as there was no instrumentation at the base. However the relative displacements between pile head and soil would tend to indicate an extension of the pile causing slight negative residual loads.

The shape of the residual load curve at the end of the C.R.P. test and the beginning of the M.T.L. test is somewhat different than the original with a high positive load being displayed at the toe. This is contrary to previously published data (Gregerson et al (1973), Chan and Hanna (1979)) whereby after loading the residual loads decreased. This phenomenon is difficult to explain but may be due to relative changes in displacement between soil and pile as shown in the insitu sand displacements displayed for the M.T.L. test (Fig. 6.29 and 6.30).

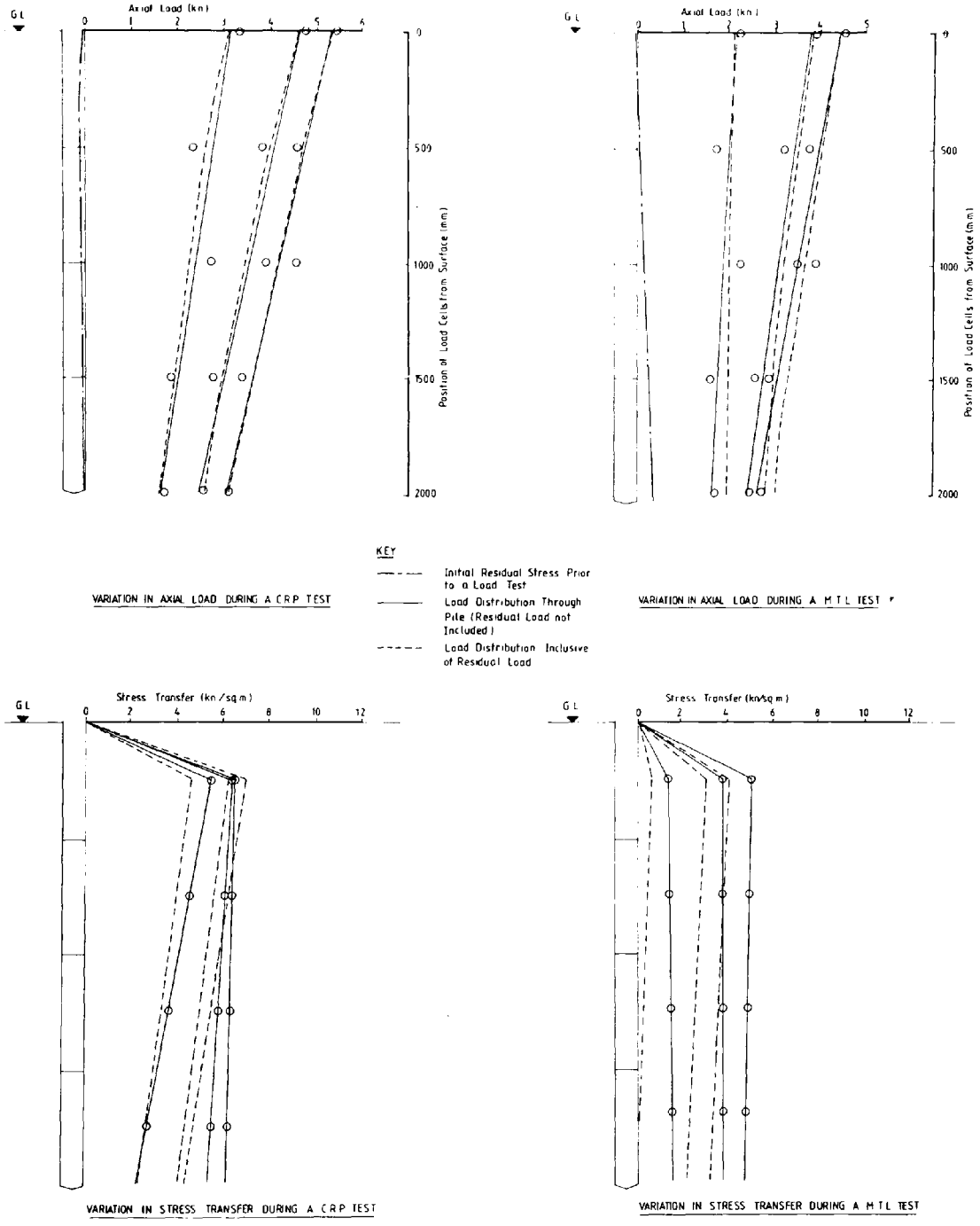

FIGURE N°6.21 SHOWING CHANGES IN AXIAL LOAD AND STRESS TRANSFER ALONG THE PILE FOR TEST 1 (Sand Only Profile)

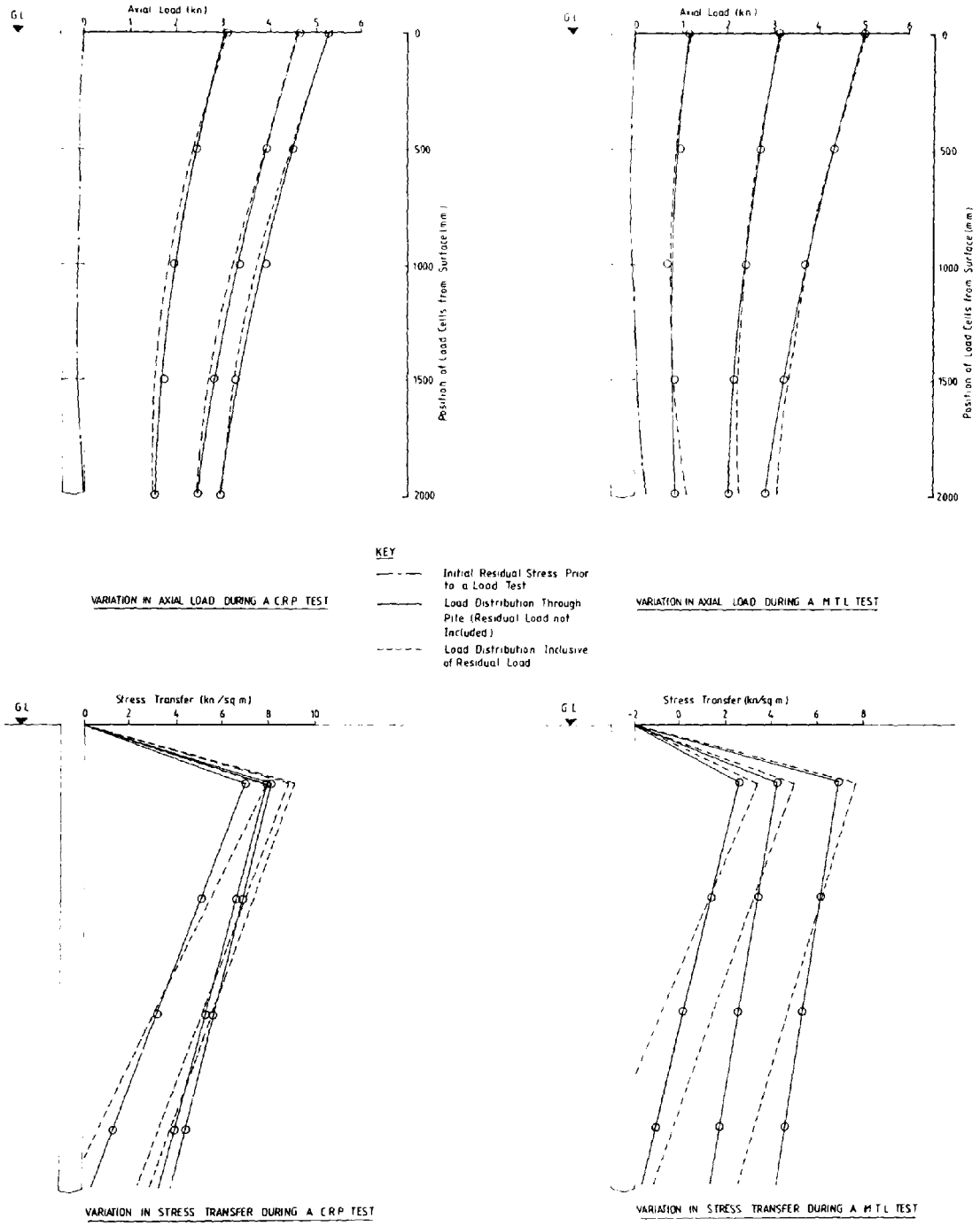

FIGURE N° 6.22 SHOWING CHANGES IN AXIAL LOAD AND STRESS TRANSFER ALONG THE PILE FOR TEST 2 (Sand Only Profile)

The same shape of residual load distribution as displayed in the M.T.L. tests for the sand only profiles was again exhibited for both the C.R.P. and M.T.L. tests in the sand over clay profile. (Fig. 6.23). The high residual toe load may be due to recovery of the clay and the generation of excess pore water pressure at the tip of the pile. Excess pore water pressure has been shown to exist under identical soil conditions (Robinson (1986)).

Robinson showed that this excess pore water pressure did not dissipate until five days after driving and therefore would produce some effect during the time scale of the test. Fellenius and Broms (1969) have shown that the dissipation of high excess pore pressures, caused by pile driving in sensitive clays, may cause appreciable down drag forces on the pile, even though relative pile soil movement may be a few millimetres. This down drag could possibly be one explanation for the large end bearing residual load encountered.

6.13 Coefficient of Earth Pressure on Pile Shaft

The equation used for determining the coefficient of earth pressure on the pile shaft (Ks) was the one suggested by Meyerhof (1953).

$$qs = Ks \gamma D \tan \delta$$

Where qs = tangential force per unit area

ks = Coefficient of earth pressure

γ = density of the soil

D = depth

δ = the angle of friction of the soil on the pile shaft

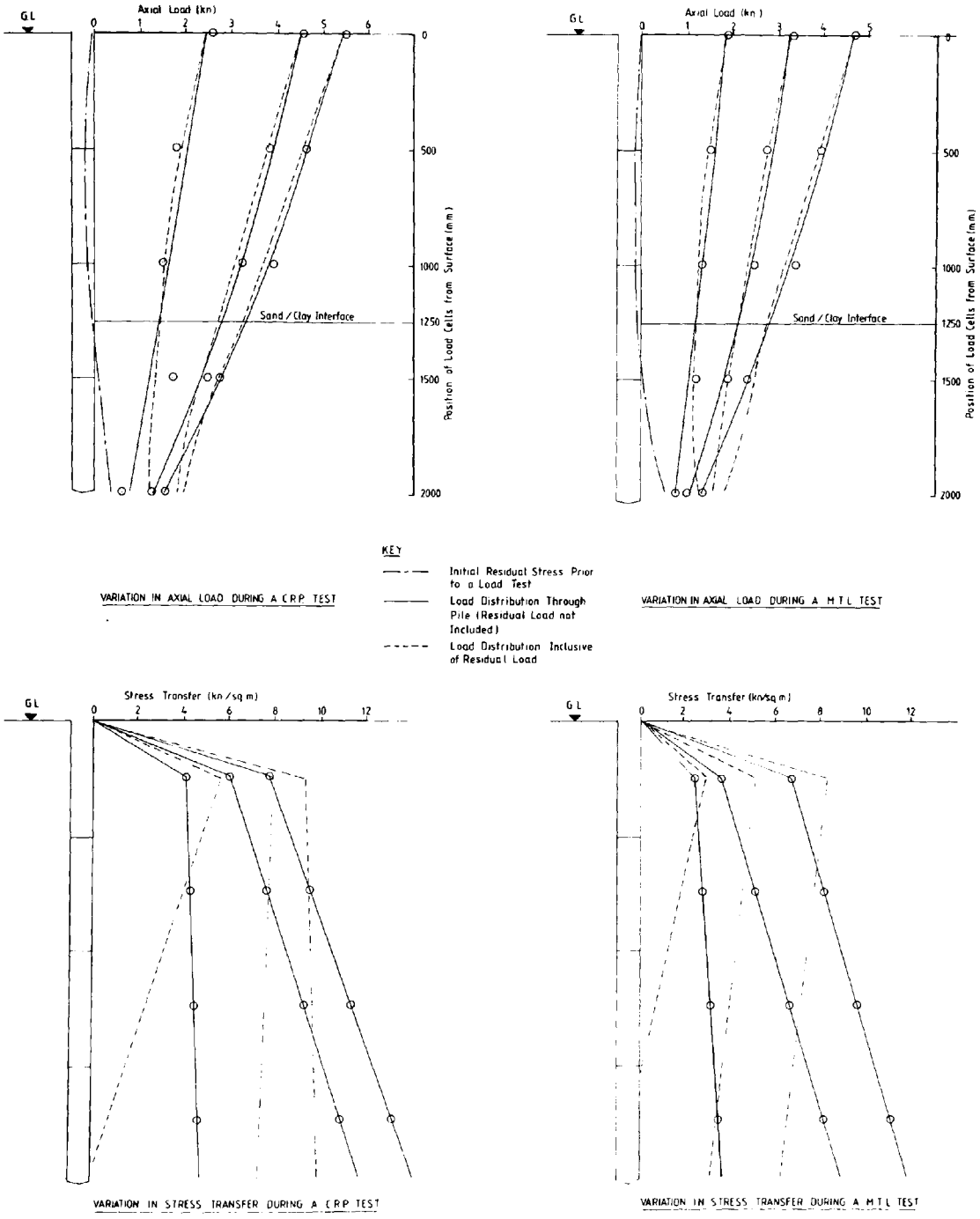

FIGURE N°6.23 SHOWING CHANGES IN AXIAL LOAD AND STRESS TRANSFER ALONG THE PILE FOR TEST 3 (Sand/Clay Profile)

Rearranging gives:

$$Ks = \frac{qs}{\gamma D \tan \delta}$$

It is accepted that this equation assumes that lateral pressures are given by normal overburden consideration with a linear increase with depth which is not the case.

Nevertheless this equation has been used as a comparison with other published data. Account of the changes in soil density along with the subsequent changes in the angle of friction has also been taken into account by reference to Fig. 6.32 and Fig. 6.1.2. These figures show insitu densities after driving and their relationships to the angle of friction.

The Ks values obtained by this method are shown in Fig. 6.24 (for the last stage of loading of the C.R.P. test) for both the adjusted and unadjusted curves.

All the values are lower than the Kp value (3.43) and all but the Ks values at the pile tip higher than the Ka value (0.291). The lowest value obtained however was only 0.077 less than Ka and therefore it can be said that the Ks value of the tip becomes equal to the Ka value.

Chaudhuri and Symons (1983) have summarised results of model investigations and the results obtained by the author appear typical with the value of Ks lying close to but not exceeding Kp. Using published data Kay (1980) plotted Ks values against pile length/diameter ratio and these results are summarised in Fig. 6.25 along with the authors' results. It can again be seen from Fig. 6.25 that the authors' results are typical with a high Ks value being displayed at shallow depths.

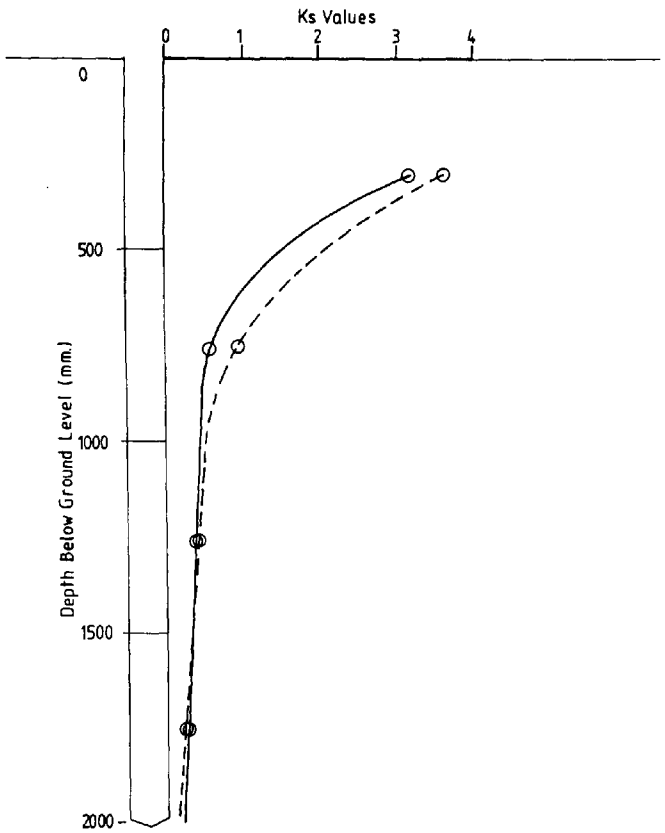

TEST N° 2 - SAND ONLY PROFILE

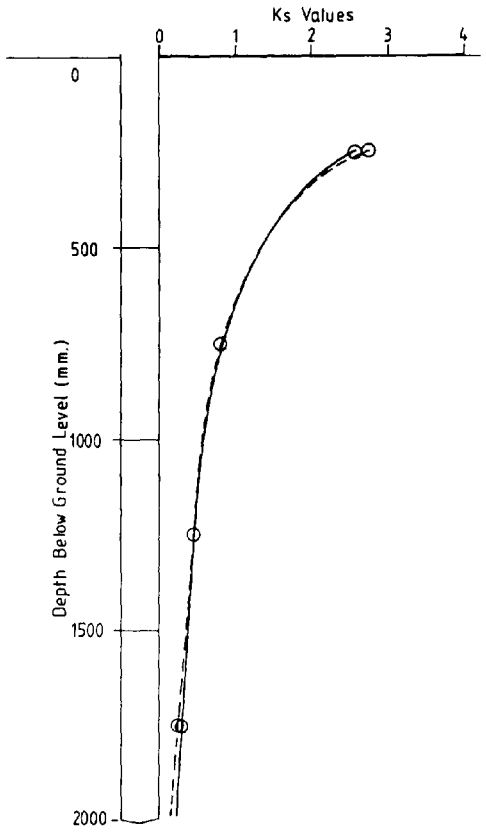

TEST N° 1 - SAND ONLY PROFILE

FIG. N° 6.24 VARIATION IN Ks VALUES ALONG THE PILE SHAFT DURING C.R.P. TESTS

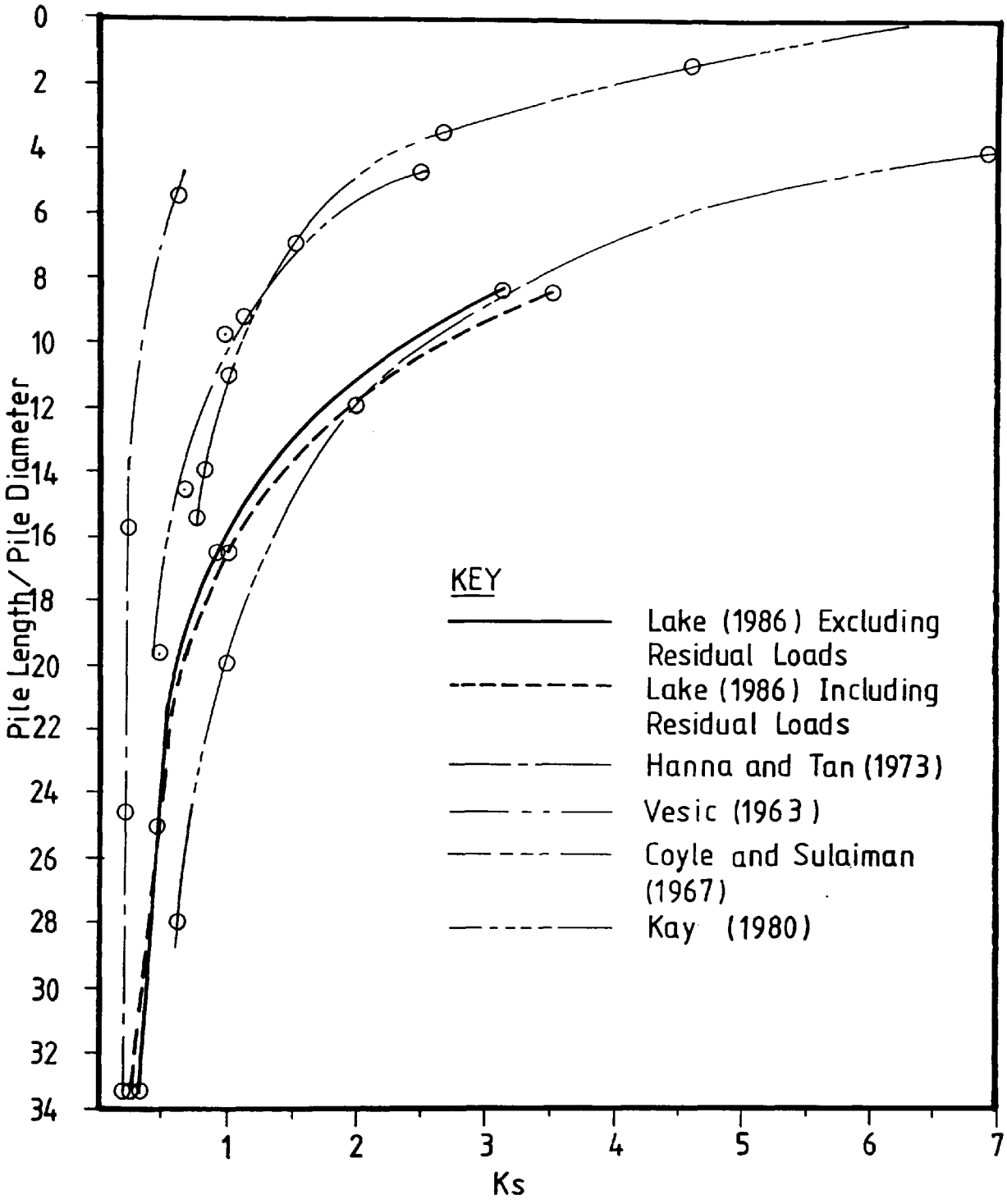

FIG. Nº. 6.25 SHOWING Ks VERSUS RELATIVE PILE LENGTH

6.14 Stress Transfer between Pile and Soil

6.14.1 Method of Determining Stress Transfer

The method of determining stress transfer is the one used by Coyle and Reese (1966) in which the load at the bottom of a pile segment is subtracted from the load at the top and then divided by the circumferential area of the pile segment. The values used for this procedure were both the adjusted and unadjusted load distribution curves and were used for comparison. It should be noted that in both cases the polyfit values were used and is a procedure similar to the one described by Gregerson et al (1973) where the 'smoothed' values of load distribution were used to calculate skin friction.

6.14.2 Sand Only Tests

6.14.3 Stress Transfer

Reccurse to Fig. 6.21 and 6.22 shows that the main feature of the graphs is the high value of skin friction at shallow depths decreasing towards the toe. This trend is shown for both the adjusted and unadjusted curves.

In order to verify that these unexpected results were correct measurement of shaft friction by two separate methods were attempted and the results compared.

The two methods were:-

(1) Applied load minus the toe load.

(2) Area enclosed by the stress transfer/embedded depth curve.

A comparison of the two methods showed aggrement of between 12% for lower loads up to 3% for the higher loads.

Similar trends have been observed by Tan (1983), Werscheing (1986) for model tests in sand. Such Authors as D'Appolonia and Romualdi (1963), Reese (1964), Thurman and D'Appolonia (1965), Hanna (1969) have suggested the progressive mobilisation of shear stress from the surface downwards. The present research shows no evidence of this phenomenon where even at the lowest loadings all load cells displayed an increased reading.

Evident from the stress transfer curves for the M.T.L. test was a negative stress transfer towards the toe of the pile for the lowest load. This would suggest that the sand at the toe is 'hung up' on the pile, an occurance that is unlikely.

No reasonable explanation can be put forward by the Author to explain this phenomenon and it will be treated as an anomaly until such time as an explanation can be found.

Also evident is that end bearing was mobilised at the lowest loads and not as previously suggested only after maximum shaft friction had been attained. Using published data from Mohan, Jain and Kumar (1963), O'Neill and Reese (1972), Baker and Holtz (1972) and Touma and Reese (1974), Tan (1983) has shown similar trends to the authors' with respect to the shaft friction/embedded depth curves.

It must be noted that these results related to piles in clay, however it will be shown that these trends are repeated to a lesser extent in the two soil medium of test 3.

In sands the mechanisms of driving and testing tends to cause lateral expansion of the soil in the vicinity of the pile base. This lateral expansion is accompanied by a vertical shortening, and the sand located above the expanding zone has a tendency to move downwards. Since both the lateral expansion and the vertical shrinkage are limited to a cylindrical zone surrounding the shaft, shearing stresses develop along the outer boundary of this zone. These shearing stresses transfer part of the weight of the sand adjoining the shaft onto the unaltered material outside the zone of expansion. This transfer is called the bin effect because it closely resembles the transfer of part of the weight of the contents of a storage bin to the wall of the bin.

This transfer of weight and the loosening of the downward annular zone of soil adjacent to the pile wall, decreases the lateral pressure on the pile shaft, thus decreasing skin friction value in the vicinity of the pile base.

This effect has been reported by Vesic (1963, 1970(a)) for piles in dense sand who also stated that the effect becomes more pronounced as punching occurs as failure is approached.

Unlike the trend suggested by Vesic is the continual drop in skin friction with depth as opposed to his contention that a constant value is reached. However, similar findings to the author have been reported by Tan (1983).

Thus the low values of shear stress at the pile toe can be explained in terms of arching from the bin effect and also punching suggested by Vesic (1963, 1970(a)).

The high shear stresses at shallow depth imply 'locking in' of the sand particles around the pile shaft at this level. One explanation for this is that the sand particles around the pile shaft try to follow the piles downward movement.

As large displacements occur the sand around the lower end of the pile slips. Thus the sand around the upper section of the pile shaft attempts to follow the pile but is prevented from doing so by the lower soil mass. This means that high lateral stresses are developed along the top of the pile. Fig. 6.32 shows graphs of changes in insitu density after all penetration tests were completed and show an increase in density towards the pile with the greater changes at shallow depth. This supports the stated reason that high lateral stresses are developed along the pile. Also recourse to Fig. 6.29 to 6.30 shows graphs of insitu vertical displacements at various depths during the C.R.P. and M.T.L. tests. The general trend of the results is for a sand displacement generally downwards or horizontal at the lowest inclinometer levels changing to upwards in the highest level of inclinometers. This phenomenon is repeated in all but the two shallower depth of inclinometers for the C.R.P. test in Test No. 1. This again lends credence to the previously described mechanism. Similar findings have been reported by Davidson and Boghrat (1983) with respect to soil movements in dense and loose sand. Thus the distribution of shear stress along the pile (high value at shallow depths with diminishing values towards the toe) is opposite to normally assume distribution from a theoretical analysis and supports the findings of Tan (1983). The effect of including residual

loads on the stress transfer curve will be discussed in Section 6.14.6.

6.14.4 Sand Over Clay Test

The stress transfer for the sand over clay tests shows a different trend from that displayed by the sand only tests. In the case of the unadjusted curves the form of stress transfer taken is that of increasing values down the pile Fig. 6.23. This supports the finding of Cooke and Price (1973) for jacked piles in London Clay. However, if residual loads are included the trend is reversed with decreasing stress transfer towards the toe. This phenomenon will be discussed in Section 6.14.6.

6.14.5 The Effect of the Inclusion of Residual Loads on the Stress Transfer Curve

In the case of the sand only tests the overall effect is to increase the value of shaft friction at shallow depths and to decrease the shaft friction at greater depths. This highlights the considerable effect that the omission of residual loads can have on the basic understanding of load transfer through end bearing and shaft friction.

In the case of the sand over Clay tests the effect of including residual loads is considerable. In effect the inclusion of the residual loads changes the form of stress transfer mechanism from low values at shallow depths and high values at lower depths to the exact opposite. This brings into question the validity of the residual loads registered.

The validity of these results have been discussed in previous sections in relation to sensitivity and stability of the load cells. It was shown that some error was possible due to these factors, however, the value of residual load obtained at the tip could not be accounted for due to the load cells misreading. The results were also consistent throughout the tests and it must therefore be concluded that the residual values obtained are valid in relation to the tests. A possible reason for this high end bearing residual load is discussed in Section 6.12.

6.15 Insitu Soil Displacements

6.15.1 General

The assumption that there is no slip between the soil and pile wall is not valid in this case as pile displacements per blow were as much as 45 mm. Therefore no projection of the curve can be accurately made beyond the limit of instrumentation. The curves have however, been extended beyond the limits of instrumentation to yield a general trend and are an extension of the actual curves produced from the inclinometer results.

6.15.2 Vertical Soil Displacements During Driving

The vertical soil displacements at various stages of driving are shown in Fig. 6.26.

The Figure highlights a number of important observations:-

(1) Soil displacements around the pile decrease with increasing depth.

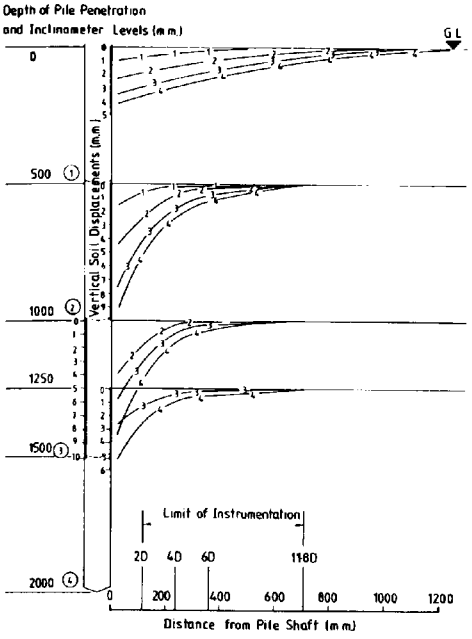

TEST 1 - SAND ONLY PROFILE

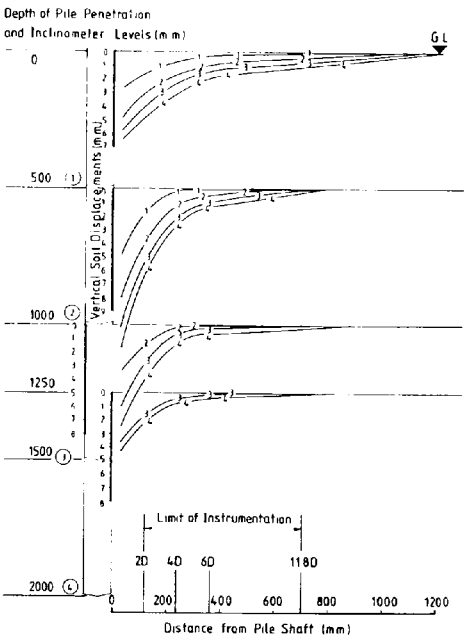

TEST 2 - SAND ONLY PROFILE

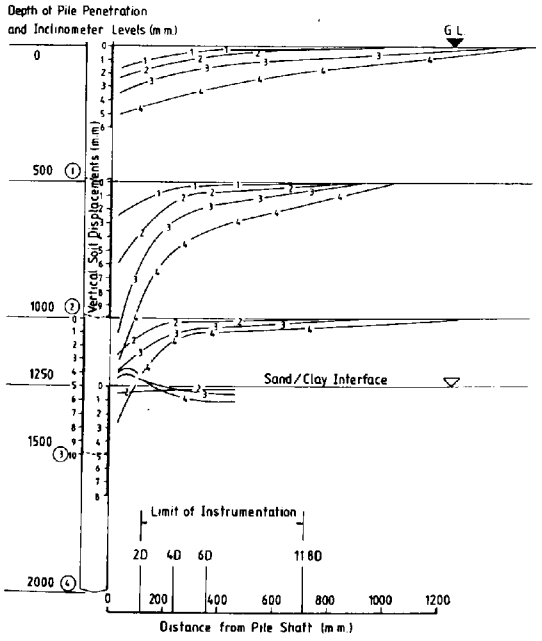

TEST 3 - SAND OVER CLAY PROFILE

—— 2 —— 2 —— Indicates Soil Displacements when Pile has been Driven 1000 mm

FIGURE N°6.26 SHOWING GROSS SOIL DISPLACEMENTS AT VARIOUS STAGES OF PILE INSTALLATION

(2) At shallow depths significant soil movements extend to 12D diminishing to a value of approximately 7D at greater depth.

(3) Observed movement of the soil under the toe was initiated at approximately 4 diameters.

(4) In the case of the sand over clay tests, heave of the clay surface was evident as the pile penetrated the clay.

The above observations will now be discussed and compared with previous research. Kay (1980) observed decreasing displacements with depth for a 110 mm diameter model pile (no end bearing). This observation also supports the argument that high lateral stresses are built up at the upper section of the pile. The sand along the upper section of the pile being prevented from moving down by the arching mechanism at the toe.

The maximum visible movement observed from the inclinometers extended to a maximum value of 12D and is greater than the figure of 5.5D in medium dense sand quoted by Robinsky and Morrison (1964) and 8D quoted by Kishida (1963). However Cooke and Price (1973) using electrolytic levels stated that discernable movement extended to 8D in London Clay. It would therefore seem that the sensitivity of the instrumentation was responsible for detecting smaller values of vertical displacements than the two previous authors could, using their measurement techniques.

It must also be stated that greater agreement with this published data is achieved at greater depths along the pile.

Robinsky and Morrison (1964) also showed that visible movement below the pile point extended to 4.5D while Meyerhof (1959) found the value to be 5D. This is in close agreement with the authors result of 4D.

That heave of the clay surface occurs due to driving is a well known phenomenon and has been reported upon by many authors e.g. Cooke and Price (1973) who reported considerable heave for jacked piles in London Clay. At the test site they found the volume of heave to be 66% of the embedded volume of the pile. The calculated volume of heave in the case of the authors' tests was on only 14% of the embedded volume of the pile. This low volume was expected to be due to the overburden pressure of the sand.

6.15.3 Vertical Soil Displacement as a Function of Pile Penetration

Evident from Fig. No. 6.27 is a 'kink' in the vertical soil displacement/pile penetration curve. This indicates that as the pile passes, the innermost set of inclinometers 'pops up' before returning to a downward movement. This 'pop up' as the pile passes the inclinometer levels indicates a change in stress from tensile to compressive, (Werscking (1986)) and is similar to the profile shown by Vesic (1967), (Fig. 6.28). Unfortunately the incomplete record of static equipment during driving (due to the relatively long scanning period) made it impractical to calculate a strain profile from the authors results.

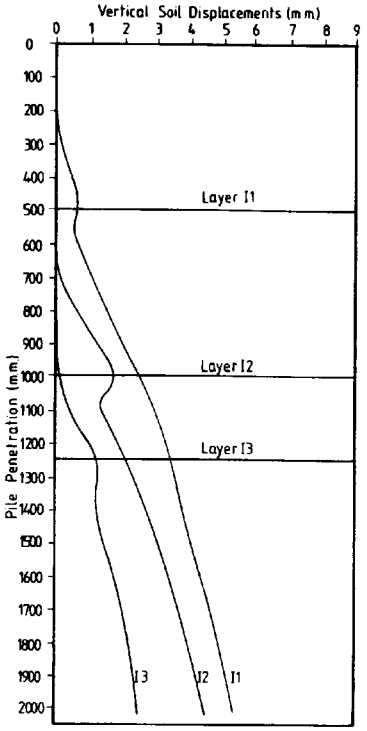

TEST 1 SAND ONLY PROFILE

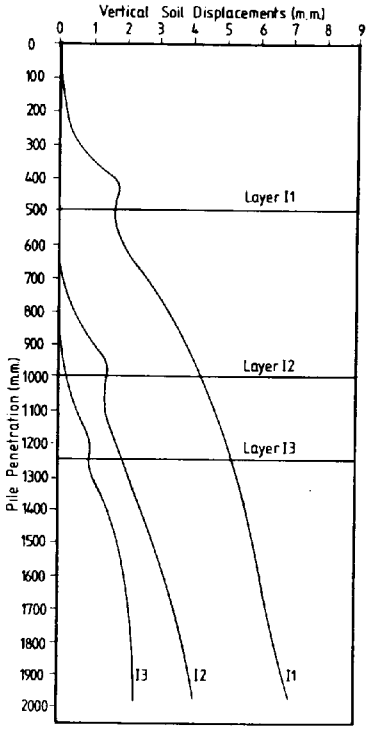

TEST 2 SAND ONLY PROFILE

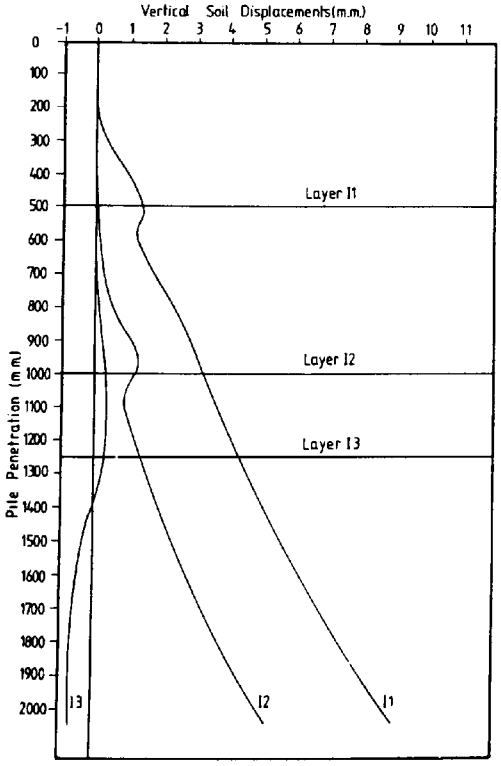

TEST 3 SAND OVER CLAY PROFILE

FIGURE N° 6.27 SHOWING VARIATIONS IN VERTICAL SOIL DISPLACEMENTS WITH PILE PENETRATION

NOTE
DISPLACEMENTS SHOWN ARE OBTAINED FROM THE INNERMOST SETS OF INCLINOMETERS FOR EACH INSTRUMENT LAYER

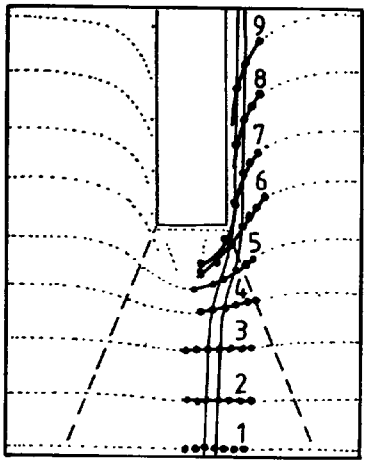

6.28 (a)

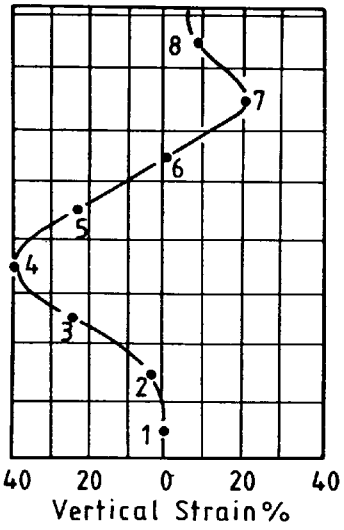

6.28 (b.)

KEY

6.28 (a) Displacements Around a Driven Pile in Sand (After Robinsky and Morrison (1964))
6 28 (b) Strains Around a Driven Pile in Sand (Deduced by Vesic (1967) from the Displacements in 6.28 (a) (Robinsky and Morrison (1964))

FIG. Nº. 6.28 STRAINS AND DISPLACEMENTS AROUND A DRIVEN PILE (After Robinsky and Morrison (1964))

6.15.4 Insitu Soil Displacements During Penetration Tests

Figure No. 6.29 to 6.31 shows graphs of insitu vertical displacements at various stages of a C.R.P. and M.T.L. tests. The significance of these results with sand displacements upwards at shallow depths has been discussed in Section 6.14.3.

This upward trend indicates high lateral stresses being developed at the top of the pile due to arching of the circular ring of sand around the pile which has again been fully discussed in Section 6.14.3

6.16 Change in Insitu Density Due to Pile Installation and Testing

A means of measuring the changes in density in a dry sand which was developed at the Polytechnic (Wersching (1983)) and described in Chapter 3, Section 3.9.6 was used in the model tests.

Figure No. 6.32 shows graphs of changes in density for the 3 tests and highlights a number of interesting points:-

(1) An increased density is exhibited along the pile shaft to an approximate radius of 7D (average percentage increase 2.09).

(2) Also density increase appears to be greatest at shallow depths (3.59% increase) diminishing with depth (1.31% increase at toe).

(3) In the case of the sand only tests a density increase is exhibited under the pile toe (average percentage increase 1.33).

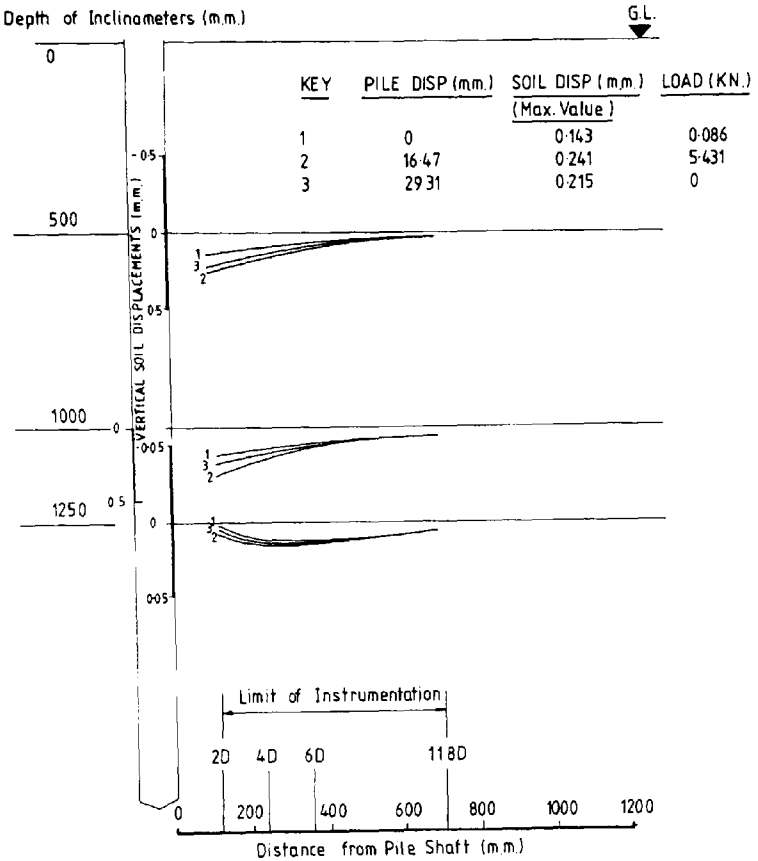

SOIL DISPLACEMENTS DURING A C.R.P. TEST

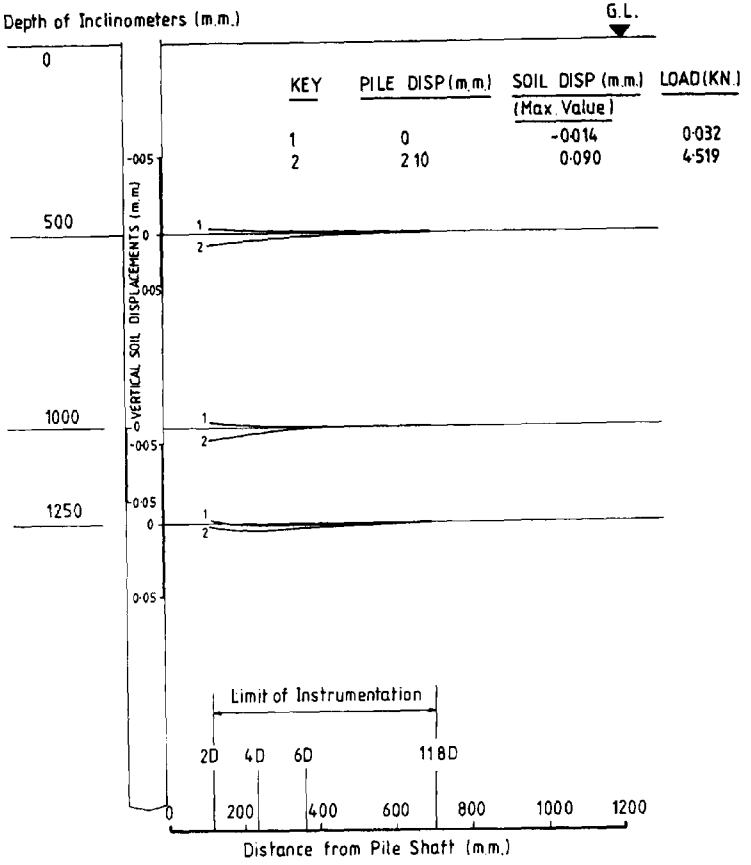

SOIL DISPLACEMENTS DURING A M.T.L. TEST

FIG. N° 6.29 SHOWING GROSS SOIL DISPLACEMENTS AT VARIOUS STAGES OF A C.R.P. AND M.T.L. TEST

TEST N°. 1 (Sand Only Profile)

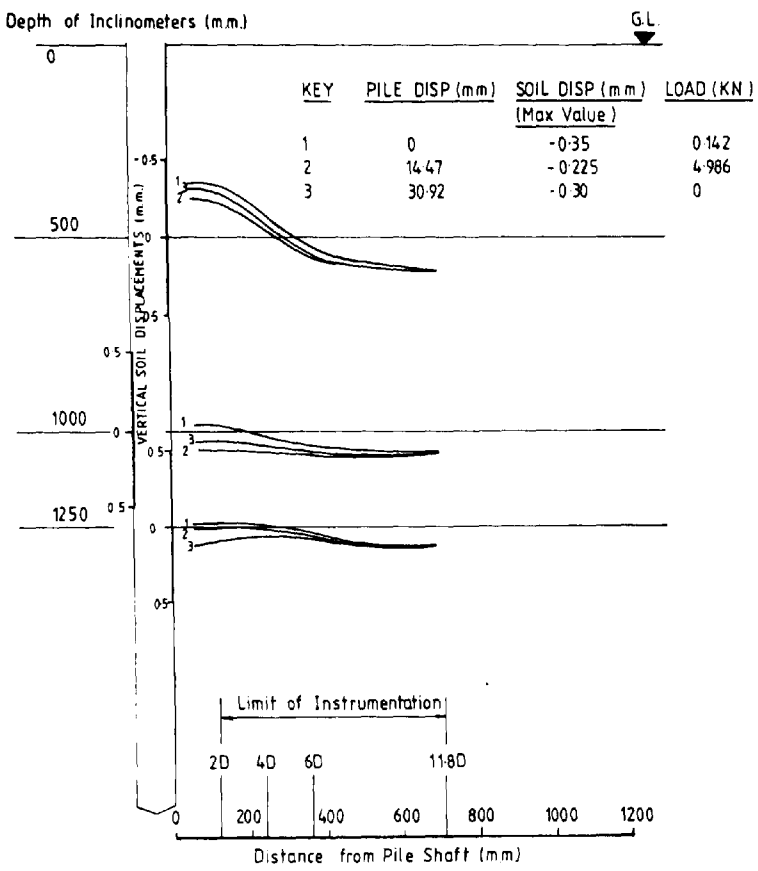

SOIL DISPLACEMENTS DURING A C.R.P. TEST

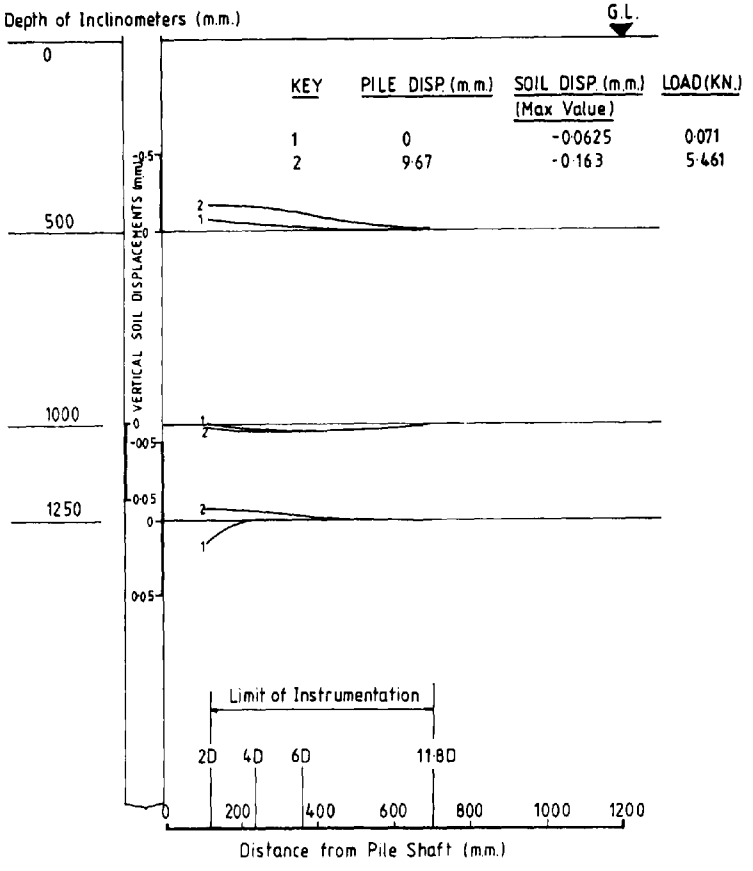

SOIL DISPLACEMENTS DURING A M.T.L. TEST

FIG. N° 6 30 SHOWING GROSS SOIL DISPLACEMENTS AT VARIOUS STAGES OF A C.R.P. AND M.T.L. TEST
TEST N°. 2 (Sand Only Profile)

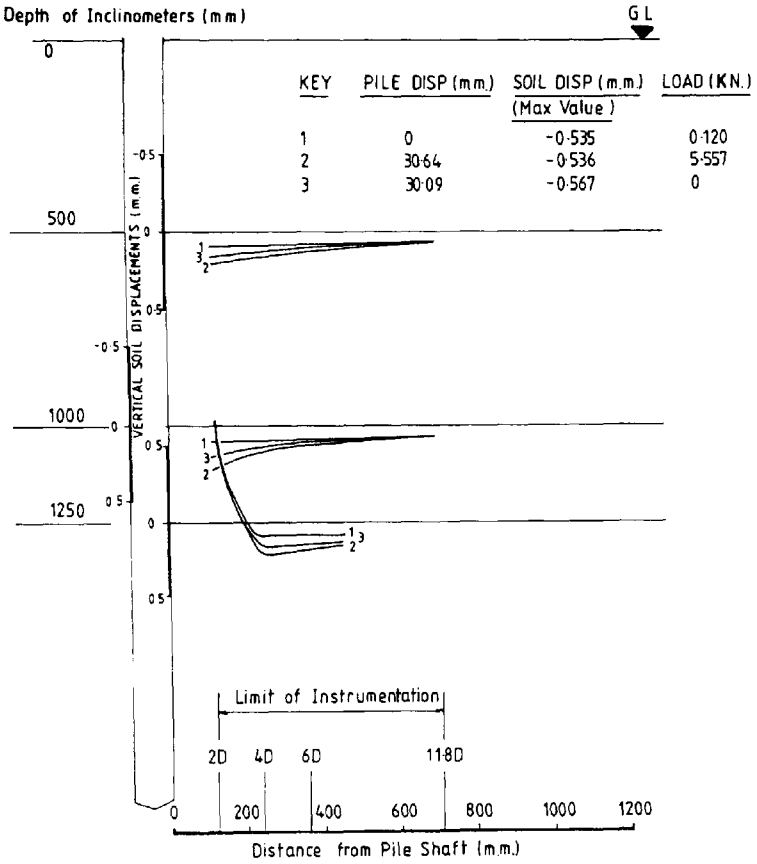

SOIL DISPLACEMENTS DURING A C.R.P. TEST

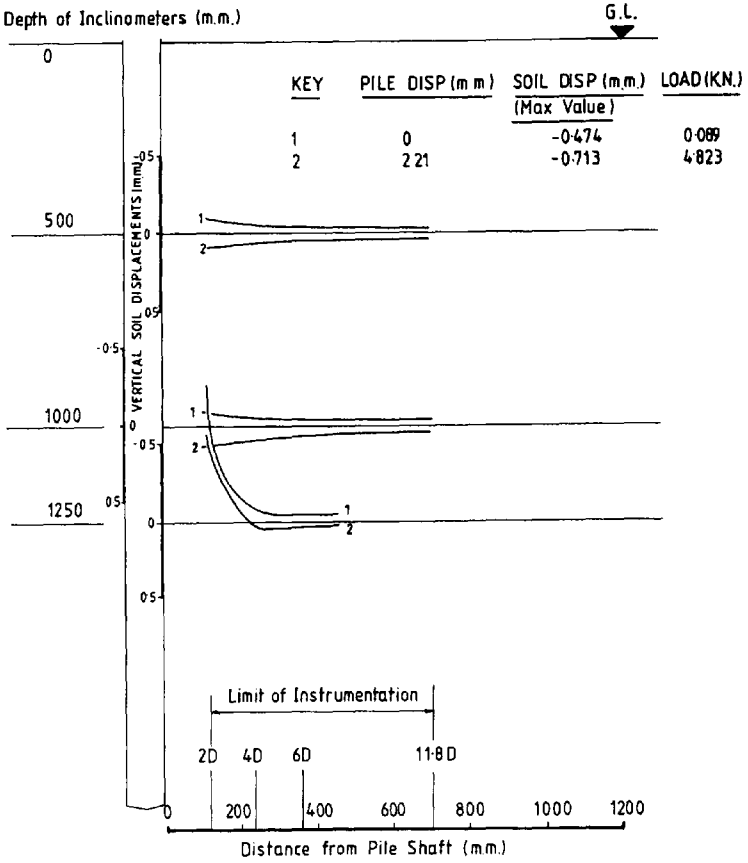

SOIL DISPLACEMENTS DURING A MTL TEST

FIG. N° 6.31 SHOWING GROSS SOIL DISPLACEMENTS AT VARIOUS STAGES OF A C.R.P. AND M.T.L. TEST

TEST N°. 3 (Sand Over Clay Profile)

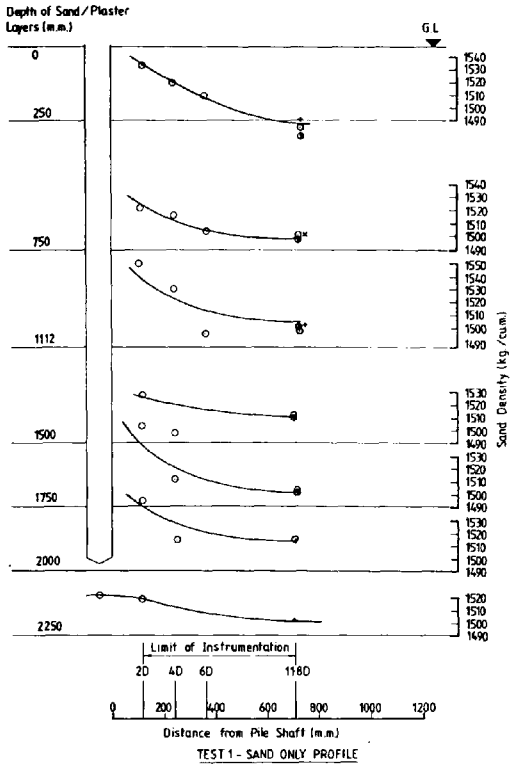

TEST 1 - SAND ONLY PROFILE

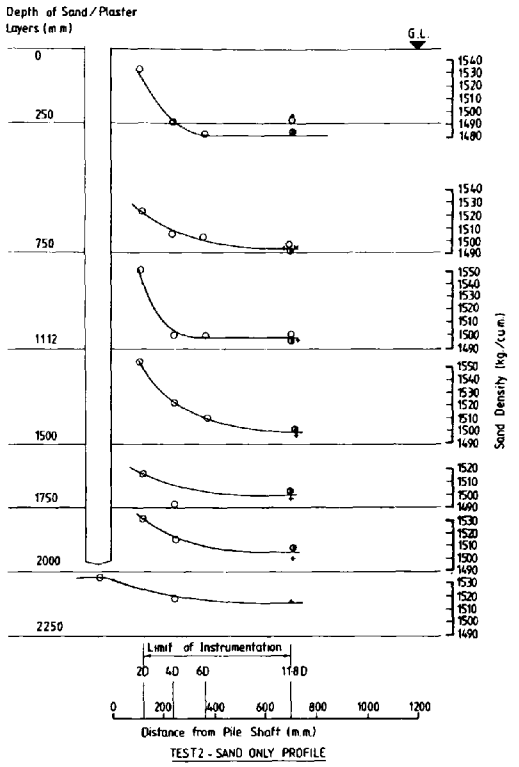

TEST 2 - SAND ONLY PROFILE

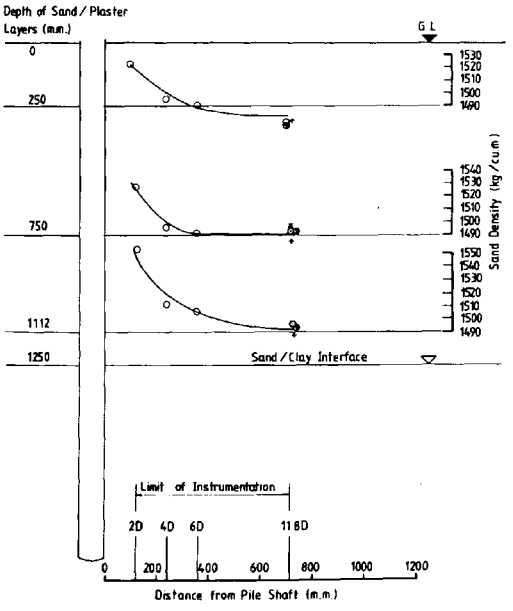

TEST 3 - SAND OVER CLAY PROFILE

KEY :-

- ○ Sand-Plaster Mixture Hydrated after all Penetration Tests
- ◉ " " " " Prior to all Tests
- • As Placed Density as Determined from a C.B.R. Mould
- × Insitu Density Check on Sand-Plaster Values Determined by 'Left in Place' C.B.R. Moulds

FIGURE N°6.32 SHOWING CHANGES IN SOIL DENSITY DUE TO PILE INSTALLATION

A high percentage increase was exhibited in the case of Test 3 (sand over clay) profile for the lowest level of density samples. This may be attributed to the close proximity of the samples to the sand/clay interface causing 'base effects'.

The zone of increased density exhibited in Figure 6.32 (7D) is in broad agreement with the values quoted by Robinsky and Morrison (1964) (5.5D), Meyerhof (1959) (5 D), and Kishida (1963) (8D).

The relatively larger percentage increases in density displayed at shallow depths combined with the slightly lower values of percentage increase at lower depths again tends to support the hypothesis that high lateral stresses are developed at the upper section of the pile due to 'locking in' of the sand particles.

Also evident from Figure 6.32 is a slight density gradient for the undisturbed sand ranging from 1490 kg/m^3 at a depth of 250 mm to 1520 kg/m^3 at a depth of 2250 mm.

6.17 Shear Stresses at the Sand Clay Interface

The effect of driving the pile and subsequent test loadings on sand movements at the sand/clay interface was monitored using the shear transducers described in Chapter 5, Section 5.1.7.

The load cells were constructed in such a way that a negative shear indicated movements towards the pile while a positive shear indicated movement away from the pile.

Figure No. 6.33 shows the changes in shear stress at the sand/clay interface during:-

(1) Driving

(2) C.R.P. Test

(3) M.T.L. Test

(4) Pull Out Test

Each case will be treated individually commencing with shear stresses due to driving.

6.17.1 (a) Driving

The nature of the driving operation (dynamic) made monitoring the shear load cells during pile installation impractical. However, the driving operation was stopped at 500 mm intervals in order to fix the next pile section in place. As a consequence it was possible to monitor the residual stresses at 500, 1000, 1500 and 2000 mm pile penetrations. At a depth of 500 mm (750 mm from the sand/clay interface) there was no change in load cell readings and hence no appreciable soil movements. At a penetration of 1000 mm (250 mm from the sand/clay interface) changes in stresses were registered on the load cells. These stresses were positive up to a radius of 2.6D, and equally negative at a radius of 7.6D. The corresponding displacement field would therefore be one of sand pushed away from the pile (causing possible densification) to a radius of 5.0D with the general mass of sand pushing inwards towards the pile at greater radii. The displacement field thus indicated is similar to classical failure patterns under deep foundations as shown in Fig. 6.34.

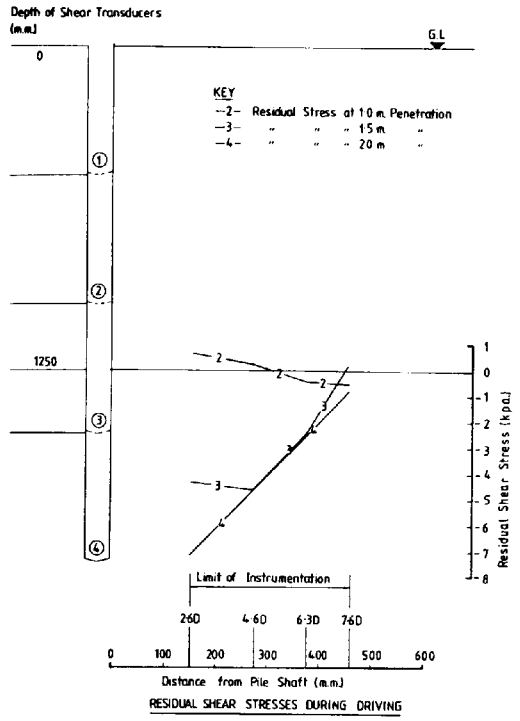

RESIDUAL SHEAR STRESSES DURING DRIVING

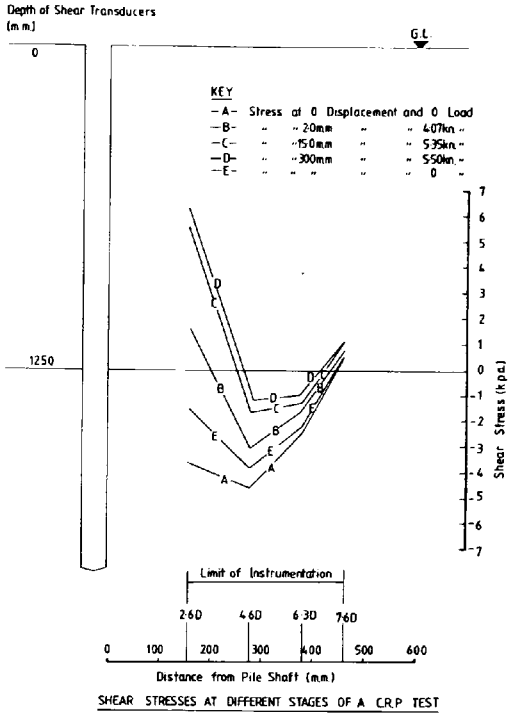

SHEAR STRESSES AT DIFFERENT STAGES OF A C.R.P TEST

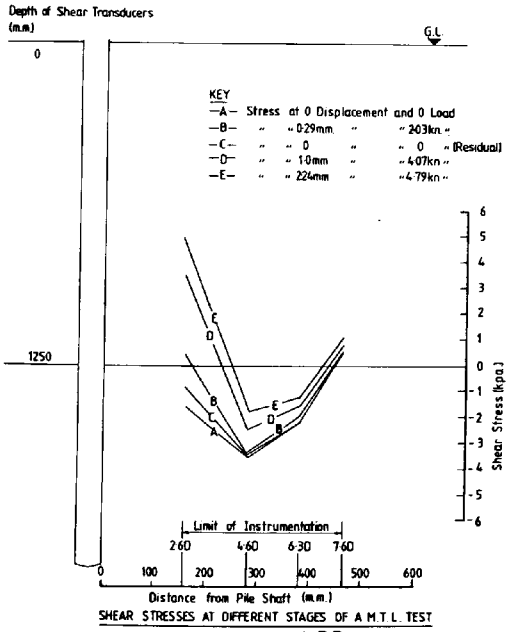

SHEAR STRESSES AT DIFFERENT STAGES OF A M.T.L. TEST

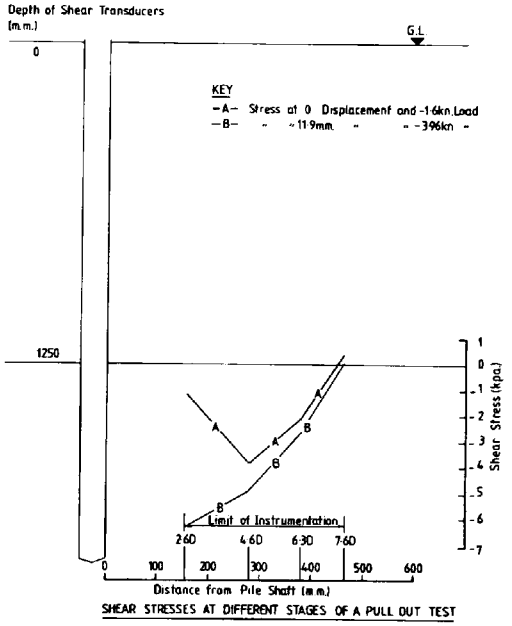

SHEAR STRESSES AT DIFFERENT STAGES OF A PULL OUT TEST

FIGURE Nº 6.33 SHOWING SHEAR STRESSES AT THE SAND/CLAY INTERFACE CAUSED BY SOIL MOVEMENT DUE TO PILE INSTALLATION

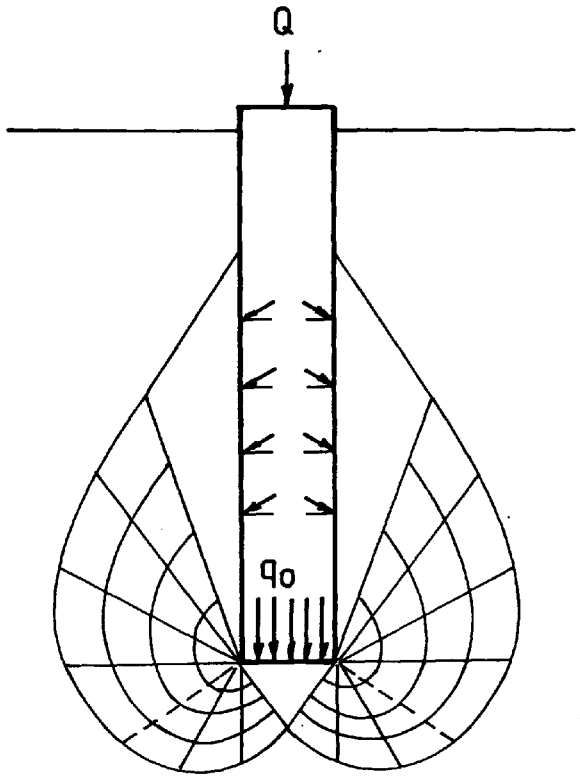

De Beer (1945)
Jaky (1948)
Meyerhof (1951)
(After Vesic (1965))

FIG. Nº. 6.34 ASSUMED FAILURE PATTERNS UNDER DEEP FOUNDATIONS

When the pile had penetrated the clay the residual stresses were entirely negative indicating that sand had travelled towards the pile on cessation of driving. The maximum decrease encountered was equal to approximately 8 Kpa.

6.17.2 (b) Shear Stresses During Penetration Tests

Figure No. 6.32 shows changes in shear stress during a C.R.P. and M.T.L. test and highlight a number of important facts:-

(1) At the beginning of the test the residual stress is entirely negative indicating sand has moved towards the pile.

(2) The initial residual stress corresponds to the final residual stress from the previous stage of loading.

(3) As the test progresses there is a positive increase in shear stress indicating sand is pushed away from the pile during loading.

(4) When the load is removed the final residual state is again negative but with a smaller negative value than the initial one. This indicates that even under conditions of no load the soil is still in a stressed state.

(5) The numerical increase in shear stress for the C.R.P. test (10.1 Kpa) is greater than that for the M.T.L. test (6.4 Kpa) showing the effect that large pile movements have on insitu sand movements.

6.17.3 Pull Out Test

As can be seen from Fig. 6.32 there is a negative change in shear stress (5.2 Kpa) which indicates sand movement towards the pile during the pull out test. This occurrance was to be expected as the sand filled the void created by retracting the pile.

6.18 Insitu Vertical Stress Changes due to Pile Installation and Test Loadings

6.18.1 General

The instrumentation used to measure insitu vertical stress changes in the soil have been fully discussed in Chapter 5, Section 5.1.6 and were of the Nottingham load cell type. Insitu checks were conducted on the load cells after calibration to ensure they were functioning correctly by comparing the values of the embedded load cells with calculated overburden values. Agreement between calculated and experimental values were within 0.5 Kpa. However, it must be noted that during the course of the tests 3 of the 6 load cells used malfunctioned.

6.18.2 Sand Only Profiles

In the case of the sand only profiles changes in vertical stresses were detected as far away as 12.5 diameters from the pile tip, although it must be stressed that the readings obtained were near the limits of the instruments accuracy. Definite changes were detected with the pile tip 4 diameters from the level of instrumentation.

It has been explained in Section 6.17.1 that the stresses obtained during the driving process were residual ones when the pile was in a state of equilibrium.

It can be seen from Fig. 6.35 and 6.36 that the zone of influence is approximately 7D and is again in broad agreement with the previously quoted authors. That the residual vertical stresses are negative is difficult to explain, but may be due to the process of some displacement and compaction below the pile tip followed by some movement adjacent to the pile sides. These movements tend to decrease the sand density in the immediate vicinity of the sides. Evidence of this effect is shown in Fig. 6.28 where Vesic (1967) has plotted vertical strain profile using results published by Robinsky and Morrison (1964). He shows a tensile stress along the pile shaft indicating a decrease in density. Recourse to Fig. 6.27 also indicates the same phenomenon. Vesic also suggested that this action nullifies some of the benefits obtained from primary compaction. Figure 6.35 and 6.36 also show changes in vertical stress during C.P.R., M.T.L. and pull out tests and in all cases display a positive change in vertical stress indicating a density increase at the instrument level.

The validity of these results come into question when they are compared to the sand over clay profile results shown in the next section.

6.18.3 Sand Over Clay Profile

Figure 6.37 indicates a drastic change in the behaviour of the load cells with predominantly positive results being

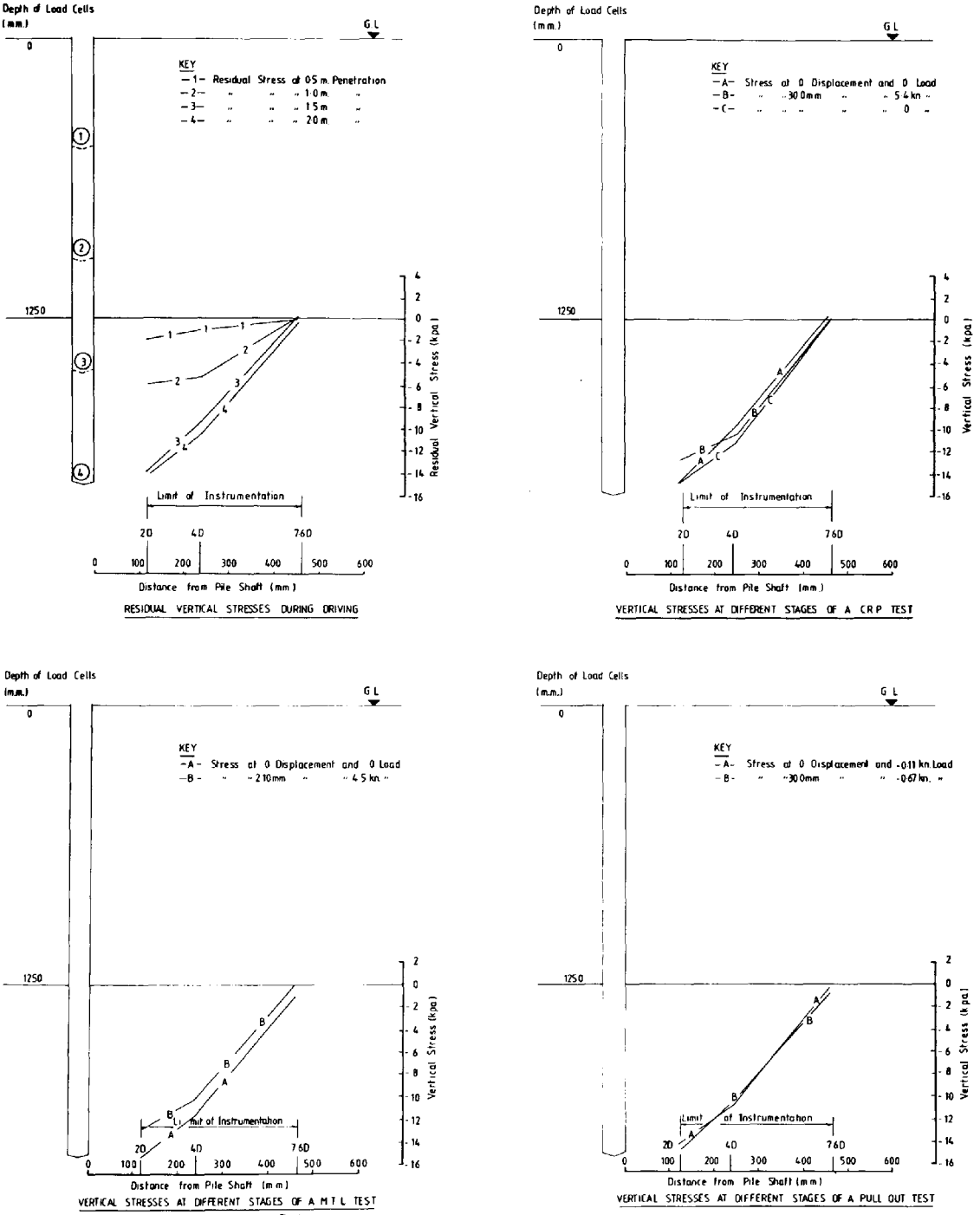

FIGURE Nº 6.35 SHOWING CHANGES IN VERTICAL STRESSES AT THE INDICATED LEVEL FOR TEST 1 (Sand Only Profile) DUE TO PILE INSTALLATION

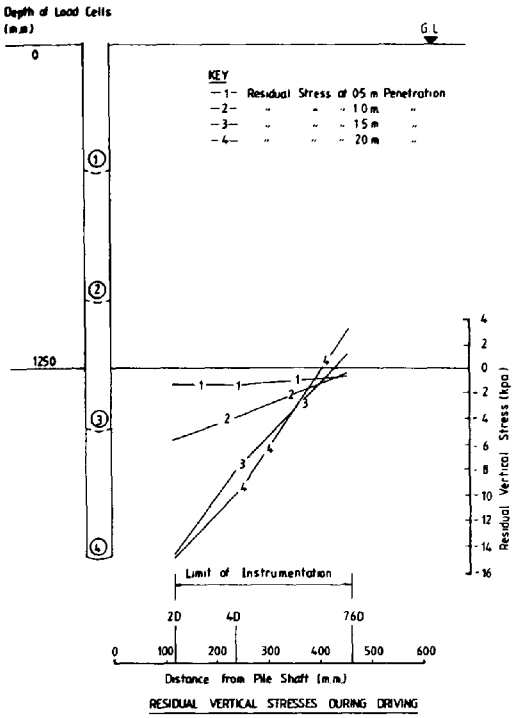

RESIDUAL VERTICAL STRESSES DURING DRIVING

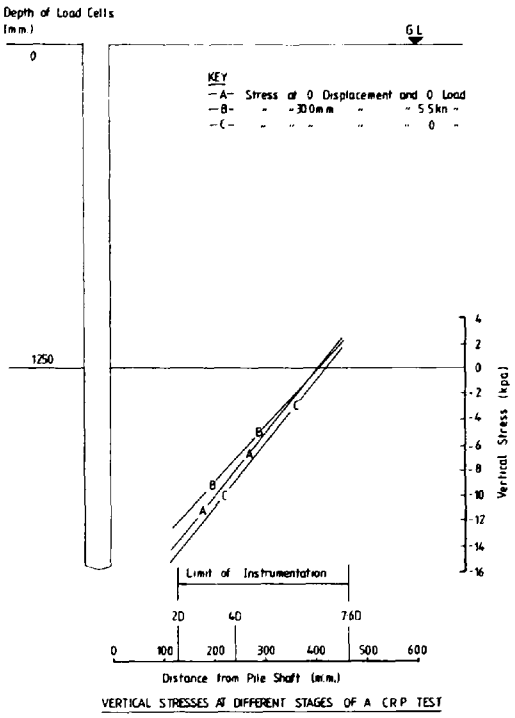

VERTICAL STRESSES AT DIFFERENT STAGES OF A CRP TEST

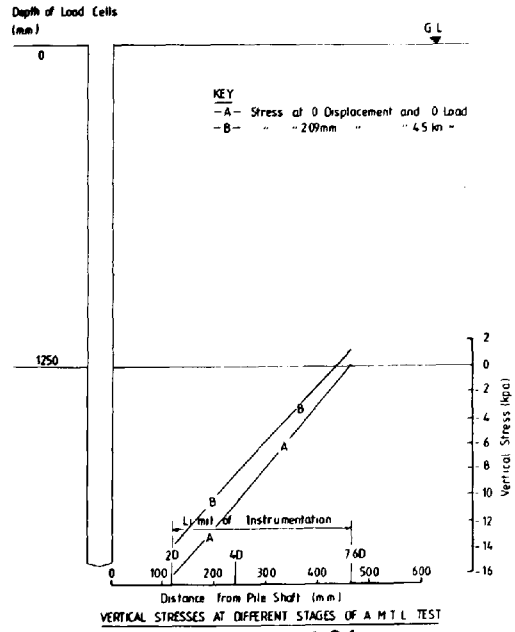

VERTICAL STRESSES AT DIFFERENT STAGES OF A MTL TEST

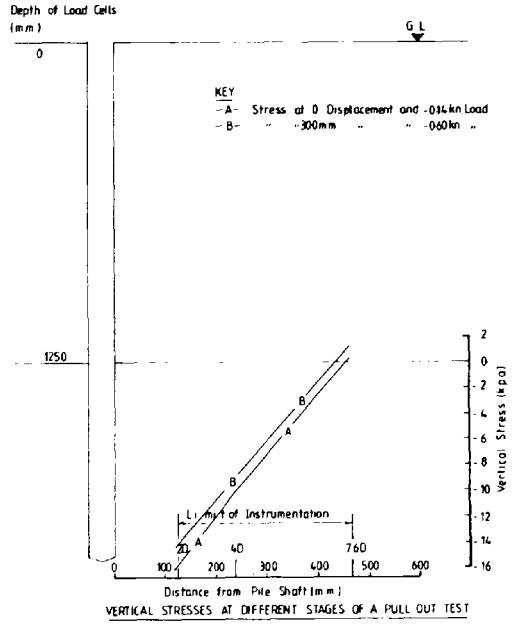

VERTICAL STRESSES AT DIFFERENT STAGES OF A PULL OUT TEST

FIGURE Nº 6.36 SHOWING CHANGES IN VERTICAL STRESSES AT THE INDICATED LEVEL FOR TEST 2 (Sand Only Profile) DUE TO PILE INSTALLATION

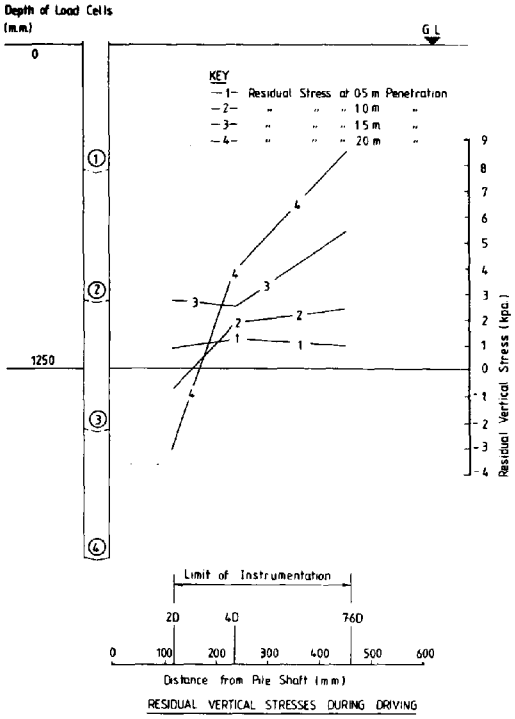

RESIDUAL VERTICAL STRESSES DURING DRIVING

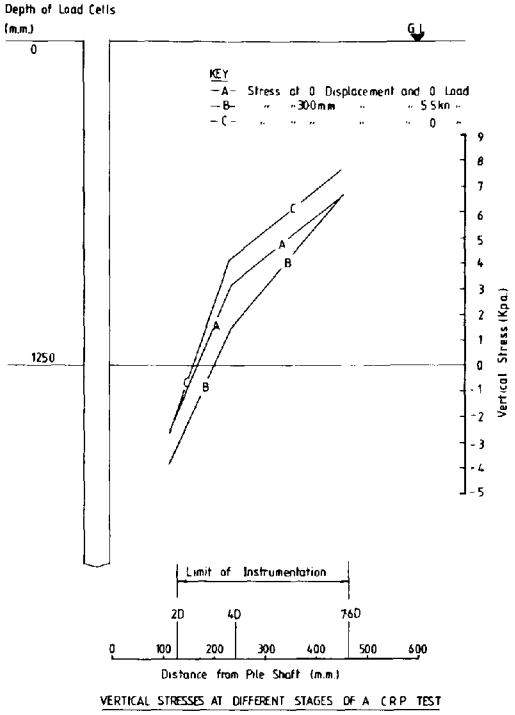

VERTICAL STRESSES AT DIFFERENT STAGES OF A CRP TEST

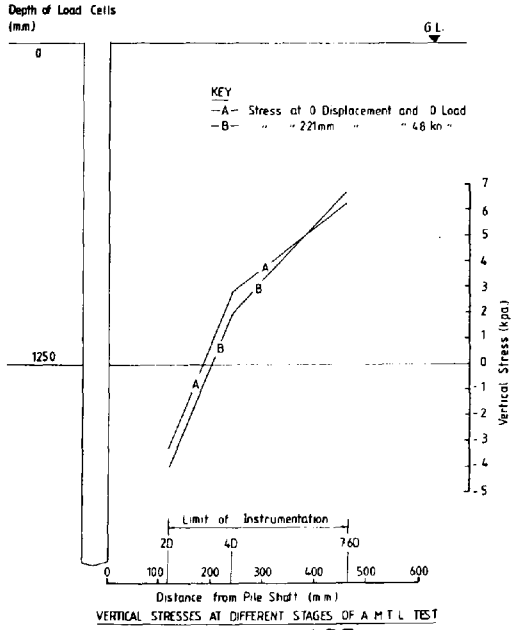

VERTICAL STRESSES AT DIFFERENT STAGES OF A M T L TEST

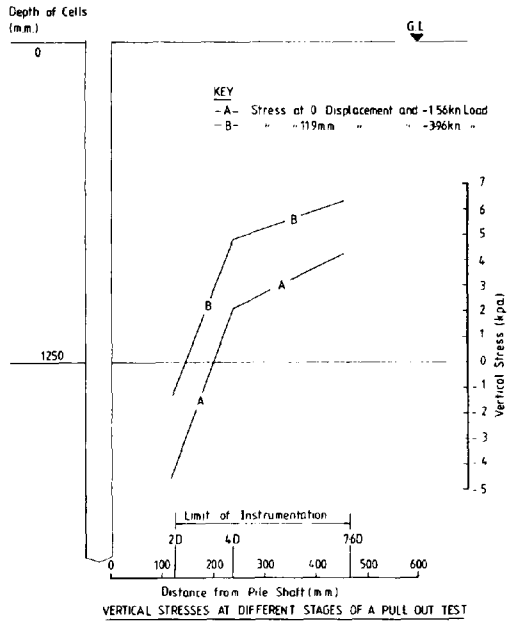

VERTICAL STRESSES AT DIFFERENT STAGES OF A PULL OUT TEST

FIGURE N° 6.37 SHOWING CHANGES IN VERTICAL STRESSES AT THE SAND/CLAY INTERFACE DUE TO PILE INSTALLATION

displayed. This tends to indicate that the rigidly confined load cells behave differently to the 'floating' load cells in the sand only tests. It would be reasonable to assume that in the case of the sand only tests the load cells displace vertically as is indicated in Fig. 6.26 (insitu vertical displacements), leading to a relief in overburden pressures. However when the load cells are rigidly confined as in test 3 an increase in overburden pressure is displayed as displaced sand presses down on the sand/clay interface. It may be said that the load cells are rigidly confined because the clay is in an undrained state due to the water-proof membrane covering the whole block. Negative values are displayed near to the pile and may indicate a slight decrease in density due to the previously described reasons. Therefore, it may be said of the sand only results that while the readings obtained were true within the context of the test the values obtained were predominantly due to vertical soil movements as opposed to changes in overburden pressure shown in the sand over clay test.

6.19 Analysis of the Clay Block

6.19.1 Dissection of the Clay after a Test

In order to study the effect of pile driving on the structure of the clay a method had to be devised whereby the clay block could be taken apart without destroying any internal features of note. In the small scale tests described in Chapter 3, a cheese wire was used to cut the clay block and expose the pile insitu. However it was found that the action of the wire left a smooth face devoid of any structure changes that

may have occurred. In an effort to remedy the shortcomings of this method the following procedure was adopted:-

(1) One side of the Braithwaite Tank used to contain the clay former (Chapter 5, Section 5.2.4) was carefully removed along with the corresponding side of the clay former.

This procedure was adopted in order to minimise the possibility of predetermined fracture lines occurring in the clay due to stress relief.

(2) Starting at the top outer edge of the block a spade was pushed horizontally into the clay to a depth of approximately 100 mm and a prising action used to remove the resulting clay 'brick'. In this way the structure of the clay face could still be seen, allowing any fracture or failure patterns to be identified.

(3) This process was then repeated from top to bottom of the clay block on a plane at right angles to a pile diameter.

(4) Once the process had been completed steps 2 and 3 were then repeated until the pile shaft was exposed.

It should be noted at this stage that any visible features of interest were recorded on film and will be shown and discussed in the ensuing sections.

(5) When the pile had been exposed the untreated surface was overlayed by a polythene membrane

and all visible structural changes in the clay sketched on it using a felt marker for later analysis.

(6) The sand/clay face was then split into a grid and moisture content samples taken with the majority being sealed in wax for later analysis of moisture migration. Some samples of obvious importance (around the pile tip) were taken for immediate moisture content determination. It was later found that this was a prudent step as an attempted analysis of the clay samples up to 6 weeks later revealed that some had dried out due to tiny pin holes in the wax coating. Enough samples were contaminated in this way to render the analysis ineffective.

(7) Finally the same procedure for dissecting the clay was used on the other half but this time with the spade vertical and working on a horizontal plane in order to determine if there were any radial cracks denoting possible fracture due to driving. Another feature also looked for was random cracks not eminating from the pile and denoting fracture due to stress relief. At each 100 mm depth 3 triaxial samples were taken and coated in wax for undrained tests to determine the variation in cohesion with depth.

The entire dissection process lasted approximately five days with the exposed clay surface being covered with polythene

during the time when the clay was not being worked upon. Nevertheless it is expected that some moisture loss would have taken place.

Unfortunately some of the triaxial samples suffered from the same fate as the moisture content samples with regard to pin holes developing in the wax coating. Despite this every effort was made to allow for this fact when determining the Cu values for each clay layer. However Fig. 6.38 shows that although there seems to be a linear increase in Cu values from the surface down, the values at the bottom appear extremely high when compared to the as placed (apparent cohesion) values. Even taking into account consolidation due to the overburden pressure the values still appear high. Therefore the results must be treated with some sceptisism although they do show a general trend of linearly increasing Cu values.

6.20 Drag down of Sand into the Clay Block Due to Driving

The small scale tests in Chapter 3 have shown that sand is dragged down into the underlying clay due to driving. This phenomenon was again repeated for the semi full scale tests. Plate 6.1 shows the pile entering the clay with a ring of sand around the pile that has been dragged down into the clay. This ring of sand extends a distance of 30 mm out from the pile wall (i.e. half a pile diameter) and 120 mm into the clay (2 diameters) before petering out. (Fig. 6.39, Plate 6.2). Again this is broadly in line with the findings of Tomlinson (1971) where he suggested that sand could be pulled down onto the clay layer by as much as 3D.

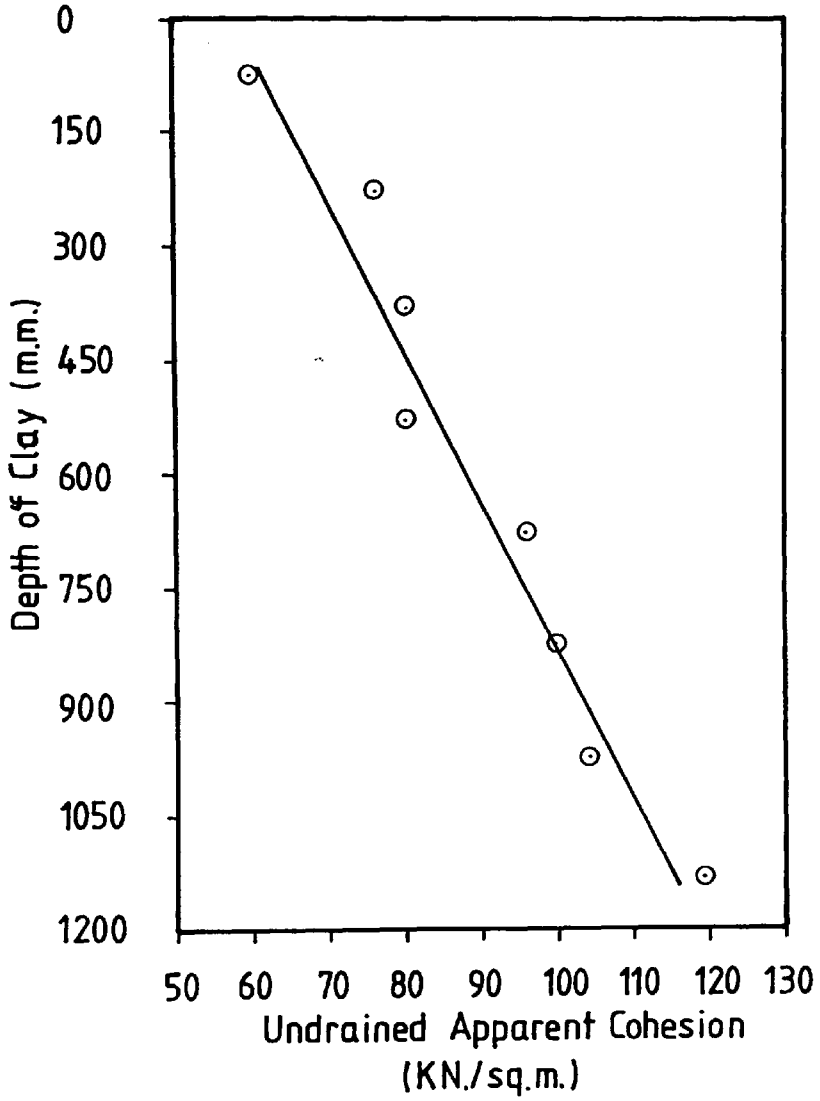

FIG. N° 6.38 SHOWING 'AS RETREIVED' COHESION VALUES OF THE RED MARL

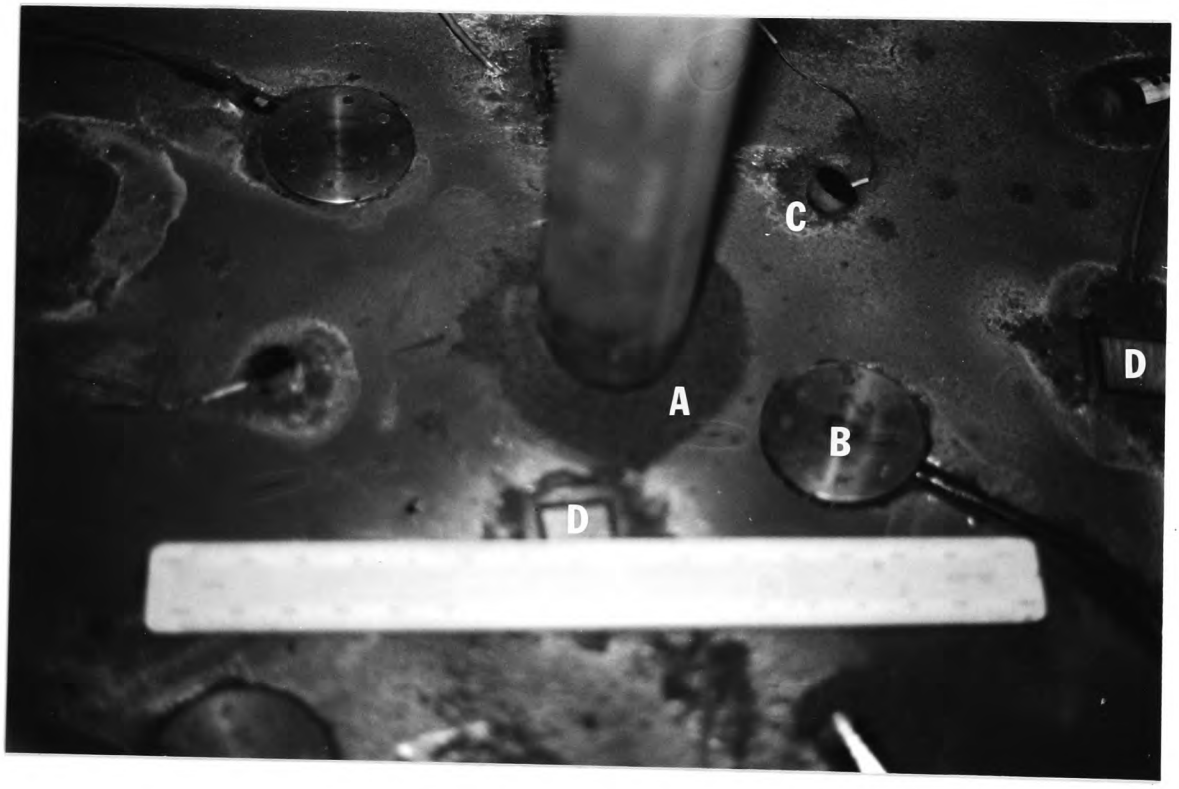

KEY:

A. Ring of Sand Dragged Down into the Clay Block

B. Nottingham Pressure Transducer

C. Inclinometers

D. Shear Transducers

PLATE 6.1 Showing Pile Entering the Clay Block

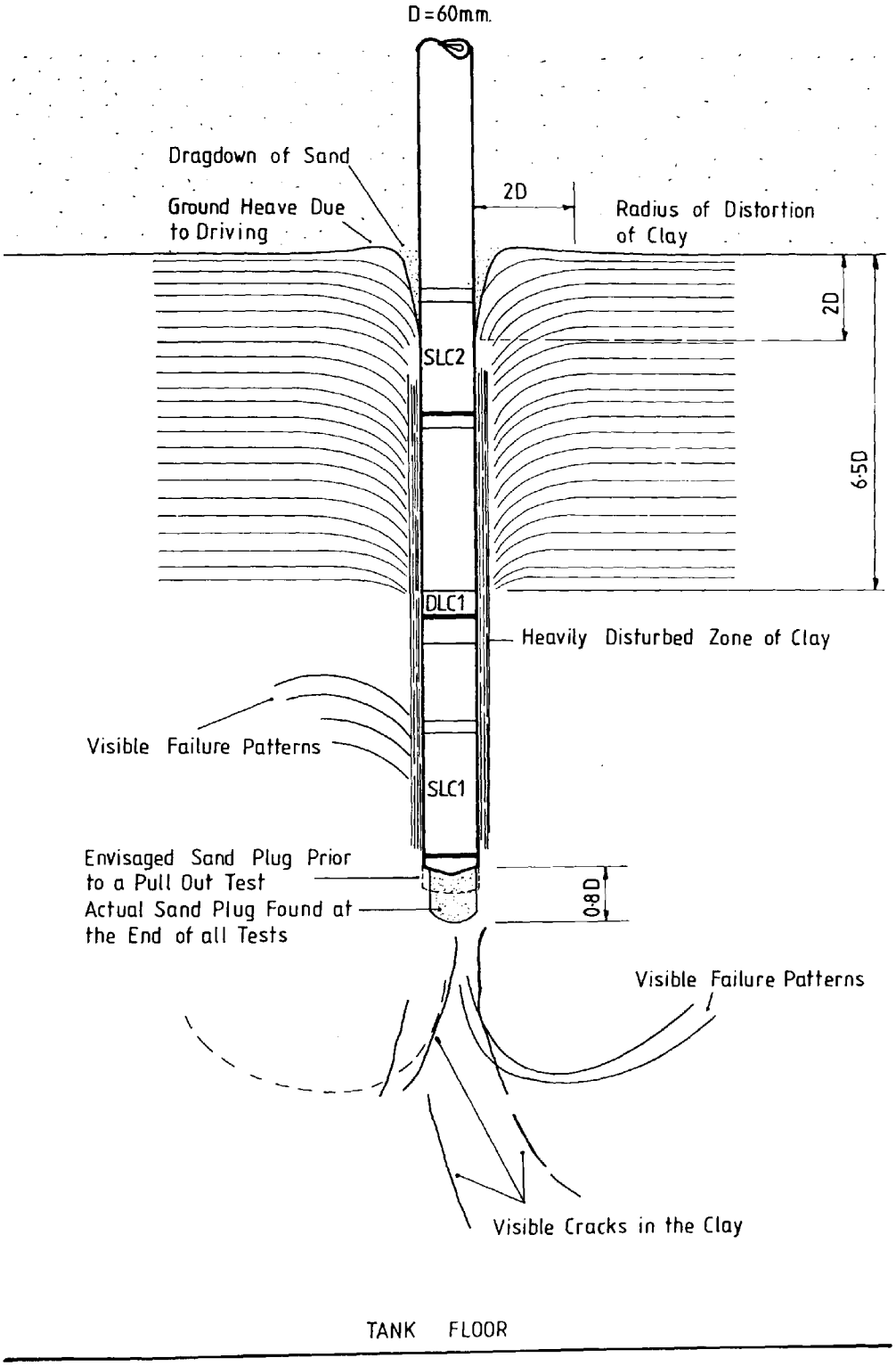

FIG. N° 6.39 SHOWING STRUCTURAL CHANGES IN THE CLAY DUE TO DRIVING

KEY:

A. Disturbed Zone of Clay

PLATE 6.2 Showing Radius of Distortion of the Clay due to Driving

6.21 Sand Plug at the Pile Tip

The small scale tests (Chapter 3) revealed a sand plug which preceded the pile tip into the clay stratum. The same phenomenon was again observed in the semi full scale tests. Meyerhof and Sastry (1978) have also reported this phenomenon where the pile tip punched a sand wedge into an underlying clay layer. Similar findings have also been reported by Werscking (1986) in which 110 mm diameter piles have been driven at a constant rate of penetration in an identical two soil system. However the plug of sand differed from those obtained by the latter authors and also what could be expected using conventional failure patterns under deep foundations (e.g. Prandtl (1921), Meyerhof (1951)) where a wedge of sand precedes the pile tip.

Plate 6.3 and Fig. 6.39 shows the sand plug obtained from test 3 and in order to explain the unusual shape recourse to the load testing sequence together with the lateral stress state of the sand below the pile tip just before entry into the clay layer must be taken.

The shape of the sand plug displayed three distinct features:-

(1) Vertical cylindrical walls

(2) Curved base

(3) Diameter of the cylinder less than the diameter of the pile.

6.21.1 Load Test History

The last test performed on the model pile was a pull out test whereby the pile was retracted from the clay a total distance of 30 mm. Thus although the depth of the sand plug

KEY:

A. Sand Plug

PLATE 6.3 Showing Sand Plug that Proceeds the Pile Tip into the Clay

6.21.2 Increase in Moisture Content at the Pile Tip

Moisture content samples taken from the clay surrounding the sand plug yielded an average value of 20.43%. This is considerably higher than the average as placed value of 18%. Physically this increase in moisture content implies a decrease in Cu value from approximately 60 Kn/m^2 to 38 Kn/m^2 (Fig. 6.1.3), and a decrease in bulk density from approximately 2150 Kg/m^3 to 2050 kg/m^3, (Fig. 6.1.4). This shows that considerable softening of the clay at the pile tip has taken place and is due in part to the sand plug acting as a sand drain.

6.22 Insitu Clay Deformation Due to Driving

6.22.1 General

It was explained in Section 6.19.1 that an attempt was made to study the effects of driving on the clay structure by carefully dissecting the clay mass after a test. While it is accepted that the method used was a crude one, a number of interesting features were observed and are discussed in the ensuing sections with regard to current theories on soil movement due to installation.

6.22.2 Soil Heave

The fact that the clay surface heaves during driving has been reported in Section 6.15.2. The volume of heave in relation to pile volume was also given. Unfortunately because the amount of heave was so small no pictorial evidence can be presented to verify the inclinometer results.

shown in Fig. 6.39 was 48 mm (0.8D) the actual depth of the sand plug before the pull out test must have been approximately 18 mm. This envisaged shape (Fig. 6.39) would also correspond more closely to the shape of the sand plug in the small scale tests where only compressive tests were undertaken.

Evidence from Plate 6.4 is that either considerable swelling of the clay has taken place after the test and prior to the pile tip being exposed or a considerable suction was developed during the pull out test. As a by product of determining the moisture content of the sand plug (11.77%) an approximate density of the sand plug was determined. The sand density thus determined was 1350 Kg/m^3 which was 10% less than the average dry density of the sand from all three tests. Thus the sand was in a fairly loose state despite being compressed between the pile and the clay during driving and penetration tests. A more logical explanation would be to assume the suction caused by retracting the pile formed the increased cavity seen in Plate 6.4 and also caused the sand to fill the resulting cavity, giving a corresponding reduction in the sand density. Also shown in Fig. 6.39 is the envisaged sand plug prior to a pull out test. The corresponding density of sand at this stage would have been approximately 1600 kg/m^3 which is a more reasonable figure considering the state of confinement of the plug. This envisaged sand plug shown in Fig. 6.39 still displays a vertical wall although much reduced from the original. This shape may well be due to high lateral stresses in the soil as the pile approaches the sand/clay interface. This occurrance has also been reported by Meyerhof and Sastry (1978) and also Werscking (1986).

PLATE 6.4 Showing the Cavity left after Removing the Sand Plug

6.22.3 Visible Clay Deformations Along the Pile Shaft

Figure 6.39 and Plate 6.2 show clearly the effect of pile driving on the clay stratum whereby the clay is distorted and dragged down in the vicinity of the pile. This radius of distortion was found to be approximately 2D and is greater than the value quoted by Tomlinson (1971) of 3/4 width of a square timber pile.

This phenomenon was only visible for the first 650 mm of penetration (11D). However this may have been due to the fairly crude method of dissection than to an actual lack of the phenomenon.

There was some pictorial evidence to suggest a zone of intensely remoulded clay (Plate 6.5) around the pile as suggested by Randolph and Wroth (1982).

However, this phenomenon was easily identified by the previously described method of placing a polythene sheet over the exposed surface and sketching all relevant features. Fig. 6.39 shows the results of this exercise including the remoulded zone of clay. From the figure it is evident that this phenomenon only occurs a limited distance from the pile wall.

6.22.4 Failure Patterns at the Pile Toe

Again Figure 6.39 shows the failure patterns evident in the clay after the test, while Plate 6.5 shows these features pictorially. The failure pattern displayed is similar to the plastic zones near a foundation with a rough base proposed by Meyerhof (1951).

KEY:

A. Visible Failure Patterns

B. Heavily Disturbed Zone of Sand

PLATE 6.5 Showing Visible Failure Patterns in the Clay at the Pile Tip Due to Driving

However, it is evident from Figure 6.39 that the point at which the plastic zone returns to the pile shaft is greater than the one diameter proposed by Meyerhof. Also evident is the zone of highly disturbed or intensely remoulded clay around the shaft (Section 6.22.3). These patterns although only approximate appear to support the failure patterns proposed by among others De Beer (1945), and Jaky (1948).

6.22.5 Fracture Lines of the Clay Block

Evident from Fig. 6.39 and Plates 6.6 and 6.7 are a number of vertical fissures in the clay stratum. These fissures become more apparent and frequent towards the centre of the block.

It would appear logical that these fissures may have been caused by stress relief due to dismantling the Braithwaite tank. However the increase in frequency as the centre of the block was approached may lead to an alternative reason. Massarsch and Broms (1977) suggested that cracks can develop in normally consolidated clay due to pile driving. These cracks around the pile increase temporarily the permeability of the soil and cause a rapid dissipation of the excess pore water pressure.

6.23 Pile Alignment

While every effort was made to avoid pile drift during driving (Plate 6.8), misalignment was evident in the case of Test 3 (Sand over Clay profile). The estimated deviation from the vertical for this test was 2° and is within the accepted limits for normal piling practises of 2 to 3 per cent of the driven pile length (Hanna (1968)). It must be stated that

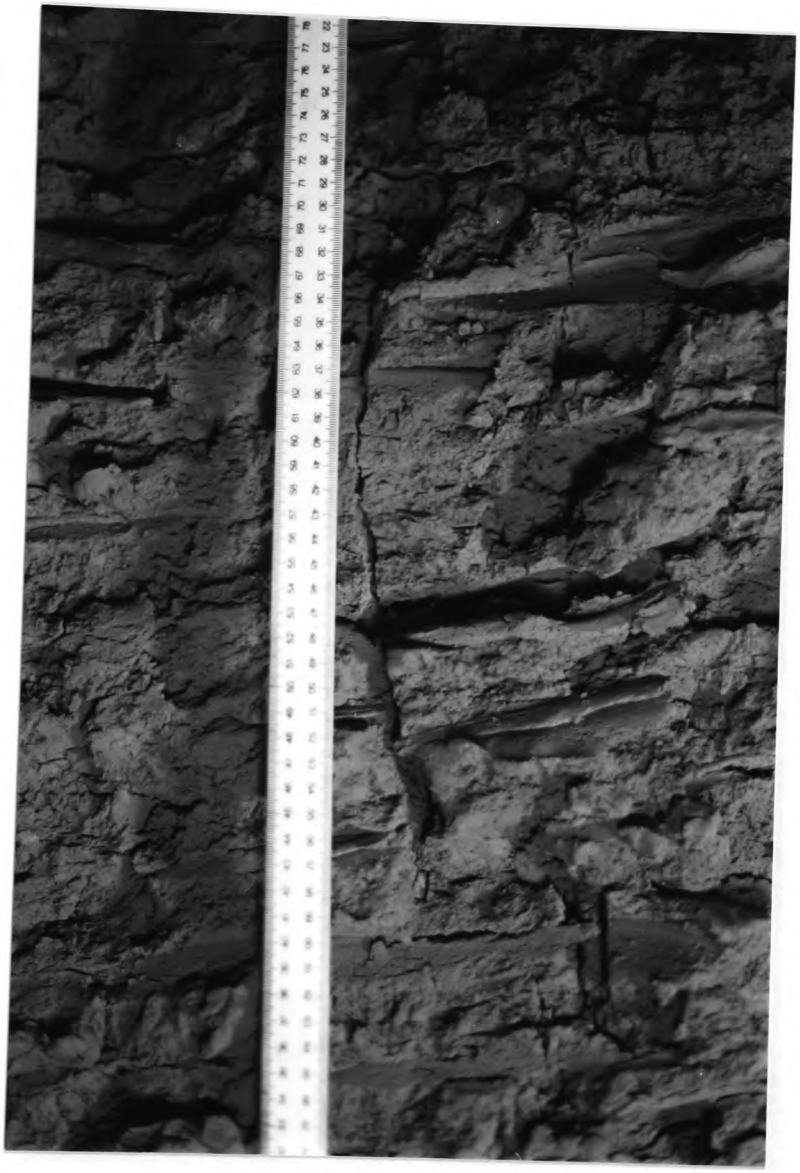

PLATE 6.6 Showing Fracture Lines in the Clay Block

PLATE 6.7 Showing Fracture Lines in the Clay Block

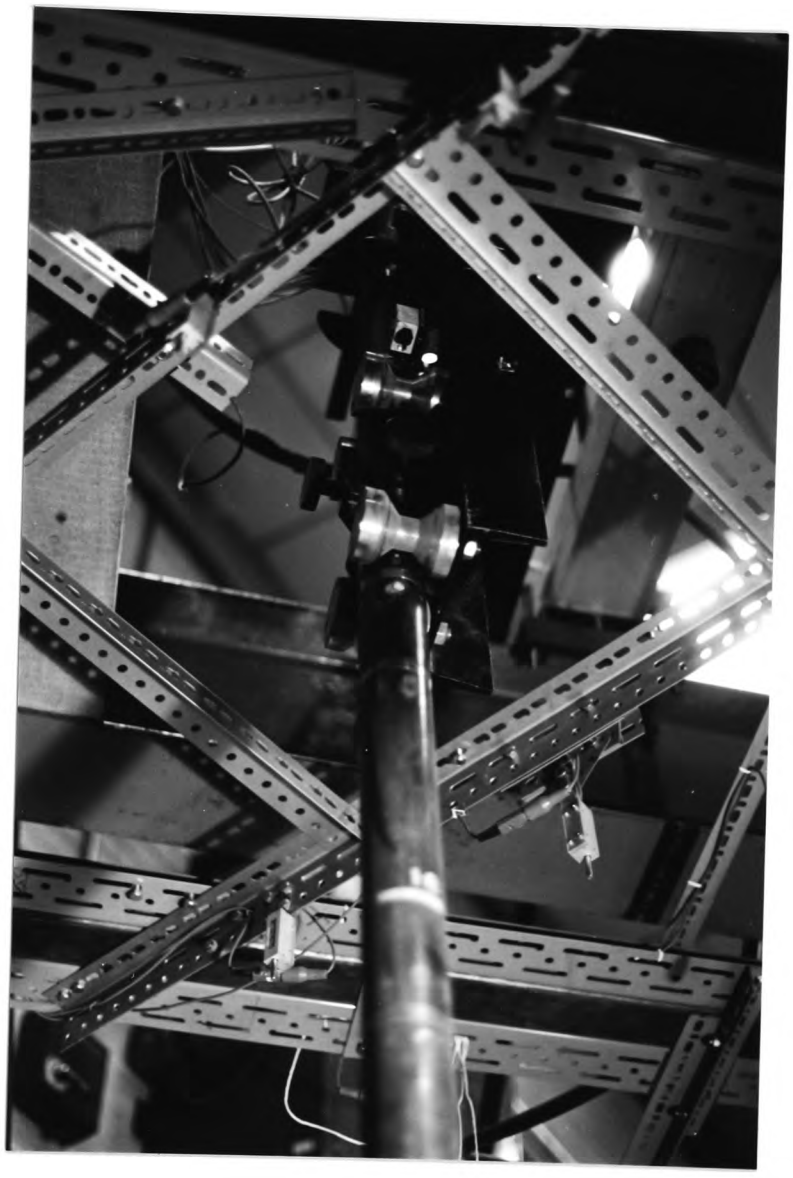

PLATE 6.8 Showing Model Pile and Pile Guides

it was only possible to measure the deviation from vertical in the case of the sand/clay test. In the case of the sand only tests the process of emptying the tank would have nullified any vertical deviation due to the sand disturbance.

Appendix 6.1

SOIL PROPERTIES

Leighton Buzzard Sand

The properties of the Leighton Buzzard sand used have been extensively researched at the Polytechnic (Kay (1980), Werscheing (1986)). Figure 6.1.1 and 6.1.2 (after Werscheing (1986)) shows the particle size distribution chart and angle of internal friction/dry density relationship respectively. From figure 6.1.1 the coefficient of uniformity (Cu) equals 1.79 and a coefficient of curvature (CC) of 1.14.

Red Keuper Marl (Mercia Mudstone)

The clay used was a red keuper Marl, the properties of which have been extensively determined by Werscheing (1986). Figure 6.1.3 and 6.1.4 (after Werscheing (1986)) show the variation in moisture content with $\log_{10}$ undrained shear strength and the variation in density with moisture content. The liquid limit (LL) of the clay was determined as 39 with the Plastic limit being 19.5. The clay can therefore be classified as a clay of medium (or intermediate) compressibility (using the plasticity chart for soil classification).

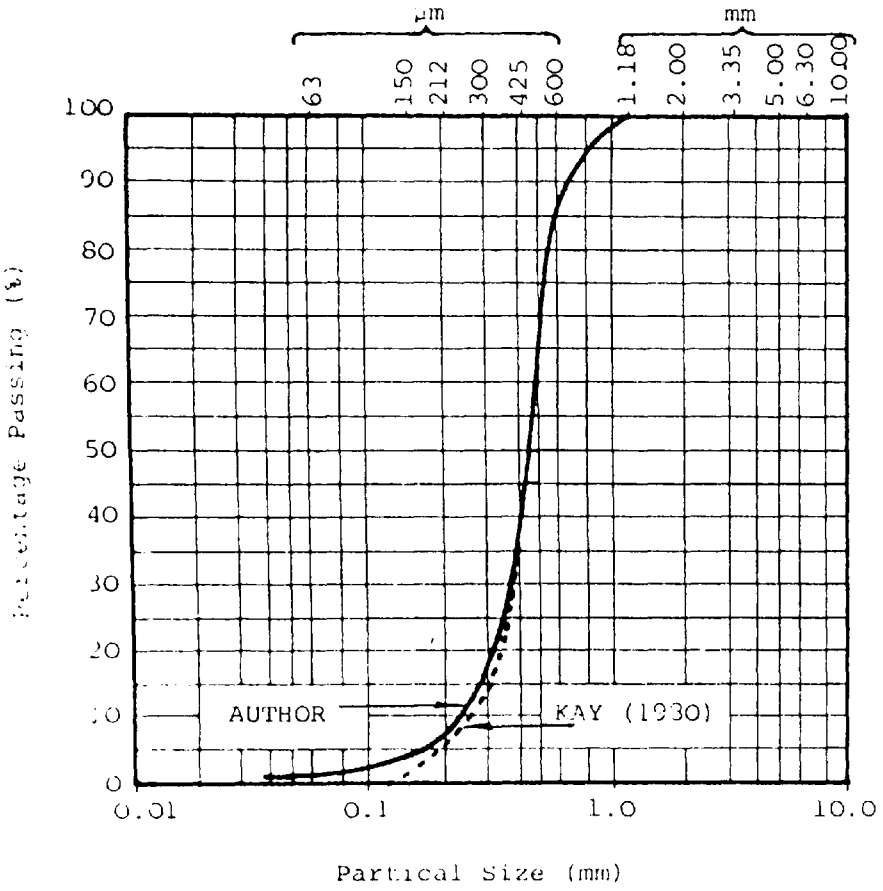

PARTICAL SIZE DISTRIBUTION FOR LEIGHTON BUZZARD SAND

FIGURE 6.1.1

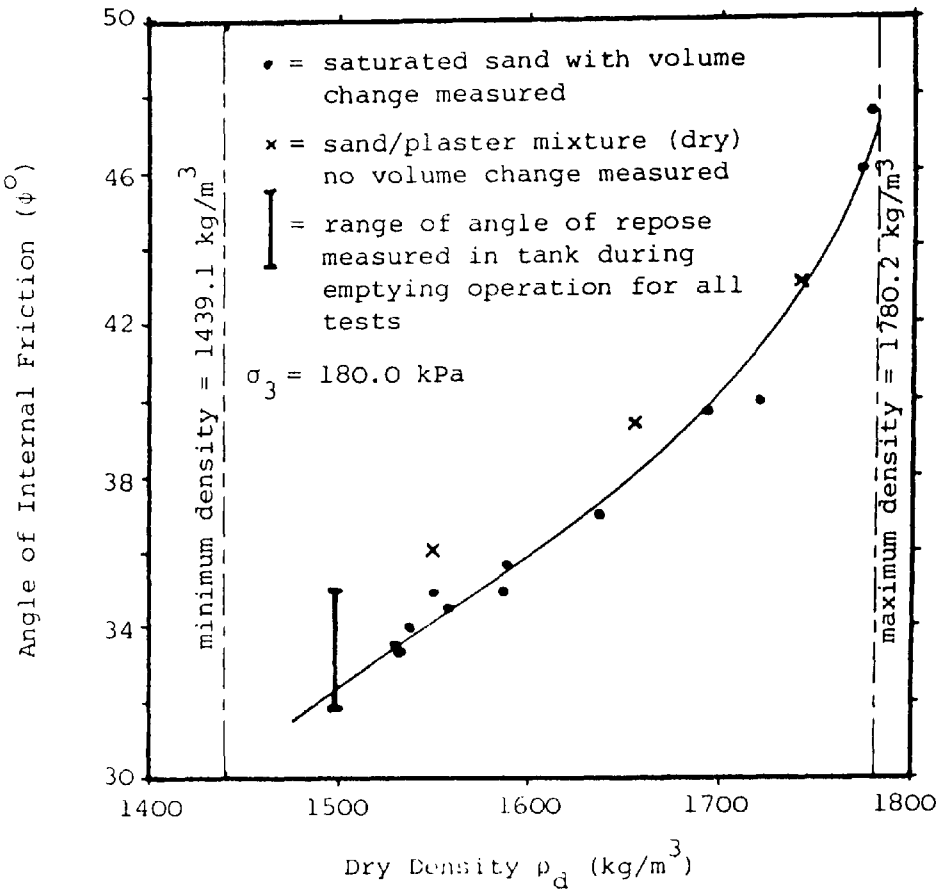

ANGLE OF INTERNAL FRICTION-DRY DENSITY RELATIONSHIP FOR LEIGHTON BUZZARD FROM 102.0 MM DIAMETER DRAINED TRIAXIAL TESTS

FIGURE 6.1.2

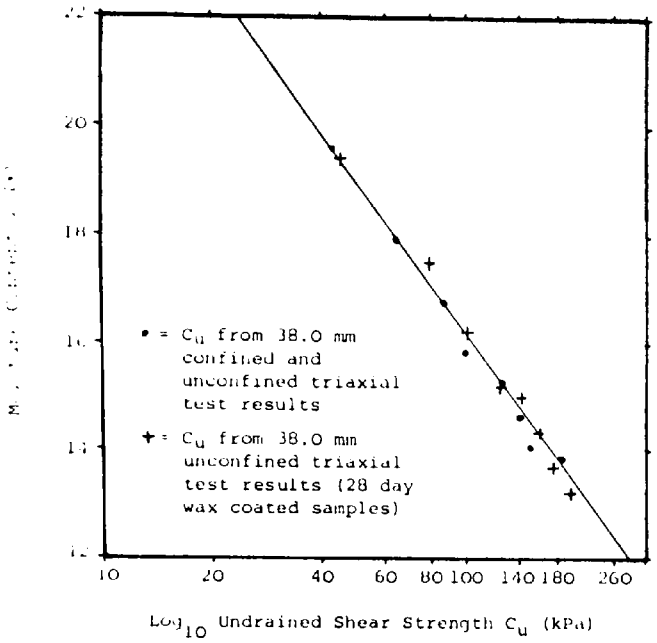

VARIATION IN UNDRAINED SHEAR STRENGTH OF CLAY WITH MOISTURE CONTENT

FIGURE 6.1.3

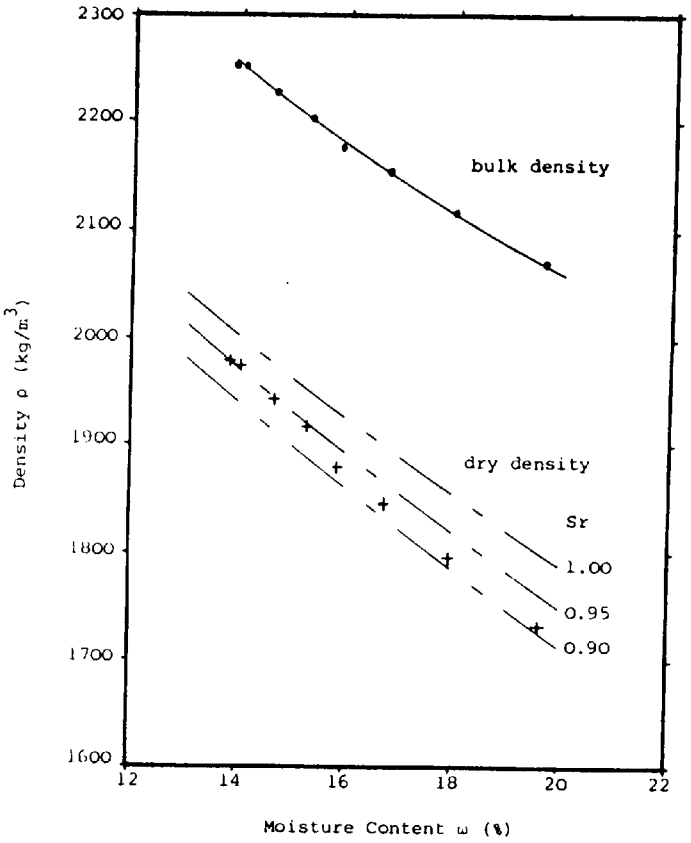

VARIATION IN BULK AND DRY DENSITY OF CLAY WITH MOISTURE CONTENT

FIGURE 6.1.4

CHAPTER 7

COMPARISON OF THEORETICAL RESPONSE WITH EXPERIMENTAL RESULTS

7.1 General Considerations

In order to compare the theoretical response of the model piles with the experimental the following procedure was adopted:-

1. The logarithmic decrement of the system was obtained by averaging data obtained from a number of acceleration/time plots, then using it as input data in the response program.

   The number of traces used in order to determine damping was based on the variation of individual plots.

2. The experimental acceleration/time curve was then integrated using a simple technique developed by the author and described in Chapter 7, Appendix 7.1

3. Having obtained the integrated displacement a comparison was made graphically with the actual displacement obtained from a long stroke L.V.D.T. (Chapter 4 Section 4.5.5).

   Because of the double check on displacement available from the L.V.D.T. the displacement trace was used as criterion for a 'best match' between theoretical and measured response.

4. Using the displacement/time plot a 'best match' was assumed to be effected when the maximum displacement from the response program corresponded to the 'set' obtained from the L.V.D.T. trace. (Section 7.3.2.).

It should be noted that in the case of the small scale pile only the set of the last blow was obtained by sighting a target on the pile with a surveying level.

7.2 Model Study Parameters

Figure 7.1 shows the input parameters used in the response program.

It should be noted that due to the complex nature of the semi full scale pile it was idealised in the following way:-

1. Each section of the model pile was weighed separately.

2. The pile was split up into 10 elements of 256 mm length.

3. Using the length of the element and its spacial position in the pile (i.e. correct weight of pile section) an equivalent cross sectional area was calculated.

4. Finally the total weight of the pile was calculated using the equivalent cross sectional area and then compared with the actual weight of the pile as a cross check.

Common to all Tests	
Number of elements	10
Time increment (secs.)	0.2×10^{-4}
Embedded length of Pile (m)	2.176
Total number of iterations	600
Density of pile material (Kg/cu.m)	7860.0
Mod. of elasticity of Pile (N/sq.m)	0.2×10^{12}
Pile element length (m)	0.256

Element No.	C/S area of element (m^2)
1	0.8×10^{-3}
2	0.15×10^{-2}
3	0.8×10^{-3}
4	0.15×10^{-2}
5	0.19×10^{-2}
6	0.14×10^{-2}
7	0.8×10^{-3}
8	0.13×10^{-2}
9	0.21×10^{-2}
10	0.14×10^{-2}

Data varies for each Test	Test 1	Test 2	Test 3
Percentage of load on pile tip	0.466	0.5625	0.3
Assumed ultimate load on Pile (N)	0.45×10^4	0.44×10^4	0.51×10^4
Duration of input force (secs.)	0.2×10^{-2}	0.2×10^{-2}	0.22×10^{-2}
Time in secs. to peak value of input force	0.78×10^{-3}	0.82×10^{-3}	0.8×10^{-3}
Peak value of input force (N)	0.5623×10^5	0.5888×10^5	0.5623×10^5
First peak acceleration (m/s^2)	0.220123×10^4	0.204×10^2	0.52×10^4
Second peak acceleration (m/s^2)	0.110594×10^4	0.15051×10^2	0.312014×10^4
Soil damping coefficient (α)	0.01	0.02	0.25
Pile damping coefficient (β)	0.99	0.98	0.75

Fig. No. 7.1 showing input data used for theoretical

Response Analysis of Model Pile

A similar procedure was adopted in the case of the small scale model pile which was split up into 2 elements with equivalent cross sectional area of 0.00496 m^2.

As can be seen from Figure 7.1 only a minimum amount of data is needed to run the program.

7.2.1 Optimum Damping Coefficients

Chapter 2 Section 2.2.4 outlined the logarithmic decrement method for determining viscous damping from Acceleration/ time plots and illustrated the variation in response obtained by changing the damping coefficient α and β.

For both the small scale and semi full scale tests the optimum damping coefficients were taken to be those which created the best match between theoretical and experimental displacement time plots.

The optimum coefficients for the tests were as follows:-

Test No.	α (Soil damping) coeff.	β (Pile damping) coeff.
Small Scale Test	0.02	0.98
1	0.01	0.99
2	0.02	0.98
3	0.25	0.75

It can be seen that in the case of the sand tests the soil damping coefficient is small while in the case of the sand over clay test (Test no. 3), as would be expected the damping coefficient is much higher.

Obviously a statistical analysis of as many different pile and soil types as possible must be carried out in order to

verify the validity of the damping coefficients.

The data needed in order to conduct such an analysis is as follows:-

1. Input Force/Time History
2. Acceleration/Time History
3. Integrated Velocity/Time History
4. Integrated Displacement/Time History

A search of the available literature has shown that while there is an abundance of acceleration/time plots, very few papers give the complete history required.

Also in order that such a study be consistent, the same type of equipment with regard to the ratio of load cell impedence, cross-sectional area to pile impedence and cross-sectional area should be employed to obtain the required data.

Goble and Rausche (1972) have pointed out the pitfalls in using data acquired by using an alternative measuring system.

Likins G. (1982) has also indicated that in order that the measured force in the load cell is indeed the force that is transmitted along the pile, certain criteria should be adhered to when considering the stiffness of the cell with regard to that of the pile.

These criteria have been discussed in Chapter 6 Section 6.1.2 and until such load cells are used with other pile sections, lengths, materials and soil variations only the author's experimental results are considered.

7.3 Model Study Results

7.3.1 Small Scale Test (Pilot Study)

Figure 7.2 shows the comparison between predicted and measured response for the model pile taken for the last blow prior to test loading.

Referring to the plot of acceleration/time it can be seen that the initial acceleration peak from the theoretical analysis compares favourably with the measured peak in both magnitude and time.
(3652 m/s^2, 0.35×10^{-3} secs - 3902 m/s^2, 0.39×10^{-3} secs respectively)

The subsequent response, although following the overall pattern of the measured acceleration/time trace does not reproduce it exactly.

As would be expected due to the close match with the acceleration/time traces the peak values for both velocity and displacement are well reproduced in the theoretical analysis. The response was obtained using the damping coefficients stated in Section 7.2.1 and the actual Ultimate Static Bearing Capacity of 1.45 KN as input parameters.

No attempt has been made in this example to demonstrate the variation in displacement/time curves due to different values of inputed Bearing Capacity. The small value of Ultimate Static Bearing Capacity makes it unreasonable to vary it enough to cause significant changes in the displacement/time plots.

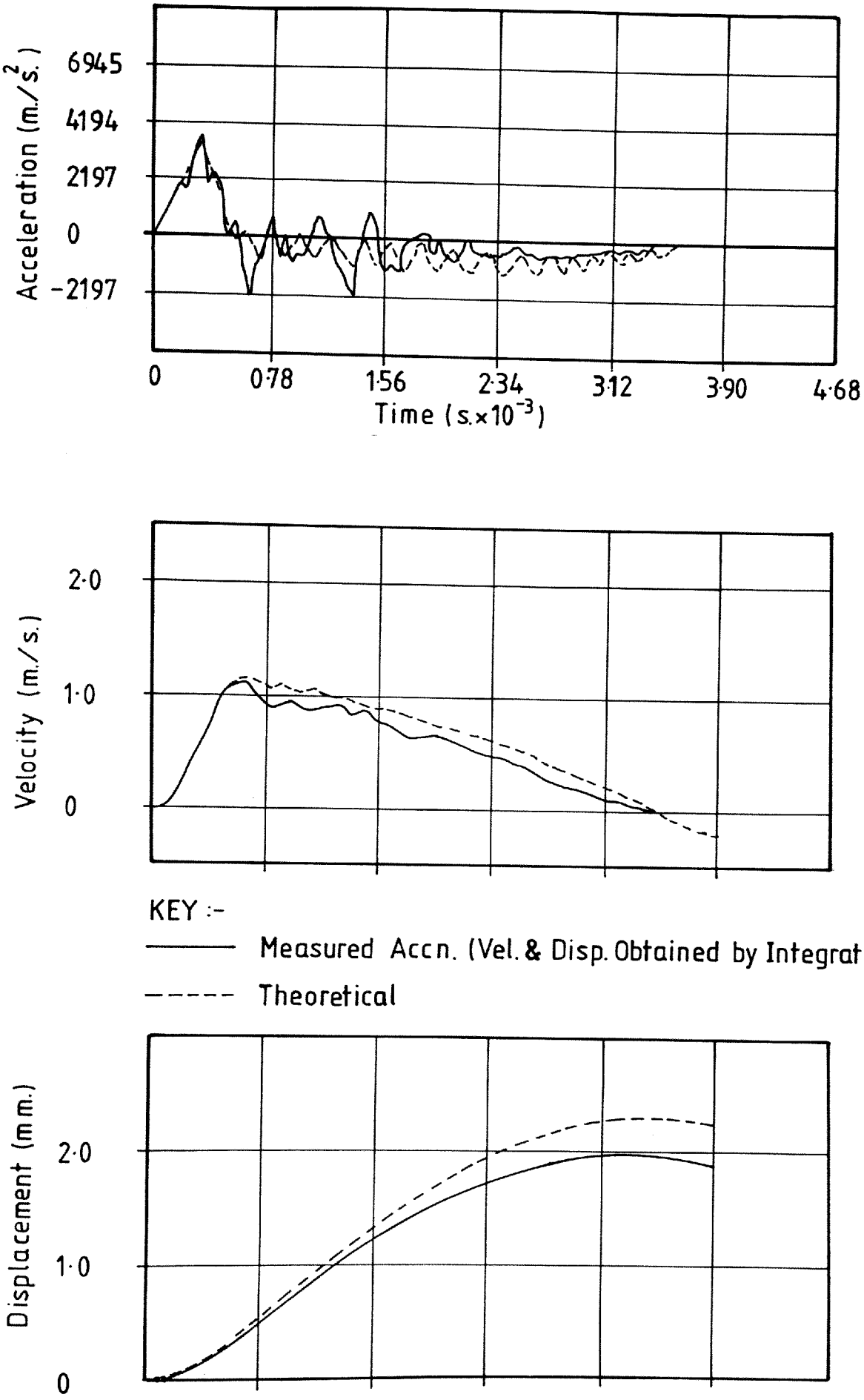

FIG. Nº. 7.2 SHOWING COMPARISON OF MEASURED AND PREDICTED DYNAMIC RESPONSE FOR THE SMALL SCALE TEST

7.3.2 Semi Full Scale Tests

In all three semi full scale tests the theoretical acceleration/time curves underestimated the measured ones to varying degrees (Fig 7.3 - 7.5). The theoretical time to the initial peak acceleration in all cases is identical to the experimental time with the overall shape of the acceleration/time curve again following but not conforming exactly to that of the experimental ones. The average percentage difference between initial experimental and theoretical peaks was 42.7%. This underestimating of peak accelerations may be due to the very short durations of the said peaks or more likely to the very complex response of the coupled pile/soil system being only approximately discretised in the response program (Section 7.1).

This pattern is again repeated in the velocity/time traces but to a lesser extent. In the case of the displacement/time traces for the two sand only tests, the theoretical, measured displacement (from L.V.D.T.) and measured displacement (double integrated from the acceleration/time curve) are extremely close to each other.

The following table shows the difference between theoretical maximum displacement for the three tests compared with the pile set obtained from the L.V.D.T. for the last blow

Test No.	Max. Displacement (m.m.)	Actual Set (m.m.)
Small Scale Test	2.2	2.1
1	10.8	11.4
2	11.63	11.4
3	4.27	4.2

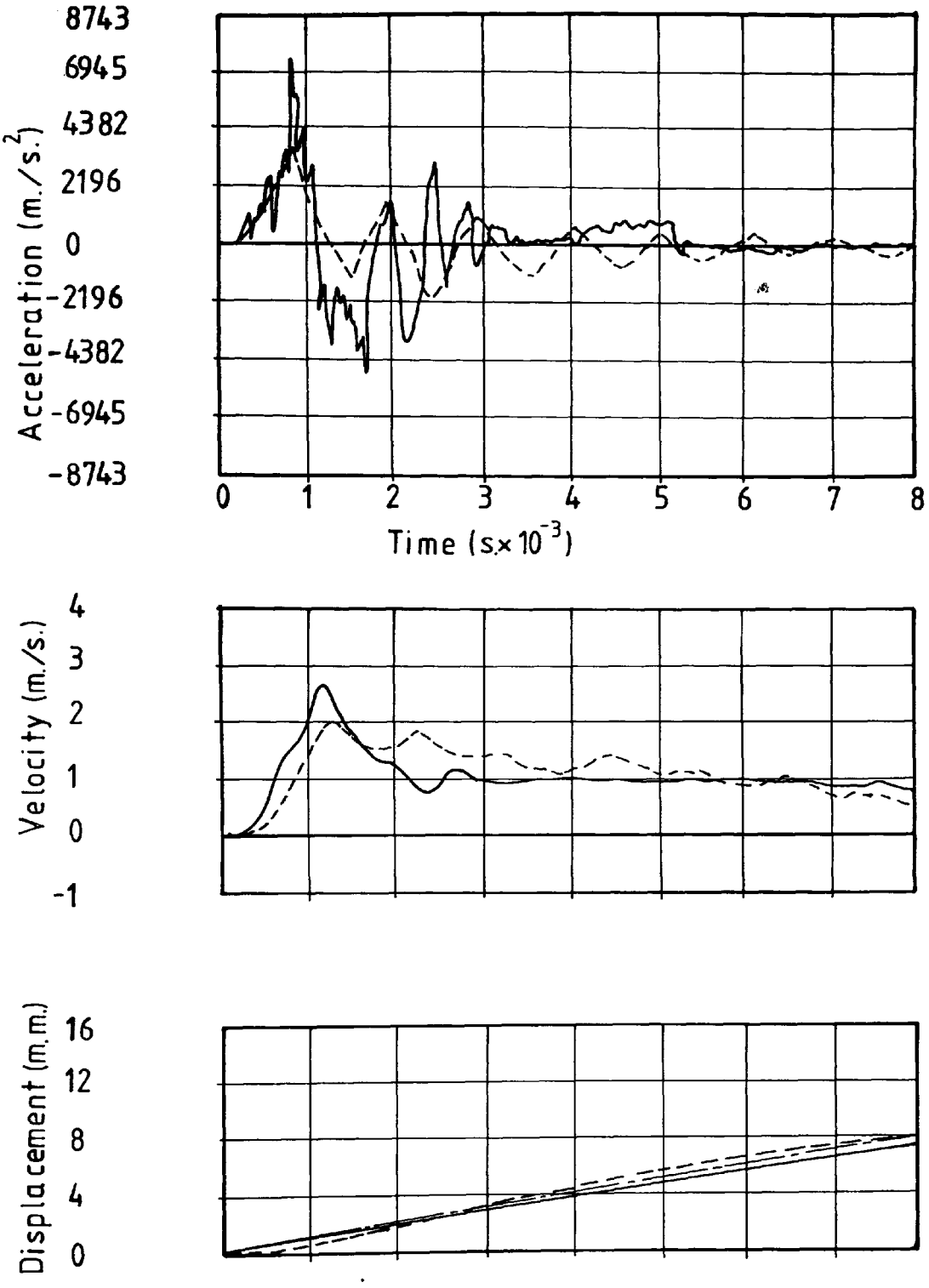

KEY :-

——— Measured Accn. (Vel. & Disp. Obtained by Integration)

— — — " Displacement (From L.V.D.T.)

– – – – Theoretical

FIG N° 7.3. SHOWING COMPARISON OF MEASURED AND PREDICTED DYNAMIC RESPONSE FOR TEST 1 (Sand Only Profile)

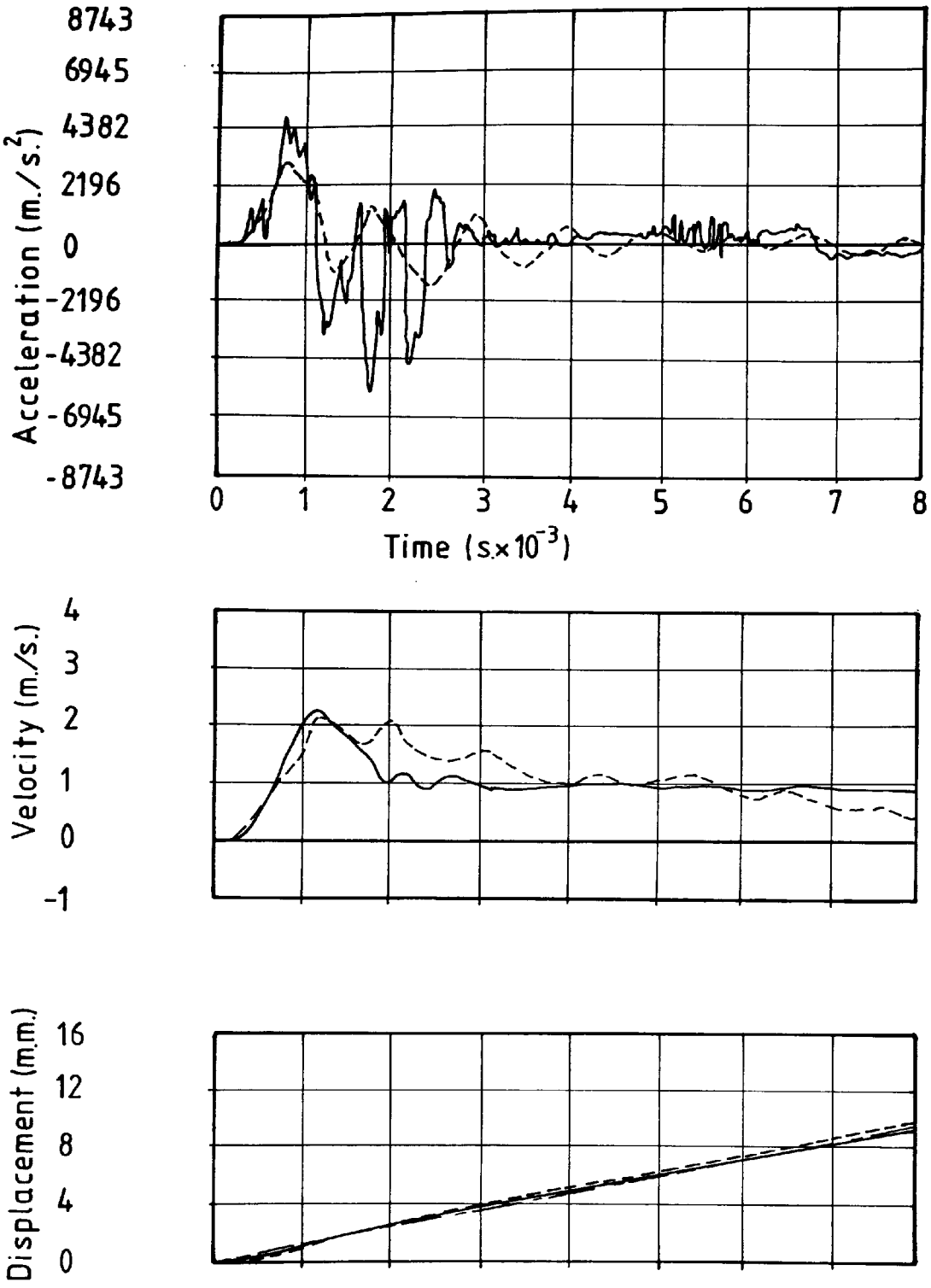

KEY :-

——— Measured Accn. (Vel. & Disp. Obtained by Integration)

—— — " Displacement (From L.V.D.T.)

---- Theoretical

FIG N° 7.4 SHOWING COMPARISON OF MEASURED AND PREDICTED DYNAMIC RESPONSE FOR TEST 2 (Sand Only Profile)

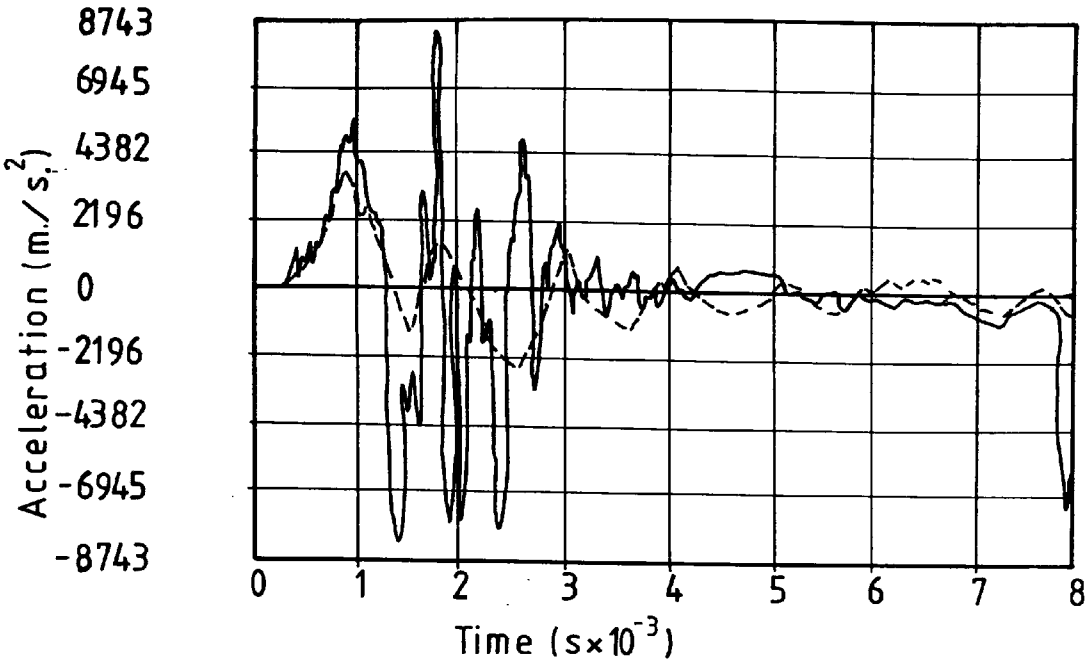

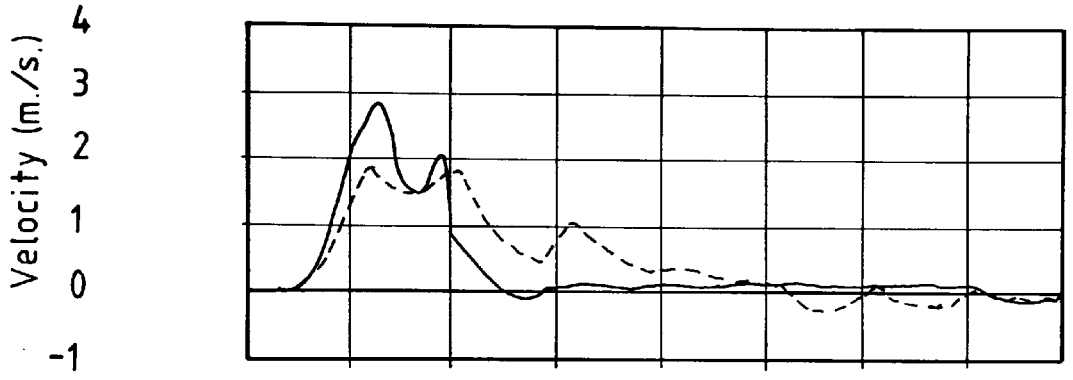

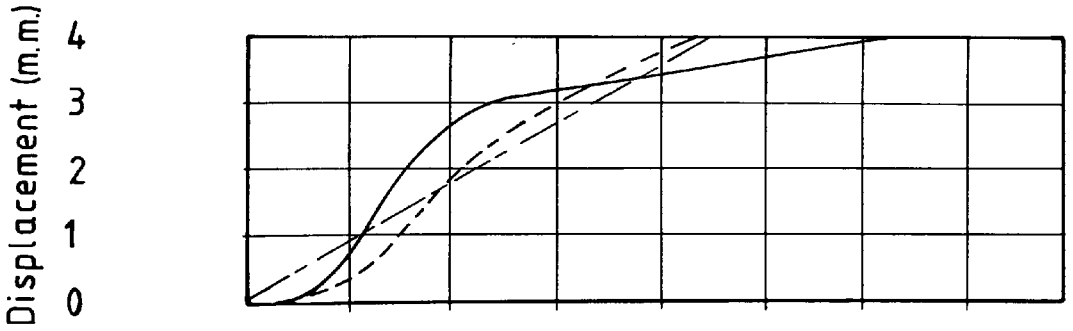

KEY:-

——— Measured Accn. (Vel. & Disp. Obtained by Integration)

— — — " Displacement (From L.V.D.T.)

---- Theoretical

FIG N° 7,5 SHOWING COMPARISON OF MEASURED AND PREDICTED DYNAMIC RESPONSE FOR TEST 3 (Sand Over Clay Profile)

In the case of Test 3 (sand over clay profile) the agreement between theoretical response and measured response for the L.V.D.T. are very close and vary somewhat from the integrated displacement/time curve. This may well be due to the 'ringing' effect indicated by the middle section of the acceleration/time trace which may have given rise to spurious results and is fully discussed in Chapter 6.

7.4 Sensitivity of Approach to Variation in the Input Parameters

In order to illustrate the sensitivity of the method to variations in the Input Parameters Test 2 (sand only profile) was chosen. Test 2 was used because of the close agreement between theoretical and experimental response.

7.4.1 Damping Parameters

As has been previously discussed in Chapter 2 Section 2.5.1 the critical damping parameter is α (the soil damping coefficient). Figure 7.6(a) shows a considerable variation in displacement response for only a small change in the value of α. It is therefore of great importance to determine correct and justifiable values of damping in order to use the method for actual bearing capacity evaluations.

7.4.2 Ultimate Static Bearing Capacity

Figure 7.6(b) shows a significant variation in displacement/time response for small variations in Ultimate Static Bearing Capacity and highlights the fact that the theoretical approach is sensitive to small changes in inputed Bearing Capacity.

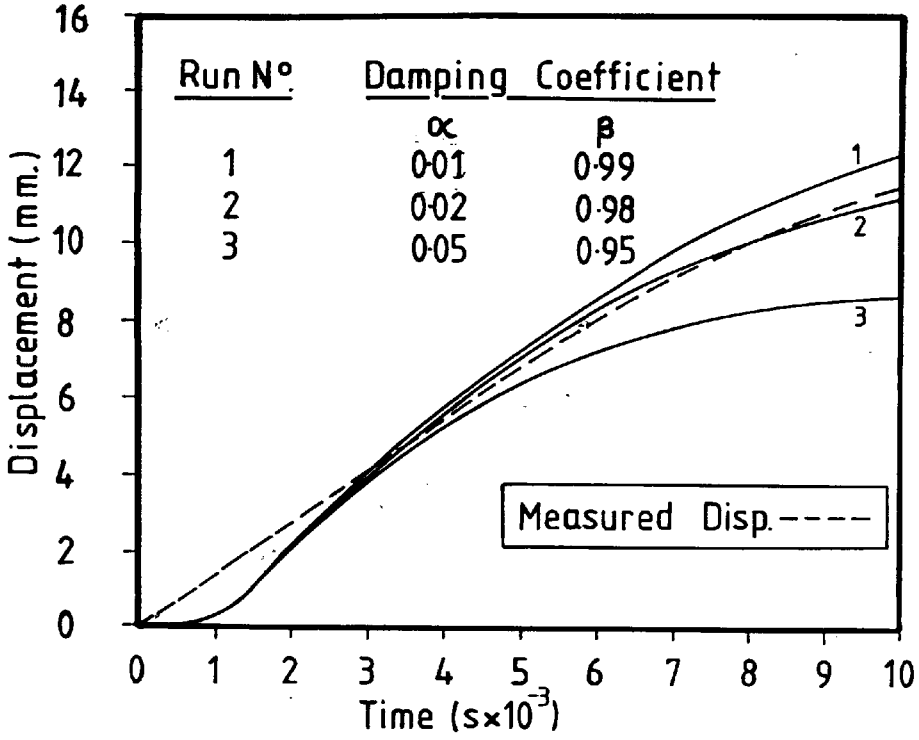

FIG N° 7.6 (a) SHOWING VARIATION IN RESPONSE FOR DIFFERENT DAMPING COEFF'S

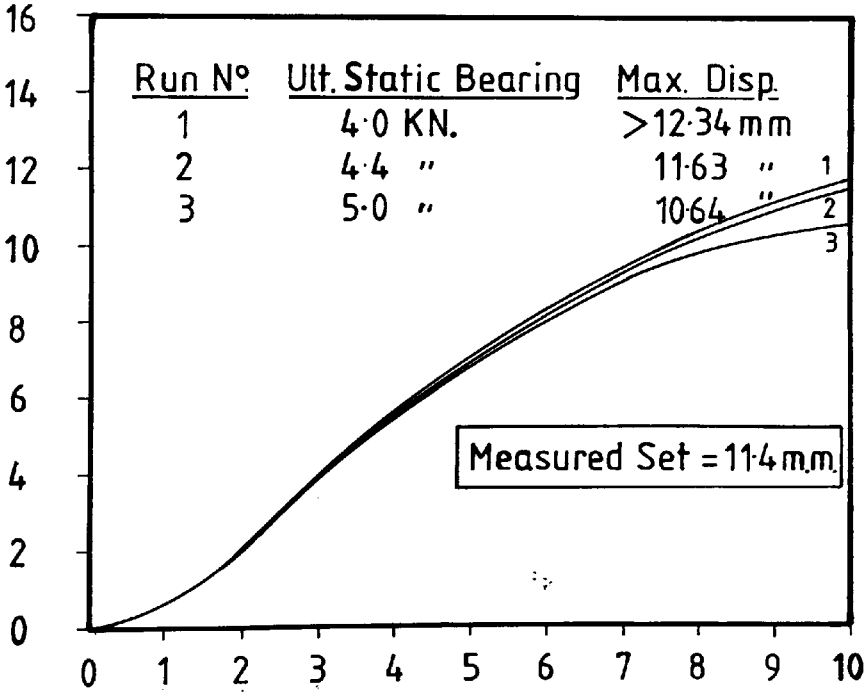

FIG N° 7.6 (b) SHOWING VARIATION IN RESPONSE FOR DIFFERENT VALUES OF ULT. STATIC BEARING CAPACITY

FIG N° 7.6 SHOWING THE VARIATION IN DISPLACEMENT RESPONSE BY CHANGING THE INPUT PARAMETERS FOR TEST 2 (Sand Only Profile)

7.5 Observations

With regard to the comparison of theoretical and experimental response of the author's results the following points should be noted:-

1. Based on the comparison of theoretical and experimental response the approach appears to be a viable one in predicting Ultimate Static Bearing Capacity.

2. In order that the first observation be confirmed without question, a great deal more data must be collected using the type of equipment developed by the author and using ordinary piles in the field. This is needed in order that a statistical base may be founded in which both confidence in the approach as well as reliable damping parameters may be obtained.

   A major refinement of the technique may be the use of direct digital sampling of the input signal at high speed. This cuts out the need to synchronise the bandwidth on the recorder with that of the sampling frequency of the analyser. If this is not accomplished satisfactorily, distortion of the true signal may result.

3. The extremely complex nature of construction of the model pile with regard to segment interfaces and its high mass to length ratio when compared with tubular steel piles of the same diameter may make the response an untypical case.

In conclusion it must be said that although the comparison between theoretical and experimental are favourable it does not mean that the approach is applicable to all hammer/pile/soil types. The only way to completely validate the approach is as previously discussed using similar monitoring and measuring equipment under different conditions to obtain a statistical base.

APPENDIX 7.1

INTEGRATION OF ACCELERATION CURVES

The procedure for integrating the acceleration curves obtained from the model pile tests falls into two distinct parts:-

1. Digitisation of Curve

The acceleration time curve was digitised as follows:-

a) An acceleration/time plot was placed on the bed of a Textronix Type plotter linked to a DEC-20 macro computer and secured.

b) Each change in acceleration was recorded on disc by moving the cursor of the Textronix and pressing the plot button. The first two points recorded in this way were used for scaling purposes in the program and need not have been on the actual curve.

c) On completion of digitising, the actual numerical values of the first two co-ordinates were fed into the computer and the other points scaled accordingly and stored on disc under a previously specified file name.

The program to accomplish the digitisation, scaling and storage was written by J. E. McBride of the Polytechnic Computer Centre.

2. Integration of Curve

In order to integrate the digitised curve a small program was written by the author which called up the stored data and operated on it in the following manner:-

a) The area under the curve formed by consecutive pairs of digitised points was calculated.

b) The process was repeated for the next pair and the algebraic sum calculated. In this way a velocity/time curve was obtained.

c) The integration scheme was then repeated until all the digitised points were used.

d) Steps a-c were then repeated for the velocity/time curve in order to obtain the displacement time curve.

e) The calculated values of displacement, velocity together with acceleration and time were then output to the mainline printer to obtain a hard copy.

In order to verify that the digitisation and integration procedures were functioning satisfactorily, previously published data (Scanlan and Tomko (1969) in the form of acceleration/time curves were integrated and compared with the corresponding integrations as shown by Scanlan and Tomko.

As can be seen from Fig. 7.1.1 the results bear close resemblance to each other thus validating the digitisation and integration approach.

It should also be noted that the measured velocity/time and displacement/time plots given by Scanlan and Tomko (1969) are actually the integration and double integration of the acceleration/time curve. No check to verify that the integrated signals were indeed correct was attempted. This is not the case with the author's work which is compared to the measured displacement/time curve obtained from a long stroke L.V.D.T. as was discussed in previous sections.

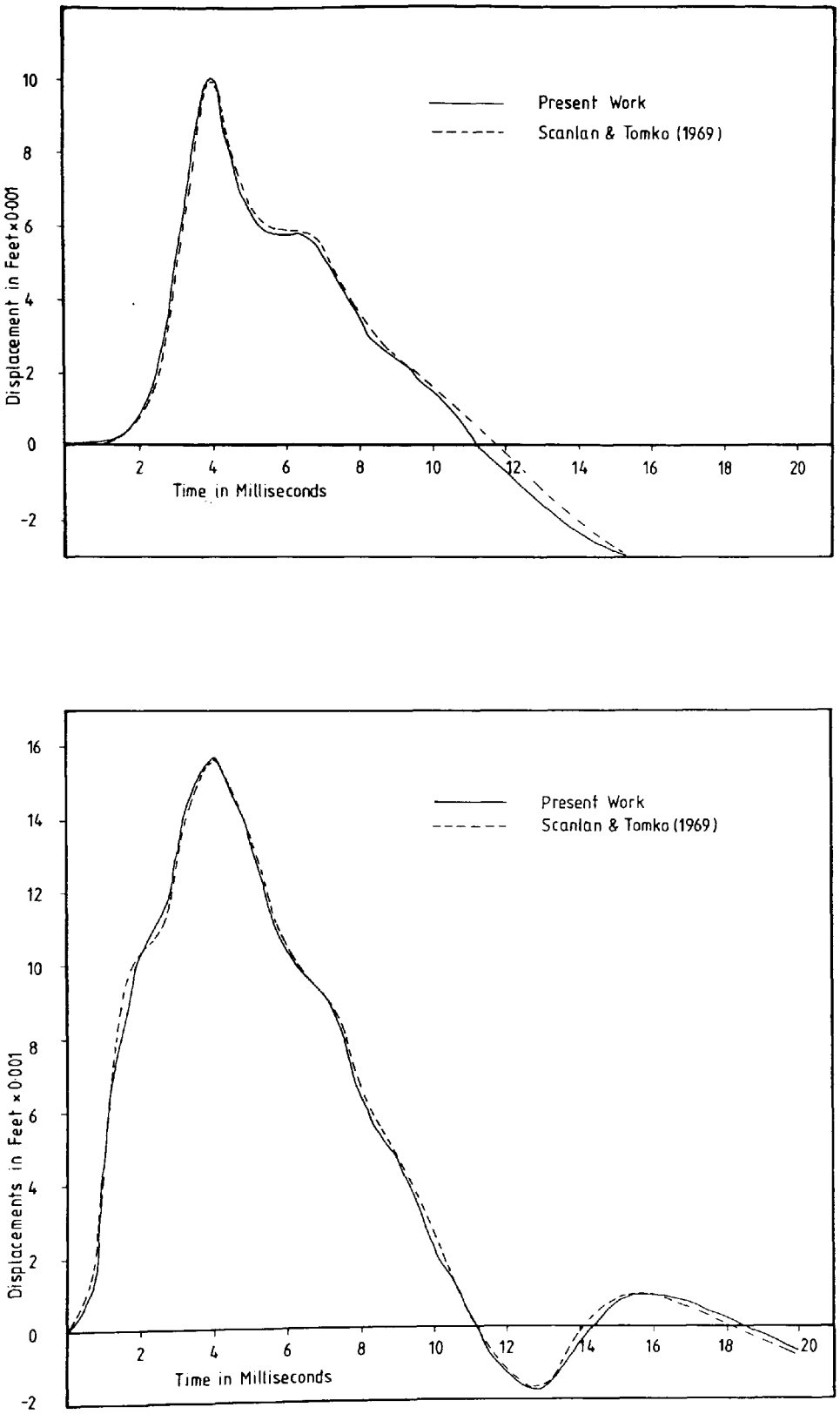

FIG. Nº 7.1.1. COMPARISON OF INTEGRATED DISPLACEMENT/TIME CURVES

CHAPTER 8

Conclusions and Proposals for Future Work

8.1 Conclusions

The conclusions drawn from the investigation fall into four distinct categories:-

(1) The design, manufacture and subsequent testing of the equipment, recording and monitoring systems.

(2) The analysis of the results of driving and the subsequent testing of the small scale pile (including dynamic tests).

(3) The analysis of the results of driving and the subsequent testing of the semi-full scale pile.

(4) The theoretical approach to the prediction of static bearing capacity from dynamic measurements and the comparison with experimental results.

While every effort was made to ensure that the semi-full scale model pile was large enough to provide a realistic indication of the behaviour of full-scale piles it is accepted that differences do exist between model and full-scale pile behaviour. Thus it is hoped that although the results of the tests are only valid for the precise experimental conditions existing in the laboratory, observations made can be related to full scale conditions and demonstrate how a pile is likely to behave in the field.

8.1.1 Piling Equipment and Monitoring Systems

The following conclusions are drawn with respect to the piling equipment and monitoring system:-

(1) The taper connectors developed for both the static and dynamic load cells although effective in resisting impact forces suffered from two major defects:-

(a) In the case of the static load cells the calibration graph for loading and unloading exhibited a hysteresis effect.

(b) The resistance to tension of the joint was insufficient to perform Pull Out Tests. Because of these defects the joints were altered to incorporate tight-fitting parallel connectors and grub screws through the pile wall to secure pile sections together. However, even with the re-designed joints loosening was in evidence due to prolonged driving (Sand Over Clay Test). Therefore it is recommended that if in the future prolonged driving is to be undertaken (i.e. over 200 blows) that a combination of the two types of connectors be adopted.

(2) The static control program written by Wersching (1986) and updated by the author performed well with only minor alterations needed for future research. The Strain sensing part of the static axial load cell stood up well to the means of installation and it may be possible at a future date to decrease the wall thickness and thus increase sensitivity.

(3) The Commodore P.E.T. Microcomputer and Orion data logger combined to give a high level of control to

the tests both with data storage (through disc drives) and Dartec jack control.

8.1.2 Small Scale Tests (Pilot Study)

Extensive tests were conducted with the dynamic systems (Chapter 3) and these highlighted the following basic facts:-

(1) The monitoring and recording equipment used was capable of accurately recording and reproducing the transient signals.

(2) The type of dynamic load cell housing used and the overall model pile construction did not effect the unconfined response of the force washers, i.e. the reproduction of the signals.

(3) A relationship between peak dynamic tip force and the modulus of elasticity of the bearing surface was shown to exist and appears to be a simple and effective means of determining E values.

8.1.3 Semi-Full Scale Tests

(1) In both the small scale and semi-full scale tests it was evident that the input force from the hammer to pile was dependant on ram impact velocity only with the same peak force being displayed for markedly different bearing surfaces.

(2) Again for both the small scale and semi-full scale tests it was shown that the transient force at the pile tip was dependant to a large degree on the rigidity of the bearing surface with the transient peak force being less than equal to or greater than

the input force (max. value being twice the input force).

(3) It is possible to detect discontinuities such as joint slackness by studying the shape of the velocity x $EA/_C$ against time curve for the input force. - Chapter 6, Section 6.2 (Fig. No. 6.1)

(4) The Pneumatically controlled driving rig designed by the author performed satisfactorily during trials and subsequent tests giving an average driving efficiency of 67.55%.

(5) The peak transient forces at the pile cap may be as high as twelve times that of the static bearing capacity.

(6) The distribution of static axial load along the pile was similar to the classical patterns shown by among others Vesic (1963), Chan and Hanna (1979).

(7) Residual loads in the pile were present after driving and were significant when estimating the distribution of load between shaft and toe and also stress transfer along the pile. In the case of these tests omission of the residual loads meant that the loads were underestimated and shaft friction overestimated, (slightly).

(8) The stress transfer observed for a dynamically driven pile indicated high values at shallow depth reducing in value towards the toe. This is in contrast to previously published data (Chapter 6,

Section 6.12) but verifies the findings of Tan (1983) and Werscheing (1986) for piles not dynamically driven. The phenomenon of decreasing stress transfer towards the pile toe is thought to be the result of high lateral stresses developed in the soil at shallow depths. Also the distribution of Ks along the pile falls within the Ka and Kp limits for all intents and purposes and again confirms the findings of Tan (1983).

(9) The static bearing capacity obtained from the CRP and MTL tests were in close agreement with each other for all the tests giving an average percentage difference of 8%.

(10) In the case of the sand over clay profile the maximum pull out load was within 10% of the shaft load in compression. For the case of the sand only tests the maximum pull out load was only 33% of the shaft friction in compression and it is therefore recommended that in order to ascertain pull out loads with any accuracy representative in-situ tests should be performed.

(11) In-situ vertical soil displacements decreased with radial distance from the pile and increasing depths. Movement was observed to a radial distance of 12D at shallow depths reducing to 7D at greater depths. Observed movement under the pile toe extended to a depth of 4D beneath the pile tip.

(12) The in-situ vertical displacements during the CRP

and MTL tests yielded a general trend of sand displacement downwards or horizontal at the deepest level of inclinometers changing to upwards at shallower depths. This phenomenon again indicates a lock-up of stresses due to arching.

(13) A zone of increased density around the pile was exhibited up to a radial distance of 7D and demonstrates the densification effect that pile driving has on loose sand.

(14) Relative sand movement across the sand/clay interface was detected - being outwards during loading and returning inwards under conditions of zero load. The converse was observed for the pull out test with the sand moving inwards while the pile was retracted. At all stages of unloading residual stresses were detected indicating that the sand remained stressed at the end of the tests.

(15) The results from the Nottingham load cells must be treated with some scepticism even though checks on the suitability of the load cell with the grain size of the sand appeared adequate. The contribution of these load cells to the data was therefore not very important and it may be wiser to exclude them in future work in order to reduce interference caused by the instrumentation.

(16) Sand was dragged down into the clay to a limited distance (2D) with little evidence thereafter. A sand plug preceeding the pile tip was also driven

into the clay. The exact effect that this plug of sand has on the properties of the clay in the vicinity of the pile tip cannot be accurately determined without additional instrumentation such as peizometers but an increase in moisture content in the clay was observed.

(17) The method of dissecting the clay block although simple proved quite effective and revealed a number of interesting features. These features can be divided into three main categories:-

(a) A zone of disturbed clay around the pile with a visible radius of distortion of 2D and similar to that proposed by Tomlinson (1971).

(b) A zone of intensely remoulded clay in the immediate vicinity of the pile and again similar to that proposed by Randolph and Wroth (1982).

(c) The failure patterns at the pile tip were easily detected from the dissected block and were similar to the plastic zones proposed by Meyerhof (1951).

(18) Finally recourse to the test results as a whole reveals the high degree of repeatability of the tests during all stages of installation and testing. It may also be said that in the case of these tests that a pile founded in sand alone has a bearing capacity comparable to that of a similar pile founded in a sand over clay medium. The significance of this

statement is that in the case of the sand only test, driving was easy (average number of blows to drive 2.0 m equals 94) whereas in the case of the sand over clay profile driving was hard and becoming progressively harder (number of blows to drive 2.0 m equals 153).

Thus the wear and tear on both the pile and driving system is less for the sand only tests although settlements needed to reach maximum working loads are much greater than in the sand/clay test.

8.1.4 Theoretical Analysis

The theoretical analysis based on the dynamic equation of motion and used to predict static bearing capacity proved quite successful with the following provisos:-

(1) Maximum peak accelerations were not numerically reproduced and may be due to the relative crudity of the soil model.

(2) Before any conclusions are drawn as to the usefulness of such an approach under field conditions a study should be conducted in the field using different hammer/pile/soil combinations.

8.2 Proposed Future Work

The research investigation described in this project raised a number of questions that could not be fully answered without using further instrumentation and were:-

(1) The phenomenon of lateral stresses on the pile formed by arching of the soil and caused by driving.

While conclusions based on the available instrumentation were drawn it would appear a logical step to introduce contact stress transducers developed at the Polytechnic (Werscheing (1986)) into the pile to measure shear and lateral forces directly.

(2) A more involved study of pile joints should be undertaken in order to eliminate the shortcomings encountered during the tests.

(3) The clay block should be instrumented using piezometers in order to study the build-up of pore water pressure around the pile tip and determine the relationship between excess pore water pressure and the increased moisture content encountered in the experiments.

(4) In the case of the sand/clay tests long-term tests should be undertaken in order to study the effects of strength regain on the value of static bearing capacity.

(5) Cyclic loading tests should also be conducted in order to study the effects that repeated reversals have on such factors as degradation of bearing capacity, shaft and base resistance, etc. This study would also be of use when constructing a more realistic soil model for use with the theoretical approach.

(6) The literature reviewed in Chapter 1 showed that the theoretical approach outlined in Chapter 2 was simple

in nature and was in need of updating.

There are three main areas in which the analysis could be improved and are:-

(1) Inclusion of residual driving stresses in the analysis.

(2) Updating of the bi-linear soil model to include such effects as degradation of soil properties.

(3) The possible inclusion of a multiple blow analysis as opposed to the single blow analysis at present used.

Although the author was aware of all these points during the investigation the time limits imposed made it impractical for him to pursue them. They are therefore left to future researchers at the polytechnic to investigate.

BIBLIOGRAPHY

AGERSCHOU, H.A. - Analysis of the Engineering News Pile Formula. J.S.M.E.D., ASCE, 88, SM5:1-11 (1962)

AIRHART, T.P., COYLE, H.M., HIRSCHE, T.J. and BUCHANAN, S.J. - Pile Soil System Response in a Cohesive Soil. ASTM, STP 444:264-294 (1969)

AUTHIER, J., FELLENIUS, B.H. - Dynamic Measurements as an Inspection Tool for Discovering Damage to Spliced and Unspliced Precast Concrete Piles - Two Case Histories. Intl. seminar on the Application of Stress - Wave Theory on Piles/Stockholm: 121-127 (1980)

AUTHIER, J., FELLENIUS, B.H. - Quake Values determined from Dynamic Measurements. Intl. seminar on the Application of Stess - Wave Theory on Piles/Stockholm: 197-215 (1980)

BATHE, K.J. and WILSON, E.L. - Numerical Methods in Finite Element Analysis. Prentice-Hall, Inc. (1976)

BARKAN, D.D. - Dynamics of Bases and Foundations. New York: McGraw-Hill (1962)

BIOT, M.A. - General Solutions of the Equations of Elasticity and Consolidation for a Porous Material. Journal of Applied Physics, Vol. 23: 91-96 (1956)

BIOT, M.A. - Theory of Propogation of Elastic Waves in a Fluid-Saturated Porous Solid, I: Low-Frequency range, II: Higher-Frequency range. Journal of the Acoustical Society of America. Vol. 28, No.2: 168-191 (1956)

BJERRUM, L., BRINCH HANSEN, J., and SEVALDSON, R. - Geotechnical Investigation for a Quay Structure in Horten. N.G.I., Pub. No. 28: 1-17 (1958)

BJERRUM, L., JOHANNESSEN, I.J. - Pore Pressures Resulting from Driven Piles in Soft Clay. Conf. on Pore Pressure and Suction in Soil, Butterworths, Sydney, Australia: 14-17 (1960)

BREDENBERG, H., BROMS, B.B. - Response of Pile Points on Rock to Transient Loading. Proc. 10th. Int. Conf. on Soil Mech. and Found. Eng., Vol. 2, Stockholm: 637-642 (1982)

BROMS, B.B., BREDENBERG, H. - Application of Stress-Wave Theory on Pile Driving - A State-of-the-Art Report. Proc. 7th. South-East Asian Geotechnical Conf. Vol. 11: 195-238 (1982)

BYCROFT, G.N. - Forced Vibrations of a Rigid Circular Plate on a Semi-Infinite Elastic Space and on an Elastic Stratum. Philosophical Trans., Royal Society, London. Ser. A, Vol. 248: 327-368 (1956)

CHAN, J.H.C., MATLOCK, H. - A Discrete Element Method for Transverse Vibrations of Beam Columns resting on Linearly Elastic or Inelastic Supports. Center for Highway Research, Report No. 56-24, The University of Texas at Austin (1972)

CHAN, J.H.C., MATLOCK, H. - A Discrete Element Method for Transverse Vibrations of Beam Columns resting on Linearly Elastic or Inelastic Supports. Preprints Offshore Technology Conf., OTC Paper No. 1841, Huston, Texas (1973)

CHAN, S.F., HANNA, T.H. - The Loading Behaviour of Initially Bent Large Scale Laboratory Piles in Sand. Can. Geot. Jnl., 16: 43-58 (1979)

CHAUDHURI, K.P.R., SYMONS, M.V. - Uplift Resistance of Model Single Piles. Proc. of the Conf. on Geotechnical Practise in Offshore Eng., ASCE, Austin, Texas: 335-355 (1983)

CHELLIS, R.D. - Pile Foundations. New York: McGraw-Hill (1961)

CLOUGH, R.W., PENZIEN, J. - Dynamics of Structures. New York: McGraw-Hill (1975)

COOKE, R.W. - Extract from Scott, R.F. Granada (1965)

COOKE, R.W., PRICE, G. - Strains and Displacements around Friction Piles. Proc. 8th. Int. Conf. in Soil Mech. and Found. Eng., Moscow, Vol. 2, No. 1: 53-60 (1973)

COOKE, R.W. - The Settlement of Friction Pile Foundations. Proc. Conf. Tall Buildings, Kuala Lumper: 7-19 (1974)

COOKE, R.W., PRICE, G., TARR, K. - Jacked Piles in London Clay: A study of Load Transfer and Settlement under Working Conditions. Geotechnique, Vol. 29, No. 2: 113-147 (1979)

COYLE, H.M., REESE, L.C. - Load Transfer for Axially Loaded Piles in Clay. J.S.M.F.D., ASCE. Vol. 92, SM2: 1-26 (1966)

COYLE, H.M., GIBSON, G.E. - Empirical Damping Constants for constants for Sands and Clays. J.S.M.F.D., ASCE, Vol. 96, SM3: 949-965 (1970)

CUMMINGS, A.E., KERKHOFF, G.O. and PECK, R.B. - Effect of Driving Piles in Soft Clay. Trans. ASCE., Vol. 115: 275-286 (1950)

CUTHBERT, L.G., DOLWIN, J.E., POSKITT, T.J. - An Instrumentation System for Monitoring Piling. Intl. Seminar on the Application of Stress-Wave Theory on Piles, Stockholm: 53-67 (1980)

CUTHBERT, L.G., POSKITT, T.J. - Development of Instruments for Offshore Piles. Ground Engineering, Jan. Edition: 29-34 (1983)

D'APPOLONIA, E. and ROMUALDI, J.P. - Load Transfer in End Bearing Steel H-Piles. J.S.M.F.E., ASCE, Vol. 89, SM2: 1-25 (1963)

D'APPOLONIA, E. and ROMUALDI, J.P. - Performance of Four Foundations on End Bearing Piles. J.S.M.F.D., ASCE, Vol. 97, SM1: 77-93 (1971)

DE BEER, E.E. - Etude des Fondations sur Pilotis et des Fondations Directes. Annales des Travaux Publics de Belgique, 46: 1-78 (1945)

DE MELLO, V.F.B. - Foundations of Buildings on Clay, State-of-the-Art Report. Proc. 7th. Int. Conf. SM and F.E: 49-136 (1969)

DISMUKE - Behaviour of Steel Piles during Installation and Service. Behaviour of Deep Foundations, ASTM., STP670: 282-299 (1979)

DOWNS, D.I. and CHIEURZZI, R. - Transmission Tower Foundations. J. Power Divn., ASCE., Vol. 92, PO2: 91-114 (1966)

FELLENIUS, B.H. and BROMS, B.B. - Negative Skin Friction for Long Piles Driven in Clay. Proc. 7th. Int. Conf. SM and F.E. Vol. 2: 93-98 (1969)

FELLENIUS, B.H., HAGEN, T. - New Pile Force Gauge for Accurate Measurements of Pile Behaviour during and following Driving. Can. Geot. Jnl. Vol. 6, Part 3: 356-362 (1969)

FLAATE, K.S. - An Investigation of the Validity of Three Pile Driving Formulae in Cohesionless Material. Pub. No. 56, N.G.I., Oslo, Norway (1964)

FOO, S.H.C. and MATLOCK, H. - Analysis of Driving of Foundation Piles. Proc. Offshore Technology Conf., Houston, Texas, OTC 2842: 281-286 (1977)

FOREHAND, P.W. and REESE, J.L. - Prediction of Pile Capacity by the Wave Equation. J.S.M.F.D., ASCE., Vol. 90, SM2: 1-25 (1964)

GLANVILLE, W.H., GRIME, G., FOX, E.N. and DAVIES, W.W. - An Investigation of the Stresses in Reinforced Concrete Piles during Driving. British Building Research Board, Technical Paper No. 20, London (1938)

GOBLE, G.G. and RAUSCHE, F. - Wave Equation Analysis of Pile Driving - WEAP Program. Prepared for the U.S. Department of Transportation, Federal Highway Administration, Implementation Division, Office of Research and Development (1976)

GOBLE, G.G. and RAUSCHE, F. - Pile Driveability Predictions by CAPWAP. Proceedings Conference on Numerical Methods in Offshore Piling, The Institute of Civil Engineers, London (1979)

GOBLE, G.G. RAUSCHE, F. and LIKINS, G.E. - The Analysis of Pile Driving. A state-of-the-Art. Intl. Seminar in the Application of Stress Wave Theory on Piles, Stockholm: 131-161 (1980)

GREGERSON, O.S., AAS, A. and DIBIAGIO, E. - Load Tests on Friction Piles in Loose Sand. N.G.I. Pub. No. 99: 19-27 (1973)

GRIMES, J.N. - The Engineering Geology and Stability of Rapid Alternating Limestone and Shale Sea Cliffs of South Glamorgan. Phd Thesis, Polytechnic of Wales, S. Wales. U.K. (1986)

HANNA, T.H. - The Bending of Long H-Section Piles. Can. Geot. Jnl., Vol. 5, No. 3: 150-172 (1968)

HANNA, T.H. - The Mechanics of Load Mobilization in Friction Piles. Journal of Materials, 4: 924-937 (1969)

HANNA, T.H., TAN, R.H.S. - The Behaviour of Long Piles Under Compressive Loads in Sand. Can. Geot. Jnl., Vol. 5, No. 3: 150-172 (1973)

HOLLOWAY, D.M., CLOUGH, G.W. and VESIC, A.S. - The Effects of Residual Driving Stress on Pile performance under Axial Loads, OTC 3306 (1978)

HOLLOWAY, D.M., AUDIBERT, J.M.E. and DOVER, A.R. - Recent Advances in Predicting Pile Drivability. 10th Annual OTC., Houston, OTC3273 (1978)

HUNTER, A.H. and DAVISSON, M.T. - Measurements of Pile Load Transfer. Performance of Deep Foundations A.S.T.M. STP444: 100-117 (1969)

ISAACS, D.V. - Reinforced Concrete Pile Formulae. Trans Instn. Engrs. Aust., 12: 313-323 (1931)

IRELAND, H.O. - Pulling Tests on Piles in Sand. Proc. 4th. Int. Conf. SM and F.E., Vol. 2: 43-54 (1957)

JAKY, J. - On the Bearing Capacity of Piles. Proc. Sec. Int. Conf., Soil Mech. and Found. Eng., 1: 100-103 (1948)

KAY, W.F. - The Development of Shaft Friction in Semi Full Scale Piles Passing through Granular Soils. Ph.D. Thesis, Polytechnic of Wales, S. Wales (1980)

KERISEL, J. - Fondations Profondes en Milieu Sableux. Proc. 5th Int. Conf. SM and F.E., Vol. 2: 73-83 (1961)

KISHIDA, H. - Stress Distribution by Model Piles in Sand. Soils and Foundations, Vol. iv, No. 1: 1-23 (1963)

KOIZUMI, Y. and ITO, K. - Field Tests with regard to Pile Driving and Bearing Capacity of Piled Foundations. Soils and Foundations, No. 3: 30 (1967)

LAMBE, T.W. and HORN, H.M. - The Influence on an Adjacent Building of Pile Driving for the M.I.T. Materials Center. Proc. 6th. Int. Conf. SM and F.E., Vol. 2: 280 (1965)

LIKINS, G. - Effective use of the Pile Driving Analyser. Manual Supplied to Users of the Goble P.D.A. System (Balkan Piling, U.K.) (1982)

LITKOUHI, S. - The Behaviour of Foundation Piles during Driving. Ph.D. Thesis, Queen Mary College, University of London (1979)

LOWERY, L.L., HIRSCH, T.J., EDWARDS, T.C., COYLE, H.M. and SAMSON, C.H. - Use of the Wave Equation to Predict Soil Resistance on a Pile during Driving. Spec. Session No. 8, 7th. Int. Conf. SM and F.E. (1969)

LO, K.Y. and STERMAC, A.G. - Induced Pore Pressures during Pile Driving Operations. Proc. 6th. Int. Conf. SM and F.E., Vol. 2: 285 (1965)

LYSMER, J. - Vertical Motion of Rigid Footings. Dept. of Civil Eng., Univ. of Michigan Report to WES, Contract Report No. 2-115 under Contract No. DA-22-079-eng-340; also a Ph.D. Dissertation, Univ. of Michigan (1965)

LYSMER, J. and RICHART, F.E. - Dynamic Response of Footings to Vertical Loading. Journ. of the SM and F.E. Divn., ASCE., SM1, Vol. 92: 65-91 (1966)

MANSUR, C.I., KAUFMAN, R.I. - Pile Tests, Low-sill Structure, Old River La. J.S.M.F.D., ASCE., Vol. 82, SM4, Proc. Paper 1079 (1956)

MASSARCH, K.R. and BROMS, B.B. - Fracturing of Soil caused by Pile Driving in Clay. Proc. 9th. Int. Conf. on SM.F.E., Vol. 1: 197-200 (1977)

MATLOCK, H. and SALANE, H.J. - Finite Difference Methods for Plate Vibration Problems. Journal of the Structural Division, ASCE., Vol. 95, ST3, Paper No. 6477: 441-456 (1969)

MATLOCK, H. and FOO, S.H.C. - Axial Analysis of Piles using a Hysteretic and Degrading Soil Model. Inst. of Civil Eng., Numerical Methods in Offshore Piling, I.C.E: 127-133 (1980)

MEYERHOF, G.G. - The Ultimate Bearing Capacity of Foundations. Geotechnique, Vol. 2: 301-332 (1951)

MEYERHOF, G.G. - The Bearing Capacity of Foundations under Eccentric and Inclined Loads. Proc. 3rd. Int. Conf. SM and F.E., Vol. 1: 440 (1953)

MEYERHOF, G.G. - Compaction of Sands and Bearing Capacity of Piles. J.S.M.F.D., ASCE., Vol. 85: SM6: 1-29 (1959)

MEYERHOF, G.G. and VALSANGER, A.J. - Bearing Capacity of Piles in Layered Soils. Proc. 9th. Int. Conf. SM., F.E., Vol. 1: 645-650 (1977)

MEYERHOF, G.G. SASTRY, V.V.R.N. - Bearing Capacity of Piles in Layered Soils, Part 2, Sand Overlying Clay. Con. Geot. Jnl., 15: 183-189 (1978)

MILLIGAN, V., SODERMAN, L. and RUTKA, A. - Experience with Canadian Varved Clays. J.S.M.F.D., ASCE, Vol. 88, SM4: 32-67 (1962)

MOHAN, D., JAIN, G.S. and KUMAR. V. - Load Bearing Capacity of Piles. Geot. Vol. 13, No. 1: 76-86 (1963)

NICHOLLS, R.A. - Negative Friction of Piled Foundations. Ph.D. Thesis, University of Wales (1973)

O'NEILL, M.W., REESE, L.C. - Behaviour of Bored Piles in Beaumont Clay. J. SMFE., ASCE., 98: 195-213 (1972)

O'NEILL, M.W., HAWKINS, R.A., AUDIBERT, J.M.E. - Installation of Pile Groups in Over-Consolidated Clays. J.G.E.D., ASCE., Vol. 108, No. GTH: 1369-1386 (1982)

OLSEN, R.E., FLAATE, K.S. - Pile Driving Formulae for Friction in Sand. J.S.M.F.D., ASCE., Vol. 93, SM6: 279-296 (1967)

ORRJE, O. and BROMS, B.B. - Effects of Pile Driving on Soil Properties. J.S.M.F.D., ASCE., Vol. 93, SM5: 59-73 (1967)

POULOS, H.G., DAVIS, E.H. - Pile Foundation Analysis and Design. John Wiley and Sons Inc. (1980)

SCANLAN, R.H., TOMKO. J.J. - Dynamic Predictions of Pile Static Bearing Capacity. J.S.M.F.D., ASCE., Vol. 95, SM2: 583-604 (1969)

SEED, H.B., REESE, L.C. - The Action of Soft Clay along Friction Piles. Trans. ASCE., Vol. 122: 731-754 (1957)

SMITH, E.A.L. - Impact and Longitudinal Wave Transmission. Transactions, ASME (1955)

SMITH, E.A.L. - Pile Driving Analysis by the Wave Equation. J.S.M.F.D., ASCE., 86: 35-61 (1960)

SODERBERG, L. - Consolidation Theory Applied to Foundation Pile Time Effects. Geot. Vol. 12: 217 (1982)

SORENSEN, T., HANSEN, B. - Pile Driving Formulae, and Investigation based on Dimensional Considerations and a Statistical Analysis. Proc. 4th. Int. Conf. SM and F.E., Vol. 2: 61-65 (1957)

SOWA, V.A. - Pulling Capacity of Concrete Cast in situ Bored Piles. Can. Geot. Jnl. Vol. 7: 482-493 (1970)

St. VENNANT, B.D. - J. Mathemat (Liouville), pp. 257 and 376 (1866)

SUNG, T.Y. - Vibrations in Semi-infinite Solids due to Periodic Surface Loadings. Symposium on Dynamic Testing of Soils, ASTM, STP, No. 156

TAN, Y.G. - Load Testing of Piled Foundations. Ph.D. Thesis, U.W.I.S.T., Cardiff, S. Wales (1983)

TAVENAS, F.A. - Load Tests Results in Friction Piles in Sand. Can. Geot. Jnl., vol. 8: 7-22 (1971)

TAVENAS, F.A., AUDY, R. - Limitations of the Driving Formulas for Predicting the Bearing Capacity of Piles in Sand. Can. Geot. Jnl., 9: 47-62 (1972)

TAVENAS, F.A., AUDIBERT, J. - Application of the Wave Equation Analysis to Friction Piles in Sand. Can. Geot. Jnl. 14: 34 (1977)

TAYLOR, D.W. - Fundamentals of Soil Mechanics. New York, Wiley (1948)

THURMAN, A.G., D'APPOLONIA, E. - Computed Movement of Friction and End-Bearing Piles embedded in Uniform and Stratified Soils. Proc. 6th. Int. Conf. SM and F.E., Vol. 2: 323-327 (1965)

TIMOSHENKO, S., GOODIER, J.M. - Theory of Elasticity. McGraw-Hill, Second Edition, p. 438 (1951)

TOMLINSON, M.J. - Some Effects of Pile Driving on Skin Friction, Installation Proceeding and Effects. Proc. Conf. on Behaviour of Pile Inst. Paper 9: 107-114 (1971)

TOMLINSON, M.J. - Pile Design and Construction Practise. London: Viewpoint Publications (1977)

TOUMA, F.T., REESE, L.C. - Behaviour of Bored Piles in Sand. Jnl. Geot. Eng. Div., ASCE., Vol. 100, No. GT7: 749-761 (1974)

VAN KOTEN, H., MIDDENDORP, P. - Interpretation of Results from Integrity Tests and Dynamic Load Tests. Intl. Seminar on the Application of Stress Wave Theory on Piles, Stockholm: 217-232 (1980)

VESIC, A.S. - Bearing Capacity of Deep Foundations in Sand. Highway Research Record, 29: 113-153 (1963)

VESIC, A.S. - Ultimate Loads and Settlements of Deep Foundations in Sand. Proc. Symposium on Bearing Capacity and Settlement of Foundations, Duke University: 53-68 (1965)

VESIC, A.S. - A Study of Bearing Capacity of Deep Foundations. Final Report, Prof. B-189, School of Civil Engineering, Georgia Inst. Tech., Atlanta, Ga. (1967)

VESIC, A.S. - Load Transfer in Pile Soil Systems. Proc. of the Conf. on Design and Installation of Pile Foundation and Cellular Structures, Bethlehem, P.A: 47-73 (1970)

WERSCHING, S.N. - A Method of Estimating the In-Situ Density of Dry Uniformly Graded Sand under Controlled Conditions of Placement. Geot. Inst. Inl., GTJODJ, Vol. 6, No. 4 pp. 196-200 (1983)

WERSCHING, S.N. - The Load Transfer of an Axially Loaded Model Pile in Sand overlying Clay. Ph.D. Thesis, Polytechnic of Wales, S. Wales, U.K. (1986)

WHITAKER, T. - Experiments with Model Piles in Groups. Geot., Vol. 7: 147-167 (1957)

WHITAKER, T. - The Constant Rate of Penetration Test for the Determination of the Ultimate Bearing Capacity of a Pile. Proc. Inst. Civ. Engs. Vol. 26: 119-123 (1963)

WHITAKER, T. - The Design of Piled Foundations. Oxford, Pergamon (1970)

WHITMAN, R.V., RICHART, F.E. - Design Procedure for Dynamically Loaded Foundations. J.S.M.F.D., ASCE., Vol. 93, SM6: 169-193 (1967)

PRANDTL, L. - Uber die Eindringungsfestigkeit Plastisher Banstoffe und die Festigkeit von Schneiden. Zeitschrift fur Angewandte Machematick und Mechanik, 1:1, 15-20 (1921)

RAMEY, G.E., HUDGINS, A.P. - Sensitivity and Accuracy of the Pile Wave Equation. Ground Engineering, Vol. 10, No. 7: 45-47 (1977)

RANDOLPH, M.F., WROTH, C.P. - Recent Developments in Understanding the Axial Capacity of Piles in Clay. Ground Engineering: 17-25 (Oct. 1982)

RAUSCHE, F. - Soil Response from Dynamic Analysis and Measurements on Piles. Ph.D. Thesis, Case Western Reserve University, Cleveland, Ohio (1970)

RAUSCHE, F., GOBLE, G.G. - Performance of Pile Driving Hammers. Journal of the Construction Division, ASCE, Vol. 98, No. 102, Proc. Paper 9188 (1972)

RAUSCHE, F., MOSES, F. and GOBLE, G.G. - Soil Resistance Predictions from Pile Dynamics. J. SMFE., ASCE., Vol. 98, No.SM9, Proc. Paper 9220 (1972)

REESE, L.C. - Load Versus Settlement for an Axially Loaded Pile. Proceedings of a Symposium on Bearing Capacity of Piles, Roorkee, India: 18-38 (1964)

REISSNER, E. - Stationare Axialsymmetrische Durch eine Schuttelmde Masse Erregte Schwingungen eines Homogenen Elastischen Halbraumes. Ingenieur-Archiv, Vol. 7, Part 6 (1936)

REMPE, D.M. - Mechanics of Diesel Pile Driving. Ph.D. Thesis, University of Illinois at Urbana - Champaign (1975)

REMPE, D.M., DAVISSON, M.T. - Performance of Diesel Pile Hammers. Proc. 9th. Int. Conf. SM. F.E., Vol. 2: 347-354 (1977)

ROBINSON, R.B. - Shaft Friction and End Bearing Resistance for Driven Piles in Layered Soils. Progress Report for Transfer of Registration from Master of Philosophy to Doctor of Philosophy, Poly. of Wales, S. Wales, U.K. (1986)

ROBINSKY, E.I., MORISSON, C.F. - Sand Displacements and Compactions around Model Friction Piles. Can. Geot. Jnl., Vol. 1, No. 2: 81 (1964)

SAMSON, C.H., HIRSCH, T.J. and LOWERY, L.L. - Computer Study of Dynamic Behaviour of Piling. J. Struct. Divn., ASCE., Vol. 89, ST4: 413-449 (1963)